



FAKULTÄT FÜR CHEMIE

Lehrstuhl für Strukturanalytik in der Katalyse

The Synthesis, Characterization and Performance of  
Well-Defined Iron Carbonyl Catalysts

Hüseyin Güler

Vollständiger Abdruck der von der Fakultät für Chemie der Technischen  
Universität München zur Erlangung des akademischen Grades eines  
Doktors der Naturwissenschaften  
genehmigten Dissertation.

Vorsitzender : Univ.-Prof. Dr. Klaus Köhler

Prüfer der Dissertation:

1. Prof. Moniek Tromp, Ph.D.  
Univ. Amsterdam / Niederlande
2. Univ.-Prof. Dr. Thomas Brück

Die Dissertation wurde am 28.05.2015 bei der Technischen Universität München  
eingereicht und durch die Fakultät für Chemie am 28.07.2015 angenommen.

**THE SYNTHESIS, CHARACTERIZATION AND  
PERFORMANCE OF WELL-DEFINED IRON CARBONYL  
CATALYSTS**

**HUSEYIN GULER**

Doctoral Thesis  
Technische Universität München  
May 2015

Hüseyin Güler: The Synthesis, Characterization and Performance of Well-Defined  
Iron Carbonyl Catalysts.

© May 2015

## ABSTRACT

---

The synthesis of well-defined, uniform iron carbonyl based complexes incorporating diphosphine ligands was performed and their performance as homogeneous catalysts evaluated. The iron carbonyl diphosphine complexes were formed by reaction of  $\text{Fe}_3(\text{CO})_{12}$  and bidentate diphosphine ligands. Detailed characterizations as well as kinetic studies were performed to provide fundamental insights in the catalyst properties. These iron carbonyl complexes were examined as homogeneous catalysts in 2-propanol-based transfer hydrogenation of ketone. The influence of different reaction parameters on the catalytic performance was investigated. The scope and limitations of the described catalyst for the reduction of a series different ketones was shown. In most cases, high conversion and selectivity are obtained. Mechanistic and kinetic studies indicate a monohydride reaction pathway for the homogeneous iron catalyst. Iron carbonyls supported on  $\gamma\text{-Al}_2\text{O}_3$  were obtained and their performance as heterogeneous catalysts evaluated.

## ZUSAMMENFASSUNG

---

Die Synthese von gut definierten einheitlichen Eisencarbonyl Komplexe mit diphosphine Liganden wurde durchgeführt und ihre katalytischen Leistungen wurden ausgewertet. Die Eisencarbonyl diphosphine Komplexe wurden durch die Reaktion von  $\text{Fe}_3(\text{CO})_{12}$  und bidentate Diphosphin-Liganden gebildet. Um grundlegende Erkenntnisse von den Eigenschaften der Katalysatoren zu erlangen, wurden detaillierte Charakterisierung als auch Kinetik durchgeführt. Diese Eisencarbonyl Komplexe wurden als homogene Katalysatoren in 2-Propanol-basierter Transfer-Hydrierung von Ketonen untersucht. Der Einfluss der verschiedenen Reaktionsparameter auf die katalytische Leistung wurde analysiert. Die Anwendungsbereich und Limitationen des definierten Katalysators wurden für die Reduktion einer Reihe verschiedener Ketone gezeigt. In den meisten Fällen wurden hohe Umwandlungen und Selektivitäten erhalten. Mechanistische und kinetische Studien zeigen einen Monohydrid Reaktionsweg für die homogenen Eisen-Katalysatoren. Eisencarbonyle imprägnierte auf  $\gamma\text{-Al}_2\text{O}_3$  wurden erhalten und ihre katalytische Leistungen wurden ausgewertet.

# INDEX

---

INTRODUCTION	1
1 LITERATURE SURVEY AND THEORY	6
1.1 IRON CARBONYLS	6
1.1.1 Mononuclear Iron Carbonyl: $\text{Fe}(\text{CO})_5$	8
1.1.2 Binuclear Iron Carbonyl Clusters: $\text{Fe}_2(\text{CO})_n$ (n: 9, 8, 7,6)	9
1.1.3 Trinuclear Iron Carbonyl Clusters: $\text{Fe}_3(\text{CO})_n$ (n: 12, 11, 10, 9)	11
1.1.4 Hexanuclear Iron Carbonyl Clusters: $[\text{Fe}_6\text{C}(\text{CO})_{16}]^{2-}$	13
1.2 PHOSPHORUS LIGANDS	15
1.2.1 DuPhos and BPE Bisphosphine Ligands	16
1.2.2 DIOP Bisphosphine Ligands	17
1.2.3 Bisphosphine Ligands	18
1.2.4 Phosphorus Ligands in Hydrogenation of Ketone	18
1.3 IRON CARBONYL CLUSTER - PHOSPHINE COMPLEXES	22
1.3.1 Iron Carbonyl Phosphorus Complexes	22
1.3.2 Reactions of Iron Carbonyls with mono-Phosphines	23
1.3.3 Reactions of Iron Carbonyls with bis-Phosphines	25
1.3.3.2 Trinuclear iron carbonyl complexes	26
1.4 REDUCTION OF CARBONYL COMPOUNDS BY TRANSFER HYDROGENATIONS	29
1.4.1 Introduction	29
1.4.2 Transfer Hydrogenation	31
1.4.3 Mechanistic Aspects of Transfer Hydrogenation	36
1.5 $\gamma$ -ALUMINA AS A SUPPORT FOR CATALYSTS	38
1.5.1 Structure of $\gamma$ -Alumina	38
1.5.2 $\gamma$ - $\text{Al}_2\text{O}_3$ / $\text{H}_2\text{O}$ Interface	40

1.5.3 $\gamma$ -Al <sub>2</sub> O <sub>3</sub> as a Support	41
1.6 IRON CARBONYL CLUSTERS SUPPORTED On $\gamma$ -Al <sub>2</sub> O <sub>3</sub>	43
1.6.1 Physisorption on $\gamma$ -Al <sub>2</sub> O <sub>3</sub>	43
1.6.2 Chemisorption on $\gamma$ -Al <sub>2</sub> O <sub>3</sub>	45
1.7 X-RAY POWDER DIFFRACTIONS	48
1.7.1 Crystal Structures	49
1.7.2 Louër Method	51
1.7.3 Visser Method	52
1.7.4 Werner Method	53
1.8 REFERENCES	54
2 EXPERIMENTAL	61
2.1 GENERAL TECHNIQUES AND METHODS	61
2.2 CHARACTERIZATION OF SUBSTANCES	61
2.2.1 Nuclear Magnetic Resonance Spectroscopy	61
2.2.2 Elemental Analysis	61
2.2.3 Mass Spectroscopy	62
2.2.4 Gas Chromatography	62
2.3 WORKING PROCEDURES	62
2.3.1 Synthesis of iron carbonyl cluster	62
2.3.2 Synthesis of Iron Carbonyl Complexes	64
2.3.3 Obtainment of Supported Iron Carbonyl Clusters on Alumina	76
2.3.4 Experimental of Transfer Hydrogenation	80
2.3.5 Experimental of Heterogeneous Catalysis	80
2.4 REFERENCES	81
3 RESULTS AND DISCUSSION	82
3.1 SYNTHESIS	82

3.2	ELEMENTAL ANALYSIS OF THE SYNTHESIZED COMPOUNDS	82
3.3	$^{13}\text{C}$ -NMR AND $^{31}\text{P}$ -NMR SPECTRA	83
3.4	FT-IR SPECTRA	85
3.5	X-RAY POWDER DIFFRACTIONS	88
3.5.1	The Powder X-ray Structure of $[\text{Et}_4\text{N}]_2[\text{Fe}_6\text{C}(\text{CO})_{16}]$ (1)	88
3.5.2	The Powder X-ray Structure of $\text{Fe}_2(\text{CO})_4(\mu\text{-CO})(\mu,\eta^2\text{-dppm})_2$ (2)	89
3.5.3	The Powder X-ray Structure of $\text{Fe}_2(\text{CO})_4(\mu\text{-CO})_3(\mu,\eta^2\text{-dppm})$ (3)	89
3.5.4	The Powder X-ray Structure of $\text{Fe}(\text{CO})_4(\eta^1\text{-dppm})$ (4)	90
3.5.5	The Powder X-ray Structure of $\text{Fe}_2(\text{CO})_4(\mu,\eta^2\text{-dppe})_2$ (5)	91
3.5.6	The Powder X-ray Structure of $\text{Fe}_2(\text{CO})_4(\mu,\eta^2\text{-dppp})_2$ (6)	92
3.5.7	The Powder X-ray Structure of $\text{Fe}_3(\text{CO})_8(\mu\text{-CO})_2(\mu,\eta^2\text{-dppm})$ (7)	92
3.5.8	The Powder X-ray Structure of $\text{Fe}_3(\text{CO})_8(\mu\text{-CO})_2(\mu,\eta^2\text{-dppe})$ (8)	93
3.5.9	The Powder X-ray Structure of $\text{Fe}_3(\text{CO})_8(\mu\text{-CO})_2(\mu,\eta^2\text{-dppp})$ (9)	94
3.5.10	The Powder X-ray Structure of $\text{Fe}_2(\text{CO})_4(\text{CO})_3(\mu,\eta^2\text{-dppp})$ (10)	95
3.6	APPLICATION OF TRANSFER HYDROGENATION	96
3.6.1	Optimization of Iron-Catalysed Transfer Hydrogenation of Ketone	96
3.6.2	Different Iron Carbonyl Precursors	103
3.6.3	Substrate scope	105
3.7	KINETIC INVESTIGATIONS OF TRANSFER HYDROGENATION	108
3.7.1	Determination of the Rate of Reaction	110
3.7.2	Different iron carbonyl precursors	113
3.7.3	Temperature Dependence	114
3.7.4	Calculation of $E_a$ using Arrhenius Equation	114

3.8	STABILITY OF CATALYSTS IN TRANSFER HYDROGENATION	117
3.9	THE EFFECT OF DIPHOSPHINE COMPLEXES ON THE CATALYST STABILITY AND FUNCTIONALITY	118
3.9.1	Ligand Parameters	118
3.9.2	Steric factors in phosphines (Tolman's cone angle)	120
3.10	APPLICATION OF HETEROGENEOUS CATALYSIS	122
3.10.1	Optimization of Iron Supported on Alumina-Catalysed Hydrogenation of Ketone	122
3.10.2	Different Iron Carbonyl Precursors	123
3.11	REFERENCES	124
4	SUMMARY AND CONCLUSION	125
4.1	Transfer Hydrogenation of Ketones	125
4.2	Heterogeneous Catalysis	126
	APPENDIX 1 MASS SPECTRA	128
	APPENDIX 2 <sup>13</sup> C-NMR SPECTRA	128
	APPENDIX 3 <sup>31</sup> P-NMR SPECTRA	128
	APPENDIX 4 FTIR SPECTRA	128
	APPENDIX 5 X-RAY POWDER DIFFRACTIONS	128



## LIST OF FIGURES

---

Figure 1 Structure of iron pentacarbonyl.....	7
Figure 2 Fe(CO) <sub>5</sub> X-ray structure .....	8
Figure 3 Fe <sub>2</sub> (CO) <sub>8</sub> structure (Hoffmann et al., 1982) .....	10
Figure 4 Fe <sub>2</sub> (CO) <sub>8</sub> structure (Poliakoff et al., 1986).....	10
Figure 5 Structures of M <sub>3</sub> (CO) <sub>12</sub> isomers: (a) M <sub>3</sub> (CO) <sub>12</sub> with no bridging CO groups ( <i>D</i> <sub>3h</sub> ); (b) M <sub>3</sub> (CO) <sub>10</sub> (μ-CO) <sub>2</sub> with two bridging CO groups ( <i>C</i> <sub>2v</sub> ); (c) M <sub>3</sub> (CO) <sub>9</sub> (μ-CO) <sub>3</sub> with three bridging CO groups ( <i>D</i> <sub>3h</sub> ).....	11
Figure 6 Structure of the [Fe <sub>6</sub> C(CO) <sub>16</sub> ] <sup>2-</sup> .....	14
Figure 7 Chiral phosphorus ligands (Tang et al., 2003) .....	15
Figure 8 Phosphor ligands such as BINAP and DuPhos (Tang et al., 2003) .....	16
Figure 9 Modification of DuPhos and BPE.....	16
Figure 10 The Modification of DIOP .....	17
Figure 11 Some of bisphosphine ligand .....	17
Figure 12 Bisphosphine Ligands .....	18
Figure 13 Structure of Fe <sub>2</sub> (CO) <sub>n</sub> (dppx) <sub>m</sub> .....	22
Figure 14 Structure of Fe(CO) <sub>4</sub> (η <sup>1</sup> -dppm), Fe <sub>2</sub> (CO) <sub>7</sub> (dppm) and Fe <sub>2</sub> (CO) <sub>5</sub> (dppm) <sub>2</sub> . ..	23
Figure 15 Structure of Fe <sub>2</sub> (CO) <sub>6</sub> (PRR')H.....	24
Figure 16 (i) a symmetrically intermolecular bridging mode, (ii) a symmetrically intramolecular bridging mode and (iii) unsymmetrically chelating mode ...	25
Figure 17 Structure of iron-diphosphine complexes .....	26
Figure 18 Structure of Fe <sub>3</sub> (CO) <sub>11</sub> (PFcPh <sub>2</sub> ) .....	26
Figure 19 Structure of Fe <sub>3</sub> (CO) <sub>n</sub> (dppx) (P-R-P = dppe, dppm, dppb, dppf, dppbz)... ..	27
Figure 20 Alumina structure.....	38

Figure 21 Schematic drawing of the first two layers in the gamma alumina structure .....	39
Figure 22 Two type of adsorption .....	44
Figure 23 Difference between single-crystal X-ray and powder X-ray .....	48
Figure 24 The schematic presentation of powder x-ray diffraction .....	49
Figure 25 $\nu(\text{CO})$ stretching vibration a) $\text{Fe}_3(\text{CO})_{12}$ , b) $\text{Fe}_2(\text{CO})_4(\text{dppe})_2$ , and $\text{Fe}_3(\text{CO})_{10}(\text{dppe})$ .....	86
Figure 26 $\nu(\text{CO})$ stretching vibration a) $\text{Fe}_3(\text{CO})_{12}$ , b) $\text{Fe}_2(\text{CO})_4(\text{dppp})_2$ , and $\text{Fe}_3(\text{CO})_{10}(\text{dppp})$ .....	87
Figure 27 $\sigma$ -donation (left) and $\pi$ -back donation (right) contributions.....	118
Figure 28 Molecular orbital theory of phosphine and carbonyl ligands.....	119
Figure 29 Tolman's cone angle for $\text{M-PR}_3$ .....	121

## LIST OF TABLES

---

Table 1 Comparison of main advantages and disadvantages of homogeneous vs. heterogeneous catalysts. ....	1
Table 2 Influence of different bases and iron sources in the Fe-catalysed transfer hydrogenation of acetophenone (Enthaler et al., 2006).....	33
Table 3 Influence of phosphorus ligand in the Fe-catalysed transfer hydrogenation of acetophenone (Enthaler et al., 2006) .....	35
Table 4 Unit cell geometry and crystal system.....	50
Table 5 Mass-Spectrum analysis of $[\text{Et}_4\text{N}]_2[\text{Fe}_6\text{C}(\text{CO})_{16}]$ (1).....	63
Table 6 Mass-Spectrum analysis of $\text{Fe}_2(\text{CO})_4(\mu\text{-CO})(\mu,\eta^2\text{-dppm})_2$ ( <b>2</b> ) and $\text{Fe}_2(\text{CO})_4(\mu\text{-CO})_3(\mu,\eta^2\text{-dppm})$ ( <b>3</b> ).....	65
Table 7 Mass-Spectrum analysis of $\text{Fe}(\text{CO})_4(\eta^1\text{-dppm})$ ( <b>4</b> ). ....	66
Table 8 Mass-Spectrum analysis of $\text{Fe}_2(\text{CO})_4(\mu,\eta^2\text{-dppe})_2$ ( <b>5</b> ).....	68
Table 9 Mass-Spectrum analysis of $\text{Fe}_2(\text{CO})_4(\mu,\eta^2\text{-dppp})_2$ ( <b>6</b> ).....	69
Table 10 Mass-Spectrum analysis of $\text{Fe}_3(\text{CO})_8(\mu\text{-CO})_2(\mu,\eta^2\text{-dppm})$ ( <b>7</b> ). ....	71
Table 11 Mass-Spectrum analysis of $[\text{Fe}_3(\text{CO})_{10}(\mu,\eta^2\text{-dppe})]$ ( <b>8</b> ).....	72
Table 12 Mass-Spectrum analysis of $[\text{Fe}_3(\text{CO})_8(\mu\text{-CO})_2(\mu,\eta^2\text{-dppp})]$ ( <b>9</b> ).....	74
Table 13 Mass-Spectrum analysis of $[\text{Fe}_2(\text{CO})_4(\mu\text{-CO})_3(\mu,\eta^2\text{-dppp})]$ ( <b>10</b> ).....	75
Table 14 Elemental analysis of iron carbonyl cluster complexes.....	83
Table 15 $^{13}\text{C}$ -NMR spectral data. Chemical shifts ( $\delta$ ) are reported in ppm. ....	84
Table 16 IR spectra ( $4000\text{-}550\text{ cm}^{-1}$ ) of compounds (1-10).....	85
Table 17 The result of the Louër solution for $[\text{Et}_4\text{N}]_2[\text{Fe}_6\text{C}(\text{CO})_{16}]$ (1).....	88
Table 18 The result of the Visser solution for $\text{Fe}_2(\text{CO})_4(\mu\text{-CO})(\mu,\eta^2\text{-dppm})_2$ ( <b>2</b> ).....	89
Table 19 The Louër solution for $\text{Fe}_2(\text{CO})_4(\mu\text{-CO})_3(\mu,\eta^2\text{-dppm})$ ( <b>3</b> ) .....	90
Table 20 The result of the Louër solution for $\text{Fe}(\text{CO})_4(\eta^1\text{-dppm})$ ( <b>4</b> ).....	90
Table 21 The Werner solution for $\text{Fe}_2(\text{CO})_4(\mu,\eta^2\text{-dppe})_2$ ( <b>5</b> ) .....	91

Table 22 The Werner solution of $\text{Fe}_2(\text{CO})_4(\mu, \eta^2\text{-dppp})_2$ (6).....	92
Table 23 The result of the Werner calculation for $\text{Fe}_3(\text{CO})_8(\mu\text{-CO})_2(\mu, \eta^2\text{-dppm})$ (7)	93
Table 24 The result of Werner solution for $\text{Fe}_3(\text{CO})_8(\mu\text{-CO})_2(\mu, \eta^2\text{-dppe})$ (8) .....	93
Table 25 The result of the Werner solution for $\text{Fe}_3(\text{CO})_8(\mu\text{-CO})_2(\mu, \eta^2\text{-dppp})$ (9) .....	94
Table 26 The Louër calculation of $\text{Fe}_2(\text{CO})_4(\mu\text{-CO})_3(\mu, \eta^2\text{-dppp})$ (10) .....	95
Table 27 Influence of base in the $\text{Fe}_3(\text{CO})_{12}$ -catalyzed transfer hydrogenation of acetophenone .....	97
Table 28 Influence of base in the $\text{Fe}_2(\text{CO})_4(\mu\text{-CO})(\mu, \eta^2\text{-dppm})_2$ (2)-catalyzed transfer hydrogenation of acetophenone.....	98
Table 29 Influence of base amount with different iron carbonyl complexes in transfer hydrogenation of acetophenone.....	100
Table 30 Influence of solvent in transfer hydrogenation of acetophenone .....	101
Table 31 Influence of solvent in the $\text{Fe}_3(\text{CO})_{12}$ -catalyzed transfer hydrogenation of acetophenone .....	102
Table 32 Influence of base and solvent in the $\text{Fe}_2(\text{CO})_4(\mu\text{-CO})(\mu, \eta^2\text{-dppm})_2$ (2)-catalyzed transfer hydrogenation of acetophenone .....	103
Table 33 Influence of the iron carbonyl complexes in transfer hydrogenation of acetophenone .....	104
Table 34 Influence of the iron carbonyl clusters in transfer hydrogenation of acetophenone .....	105
Table 35 Influence of the iron carbonyl clusters in transfer hydrogenation of acetophenone .....	106
Table 36 Calculation of experimental data's .....	116
Table 37 Influence of the iron carbonyl clusters in transfer hydrogenation of acetophenone .....	117

## LIST OF SCHEMES

---

Scheme 1 Production of $\text{Fe}_2(\text{CO})_9$ .....	7
Scheme 2 Production of $\text{Fe}_3(\text{CO})_{12}$ .....	7
Scheme 3 Threshold Values $E_t$ of $\text{Fe}_2(\text{CO})_8^+$ , $\text{Fe}_2(\text{CO})_7^+$ , $\text{Fe}_2(\text{CO})_6^+$ , $\text{Fe}_2(\text{CO})_5^+$ .....	10
Scheme 4 Fluxionality of triiron dodecacarbonyl .....	12
Scheme 5 Bridge opening - bridge closing mechanism.....	12
Scheme 6 the synthesis of vitamin B and co-enzyme A.....	19
Scheme 7 Hydrogenation of $\beta$ -keto esters .....	19
Scheme 8 Hydrogenation of simple aromatic ketones .....	20
Scheme 9 Direct hydrogenation of ketone.....	21
Scheme 10 The demonstration of merry-go-round mechanism .....	28
Scheme 11 Mechanism of transfer hydrogenation .....	29
Scheme 12 Carbonyl hydrogen transfer reduction .....	31
Scheme 13 Example of Meerwein-Ponndorf-Verley reaction with Al complex.....	36
Scheme 14 Inner- (a) vs. outer- (b) sphere mechanism. ....	37
Scheme 15 The relations between transition aluminas, depending on the initial hydroxide and temperature .....	39
Scheme 16 The interaction of $\gamma\text{-Al}_2\text{O}_3$ .....	40
Scheme 17 The rehydroxylation of Al–O–Al bonds .....	41
Scheme 18 The physisorption of iron carbonyl on gamma alumina .....	44
Scheme 19 The chemisorption of iron carbonyl on gamma alumina .....	46
Scheme 20 The chemisorption of $\text{Fe}_3(\text{CO})_{12}$ and $\text{Fe}(\text{CO})_5$ on gamma alumina .....	46
Scheme 21 Carbonyl hydrogen transfer reduction .....	96
Scheme 22 The representation of the whole process and of the two steps.....	110
Scheme 23 Carbonyl hydrogenation.....	122

## LIST OF DIAGRAMS

---

Diagram 1 Potential energy diagram for chemisorption and physisorption .....	43
Diagram 2 Energy of adsorption depending on distance (d) of adsorbate molecule...	45
Diagram 3 Comparison of base amount and $\text{Fe}_3(\text{CO})_{12}$ and $\text{Fe}_2(\text{CO})_5(\text{dppm})_2$ .....	99
Diagram 4 Comparison of base amount and iron carbonyl complexes .....	100
Diagram 5 Representative plot of typical reaction profile for the TH of AcPh .....	108
Diagram 6 Initial rates vs. acetophenone/isopropanol in TH. ....	109
Diagram 7 Initial rates vs. acetophenone/sodium isopropylate in TH.....	110
Diagram 8 Comparison of different iron carbonyl sources in TH of acetophenone .	113
Diagram 9 Simulated reaction profiles using the proposed model.....	115

## NOMENCLATURE

---

Å	Angstrom
A(s <sup>-1</sup> )	Reaction rate
AcPh	Acetophenone
DFT	Density functional theory
dppb	1,4-Bis(diphenylphosphino)butane
dppbz	1,2-Bis(diphenylphosphanyl)benzene
dppe	1,2-Bis(diphenylphosphino)ethane
dppf	1,1'-Bis(diphenylphosphino)ferrocene
dppm	1,1-Bis(diphenylphosphino)methane
dppp	1,3-Bis(diphenylphosphino)propane
dppv	1,2-bis(diphenylphosphino)ethylene
Dppx	Bis(diphenylphosphino)
ee's	Enantioselectivities
eq	Equivalent
GC	Gas chromatography
GC-MS	Gas chromatography– mass spectrometry
IR	Infrared
MS	Mass spectrometry
NMR	Nuclear magnetic resonance
°C	Degree Celsius
ppm	Parts-per-million 10 <sup>-6</sup>
TOF	Turnover frequency
XRD	X-ray Diffraction
ν	Vibration

# INTRODUCTION

---

Catalysis is a key technology to decrease the energy consumption, to achieve high atom efficiency, to generate advantageous economics and for the advancement of green chemistry (Anastas et al., 2002). Catalysis is the increase in the rate of a chemical reaction due to the participation of an additional substance called a catalyst. The phenomenon of catalysis is a concept known for almost 200 years. The technological revolution in the last century had not been possible without catalysis and nowadays a large majority of the manufacture in the chemical industry is carried out by means of catalytic processes (Chorkendorff et al., 2007). In the future, catalysis will take a key role in helping to overcome major challenges.

Catalysts can be divided into heterogeneous and homogeneous catalysis. Also afterwards heterogenized catalysts were also introduced. A catalyst is called a homogeneous catalyst, when the catalyst is in the same phase as reactant/substrate. A catalyst is called heterogeneous when the catalysts and substrates are in different phases. The major advantages and disadvantages of heterogeneous vs. homogeneous catalysts are summarized in the following table 1.

Table 1 Comparison of main advantages and disadvantages of homogeneous vs. heterogeneous catalysts.

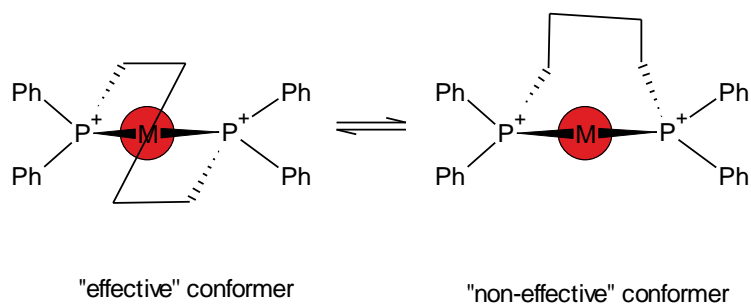
Property	Homogeneous	Heterogeneous
<b>Catalyst recovery</b>	Difficult and expensive	Cheap and easy
<b>Thermal stability</b>	Poor	Good
<b>Selectivity</b>	Excellent/good	Good/poor
<b>Recyclability</b>	Can be very difficult	Easy
<b>Stability</b>	Often decompose over 100°C	Stable to high temperature
<b>Active Site</b>	Small active site	Uniform active site



The development of homogeneous catalysts has focused on active transition metals with simple ligands, which can be P, N, O, S, Se, C and Te ligand. The ligands can change the electronic and steric effects of the active centres of catalysts. Simple changes to the structure of the ligand can completely alter the product distribution, activity or enantioselectivity of a transition metal catalysed reaction. The transition metal catalysts show high turnover frequencies (TOF) and product selectivities (Sues et al., 2014). Generally, illustrative homogeneous catalysts include the rhodium-based compound known as Wilkinson's catalyst and the iridium-based Crabtree's catalyst. The main principle of chemists is that to develop new alternatives with using more abundant, cheap, and less toxic materials.

Recently, there has been an increasing interest to iron in substituting other toxic or expensive second row or third row transition metals. The most widely used transition metal catalyst is ruthenium. Also ruthenium compounds are considered toxic and cancerogenic. In this regards, iron compounds take an important role in field of organometallic chemistry (Jang et al., 1998).

The effect of bidentate diphosphine ligands has played an important role in the development of transition metal catalysed hydrogenation. Bidentate diphosphine ligands show also reasonable enantioselectivity in asymmetric hydrogenation of dehydroamino acid derivatives (Ager et al., 1997). Bidentate diphosphine ligands containing transition metal catalysts have shown good catalytic performance and enantioselectivities in hydrogenation of  $\alpha$ -ketones, esters and amides (Ager et al., 1997). A probable reason is that seven-membered chelate ring of bidentate diphosphine metal complex is conformationally flexible.



The multidentate ligands show that the bridging ligands increase the stability of the metal atom and thus can be created stable compounds for the study with multimetallic

complexes (Masters et al., 1978 and Bahsoun et al., 1982). For this reason, bidentate diphosphine ligands have taken an important role in transfer hydrogenation study. Bis(diphenylphosphino) methane, ethane and propane (resp. dppm, dppe, and dppp) were chosen as an additional ligand in this research. Bidentate diphosphine ligands containing iron carbonyl clusters show increase activity compared to iron carbonyl complexes.

In the homogeneous catalysis, the catalytic reduction of ketones using organometallic complexes play an important role in the production of alcohols for use in the pharmaceutical, fragrance, agrochemical and flavour industry (Meyer, 2009). For this reason, iron carbonyls complexes were synthesized from the reaction between iron carbonyls and bidentate diphosphine ligands and the complexes were characterized by the help of NMR, mass spectroscopy, elemental analysis and IR techniques. The catalytic behaviour of the iron carbonyl complexes was examined in the homogeneous hydrogenation catalyst. In addition, the effect of bidentate diphosphine ligands on the catalyst stability and functionality is investigated. We researched the effect of catalyst, ligands, base and amount of solvent to optimize the catalytic reaction.

The majority of the development of heterogeneous catalysts has focused on the surface metallic chemistry, which consists of the catalytic active metal on an inert support surface. In heterogeneous catalysis, the catalysts allow the reaction under reduced or elevated temperature and pressure.

Direct interaction between iron carbonyl clusters and surface hydroxyl groups of inorganic oxides is an excellent approach to define the activity of metal-metal or metal-ligand bonds (Hugues et al., 1982). In our study, iron carbonyls and iron carbonyl bidentate diphosphine complexes were supported on gamma alumina. The catalytic activity of the iron carbonyls and their complexes were examined in direct hydrogenation and was determined using GC-MS. In addition the effect of coordinating ligands on the catalyst stability and functionality was investigated.

### *i. Thesis Outline*

In the chapter one, iron carbonyls, phosphorus ligands, and iron carbonyl complexes are presented in detail. The basic information about the reduction of carbonyl compounds by transfer hydrogenations is given also. The effect of hydrogen donors, base amount and different ligands in homogeneous catalysis are presented and mechanistic aspect of transfer hydrogenation is explained briefly. The previous researches about transfer hydrogenation using iron carbonyls are also mentioned here. Iron carbonyl supported on gamma alumina is presented also in first chapter.

In the chapter two ‘general techniques and methods’, ‘characterization of substances’ and ‘application of transfer hydrogenation and heterogeneous catalysis’ are described in detail.

In the chapter three, the  $\text{Fe}(\text{CO})_5$ ,  $\text{Fe}_2(\text{CO})_9$ ,  $\text{Fe}_3(\text{CO})_{12}$ ,  $[\text{Et}_4\text{N}]_2[\text{Fe}_6\text{C}(\text{CO})_{16}]$  and their complexes are examined for their ability to serve as catalysts for the  $>\text{C}=\text{O}$  reduction of acetophenone under the conditions of transfer hydrogenation. In order to examine the factors influencing the catalytic performance, the reaction parameters (temperature, reaction time, and catalysts) are determined by GC. In this chapter, performances of iron carbonyl phosphorus complexes were also explained in field of transfer hydrogenation. Application of iron carbonyl complexes supported on gamma alumina is investigated in this chapter. Applications of iron carbonyl cluster supported on gamma alumina are presented in heterogeneous catalysis. The results of asymmetric transfer hydrogenation and heterogeneous catalysis are discussed in detail. Iron carbonyl bisphosphine complexes and ionic hexanuclear iron carbonyl salt show good activity in the reduction of acetophenone. High conversion and selectivity is obtained using the  $[\text{Et}_4\text{N}]_2[\text{Fe}_6\text{C}(\text{CO})_{16}]$  compound as iron precursor.  $\text{Fe}(\text{CO})_5$ ,  $\text{Fe}_2(\text{CO})_9$  and  $\text{Fe}_3(\text{CO})_{12}$  indicated no catalytic activity in transfer hydrogenation. The highest conversions are obtained, when  $\text{Fe}_2(\text{CO})_5(\text{dppm})_2$  is used as a catalyst. The mechanism of asymmetric transfer hydrogenation is calculated and displayed at different temperature by using to three catalysts, which are  $\text{Fe}_3(\text{CO})_{12}$ ,  $\text{Fe}_2(\text{CO})_5(\text{dppm})_2$  and  $\text{Fe}_2(\text{CO})_4(\text{dppe})_2$ .

The results of heterogeneous catalysis with using iron carbonyls supported on  $\gamma\text{-Al}_2\text{O}_3$  are displayed in chapter three. The optimisation of the reaction parameters

(temperature, reaction time, and catalysts) for heterogeneous system is identified. The summary and conclusion take the place in chapter four.

# LITERATURE SURVEY AND THEORY

## 1.1 IRON CARBONYLS

---

Iron pentacarbonyl was synthesized at first in 1891 by Mond (Mond et al., 1891) and  $\text{Fe}(\text{CO})_5$  is prepared by the reaction of fine iron particles with carbon monoxide. Iron carbonyls are used as a precursor to obtain iron carbonyl clusters and their complexes, which are reactive as homogeneous and heterogeneous catalysis.

To understand the catalytic behaviour of iron carbonyl clusters, the chemical and physical properties of iron carbonyl clusters should be known. This chapter describes some of the chemical and physical properties of iron carbonyl clusters, their structures and their fluxionality at defined temperature.

Iron carbonyl clusters and their complexes take an important role in organo-transition metal chemistry, homogenous and heterogeneous catalysis. Iron carbonyls are reactive intermediates for the preparation of organometallic complexes, because a great variety of mixed organo-iron complexes exist. The organo-iron complexes include mostly other ligands than carbonyl to change the reactivity or catalytic activity. As for other organometallic complexes, organo-iron complexes are commonly coordinated by diphosphines and amine/imine ligands. Iron carbonyl phosphine clusters were produced to examine the catalytic properties for carbon monoxide hydrogenation of ketones.

The simplest iron carbonyl precursor to obtain another iron carbonyl clusters is iron pentacarbonyl. Diiron nonacarbonyl, triiron dodecacarbonyl and hexanuclear iron carbonyl ( $[\text{Fe}_6\text{C}(\text{CO})_{16}]^{2-}$ ) are prepared from the iron pentacarbonyl. Pentacarbonyl iron is an orange liquid, was first prepared from the iron and carbon monoxide by Mond and Berthelot more than hundred years ago (Mond et al., 1891). The structure of iron pentacarbonyl is a trigonal bipyramid (Figure 1) and its room temperature  $^{13}\text{C}$ -NMR shows only a single signal. The  $^{13}\text{C}$ -NMR shows, that all of five CO have a same chemical behaviour. The difference between Fe–CO (equatorial) and Fe–CO (axial) bond lengths hasn't been defined clearly (Braga et al., 1993).

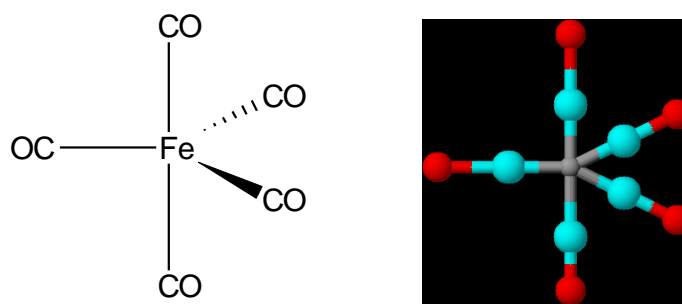
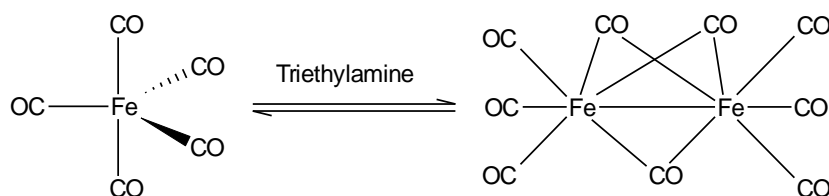


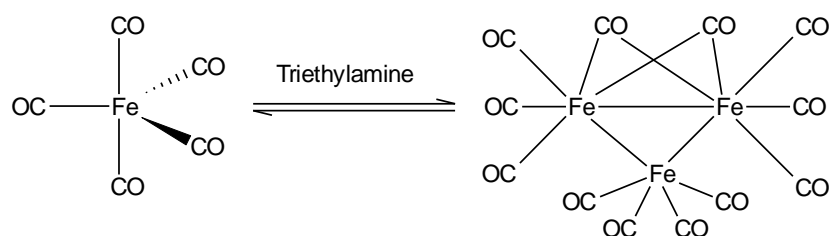
Figure 1 Structure of iron pentacarbonyl

Photolysis of one the carbonyl groups from the iron pentacarbonyl results in a coordinatively unsaturated fragment,  $\text{Fe}(\text{CO})_4$ , which reacts with iron pentacarbonyl (Scheme 1) to obtain diiron nonacarbonyl. Diiron nonacarbonyl is produced in the form of golden coloured plates.



Scheme 1 Production of  $\text{Fe}_2(\text{CO})_9$

The anionic species,  $[\text{Fe}(\text{CO})_4]^{2-}$  and  $[\text{HFe}(\text{CO})_4]^-$  are obtained from  $\text{Fe}(\text{CO})_5$  with sodium amalgam ( $\text{Na}/\text{Hg}$ ) by reduction of carbon monoxide (Wang et al., 1993).  $\text{Fe}_3(\text{CO})_{12}$ , the black-green trinuclear carbonyl, is synthesized from the reaction between iron pentacarbonyl, triethylamine and hydrochloric acid (Scheme 2) (Babin et al., 1903).



Scheme 2 Production of  $\text{Fe}_3(\text{CO})_{12}$

The colour can change with nuclearity of the neutral clusters: the simplest anion,  $\text{Fe}(\text{CO})_4^{2-}$  is colourless,  $\text{Fe}_2(\text{CO})_8^{2-}$  is orange-red,  $\text{Fe}_3(\text{CO})_{11}^{2-}$  is dark red and  $\text{Fe}_4(\text{CO})_{13}^{2-}$  is brown-black (Silver et al., 1993).

### 1.1.1 Mononuclear Iron Carbonyl: Fe(CO)<sub>5</sub>

Iron pentacarbonyl was prepared at first in 1891 by Mond (Mond et al., 1891) and its trigonal-bipyramidal structure (Figure 2) was determined by Ewens (Ewens et al., 1938).

Iron carbonyl is described as a yellow liquid, with the formula Fe(CO)<sub>5</sub> and a boiling point of 102,8°C. The pale yellow liquid cools to a pale yellow solid, which melts between -19,5°C and -20°C. The solid state of iron pentacarbonyl is obtained as a colourless compound. Also iron carbonyl regains yellow colour when heated up again (Ewens et al., 1938).

Compared to Fe<sub>2</sub>(CO)<sub>9</sub>, and Fe<sub>3</sub>(CO)<sub>12</sub>, the mononuclear complex Fe(CO)<sub>5</sub> has been studied more experimentally (Beagley et al., 1974) and theoretically (Luthi et al., 1985).

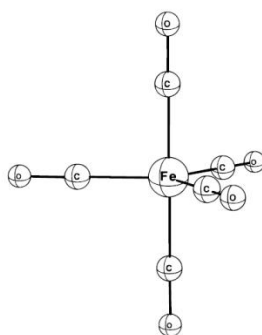


Figure 2 Fe(CO)<sub>5</sub> X-ray structure

Among the previous theoretical studies of Fe(CO)<sub>5</sub>, many DFT studies were published (Handy et al., 1996). But the first comprehensive study of monometal carbonyls was the 1995 study of Jonas and Thiel (Jonas et al., 1995). The experimental Fe-C bond distances and gas-phase electron diffraction of X-ray diffraction were examined.

Several decomposing methods were published for iron pentacarbonyl. But the best method of decomposing the iron pentacarbonyl was found to be treatment with alcoholic potash solution at 100°C. When a bulb containing iron carbonyl is broken in alcoholic potash solution, colourless tabular crystals are produced. Another decomposition method of iron pentacarbonyl is oxidation by the air (Dewar et al.,

1905) and it is forming to a red-brown precipitate, which is insoluble in organic solvents.

The industrially most important iron carbonyl which is preferred in the context of this invention is iron pentacarbonyl  $\text{Fe}(\text{CO})_5$ . Iron pentacarbonyl is used industrially as a raw material for preparing fine iron powder (known as carbonyl iron powder) by thermal decomposition with the exclusion of air or for preparing fine iron oxide powders by combustion. We synthesized mononuclear iron carbonyl complexes such as  $\text{Fe}(\text{CO})_4(\text{dppm})$  and their catalytic activities were examined in transfer hydrogenation of ketone to alcohol.

### **1.1.2 Binuclear Iron Carbonyl Clusters: $\text{Fe}_2(\text{CO})_n$ (n: 9, 8, 7,6)**

$\text{Fe}_2(\text{CO})_9$  is a member of binuclear iron carbonyl clusters and was obtained at first in 1905 (Dewar et al., 1905). Diiron nonacarbonyl contains nine carbonyl ligands around of two irons that three of them are bridging carbonyl ligands and its bridging carbonyl structure was characterized in 1939 (Powell et al., 1939). Diiron nonacarbonyl is insoluble in apolar solvents, which are such as ether, petroleum-ether and benzene but it is soluble in dimethoxymethane, alcohol and acetone, and much more soluble in pyridine.

Diiron nonacarbonyl decomposes by air or moisture. When  $\text{Fe}_2(\text{CO})_9$  is dissolved in dimethoxymethane, alcohol, acetone, or pyridine solution, the compound becomes much more sensitive to air and moisture, and deposits a reddish precipitate (Dewar et al., 1905).

$\text{Fe}_2(\text{CO})_9$  is used industrially as a precursor for preparing  $\text{Fe}(\text{CO})_4\text{L}$  and  $\text{Fe}(\text{CO})_3(\text{diene})$  compounds. It is a more reactive source of  $\text{Fe}(0)$  than  $\text{Fe}(\text{CO})_5$  and less dangerous to handle because it is nonvolatile.

$\text{Fe}_2(\text{CO})_8$  was prepared in 1971 (Poliakoff et al., 1986) and characterized in 1986 (Hoffmann et al., 1982). In fact, two different  $\text{Fe}_2(\text{CO})_8$  structures were identified, the primary product has two bridged carbonyls (Hoffmann et al., 1982). In this structure, any iron-iron bond was detected.



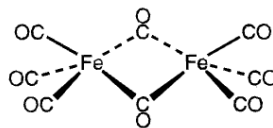


Figure 3  $\text{Fe}_2(\text{CO})_8$  structure (Hoffmann et al., 1982)

The second structure of  $\text{Fe}_2(\text{CO})_8$  produced four years later than first structure by Fletcher (Poliakoff et al., 1986) was defined as any of bridging carbonyl in this structure. The IR spectrum is consistent with the  $D_{2h}$  geometry predicted from theory (Hoffmann et al., 1982). In this structure, an iron-iron bond instead of two bridging carbonyl is determined.

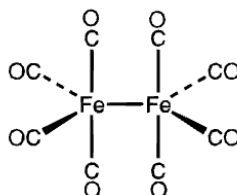
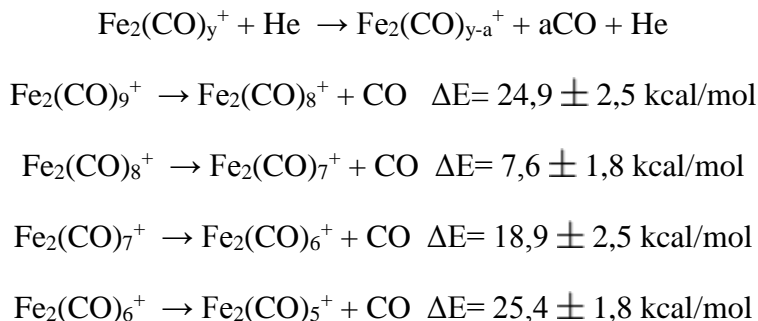


Figure 4  $\text{Fe}_2(\text{CO})_8$  structure (Poliakoff et al., 1986)

Examples of the threshold curves recorded for the CID of  $\text{Fe}_2(\text{CO})_y^+$  are shown in scheme 3 (Markin et al., 2000). The sequential elimination of CO ligands from  $\text{Fe}_2(\text{CO})_y^+$  ( $y = 1-9$ ) is observed:



Scheme 3 Threshold Values  $E_t$  (eV) of  $\text{Fe}_2(\text{CO})_8^+$ ,  $\text{Fe}_2(\text{CO})_7^+$ ,  $\text{Fe}_2(\text{CO})_6^+$ ,  $\text{Fe}_2(\text{CO})_5^+$

The experimental reaction energies show that  $\text{Fe}_2(\text{CO})_9^+$  and  $\text{Fe}_2(\text{CO})_6^+$  are quite stable, while  $\text{Fe}_2(\text{CO})_8^+$  loses a carbonyl ligand very easily (Jang et al., 1998).

Binuclear iron carbonyl complexes such as  $\text{Fe}_2(\text{CO})_7(\text{dppm})$  were synthesized and their catalytic activities were examined in transfer hydrogenation of ketone to alcohol.

### 1.1.3 Trinuclear Iron Carbonyl Clusters: $\text{Fe}_3(\text{CO})_n$ (n: 12, 11, 10, 9)

Trinuclear metal carbonyl clusters were produced and isolated as  $\text{Fe}_3(\text{CO})_{12}$  by Dewar (Dewar et al., 1907). The trimeric structure of  $\text{Fe}_3(\text{CO})_{12}$  was established using cryoscopy technique in  $\text{Fe}(\text{CO})_5$ , which is for determining the molecular weight of a substance by dissolving it and measuring the freezing point of the solution (Hieber et al., 1930 and Hieber, 1932). The correct isosceles triangular structure of  $\text{Fe}_3(\text{CO})_{12}$  with two bridging carbonyl groups  $\text{Fe}_3(\text{CO})_{10}(\mu\text{-CO})_2$  (Figure 5) was determined by X-ray diffraction in 1966 (Wei et al., 1966). More absolute geometrical parameters for  $\text{Fe}_3(\text{CO})_{12}$  were determined by Cotton (Cotton et al., 1974) and were determined later by Braga (Braga et al., 1994).

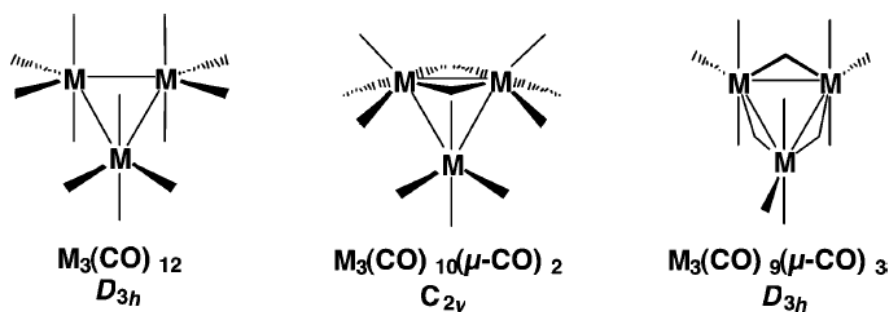


Figure 5 Structures of  $\text{M}_3(\text{CO})_{12}$  isomers: (a)  $\text{M}_3(\text{CO})_{12}$  with no bridging CO groups ( $D_{3h}$ ); (b)  $\text{M}_3(\text{CO})_{10}(\mu\text{-CO})_2$  with two bridging CO groups ( $C_{2v}$ ); (c)  $\text{M}_3(\text{CO})_9(\mu\text{-CO})_3$  with three bridging CO groups ( $D_{3h}$ )

The structure of  $\text{Fe}_3(\text{CO})_{12}$  cluster is highly fluxional. Cotton published that the fluxionality of triiron dodecacarbonyl is a result of the merry-go-round mechanism (Scheme 4) (Cotton et al., 1974). In 1976, Johnson proposed a mechanism going via a  $\text{Fe}_3(\text{CO})_{10}(\mu_3\text{-CO})_2$  intermediate and transition state, stated in middle of scheme 4, as a result of rotation of the  $\text{Fe}(\text{CO})_4$  edges (Johnson et al., 1976).

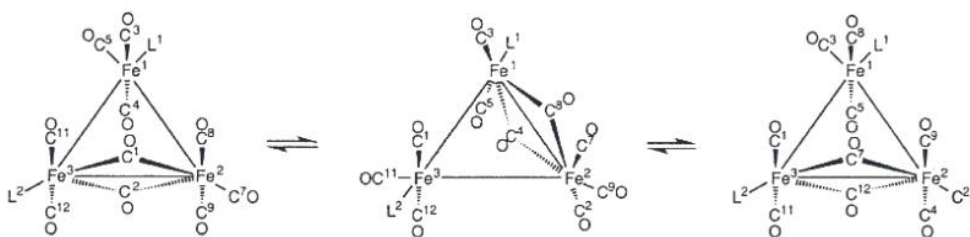
Dynamic NMR investigation of  $\text{Fe}_3(\text{CO})_{12}$  derivatives was published at first in 1981. Johnson examined the  $^{13}\text{C}$ -NMR spectrum of trinuclear iron carbonyl phosphine

complex,  $[\text{Fe}_3(\text{CO})_{11}\{\text{P}(\text{OR})_3\}]$ , that showed carbonyl signals at  $-90^\circ\text{C}$  (Benfield et al., 1981). Johnson explained the fluxionality based on an icosahedron  $\leftrightarrow$  cube octahedron  $\leftrightarrow$  icosahedron rearrangement.



Scheme 4 Fluxionality of triiron dodecacarbonyl

In 1989, the fluxionality of triiron dodecacarbonyl derivative was also examined and its fluxionality was found, the intensity of the carbonyl at  $-101^\circ\text{C}$  was different than at  $-90^\circ\text{C}$  according to NMR. The mechanism of fluxionality of  $\text{Fe}_3(\text{CO})_{12}$  and its derivatives was proposed at different temperatures (Bino et al., 1980). The mechanism involves the rotation of the  $\text{Fe}_3$  triangle around the  $S_{10}$  axis of the carbonyl icosahedron defined by carbonyls C(6)O and C(10)O (Scheme 5). As the carbonyl bridge opens on one Fe-Fe edge, another closes on a second Fe-Fe edge and this mechanism is described as a concerted *bridge opening - bridge closing mechanism* (Bino et al., 1980). This mechanism is described utilizing the slow rotation of bonds of molecule at low temperatures.



Scheme 5 Bridge opening - bridge closing mechanism

Johnson developed a mechanism and named as the Johnson mechanism. By the help of this mechanism, he explained rotations of the  $\text{Fe}(\text{CO})_4$  groups (Johnson et al., 1980).

The Johnson libration mechanism (Scheme 5) and the Mann concerted bridge opening-bridge closing mechanism (Scheme 5) differ in the pathway followed by the

iron triangle during the fluxional pathway (Johnson et al., 1980). In the Johnson mechanism all the equatorial carbonyls ( $C^5O$ ,  $C^6O$ ,  $C^7O$ ,  $C^{10}O$ ), which are shown in scheme 5, move out of the plane defined by the iron triangle (Johnson et al., 1997). In the Mann concerted bridge opening - bridge closing mechanism,  $C^5O$  and  $C^7O$ , which are shown in scheme 4, move out of the plane defined by the iron triangle, while  $C^6O$  and  $C^{10}O$  remain in the plane. Mann published a rebuttal of Johnson the concerted bridge opening - bridge closing mechanism (Mann et al., 1997). Between these two mechanisms little differences were found (Adams et al., 2001). By the help of low temperature have been isolated three different iron carbonyl structure.

Carbonyl iron is used inter alia for the preparation of inductors, pigments, as dietary supplements, (Fairweather-Tait et al., 2002) in the production of radar-absorbing materials in the stealth technology, (Richardson et al., 2002) and in Thermal spraying. We synthesized mononuclear iron carbonyl complexes such as  $Fe_3(CO)_5(dppm)_2$  and their catalytic activities were examined in transfer hydrogenation of ketone to alcohol.

#### 1.1.4 Hexanuclear Iron Carbonyl Clusters: $[Fe_6C(CO)_{16}]^{2-}$

A metal carbido complex is an organometallic compound or coordination complex that contains the carbon ligand. The most studied multi nucleic iron carbonyl carbido clusters are  $[Fe_6C(CO)_{16}]^{2-}$ ,  $[Fe_5C(CO)_{14}]^{2-}$ ,  $[Fe_5C(CO)_{15}]$ ,  $[Fe_4C(CO)_{12}]^{2-}$ ,  $[Fe_4C(CO)_{12}H]^-$  and  $[Fe_4C(CO)_{13}]$  in last century (Hill et al., 1990). The first carbidocarbonyl iron cluster  $[Fe_5C(CO)_{15}]$  was isolated in very low yield from the reaction of triiron dodecacarbonyl with methylphenylacetylene and characterized by X-ray diffraction by Braye (Braye et al., 1962). Using X-ray diffraction, churchill defined geometric structure of  $[Fe_5C(CO)_{15}]$  and the position of carbide carbon.  $[Fe_5C(CO)_{15}]$  includes a square pyramidal  $Fe_5$  core with the carbide carbon, which is determined  $0.08\text{\AA}$  below the centre of the square plane (Churchill et al., 1971).

The hexanuclear iron carbide carbonyl cluster is known as a dianion.  $[Fe_6C(CO)_{16}]^{2-}$  was synthesized by the reaction of  $Fe(CO)_5$  with a metal carbonyl anions,  $Fe(CO)_4Na$  at elevated temperatures, contains an octahedral  $Fe_6C$  core, with the carbon atom situated at its center (Churchill et al., 1971).

The defining characteristic feature of hexanuclear iron carbonyl clusters is the lone carbon atom, bound only to metal atoms. These affects are secondary when compared with the potential for chemistry at this carbon atom, caused by its surrounding metal atoms. In neither  $\text{Fe}_5\text{C}$  nor  $\text{Fe}_6\text{C}$ , has the carbon atom been observed to have any reactivity due to surrounding metal atoms (Tachikawa et al., 1981).

The essential geometry of the  $[\text{Fe}_6\text{C}(\text{CO})_{16}]^{2-}$  dianion is shown in Figure 6. There are thirteen terminal carbonyl ligands; two per iron atom except for Fe(4), which is associated with three. There are three carbonyl bridges: Fe(5)-[C(1)-O(1)]-Fe(1) and the symmetry related Fe(5)-[C(1')-O(1')]-Fe(1'), in which Fe(1)-C(1) = 1,79 Å and Fe(5)-C(1) = 2,19 Å; and the system Fe(2)-[C(5)-O(5)]-Fe(3), lying in the mirror plane of the dianion, in which Fe(2)-C(5) = 1,94 Å and Fe(3)-C(5) = 2,16 Å (Churchill et al., 1971).

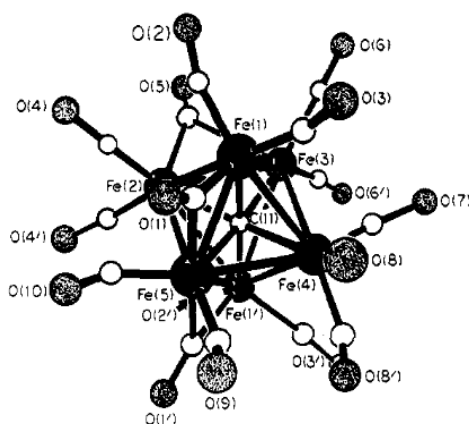


Figure 6 Structure of the  $[\text{Fe}_6\text{C}(\text{CO})_{16}]^{2-}$

$[\text{Fe}_6\text{C}(\text{CO})_{16}]^{2-}$  exhibits considerable thermal stability and also shows stability toward aerobic oxidation not shared by the simple iron carbonyl anions. The solid  $[\text{Fe}_6\text{C}(\text{CO})_{16}]^{2-}$  is partially decomposed after exposure to air for three days. The structure of the  $[\text{Fe}_6\text{C}(\text{CO})_{16}]^{2-}$  anion is resemble to the other known molecular carbides, which are  $\text{Ru}_6\text{C}(\text{CO})_{17}$  and  $\text{Ru}_6\text{C}(\text{CO})_{14}$  (Adams et al., 1989). We synthesized hexanuclear iron carbonyl complexes such as  $[\text{Fe}_6\text{C}(\text{CO})_{16}]^{2-}$  and their catalytic activities were examined in transfer hydrogenation of ketone to alcohol. By the help of different nuclearities, the catalytic properties of mono-, bi-, tri- and hexanuclear iron carbonyls were compared with each other.

## 1.2 PHOSPHORUS LIGANDS

This section will be introduced phosphorus-containing ligands and their influence in the catalytic reactions will be investigated. At first as phosphorus ligands and will be classified as systematic by types. The application of phosphorus ligands and their metal complexes as homogeneous catalysts will be referred to the role of iron carbonyl complex reduction of ketones. This part has been formed in order to understand these ligands and their catalytic affects.

The development of phosphorus ligands takes an important role in hydrogenation catalysis. In fact, the exploration of chiral phosphorus ligands for asymmetric hydrogenation is a continuous effort which started in the late 1960s (Ojima, 2000).

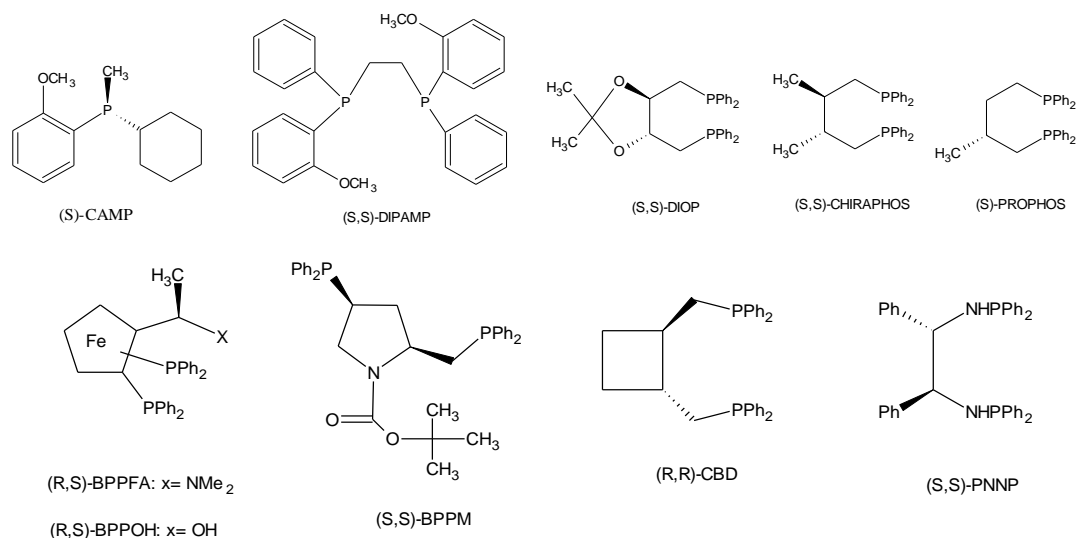
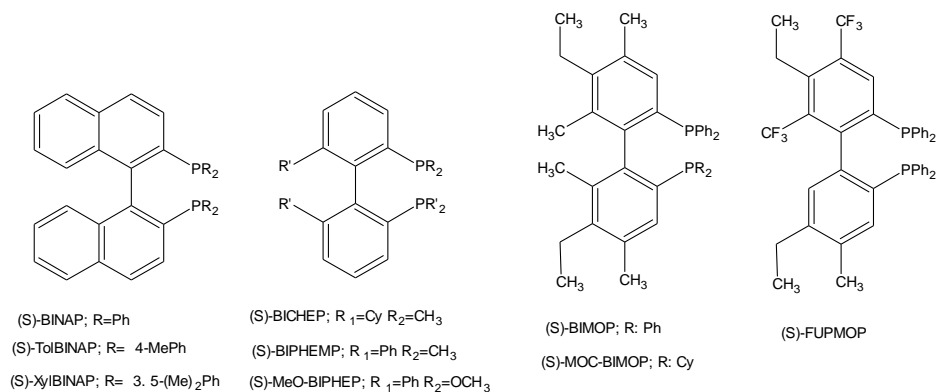


Figure 7 Chiral phosphorus ligands (Tang et al., 2003)

Many phosphorus ligands such as BINAP and DuPhos were produced at 1980s and new phosphorus ligands were designed and discovered (Tang et al., 2003).



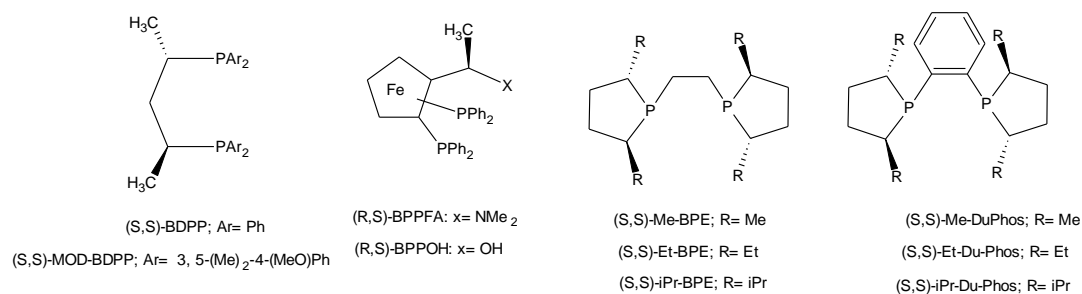


Figure 8 Phosphor ligands such as BINAP and DuPhos (Tang et al., 2003)

### 1.2.1 DuPhos and BPE Bisphosphine Ligands

Since Burk's group published good results with phosphine ligands in the hydrogenation of olefins and ketones, many bisphosphines have been synthesized based on the structural modifications of DuPhos and BPE ligands (Figure 9) (Tang et al., 2003).

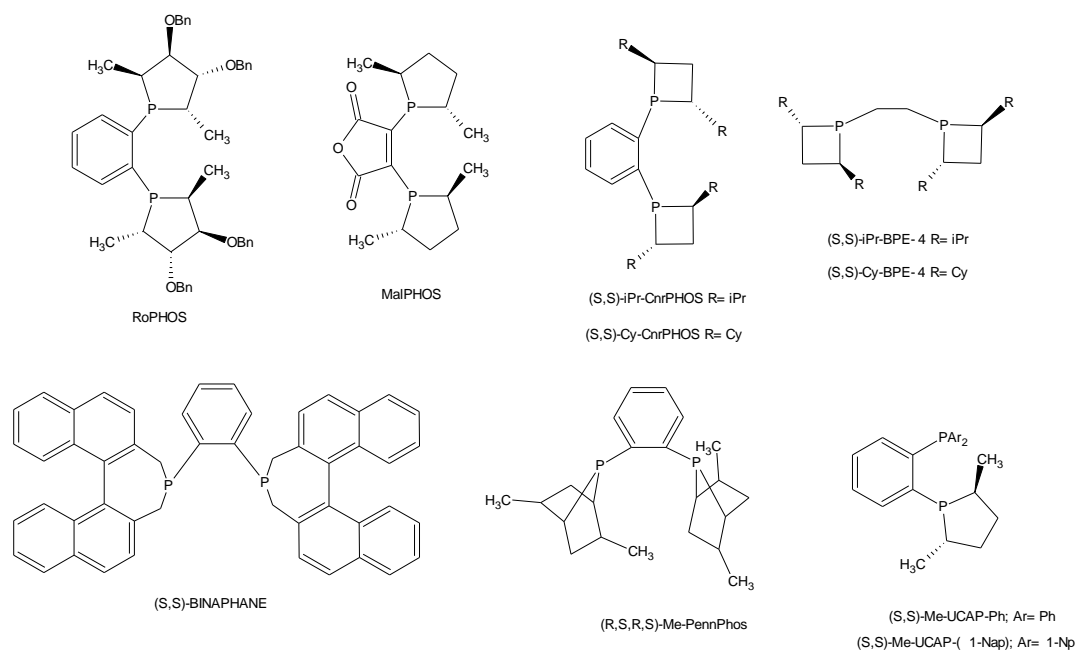


Figure 9 Modification of DuPhos and BPE

The new modified DuPhos and BPE ligands were obtained with ether, ketal, or hydroxyl groups at different positions of the phospholanes. These new synthesized ligands show the high activity in hydrogenation. Holz and co-workers have published the bisphospholane ligand, which contains a maleic anhydride and is named MalPhos. With this ligand, high enantioselectivities were obtained in hydrogenation of ( $\beta$ -acylamino)acrylates (Holz et al., 2000).

The bisphosphetane ligands such as CnrPhos and BPE-4 ligands were obtained by Marinetti (Marinetti et al., 2001). These bisphosphetane ligands have shown good enantioselectivities in transition metal-catalysed hydrogenation. PennPhos, which was developed by Zhang, has different hydrogenation properties compared to other DuPhos-type ligands (Jiang et al., 1998).

### 1.2.2 DIOP Bisphosphine Ligands

Kagan and co-workers synthesized new variations of DIOP for asymmetric hydrogenation. However, DIOP itself only includes medium enantioselectivities in the hydrogenation of amino acid derivatives (Tang et al., 2003). A probable reason is that the seven-membered DIOP metal complex ring is conformationally flexible. The conformations of DIOP transition metal complexes such as Rh and Fe identified in Figure 10 can cause its low efficiency (Tang et al., 2003).

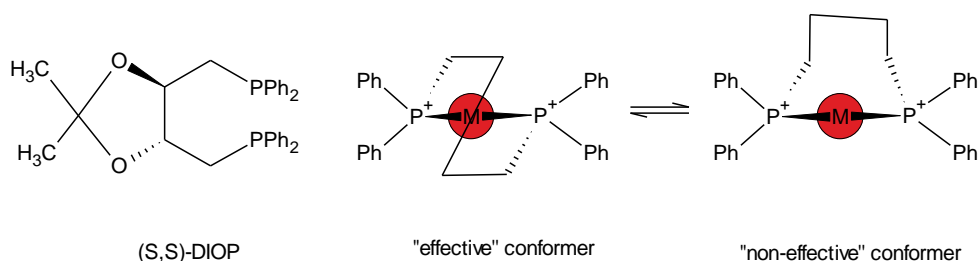


Figure 10 The Modification of DIOP

To fix the structural flexibility of DIOP ligand, a stable 1,4-diphosphine ligand BICP was identified by Zhang with two five-membered carbon rings on BICP ligand (Figure 11) (Cao et al., 1999). BICP ligand (Figure 11) has shown good activity for the hydrogenation of amino acid and the (*S,R,R,S*)-DIOP has shown good enantioselectivity for the hydrogenation of arylenamides. Although, low enantioselectivity was obtained with the isomeric ligand (*S,S,S,S*)-DIOP (Kagan et al., 1979).

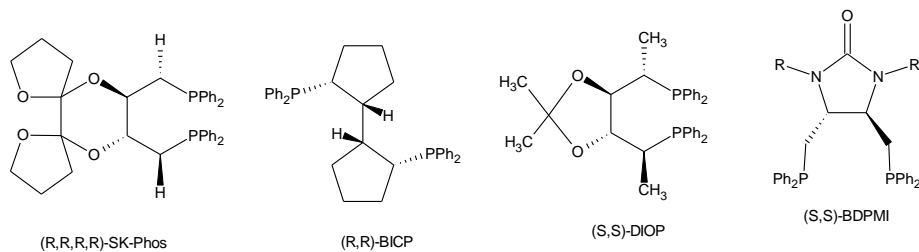


Figure 11 Some of bisphosphine ligand



### 1.2.3 Bisphosphine Ligands

The first bisphosphine-DIPAMP was obtained by Knowles and was proven active for hydrogenation. A series of bisphosphine ligands was synthesized, such as BisP by Imamoto, and the phosphorus ligands attracted much attention (Figure 12) (Imamoto et al., 1998).

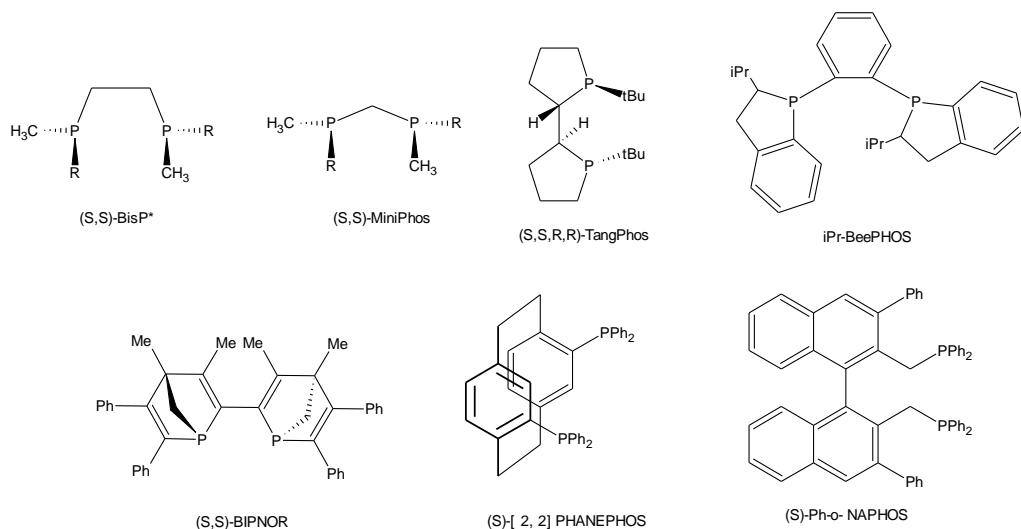


Figure 12 Bisphosphine Ligands

The bisphosphine ligands exhibited remarkable activity and enantioselectivity in hydrogenation of amino acids and enamides (Yasutake et al., 2001 and Gridnev et al., 2001).

Mathey and co-workers have synthesized a bisphosphine ligand BIPNOR containing two chiral bridgehead phosphorus centers. BIPNOR has shown excellent enantioselectivities in the hydrogenation of cinnamic acids and methylenesuccinic acids (Robin et al., 1997 and Mathey et al., 1998).

### 1.2.4 Phosphorus Ligands in Hydrogenation of Ketone

During the last decades, many scientists have concentrated on the study of phosphorus ligands and their catalytic activity in the hydrogenation of ketone. Phosphorus ligand containing transition-metal complexes increase the catalytic activities and enantioselectivities. Therefore phosphorus ligands have taken an important role in the study of the hydrogenation catalysis.

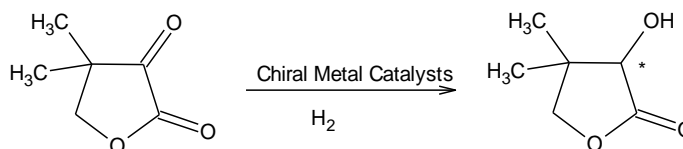
### 1.2.4.1 Hydrogenation of Functionalized Ketones

The hydrogenation of unsaturated ketones has been accepted as a difficult area since present hydrogenation catalysts prefer to hydrogenate the C=O bond rather than C=C double bond (Spogliarich et al., 1992). For example, the DIOP ligands containing transition-metal complexes have shown excellent chemoselectivity for hydrogenation of carbon monoxide over a carbon-carbon double bond (Spogliarich et al., 1992).

#### *$\alpha$ -Keto Esters*

The hydrogenation of R-keto esters has been studied with Rh, Ru and Fe catalysts (Scheme 6). The chiral ligand containing transition metal catalysts have shown good reactivities and ee's in hydrogenation of some  $\alpha$ -ketones, esters and amides. Several neutral Rh and Ru catalysts with chiral ligands such as MCCPM, Cy,Cy-oxoProNOP, Cp,Cp-IndoNOP, and Cr(CO)<sub>3</sub>-Cp,Cp-IndoNOP have shown excellent reactivities and enantioselectivities in hydrogenation of some R-keto esters or amides (Tang et al., 2003).

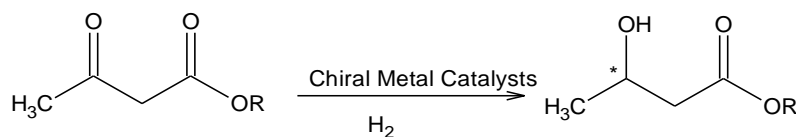
Chiral metal catalysts are used to hydrogenate (R)-pantolactone, whose product is a key intermediate in the synthesis of vitamin B and co-enzyme A (Scheme 6) (Tang et al., 2003).



Scheme 6 the synthesis of vitamin B and co-enzyme A

#### *$\beta$ -Keto Esters*

The hydrogenations of  $\beta$ -keto esters have been using chiral transition-metal catalysts (Ager et al., 1997). With a BINAP containing transition metal such as Ru, a series of  $\beta$ -keto esters have been hydrogenated to give chiral  $\beta$ -hydroxyl esters with good enantioselectivities (Scheme 7) (Noyori et al., 1987).



Scheme 7 Hydrogenation of  $\beta$ -keto esters

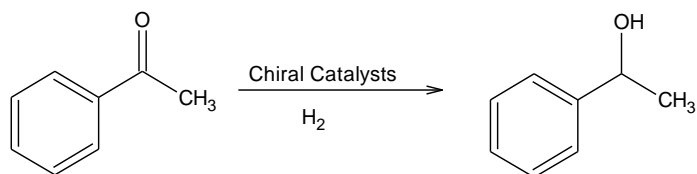
#### 1.2.4.2 Hydrogenation of Unfunctionalized Ketones

The hydrogenation of unfunctionalized ketones is a more difficult topic than the hydrogenation of functionalized ketones (Fehring et al., 1987). Due to the lack of secondary coordination to the metal, most Rh, Fe or Ru catalysts, which are quite effective for functionalized ketones, cannot provide high enantioselectivity and reactivity for the hydrogenation of unfunctionalized ketones. However, the hydrogenation of ketones has been studied in the last decades due to the discovery of efficient catalytic systems.

Bisphosphine containing transition-metal catalysts are usually used to obtain chiral alcohols from the reduction of unsaturated ketones. Functionalized olefins can be hydrogenated with excellent enantioselectivity (Okhuma et al., 2000).

#### 1.2.4.3 Aromatic Ketones

The enantioselective hydrogenation of simple aromatic ketones has been studied with some chiral bisphosphine- transition metal complexes (Scheme 8). The results of catalytic experiments show that bisphosphine ligands increase the catalytic activity of transition metal complexes in transfer hydrogenation of aromatic ketones. The DIOP-Rh complex with a tertiary amine was examined in the reduction of acetophenone and from the catalysis was obtained enantioselectivities of 80% and 87% (Toros et al., 1980). The DIOP transition-metal complex with a tertiary amine, was examined with *t*BuOK as the base and 2-propanol as the solvent, and was found to be very active for the hydrogenation of simple aromatic ketones (Doucet et al., 1998).

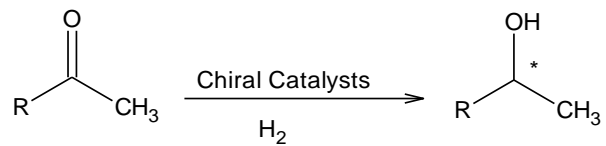


Scheme 8 Hydrogenation of simple aromatic ketones

#### 1.2.4.4 Aliphatic Ketones

The hydrogenation of simple aliphatic ketones has been studied with Fe, Os, Ru and Rh catalyst (Scheme 9). The Penn-Phos containing complexes combined with 2,6-lutidine and potassium bromide, have given good results in the hydrogenation of

aliphatic ketones (Jiang et al., 1998). From the hydrogenation of tert-butyl methyl ketone, the chiral alcohol was obtained in 94% enantioselectivity. From the reduction of isopropyl methyl ketone and n-butyl methyl ketone, chiral alcohols were obtained in 85% and 75% enantioselectivity (Jiang et al., 1998).



Scheme 9 Direct hydrogenation of ketone

### 1.3 IRON CARBONYL CLUSTER - PHOSPHINE COMPLEXES

The following sections deals with the iron carbonyl clusters and their reactions with bisphosphine ligands will be explained within this work. The iron carbonyl cluster bisphosphine complexes and their fluxionality will be referred in detailed.

Several researches have focused on the reaction between mono- or bidentate phosphines with  $[M_3(CO)_{12}]$  ( $M= Fe, Ru$  and  $Os$ ) in the last decades. Tertiary phosphine substituted iron carbonyl complexes were synthesized (Figure 13).

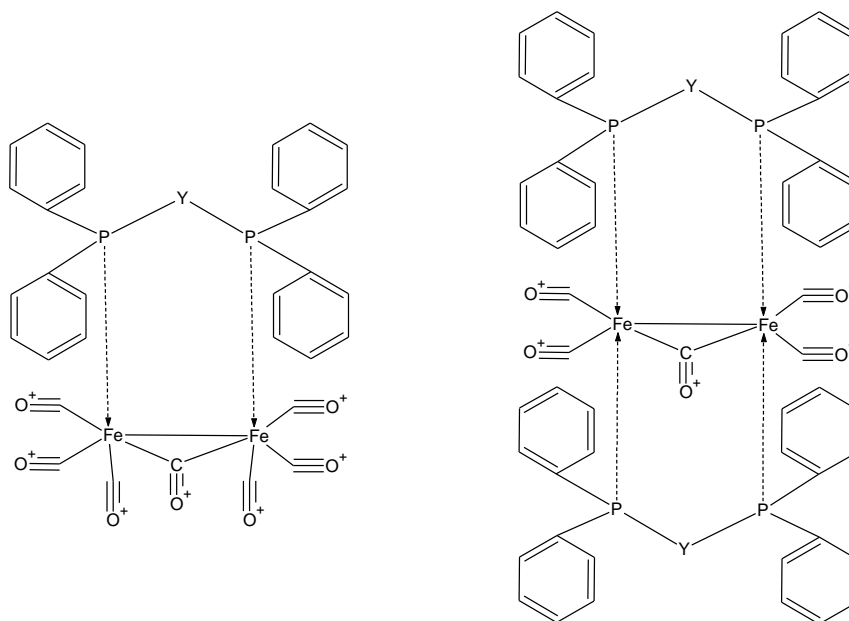


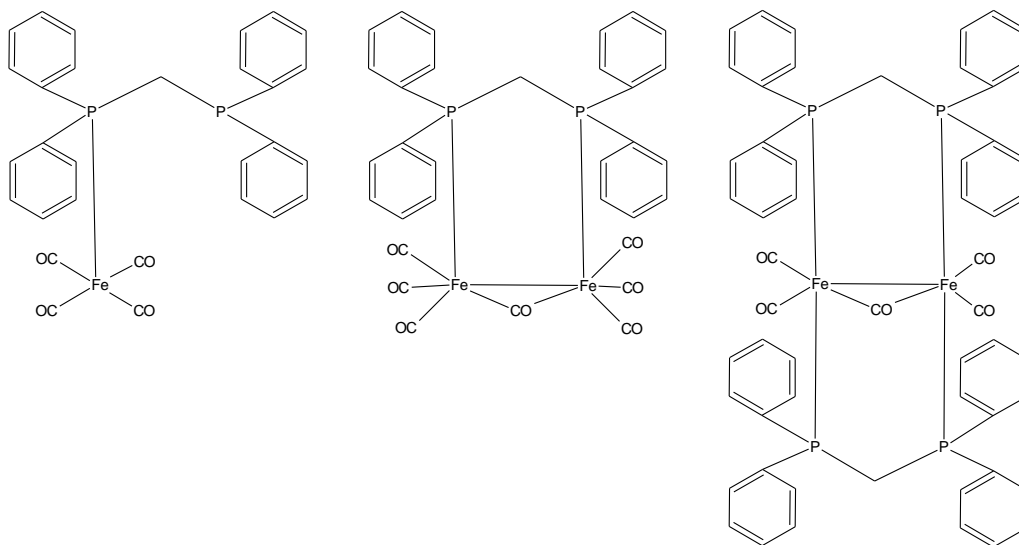
Figure 13 structure of  $Fe_2(CO)_n(dppx)_m$

#### 1.3.1 Iron Carbonyl Phosphorus Complexes

In the last decades, there was an interest in the preparation and properties of iron carbonyl cluster complexes stabilized with multidentate ligands. Multidentate ligands stabilize iron carbonyl cluster based on their structural effect. Multidentate ligands show that the presence of bridging or capping ligands increase the stability of the metal atom and thus provide useful compounds for the study of catalysis by cluster complexes (Masters et al., 1978 and Bahsoun et al., 1982). The bis(diphenylphosphino)methane (dppm) has attracted particular attention because of its tendency to act as a bridging ligand in poly-nuclear metal complexes (Cartwright et al., 1986).

The reaction of dppm with  $\text{Fe}_3(\text{CO})_{12}$  results giving the substituted derivatives  $\text{Fe}(\text{CO})_4(\eta^1\text{-dppm})$ ,  $\text{Fe}_2(\text{CO})_7(\text{dppm})$  and  $\text{Fe}_2(\text{CO})_5(\text{dppm})_2$  (Cartwright et al., 1986).

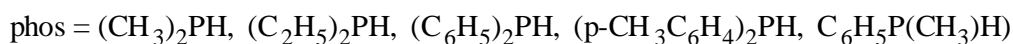
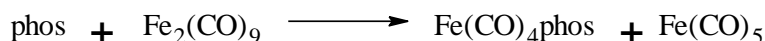
Figure 14 Structure of  $\text{Fe}(\text{CO})_4(\eta^1\text{-dppm})$ ,  $\text{Fe}_2(\text{CO})_7(\text{dppm})$  and  $\text{Fe}_2(\text{CO})_5(\text{dppm})_2$ .



### 1.3.2 Reactions of Iron Carbonyls with mono-Phosphines

Reactions of iron carbonyls  $\text{Fe}(\text{CO})_5$ ,  $\text{Fe}_2(\text{CO})_9$ , and  $\text{Fe}_3(\text{CO})_{12}$  with *mono*-phosphines have been studied in considerable detail.

When equivalent molar quantities of various secondary phosphines and diiron nonacarbonyl are allowed to react, the appropriate phosphine iron tetracarbonyl may be obtained in high yield along with iron pentacarbonyl (Manuel et al., 1966).



The product of this reaction is yellow to gold solids or liquids. The liquid products are air sensitive, but the two solids  $\text{Fe}(\text{CO})_4[\text{P}(\text{C}_6\text{H}_5)_2\text{H}]$  and  $\text{Fe}(\text{CO})_4[\text{P}(p\text{-CH}_3\text{C}_6\text{H}_4)_2\text{H}]$  are not particularly air sensitive. The defined mono-phosphine iron complexes are thermally stable at room temperature (Treichel et al., 1972).

A crystal structure of  $\text{Fe}(\text{CO})_4[\text{P}(\text{C}_6\text{H}_5)_2\text{H}]$  has been established; the phosphine group is substituted on the axial position of a trigonal bipyramid. The complexes described appear to have the same structure since the carbonyl stretching frequencies of all  $\text{Fe}(\text{CO})_4$ -phosphine complexes are all very similar (Kilbourn et al., 1968).

In each secondary phosphine-Fe<sub>2</sub>(CO)<sub>9</sub> reaction two additional classes of product are obtained in small yield. One of these is the expected phosphide-bridged species Fe<sub>2</sub>(CO)<sub>6</sub>(PR<sub>2</sub>)<sub>2</sub>, members of a class of compounds which is previously known, having either diphosphines or secondary phosphines. The secondary group of compounds have the molecular formula Fe<sub>2</sub>(CO)<sub>6</sub>(PR<sub>2</sub>)H; the geometry of these compounds was characterized as Fe<sub>2</sub>(CO)<sub>6</sub>(PR<sub>2</sub>)<sub>2</sub>, except that a bridging hydride has replaced one of the bridging phosphide groups (Figure 15) (Cooke et al., 1968 and Dobbie et al., 1970).

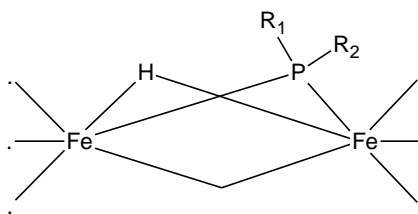


Figure 15 Structure of Fe<sub>2</sub>(CO)<sub>6</sub>(PRR')H

From the reaction of Fe(CO)<sub>4</sub>[PR<sub>2</sub>H] complex with butyl lithium, phosphine is metallated, and the resulting lithio complex Fe(CO)<sub>4</sub>[PR<sub>2</sub>]Li is a useful intermediate for further syntheses. When the complex is treated with Fe<sub>2</sub>(CO)<sub>9</sub>, stirred at 25°C, then Fe<sub>2</sub>(CO)<sub>6</sub>(PR<sub>2</sub>)H is obtained (Triechel et al., 1972).

Iron carbonyl and its monodentate phosphine derivatives, Fe(CO)<sub>3</sub>(PR<sub>3</sub>)<sub>2</sub>, appear to be stereochemically non-rigid molecules at ambient temperature and below (Mann et al., 1971). The barrier to an intramolecular isomerization process might be increased if a bidentate ligand is employed rather than two monodentate ligands (Akhtar et al., 1972).

The iron carbonyl Fe<sub>2</sub>(CO)<sub>9</sub> represented in principle an attractive complex for an extension of these studies to the diiron centre. The effect of diphosphine-bridged derivatives such as [Fe<sub>2</sub>(CO)<sub>6</sub>(μ-CO)(μ-R<sub>2</sub>CH<sub>2</sub>PR<sub>2</sub>)] is well established in stabilizing binuclear metal centres (Chaudret et al., 1988).

### 1.3.3 Reactions of Iron Carbonyls with bis-Phosphines

#### 1.3.3.1 Binuclear iron carbonyl complexes

In several works, the unsymmetrically disubstituted Fe-Fe model was published, which contains dppp, dppe, dppm, dppv,  $\text{Ph}_2\text{PCH}_2\text{C}(\text{CH}_3)(\text{CH}_2\text{PPh}_2)\text{CH}_2\text{PPh}_2$ , *o*-( $\text{PPh}_2$ ) $\text{C}_6\text{H}_4$  and  $\text{RN}(\text{PPh}_2)_2$  ligands. The complexes exhibit the same characteristics in electrochemistry and protonation (Wang et al., 2008).

There are three possible coordination models for diphosphine or diphosphite  $\text{R}_2\text{PXPR}_2$  acting as bidentate ligands in diiron complexes. They are shown in figure 16 as (i) a symmetrically intermolecular bridging mode, (ii) a symmetrically intramolecular bridging mode and (iii) an unsymmetrically chelating mode (Wang et al., 2008).

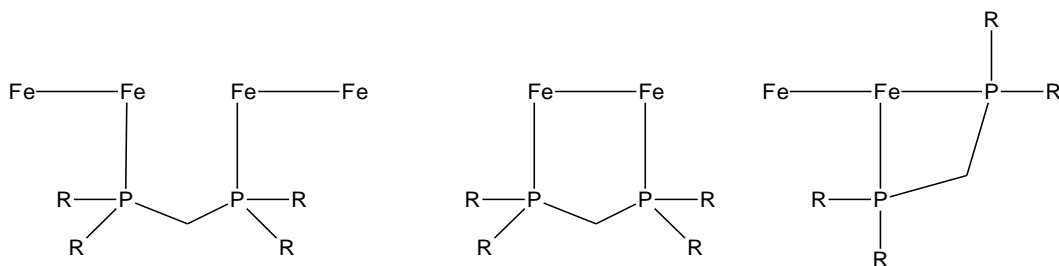


Figure 16 (i) a symmetrically intermolecular bridging mode, (ii) a symmetrically intramolecular bridging mode and (iii) an unsymmetrically chelating mode

The diiron derivative,  $\text{Fe}_2(\text{CO})_7(\text{dppm})$  has been prepared by the thermally initiated reaction between  $\text{Fe}_2(\text{CO})_9$  and dppm (Cotton et al., 1974). This complex was also characterized by a X-ray crystal structure analysis which showed the molecule to consist of two  $\text{Fe}(\text{CO})_3$  units linked by a Fe-Fe bond bridged by the dppm ligand and a carbonyl ligand (Cotton et al., 1974).

The complex  $\text{Fe}_2(\text{CO})_5(\text{dppm})_2$  was characterized and the structure of this complex is thus established as that shown in figure 17. This complex is analogous to the complexes  $\text{Fe}_2(\text{CO})_5(\text{Me}_2\text{PCH}_2\text{PMe}_2)_2$  (King et al., 1984),  $\text{Fe}_2(\text{CO})_5\{(\text{PR}_2)_2\text{NMe}\}_2$  ( $\text{R} = \text{F}, \text{OMe}$ ) (King et al., 1978), which have very similar infrared spectra to that observed for  $\text{Fe}_2(\text{CO})_5(\text{dppm})_2$ .



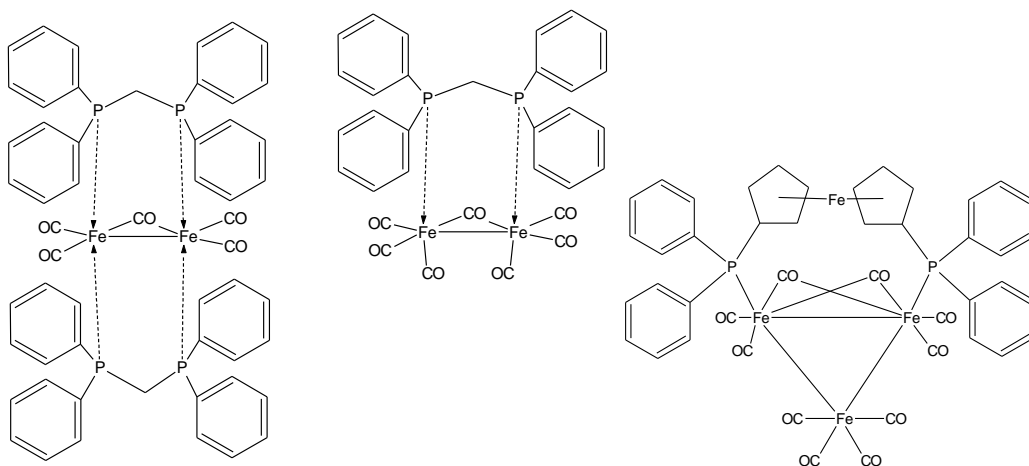


Figure 17 Structure of iron-diphosphine complexes

### 1.3.3.2 Trinuclear iron carbonyl complexes

Trinuclear iron clusters were prepared from the reaction of  $\text{Fe}_3(\text{CO})_{12}$  with ligand (Roberts et al., 1970). The fluxionality of trinuclear iron carbonyl clusters was studied and the structure of triiron carbonyl phosphine clusters was defined by Marshall (Lentz and Marshall, 1991)

$\text{Fe}_3(\text{CO})_{12}$  can be activated for substitution reactions by the diphenylketyl radical anion to produce, for example  $\text{Fe}_3(\text{CO})_{11}(\text{PFcPh}_2)$ , which is produced under mild thermal and photochemical conditions. The decomposition compound of this complex is  $\text{Fe}(\text{CO})_4(\text{PFcPh}_2)$  (Chacon et al., 1990).

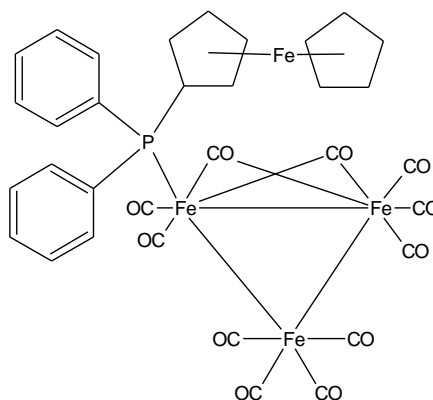


Figure 18 Structure of  $\text{Fe}_3(\text{CO})_{11}(\text{PFcPh}_2)$

The reaction of  $\text{Fe}_3(\text{CO})_{12}$  with bidentate phosphines using  $\text{Me}_3\text{NO} \cdot 2\text{H}_2\text{O}$  as a decarbonylating agent, in 1:1:2 molar ratio, produces the dppe, dppb, dppf and dppbz iron complexes in practically equal yield when the reaction is stopped 10-15 min after

the addition of  $\text{Me}_3\text{NO}\cdot 2\text{H}_2\text{O}$ . All these complexes were stable in the solid state and in solution, but slowly decomposed when stored for a long period of time under argon in the freezer (Stein et al., 1996).

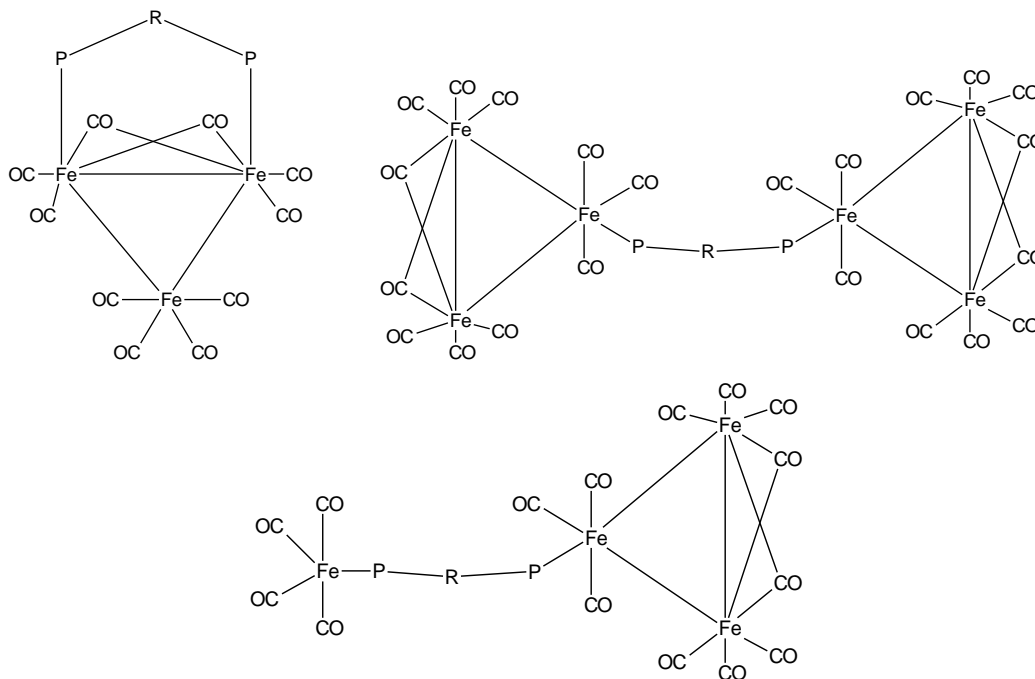


Figure 19 Structure of  $\text{Fe}_3(\text{CO})_n(\text{dppx})$  ( $\text{P-R-P} = \text{dppe}, \text{dppm}, \text{dppb}, \text{dppf}, \text{dppbz}$ )

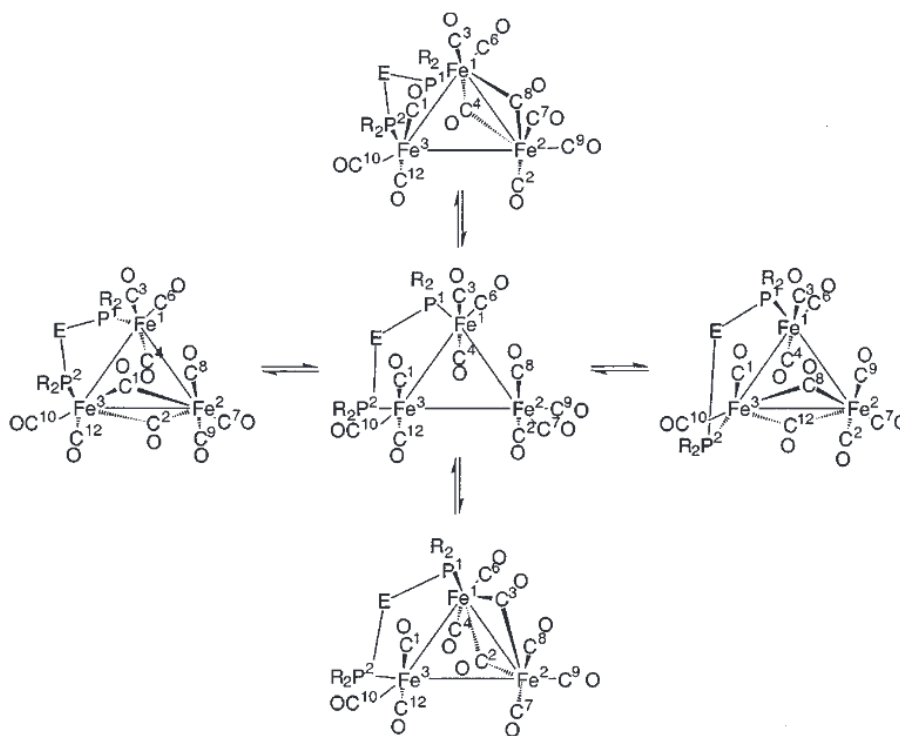
### ***The fluxionality of triiron carbonyl phosphino clusters***

The fluxionality of triiron carbonyl phosphine clusters was studied by Marshall in 1991 and is termed bridge opening – bridge closing mechanism (Lentz and Marshall, 1991).

The bridge bonds have been identified between Fe1 and Fe2 in scheme 10. The bridge bonds are then opened and begin to occur either between Fe1-Fe3 or Fe2-Fe3. The bridge opening – bridge closing mechanism is extremely facile and cannot be stopped. In the cases of the  $[\text{Fe}_3(\text{CO})_{10}\text{L}_2]$  ( $\text{L}_2 = \text{dppm}, \text{Ph}_2\text{PNHPPH}_2, (\text{EtO})_2\text{POP}(\text{OEt})_2$ ) complexes (Adams et al., 2001). The only one example of it being stopped is  $[\text{Fe}_3(\text{CO})_{11}(\text{CNCF}_3)]$  and related complexes, where the  $\text{CNCF}_3$  is tightly held into a  $\mu_2$ -bridging position (Lentz et al., 1991).

The strain produced by the chelate ring has a tendency to open the  $\text{Fe}(\mu\text{-CO})_2\text{Fe}$  bridge. The strain increases from  $[\text{Fe}_3(\text{CO})_{10}(\text{dppm})]$  to  $[\text{Fe}_3(\text{CO})_{10}\{(\text{EtO})_2-$

POP(OEt)<sub>2</sub>}. The clearest demonstration of merry-go-round mechanism occurs with [Fe<sub>3</sub>(CO)<sub>10</sub>(dppm){P(OMe)<sub>3</sub>}].



Scheme 10 The demonstration of merry-go-round mechanism

## 1.4 REDUCTION OF CARBONYL COMPOUNDS BY TRANSFER HYDROGENATIONS

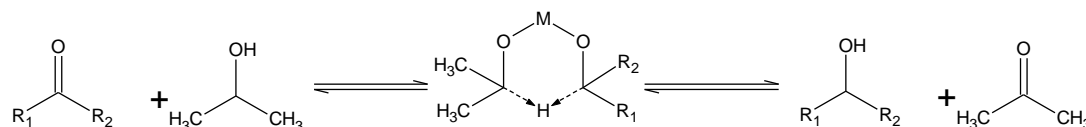
---

### 1.4.1 Introduction

The application of the iron carbonyl cluster bisphosphine complexes in catalytic reaction will be referred in detailed. This section is very important to understand, why the iron carbonyl bisphosphine clusters are active in transfer hydrogenation.

The reaction of transfer hydrogenation was discovered in the 1920s by Meerwein, where aluminium isopropoxide or sodium isopropoxide was used to promote the transfer of hydrogen from isopropanol to a ketone, and ketones were converted to the corresponding secondary alcohols as a product (Meerwein et al., 1920). Transfer hydrogenation is named as “reduction of multiple bonds with the help of a hydrogen donor in presence of a catalyst”. In this reason, isopropanol is used usually as a hydrogen donor and as well as solvent in transfer hydrogenation. The reduction of ketones takes an important role in the pharmaceutical and chemical industry for the production of alcohols.

To explain the mechanism of transfer hydrogenation, the hydrogenation path should be identified. The hydride is transferred via a six-membered transition state, in which the ketone and isopropanol are coordinated to the aluminium or sodium ion. An aluminium or sodium ion enables the hydride transfer from isopropanol to the corresponding ketone (Scheme 11). The reaction is in equilibrium and an excess of isopropanol is used to drive the reaction to the reduction. The presence of excess of acetone leads to oxidation of alcohol (Zassinovich et al., 1992). The effect of the metal in transfer hydrogenation is defined in the transition state, that the metal carries the hydrogen from the isopropanol to the ketone.



Scheme 11 Mechanism of transfer hydrogenation

Among the methodologies of the reduction of carbonyl compounds, the addition of hydrogen from a suitable donor to a C=O double bond has received increasing

attention since the mid-nineties. Transfer hydrogenation has become the procedure of choice for the preparation of alcohols from ketones or aldehydes.

Hydrogen transfer has compared favourably to alternative techniques (direct hydrogenation and hydrosilylation) available for this transformation, largely due to its simplicity. Iron catalyst benign and low-cost reducing agents and a large variety of metal catalysts increase the catalytic activity and selectivity by transfer hydrogenation, because metals carry the hydrogen from the isopropanol to the ketone. Selective carbonyl hydrogenation is an important method for the synthesis of both fine and bulk chemicals (Blaser et al., 2003 and Ryander et al., 1990).

In recent years, there has been an interest in the replacement of established transition-metal catalyst with iron-based species within catalytic applications (Enthaler et al., 2008). Iron presents an important alternative to the precious metals used currently:

- Inexpensive,
- Abundant,
- Non-toxic,
- Environmentally benign.

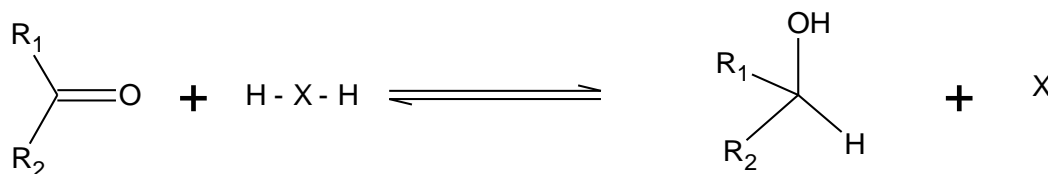
Furthermore, the amount of metal traces allowed to be used in the pharmaceutical industry is a hundred times greater for iron than for platinum, iridium, palladium, ruthenium or rhenium (Naud et al., 2007).

Much attention has been given to di-, tri- and tetra dentate ligands bearing phosphorus or nitrogen donors such as bis(diphenylphosphino)methane, porphyrin and diimino-diphosphine system for iron-catalysed hydrogenations (Legaditis et al., 2011). The metals can coordinate very easily to the nitrogen atoms using their pi-acceptor properties. The redox-active ligands such as bis(imino)pyridine and porphyrin are used to stabilize the iron center, which can be modified to give diversity, activity, and selectivity (Andersson et al., 2008). The bis(imino)pyridine ligands have four accessible oxidation states and participate in redox reactions which enables the metal to mediate multiple electron processes. This feature is thought to be critical for the iron-catalyzed [2+2] cycloaddition reaction of dienes to afford the corresponding bicyclo-[3,2,0]-heptane. The reaction does not proceed in the presence

of redox inactive ligands, for example, a pyridine bis(carbene) ligand. The reaction does not proceed in the presence of redox inactive ligands, for example, a pyridine bis(carbene) ligand. (Vijayendran et al., 2012).

### 1.4.2 Transfer Hydrogenation

For the transfer hydrogenation of carbonyl compounds, a hydrogen donor is named as the reducing agent and also as a hydrogen source. The hydrogen donor contains usually two hydrogens. A suitable promoter can be mobilized to add to an unsaturated functional group in the substrate. At the same time the hydrogen donor forms its dehydrogenated counterpart, X (Scheme 12). In the large majority of cases the two hydrogen donors aren't equivalent and they are transferred sequentially, one to the carbonyl carbon as a hydride and the other to the oxygen as a proton (Andersson et al., 2008).



Scheme 12 Carbonyl hydrogen transfer reduction

Formation of a side-product, which is shown in scheme 12, is the main drawback of the H-transfer process when compared with process such as catalytic hydrogenation. The presence of side-product in the reaction mixture can lead to complications for the isolation of a product and separation of the catalyst.

Also, upon losing two hydrogen atoms the hydrogen donors becomes itself a hydrogen acceptor. After losing hydrogen atoms the hydrogen source may be in competition with the ketone until equilibrium (Andersson et al., 2008). When great amount of hydrogen source is used, the hydrogen donors continue to be a hydrogen source.

### 1.4.2.1 Hydrogen Donors and Base

As the hydrogen source just two compounds can be used, which are isopropanol, formic acid and its salts, in the transition metal-catalysed transfer hydrogenation of carbonyl compounds (Andersson et al., 2008).

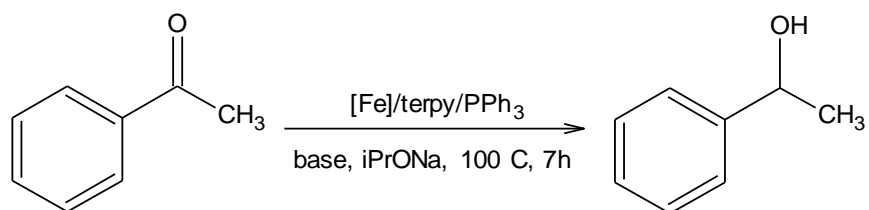
When using isopropanol as the reducing material, the reaction is under thermodynamic control and the large excess of the hydrogen donor shifts the equilibrium to the product side (Andersson et al., 2008). The benefits of isopropanol are

- cheap,
- good solvent,
- easily disposable,
- recyclable,
- environmentally benign.

When using isopropanol as a reducing agent, the base (sodium isopropoxide) is usually necessary to enable the extraction of hydrogen from the alcohol, which is used as a hydrogen source. The amount of base can vary over a wide range depending on the nature of the catalyst (Andersson et al., 2008). Usual base to metal ratios for transfer hydrogenation are between 5 to 1 and 50 to 1. In our research, base to metal ratio is 5 to 1 to release the hydrogen from the alcohol. The best catalytic activity was obtained from the rate 5 to 1 in our experiments.

The influence of base and iron catalyst was examined by Beller et al. and they obtained the best results with  $\text{Fe}_2(\text{CO})_9$  and  $\text{Fe}_3(\text{CO})_{12}$  in the presence of catalytic amounts of sodium isopropoxide or sodium tert-butyrate. The most used bases for transfer hydrogenation such as NaOH, KOH, and *t*BuOK showed low activity in the Beller model reaction. Also, different inorganic bases such as  $\text{K}_2\text{CO}_3$ ,  $\text{Cs}_2\text{CO}_3$  and  $\text{K}_3\text{PO}_4$  as well as nitrogen containing organic bases such as  $\text{NEt}_3$ ,  $\text{N}(i\text{Pr})_2\text{Et}$ , DBU and DABCO were ineffective (Table 2) (Enthaler et al., 2006).

Table 2 Influence of different bases and iron sources in the Fe-catalysed transfer hydrogenation of acetophenone (Enthaler et al., 2006)



Entry	Iron source	Base	Yield [%]
1	[Fe <sub>3</sub> (CO) <sub>12</sub> ]	<i>i</i> PrONa	78
2	[Fe <sub>3</sub> (CO) <sub>12</sub> ]	LiOH	2
3	[Fe <sub>3</sub> (CO) <sub>12</sub> ]	NaOH	< 1
4	[Fe <sub>3</sub> (CO) <sub>12</sub> ]	KOH	< 1
5	[Fe <sub>3</sub> (CO) <sub>12</sub> ]	<i>t</i> BuOK	12
6	[Fe <sub>3</sub> (CO) <sub>12</sub> ]	<i>t</i> BuONa	76
7	[Fe <sub>3</sub> (CO) <sub>12</sub> ]	K <sub>2</sub> CO <sub>3</sub>	3
8	[Fe <sub>3</sub> (CO) <sub>12</sub> ]	Cs <sub>2</sub> CO <sub>3</sub>	3
9	[Fe <sub>3</sub> (CO) <sub>12</sub> ]	K <sub>3</sub> PO <sub>4</sub>	< 1
10	[Fe <sub>3</sub> (CO) <sub>12</sub> ]	Pyridine	1
11	[Fe <sub>3</sub> (CO) <sub>12</sub> ]	NEt <sub>3</sub>	2
12	[Fe <sub>3</sub> (CO) <sub>12</sub> ]	N( <i>i</i> Pr) <sub>2</sub> Et	< 1
13	[Fe <sub>3</sub> (CO) <sub>12</sub> ]	DBU	< 1
14	[Fe <sub>3</sub> (CO) <sub>12</sub> ]	DABCO	< 1



Table 2 Influence of different bases and iron sources in the Fe-catalysed transfer hydrogenation of acetophenone (Enthaler et al., 2006)

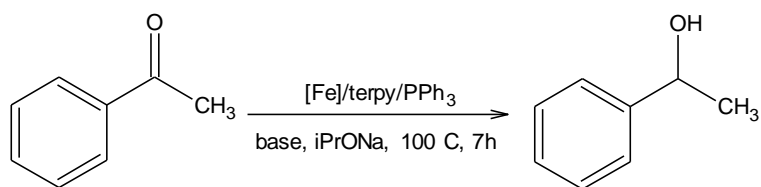
Entry	Iron source	Base	Yield [%]
15	[Fe <sub>3</sub> (CO) <sub>12</sub> ]	-	0
16	[Fe <sub>2</sub> (CO) <sub>9</sub> ]	<i>t</i> PrONa	84
17	[Fe(CO) <sub>5</sub> ]	<i>t</i> PrONa	2
18	[CpFe(CO) <sub>2</sub> I]	<i>t</i> PrONa	3
19	[Et <sub>3</sub> NH][HFe(CO) <sub>4</sub> ]	<i>t</i> PrONa	11
20	FeCl <sub>2</sub>	<i>t</i> PrONa	45
21	FeBr <sub>2</sub>	<i>t</i> PrONa	9
22	FeSO <sub>4</sub> ·7H <sub>2</sub> O	<i>t</i> PrONa	9
23	Fe(acac) <sub>2</sub>	<i>t</i> PrONa	17
24	Fe(acac) <sub>3</sub>	<i>t</i> PrONa	3

#### 1.4.2.2 Ligand Effect

Diverse ligands have been developed for the synthesis of Fe, Ru, Os, Rh and Ir complexes, which have been used in hydrogen transfer reduction. The diverse ligands differ in the number and identity of the donor atoms and in symmetry properties.

Beller et al. examined the nature of their synthesized ligands. In the substitution pattern of PPh<sub>3</sub> with electron-donating or electron-withdrawing groups, more basic and steric hindered phosphine decreased the yield of 1-phenylethanol. They got the best catalytic activity with PPh<sub>3</sub>, dppe and dppe (Enthaler et al., 2006).

Table 3 Influence of phosphorus ligand in the Fe-catalysed transfer hydrogenation of acetophenone (Enthaler et al., 2006)

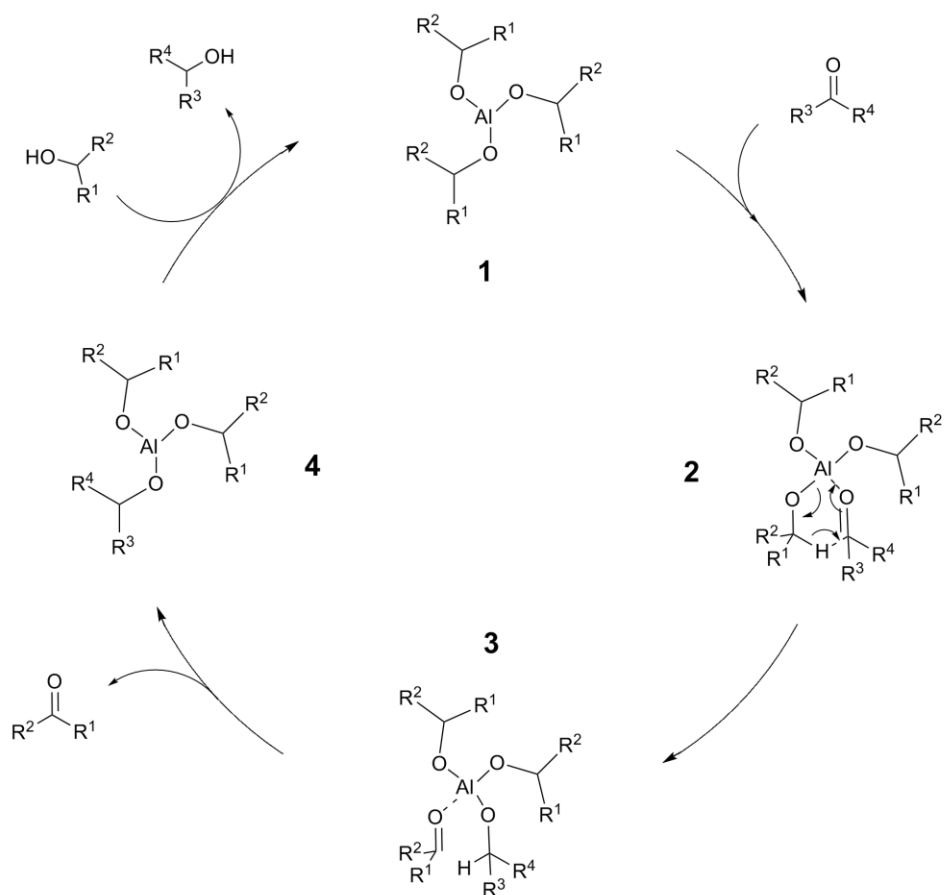


Entry	Phosphine	Conversion [%]
1	PPh <sub>3</sub>	78
2	P( <i>p</i> -MeO-C <sub>6</sub> H <sub>4</sub> ) <sub>3</sub>	13
3	P( <i>p</i> -Me-C <sub>6</sub> H <sub>4</sub> ) <sub>3</sub>	22
4	P( <i>p</i> -F-C <sub>6</sub> H <sub>4</sub> ) <sub>3</sub>	23
5	P(3,4-CF <sub>3</sub> -C <sub>6</sub> H <sub>4</sub> ) <sub>3</sub>	5
6	PCy <sub>3</sub>	11
7	P( <i>t</i> Bu) <sub>3</sub>	32
8	P(OPh) <sub>3</sub>	8
9	P(O <i>i</i> Pr) <sub>3</sub>	7
10	Ph <sub>2</sub> PCH <sub>2</sub> PPh <sub>2</sub>	64
11	Ph <sub>2</sub> P(CH <sub>2</sub> ) <sub>2</sub> PPh <sub>2</sub>	50
12	Ph <sub>2</sub> P(CH <sub>2</sub> ) <sub>4</sub> PPh <sub>2</sub>	3
13	Ph <sub>2</sub> P(CH <sub>2</sub> ) <sub>6</sub> PPh <sub>2</sub>	3

### 1.4.3 Mechanistic Aspects of Transfer Hydrogenation

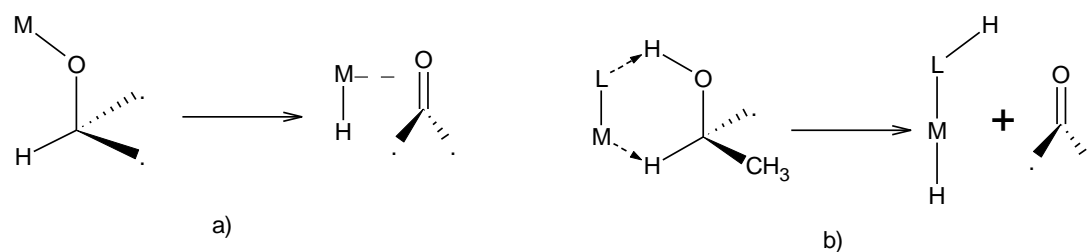
Two general procedures have been reported for the hydrogen transfer in the catalytic hydrogenation reaction, which are direct hydrogen transfer and the hydrogen route. Both mechanisms are shown in scheme 13 and 14 (Samec et al., 2006).

In the direct hydrogen transfer, the donor and the acceptor are both coordinated to the metal and the hydride is transferred from the alkoxide to the ketone in a six-membered transition state. Isopropanol and ketone were coordinated to the metal by the help of sodium isopropoxide. The metal is used in this mechanism as a Lewis acid, which is activating the substrate towards the nucleophilic attack of the hydride. The mechanism is named as the Meerwein-Ponndorf-Verley reaction and is shown in the following scheme 13 (Samec et al., 2006).



Scheme 13 Example of Meerwein-Ponndorf-Verley reaction with aluminum complex

The hydridic route involves formation of a metal hydride by interaction of the catalyst, which is iron carbonyl diphosphino clusters in our study, with the isopropanol and this hydride is subsequently transferred to the substrate. The hydridic route is divided by two as the monohydridic route and the dihydridic route in scheme 14 (Gladiali et al., 2006 and Pamies et al., 2001). The hydride is transferred in the inner sphere of the metal or it can be transferred in the outer sphere of the metal. The outer sphere mechanism can be a single process or can be in two steps (Samec et al., 2006).



Scheme 14 Inner- (a) vs. outer- (b) sphere mechanism.

## 1.5 $\gamma$ -ALUMINA AS A SUPPORT FOR CATALYSTS

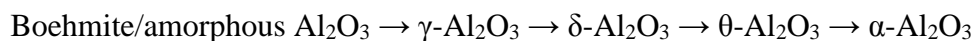
---

In this section, the important aspects of gamma-alumina to take into consideration as a support for catalytic applications will be defined. The  $\gamma$ -Al<sub>2</sub>O<sub>3</sub> was used as a support to obtain iron carbonyl supported on it in heterogeneous catalysis study.

Among the different transition alumina known, gamma alumina is the most important for the catalytic applications as a catalyst and catalyst support in the industries (Wefers, 1990). The  $\gamma$ -Al<sub>2</sub>O<sub>3</sub> takes an important role as a support for catalytic applications by reason of its chemical and hydrothermal stability. The gamma-alumina is typically prepared by thermal dehydration of coarse particles of well-defined boehmite at a temperature above 400–450 °C.

### 1.5.1 Structure of $\gamma$ -Alumina

The main properties of the microstructure of the gamma-alumina are generally explained with the oxide, which are obtained by the thermal dehydration (calcination) of aluminium hydroxides and oxyhydroxides. The transformation sequence during this process gives the metastable phases of alpha-alumina as a function of the calcination temperature (Wolverton et al., 2000).



The  $\gamma$ -Al<sub>2</sub>O<sub>3</sub> is obtained at temperatures between 350 and 1000 °C and it is formed from crystalline (Latella et al., 1997) or amorphous (Chou et al., 1991) alumina precursors. Gamma-alumina is stable at temperatures as high as 1200 °C.

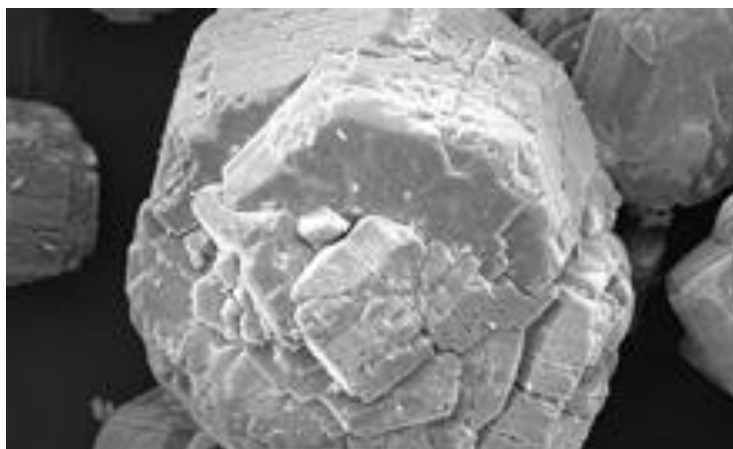


Figure 20 Alumina structure

The  $\gamma\text{-Al}_2\text{O}_3$  is determined as cubic with space group Fd-3m. The structure is described as a defect cubic spinel structure with vacancies on part of the cation positions. The unit cell contains 32 oxygen and 64/3 aluminium ions. The aluminium ions occupy the octahedral and tetrahedral positions (Song et al., 2005).

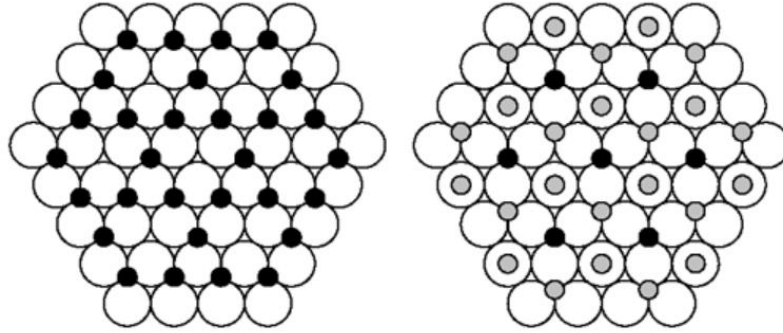
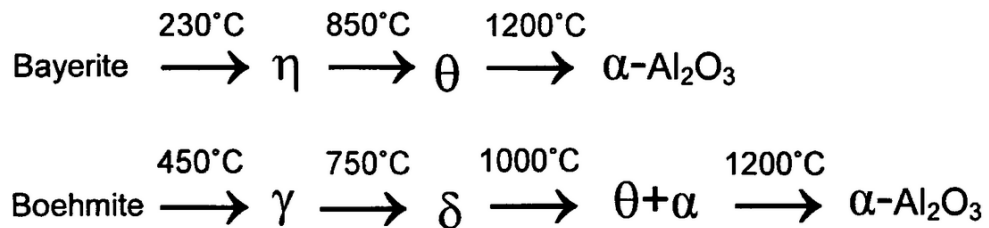


Figure 21 Schematic drawing of the first two layers in the gamma alumina structure

Tetragonal gamma alumina can be obtained from crystalline boehmite, which is produced between 450–750 °C (Paglia et al., 2004). The tetragonal structure distortion can be reduced by the help of the increase of the temperature, but in no way cubic  $\gamma\text{-Al}_2\text{O}_3$  can not be obtained. One transition phase of the alumina was identified above 750 °C, designated as gamma alumina, which is precursor for the structure of alpha alumina above 900 °C.

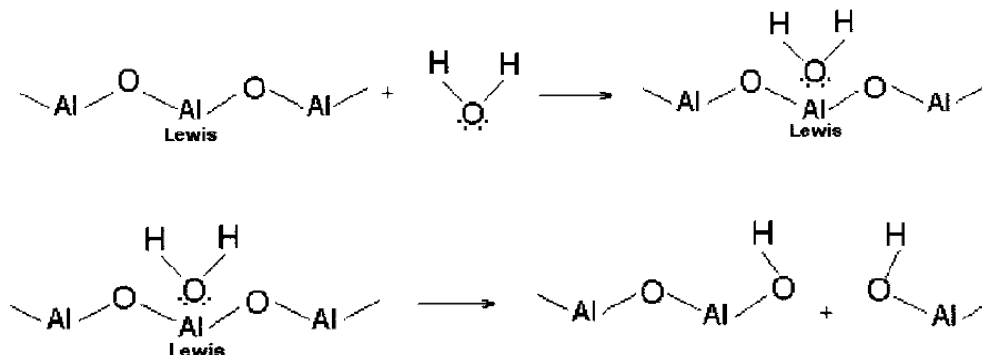
Many thermal decomposition methods for synthesis of  $\gamma\text{-Al}_2\text{O}_3$  such as precipitation and hydrolysis has been improved the oxide's textural properties and hydrothermal stability (Zhang et al., 2004).



Scheme 15 The relations between transition aluminas, depending on the initial hydroxide and temperature

### 1.5.2 $\gamma$ -Al<sub>2</sub>O<sub>3</sub>/ H<sub>2</sub>O Interface

The presence of Lewis acid sites and basic sites at  $\gamma$ -Al<sub>2</sub>O<sub>3</sub> surface allows its rehydroxylation by interaction with water, thus Lewis acid sites and basic sites can be converted into surface hydroxy groups (Ionescu et al., 2002). The interaction of  $\gamma$ -Al<sub>2</sub>O<sub>3</sub> was published as a two-step process under atmospheric conditions and both steps are shown in following scheme 16. That involves non-dissociative adsorption of H<sub>2</sub>O on Lewis sites (Trueba et al., 2005).



Scheme 16 The The interaction of  $\gamma$ -Al<sub>2</sub>O<sub>3</sub>

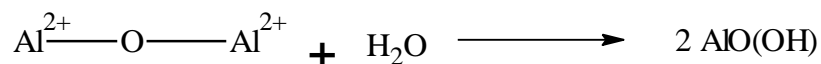
By the help of the rehydration, the tetrahedral coordinated alumina surface can eliminate and the hydroxylation of the octahedral alumina can increase (Tsyganenko et al., 1996). Therefore the reactivity of gamma alumina towards water depends on the layers exposed at each surface.

The oxide particles can be dispersed in water, so the (hydro)oxo groups on the gamma alumina surface at the solid-liquid interface can relate with protons to form positive charged complexes on the surface (Schwarz et al., 1995). The interaction between the water and the surface of gamma alumina is occurred with the help of the dissolution of the alumina oxide by adsorption of hydrogen ions (Wehrli et al., 1990). In earlier research, the extent of dissolution was accepted to be controlled by thermodynamics. However, nowadays there is a general agreement about this process usually between oxide and water interface that is controlled by slow chemical reactions occurring (Brown et al., 1999).

The hydroxyl groups of the gamma alumina surface determine its chemical, electrochemical properties, and in addition, the activity. Thus, the release of alumina ions are influenced by any process that modifies the hydroxyl group coverage of the

oxide, such as temperature of calcination and cooling conditions, adsorption on surfaces, irreversible exchange of OH groups (Trueba et al., 2005).

The different types of alumina ions (Al-O-Al) present on the surface show good activity during the first treatment, since a decrease of the concentration of alumina ions in solution is obtained upon against treatment with acid or base. They suggested that continuation of the etching is preceded by the rehydroxylation or hydrolysis of Al-O-Al bonds in the following Scheme 17 (Trueba et al., 2005).



Scheme 17 The rehydroxylation of Al-O-Al bonds

### 1.5.3 $\gamma$ -Al<sub>2</sub>O<sub>3</sub> as a Support

Heterogeneity effects of  $\gamma$ -Al<sub>2</sub>O<sub>3</sub> were first defined in 1978 by Leckie (Davis et al., 1978). After this explanation, many heterogeneity models a great variety of inorganic compounds such as metal carbons, oxides, mixed oxides, clays, and humic substances have been used to describe proton-binding behavior at oxide/solution interfaces (Trueba et al., 2005). The surface heterogeneity information can help to understand and to regulate the adsorption mechanism.

In the preparation of supported catalyst, low soluble solvent by simple impregnation or by homogeneous deposition-precipitation, ion exchange, and specific adsorption is used. In the other preparation of supported catalyst is used by considering the nature and strength of the support-precursor interactions. Common subsequent steps are washing with the insoluble solvent and drying under vacuum by irreversible transformation of the catalyst (Trueba et al., 2005).

In spite of the impregnation advantages of metal from a liquid phase, the use of the metal is inefficient. But the metals can be impregnated different conditions on alumina. Its incomplete loading and reduction and uncontrolled sintering during high-temperature salt decomposition influence to its efficiency. Organic solvents, solvents vapour, and solid phases have been examined as the impregnation phase. The easiest way for preparing impregnated metal catalysts consists in mounting metallic atoms or small metal clusters in their zero-valence state onto a pre-treated gamma alumina. So



that the need for any subsequent activation eliminates and the catalyst may be obtained in a single preparation step (Zhang et al., 2004).

$\gamma$ -Al<sub>2</sub>O<sub>3</sub>s are used as a pre-shaped structured support for preparing multiphase catalysts. In formation of an active phase dispersed on a carrier or a support (Schwarz et al., 1995). The properties of the active phase depend on the supported complex and the support surface.

## 1.6 IRON CARBONYL CLUSTERS SUPPORTED ON $\gamma$ - $\text{Al}_2\text{O}_3$

In this section, iron carbonyl clusters supported on gamma alumina will be referred.

Surface organometallic chemistry can be considered as an important part of heterogeneous catalysis and surface science. However, the intrinsic challenges in the surface chemistry studies, a few basic descriptions and elementary steps were elucidated just at a molecular stage. To study the reactivity of metal-metal or metal-ligand bonds of carbonyl clusters toward the hydroxyl groups of a surface, direct interaction between metal carbonyl clusters and the surface hydroxyl group of the divided oxides is considered as a most likely approach (Hugues et al., 1982).

Surface hydroxyl group of  $\gamma$ - $\text{Al}_2\text{O}_3$  can be oxidized by zero valence iron carbonyls with simultaneously release of hydrogen. The iron carbonyl clusters,  $\text{Fe}(\text{CO})_5$  and  $\text{Fe}_3(\text{CO})_{12}$  compounds, are transformed to  $[\text{HFe}_3(\text{CO})_{11}]\text{Al}$  complex at the same time during the oxidation of hydroxyl group (Hugues et al., 1982).

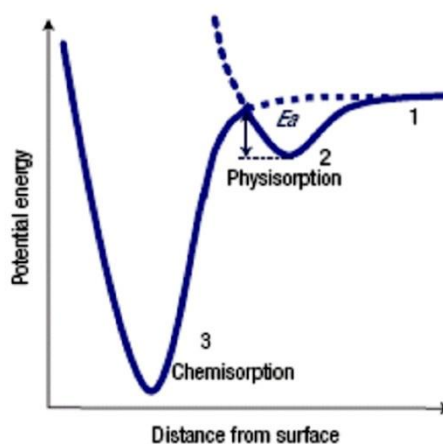


Diagram 1 Potential energy diagram for chemisorption and physisorption

The iron carbonyl on the gamma alumina can be obtained from two type of adsorption, which are described as chemisorption and physisorption (Diagram 1). Chemisorption and physisorption of iron carbonyl clusters on the  $\gamma$ - $\text{Al}_2\text{O}_3$  have been studied by many researchers, using features of hydroxyl group on  $\gamma$ - $\text{Al}_2\text{O}_3$ .

### 1.6.1 Physisorption on $\gamma$ - $\text{Al}_2\text{O}_3$

Physisorption or physical adsorption is the mechanism by which iron carbonyl is stored in the molecular form without dissociating on the support surface (Figure 22).

In case the barrier is lower than the energy of free molecular, all the molecules physisorbed can quickly form a chemical bond with the adsorbent surface and chemisorption will occur rapidly (Artioli, 2008). Responsible for the molecular adsorption of iron carbonyl clusters are van der Waals forces, between the molecules and the atoms on the support surface.

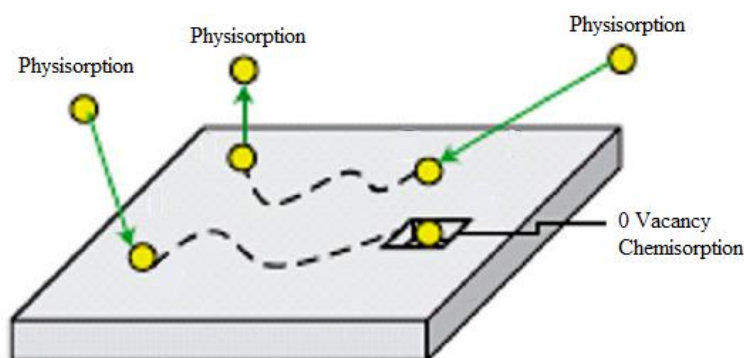
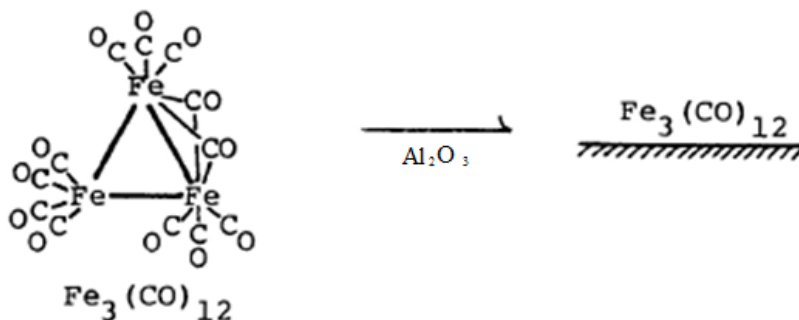


Figure 22 Two type of adsorption

In electrostatic interactions, for a given adsorbate molecule, the charges and van der Waals radii of the surface atoms are important. The minimum of the potential curve consists at a distance from the surface and the average distance is approximately the sum of the van der Waals radii of the adsorbent atom and the adsorbate molecule.



Scheme 18 The physisorption of iron carbonyl on gamma alumina

Initially, physisorbed iron carbonyl cluster was characterized by Hugues in 1980 (Hugues et al., 1980). To adsorb more quantity of iron carbonyl on the surface are used generally physisorption as adsorption type. The iron carbonyl cluster physisorbed on gamma alumina can be loaded at high quantity more than two percent (Hugues et al., 1982). After the adsorption of  $\text{Fe}_3(\text{CO})_{12}$  or  $\text{Fe}(\text{CO})_5$ , the supported

cluster are obtained same as the initial carbonyl complex and can be extracted again in a hexane (or an organic solvent) solution.

### 1.6.2 Chemisorption on $\gamma\text{-Al}_2\text{O}_3$

Chemisorption is a special form of adsorption. Chemisorption is an activated process, that is, the adsorbate has a minimum of energy in order to be adsorbed. Chemisorption or physisorption states depend on the presence of an energetic barrier. The adsorbate can be bonded to the adsorbent chemically, only if it has more energy of the free molecules than barrier; otherwise it will be desorbed. (Artioli, 2008).

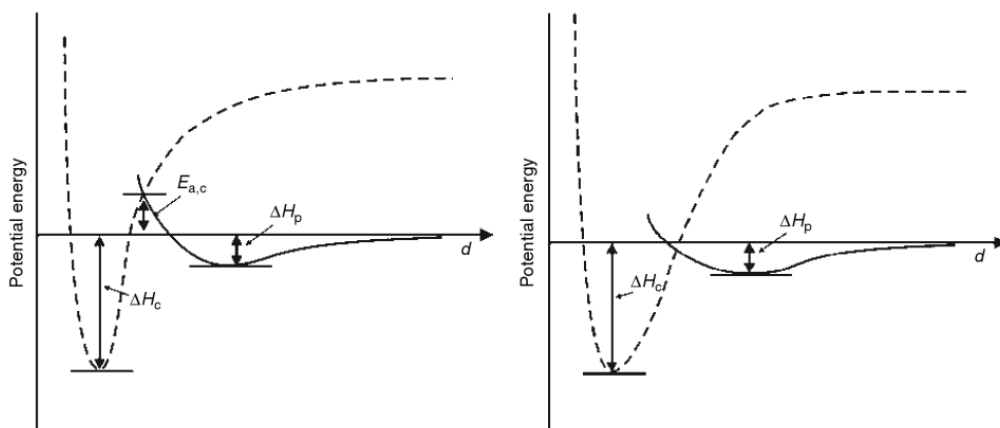


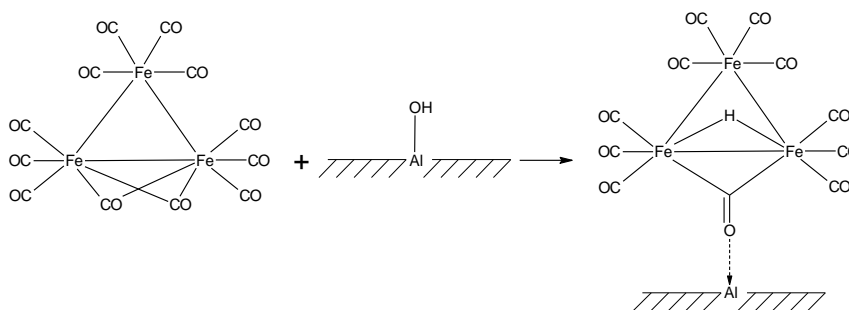
Diagram 2 Energy of adsorption depending on distance (d) of adsorbate molecule (Artioli, 2008)

In the diagram 2, solid line is for the physisorption, and dashed is for the chemisorption, where the energy required is higher enthalpy. On the left of diagram 2 is case of activated chemisorption.

The study about supported iron carbonyl clusters have focused on chemisorption of metal atoms onto inorganic oxides. Supported catalysts play an important role in comparison of the homogeneous and heterogeneous systems (Iwasawa et al., 1983).

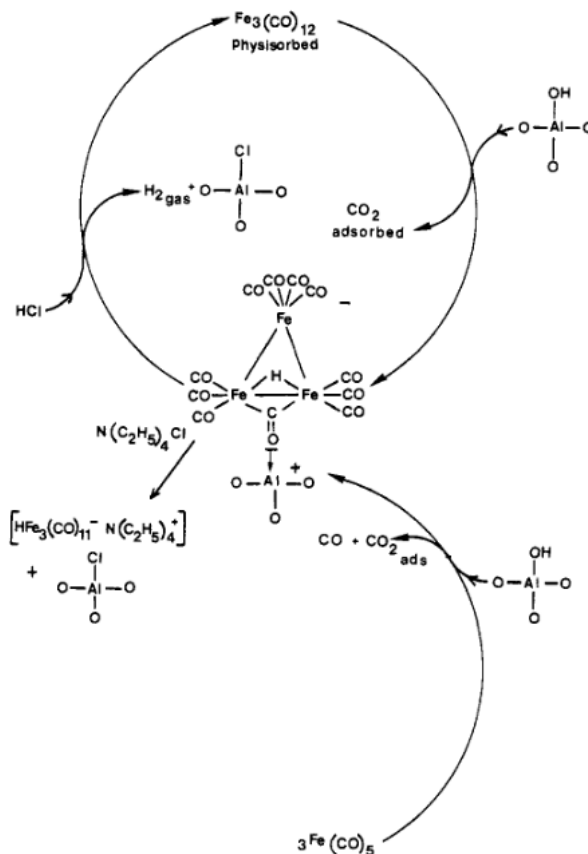
To support  $\text{Fe}_3(\text{CO})_{12}$  onto the pretreated  $\gamma\text{-Al}_2\text{O}_3$ , 1.1 carbon monoxide per triiron dodecacarbonyl may be transformed.  $\gamma\text{-Al}_2\text{O}_3$  is treated in the following way: the support is heated up to  $180^\circ\text{C}$  for one hour to remove water and is heated slowly under vacuum ( $10^{-4}$  torr) up to  $500^\circ\text{C}$  for 14 hours. The maximum quantity of  $\text{Fe}_3(\text{CO})_{12}$  that can be chemisorbed in the form of species on  $\gamma\text{-Al}_2\text{O}_3$  is 2.0 percent (Hugues et al., 1982). Also the transformations of 1.9 CO molecules can be observed

over  $\text{Al}_2\text{O}_3$  powder (ALON-C) which has the less capability for the adsorption of CO formed by decarbonylation (Iwasawa et al., 1983).



Scheme 19 The chemisorption of iron carbonyl on gamma alumina

One carbon monoxide of  $\text{Fe}_3(\text{CO})_{12}$  is oxidized to  $\text{CO}_2$  (or adsorbed carbonates) by the reaction of the cluster with the basic hydroxyl group of  $\text{Al}_2\text{O}_3$  and the  $[\text{HFe}_3(\text{CO})_{11}](\text{Al})$  is produced. From formations of  $\text{Fe}_3(\text{CO})_{12}$  and  $\text{Fe}(\text{CO})_5$ ,  $[\text{HFe}_3(\text{CO})_{11}](\text{Al})$  are obtained as a same product by the chemisorption of iron carbonyls on  $\gamma\text{-Al}_2\text{O}_3$  by hexane solution (Hugues et al., 1982).



Scheme 20 The chemisorption of  $\text{Fe}_3(\text{CO})_{12}$  and  $\text{Fe}(\text{CO})_5$  on gamma alumina

The anionic  $[\text{HFe}_3(\text{CO})_{11}](\text{Al})$  complex can be extracted from the support surface by organic polar solvents, which are dichloromethane, chloroform, methanol, or ethanol (Hugues et al., 1982). To examine the catalytic performance of supported iron carbonyl complexes, apolar solvents such as hexane must be used. In case of using polar solvents, the adsorbed iron carbonyl complexes are extracted from the surface.

## 1.7 X-RAY POWDER DIFFRACTIONS

Powder XRD developed rapidly, by the contribution of physicist William Lawrence Bragg and his father William Henry Bragg. In 1912-1913, the son W. L. Bragg developed a well-known Bragg's law (Bragg, 1913). This development changed the point of view of physics, chemistry, crystallography, mineralogy and medicine. The material analysis method of powder XRD was devised in 1916 by Peter Joseph William Debye and P. Scherrer (Debye et al., 1917) in Germany and in 1917 by A. W. Hull (Hull, 1917) in United States. In the following figure, the difference between single-crystal X-ray diffraction and X-ray powder diffraction is displayed (Figure 23).

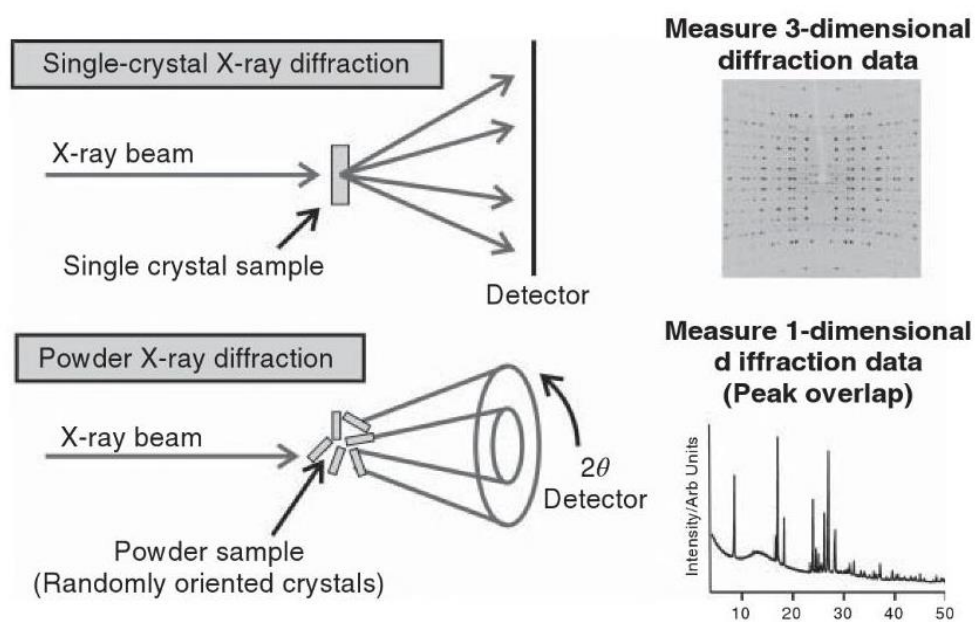


Figure 23 Difference between single-crystal X-ray and powder X-ray

The instrument used for the method is X-ray diffractometer, which consist of three basic elements, (i) an X-ray tube, (ii) a sample holder, and (iii) an X-ray detector. Figure 24 shows the schematic presentation of powder x-ray diffraction.

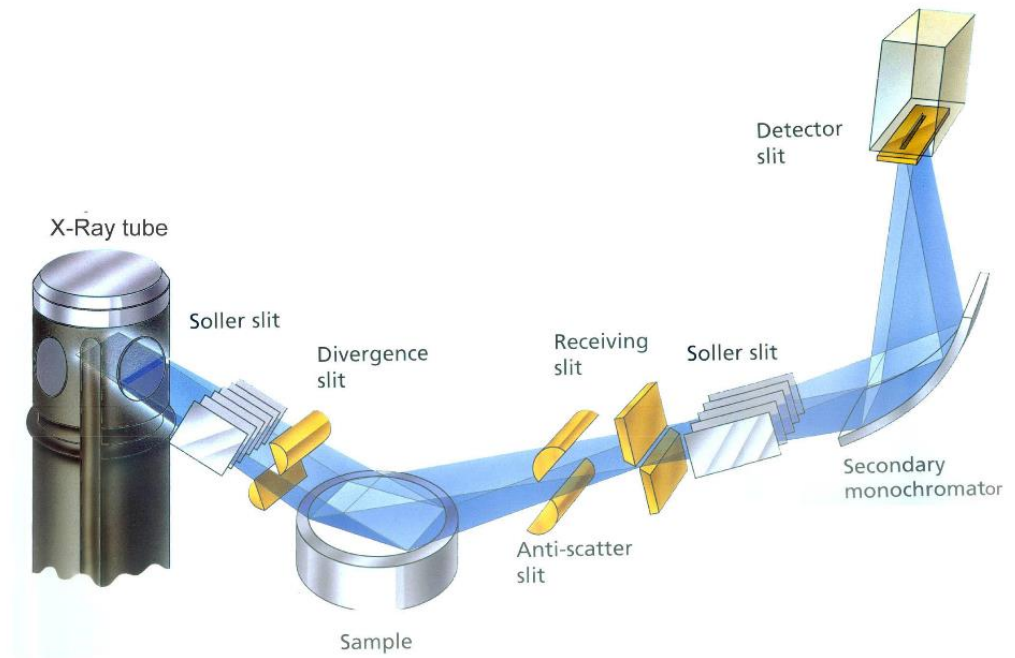


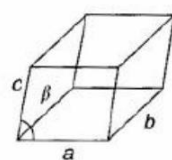
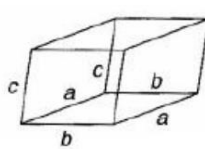
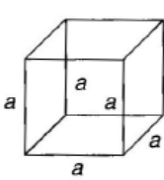
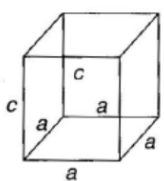
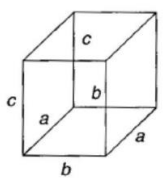
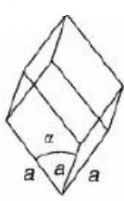
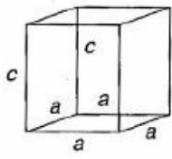
Figure 24 The schematic presentation of powder x-ray diffraction

### 1.7.1 Crystal Structures

In this section, the main definitions to understand X-ray will be described. *Crystalline solid* is defined as the atoms or ions arrange in a pattern that repeats itself in three dimensions to form a solid and it has long-range order. *Amorphous solid* is materials with only short-range order. *Space lattice* is a network composed of an infinite 3D array of points, which is coinciding with atom positions (center of spheres). The *unit cell* can be defined as the repeating unit in a space lattice. Also it is described as small repeating entity of the atomic structure and the basic building block of the crystal structure. It defines the entire crystal structure with the atom positions within. The unit cell geometries are shown in the following table 4.



Table 4 Unit cell geometry and crystal system

System	Axial lengths and angles	Unit cell geometry
<b>Monoclinic</b>	$a \neq b \neq c, \alpha = \gamma = 90^\circ, \neq \beta$	
<b>Triclinic</b>	$a \neq b \neq c, \alpha \neq \beta \neq \gamma \neq 90^\circ$	
<b>Cubic</b>	$a = b = c, \alpha = \beta = \gamma = 90^\circ$	
<b>Tetragonal</b>	$a = b \neq c, \alpha = \beta = \gamma \neq 90^\circ$	
<b>Orthorhombic</b>	$a \neq b \neq c, \alpha = \beta = \gamma \neq 90^\circ$	
<b>Rhombohedral</b>	$a = b = c, \alpha = \beta = \gamma \neq 90^\circ$	
<b>Hexagonal</b>	$a = b \neq c, \alpha = \beta = 90^\circ, \gamma = 120^\circ$	

### 1.7.2 Louër Method

The dichotomy Louër method for the indexing of powder diffraction patterns was published in 1972 (Louër et al., 1972). The dichotomy method is based on the variation of the lengths of interaxial angles and cell edges. The Louër method is searched in the n-dimensional space; n is the number of undetermined unit cell parameters. The method was first applied to orthorhombic (n = 3) and higher symmetries (n = 1 and 2) with a high success rate (Boultif et al., 1991). Then, an optimization of the program (DICVOL) and an extension to monoclinic systems (n = 4) were published in 1982 (Louër & Vargas, 1982).

The parameters (a, b, c,  $\beta$ ) of the unit cell from powder diffraction data can be formulated by the help of following equation:

$$Q(hkl) = f(A, C, \beta) + g(B)$$
$$f(A, C, \beta) = h^2/A^2 + l^2/C^2 - 2hl \cos \beta/AC$$
$$g(B) = k^2/B^2,$$
$$A = a \sin \beta, B = b \text{ and } C = c \sin \beta.$$

The four-dimensional domain is defined by the intervals, which are  $[A, A_+]$ ,  $[B, B_+]$ ,  $[C, C_+]$  and  $[\beta_-, \beta_+]$ . The whole space is then covered by increasing of the integers n, m, t and v in the intervals where the scanning steps p and  $\theta$  have been chosen as 0.40Å and 5° respectively (Boultif et al., 1991).  $A_0$ ,  $B_0$ , and  $C_0$  parameters are the lowest values for the A, B and C.

$$[A_- = A_0 + np, A_+ = A_- + p],$$
$$[B_- = B_0 + mp, B_+ = B_- + p],$$
$$[C_- = C_0 + tp, C_+ = C_- + p],$$
$$[\beta_- : 90 + v\theta, \beta_+ = \beta_- + \theta],$$

Calculated lines  $[Q_-(hkl), Q_+(hkl)]$  are generated and compared with the observed data from X-ray powder diffractometer, within the limits of experimental error. Later, the unit cell parameters are refined by a least-squares treatment (Boultif et al., 1991). The mathematical analysis of the dichotomy procedure for determining of unit cell geometry powder diffraction patterns has resulted in the computer program

(DICVOL); its efficiency in indexing accurate powder diffraction data has been demonstrated by a very high success rate.

### 1.7.3 Visser Method

The dichotomy Visser method for the automatic indexing of powder diffraction patterns was published first in 1969. The unit cell parameters ( $a, b, c, \beta$ ) from powder diffraction data can be formulated the help of the reciprocal lattice using the six constant in the following equation (Visser, 1969):

$$(2 \sin \theta/\lambda)^2 = 1/d^2 = h^2a^{*2} + k^2b^{*2} + l^2c^{*2} \\ +kl.2b^*c^* \cos \alpha^* + hl.2a^*c^* \cos \beta \\ +hk.2a^*b^* \cos \gamma^*$$

Visser defined  $Q = 10^4/d^2$  and wrote

$$Q(hkl) = h^2A + k^2B + l^2C + kLD + hLE + hkF.$$

The procedure used in program 'ITO' is simple. One- and two-parameter problems can probably be solved more effectively by a systematic trial-and-error method (Werner, 1964). Any two points in the reciprocal lattice, together with the origin, define a plane in the reciprocal lattice, corresponding to a crystallographic zone. The values of Q can be Q' and Q'' (Visser, 1969). Other points can be found by following calculating:

$$Q_{m,n} = m^2Q' + n^2Q'' + mnR$$

With the help of the above equation might be able to find the value of R belonging to the Q' and Q'' of a set of Q values (Visser, 1969):

$$R = (Q_{m,n} - m^2Q' - n^2Q'')/mn \quad (4)$$

The most frequent reason for failure in obtaining a correct reciprocal lattice is the inaccuracy of the input data. The errors in the diffraction angles should not exceed  $0.03^\circ$  ( $2\theta$ ) (Visser, 1969). The mathematical analysis of the dichotomy procedure for indexing unit cell geometry powder diffraction patterns has resulted in a significant improvement of the computer program (Ito); its efficiency also in indexing accurate powder diffraction data has been demonstrated by a very high success rate.

#### 1.7.4 Werner Method

The applications to facilitate the indexing of powder patterns were described in 1964 (Werner 1964). The method is based on a systematic trial-and-error method. The program contains separate routines for cubic, tetragonal, hexagonal, orthorhombic, monoclinic and triclinic symmetries. Approximations based on the symmetry and the  $d$  spacing of the 20th line has been proposed for unit-cell volumes (Kohlbeck & Hörl, 1976; Shirley, 1980). The reciprocal-cell relationship may be described (Werner et al., 1985):

$$Q(hkl) = h^2x_1 + k^2x_2 + l^2x_3 + hlx_4 + hlx_5 + klx_6$$

For monoclinic and higher symmetries the parameters  $x_i$  were found by Cramer's rule. In order to minimize the computing time, sub-matrices were saved and used until elements within them were changed. This procedure was repeated for each basis-line set (Werner et al., 1985).

This procedure is used because of the large number of basis-line sets needed for the symmetry (Werner et al., 1985). The mathematical analysis of the dichotomy procedure for determining of unit cell geometry powder diffraction patterns has resulted in the computer program (TREOR); its efficiency in indexing accurate powder diffraction data has been demonstrated by a very high success rate.

## 1.8 REFERENCES

- Adams H. A., Bailey N. A., Bentley G. W., Mann B. E., *J. Chem. Soc. Dalton Trans.*, 1989, 1831.
- Adams H., Agostinho S. C. M., Chomka K., Mann B. E., Smith S., Squires C., Spey S. E., *Can. J. Chem.*, 2001, 79, 760-774.
- Ager D. J., Laneman S. A., *Tetrahedron: Asymmetry*, 1997, 8, 3327.
- Akhtar M., Ellis P. D., MacDiarmid A. G., Odom J. R., *Inorg. Chem.*, 1972, 11, 2917
- Anastas P. T., Kirchhoff M. M., *Acc. Chem. Res.*, 2002, 35, 686-294
- Andersson P. G., Munslow I. J., *Modern Reduction Methods, Willey-VCH*, 2008
- Artioli Y., *Encyclopedia of Ecology*, 2008, 5(1), 60-65
- Babin V. N., Belousov Y. A., Dobryakova I. V., Nekrasov Y. S., Syrkin V. G., Uel'skii A. A., *Russian Chemical Bulletin.*, 2004, 53, 1903.
- Bahsoun A. A., Osborn J. A., Voelker C., Bonnet J. J., LAvigne G., *Organometallics*, 1982, 1, 1114.
- Beagley B., Schmidling D. G., *J. Mol. Struct.*, 1974, 22, 466
- Beck G., *Synlett*, 2002, 837
- Benfield R. E., Gavens P. D., Johnson B. F. G., Mays M. J., Aime S., Milone L., Osella D., *J. Chem. Soc. Dalton Trans.*, 1981, 1249.
- Bino A., Cotton F.A., Lahuerta P., Puebla P., and Usón R., *Inorg. Chem.*, 1980, 19, 2357.
- Blaser H. U., Malan C., Pugin B., Spindler F., Steiner H. and Studer M., *Adv. Synth. Catal.*, 2003, 343, 103
- Bolm C., Legros J., Le Paih J., Zani L., *Chem. Rev.*, 2004,104,6217
- Boultif A. and Louër D., *Journal of Applied Crystallography*, 1991, 24, 987-993
- Boultif A. and Louër D., *Journal of Applied Crystallography*, 2004, 37, 724-731
- Braga D., Grepioni F., Ferrugia L. J., Johnson B. F. G. J., *J. Chem. Soc.*, 1994, 2911.
- Braga D., Grepioni F., Orpen A.G, *Organometallics.*, 1993, 12, 1481.

- Bragg W. L., *Proc. Cambridge Philos. Soc.*, 1913, 17, 43
- Braye E. H., Dahl L. F., Hubel W., Wampler D. L., *J. Am. Chem. Soc.*, 1962, 84, 4633-4639.
- Brown G. E. Jr., Henrich V. E., Casey W. H., Clark D. L., Eggleston C., Felmy A., Goodman D. W., Grätzel M., Maciel G., McCarthy M. I., Neilson K. H., Sverjensky D. A., Toney M. F., Zachara J. M., *Chem. Rev.*, 1999, 99, 77-174.
- Cao P., Zhang X. J., *Org. Chem.*, 1999, 64, 2127
- Cartwright S., Clucas J. A., Dawson R. H., Foster D. F., Harding M. M., Smith A. K., *J. Organomet. Chem.*, 1986, 302, 403-412
- Chacon S. T., Cullen W. R., Bruce M. I., Shawkataly O. B., Einstein F. W. B., Jones R. H., Willis A. C., *Can. J. Chem.*, 1990, 68, 2001-2010.
- Chaudret B., Delavaux B., Poilblanc R., *Coord. Chem. Rev.*, 1988, 86, 191.
- Chorkendorff I., Niemantsverdriet J. W., *Concepts of Modern Catalysis and Kinetics*, 2007, 477
- Chou T. C., Adamson D., Mardinly J., Nieh T. G., *Thin Solid Films*, 1991, 205, 131-139.
- Churchill M. R., Wormald J., Knight J., Mays M. J., *J. Am. chem. Soc.*, 1971, 93, 3073-3074.
- Cooke M., Green M., Kirkpatrick D., *ibid*, 1968, 1507.
- Cotton F. A., Hunter D. L., *Inorg. Chem. Acta*, 1974, 11, L9.
- Cotton F. A., Troup J. M., *J. Am. Chem. Soc.*, 1974, 96, 4155.
- Cotton F. A., Troup J. M., *J. Am. Chem. Soc.*, 1974, 96, 4422.
- Davis J. A., Leckie J. O., *J. Colloid Interface Sci.*, 1978, 67, 90-107.
- Debye P., Scherrer P., *Physik. Z*, 1917, 27, 277
- Dewar J., Jackson F. R. S., Jones H. O., *Proc. R. Soc. (London) A*, 1905, 76, 558.
- Dewar J., Jones H. O., *Proc. R. Soc.*, 1907, 79A, 66.
- Dobbie R., Whittaker D., *J. Chem. Soc. D.*, 1970, 796.

Doucet H., Ohkuma T., Murata K., Yokozawa T., Kozawa M., Katayama E., England A. F., Irariya T., Noyori R., *Angew. Chem., Int. Ed. Engl.* 1998, 37, 1703

Enthaler S., Bernhard H., Giulia E., Junge K., Beller M., *Chem. Asian J.*, 2006, 1, 598-604

Enthaler S., Junge K., and Beller M., *Angew. Chem., Int. Ed.*, 2008, 47, 3317

Ewens R. V. G., Lister M. L., *Trans. Faraday Soc.*, 1938, 35, 681.

Fairweather-Tait, S. J., *Teucher, BNutrition Reviews*, 2002, 60 (11), 360–367.

Farrar D. H., Luniss J. A., *J. Chem. Soc. Dalton Trans.*, 1987, 1249.

Fehring V., Selke R., *Angew. Chem., Int. Ed. Engl.* 1998, 37, 1827.

Fletcher S. C., Poliakoff M., Turner J. J., *Inorg. Chem.*, 1986, 25, 3597.

Gladioli S., Alberico E., *Chem. Soc. Rev.*, 2006, 35, 226-236.

Gridnev I. D., Higashi N., Asakura K., Imamoto T., *J. Am. Chem. Soc.*, 2000, 122, 7183

Gridnev I. D., Higashi N., Imamoto T., *J. Am. Chem. Soc.*, 2001, 123, 4631.

Gridnev I. D., Yasutake M., Higashi N., Imamoto T., *J. Am. Chem. Soc.*, 2001, 123, 5268.

Haack K. J., Hashiguchi S., Fujii A., Ikariya T., Noyori R., *Angew. Chem., Int. Ed.*, 1997, 36, 285-288.

Handy N. C., Schaefer H. F., *J. Phys. Chem.* 1996, 100, 6003.

Hashiguchi S., Fujii A., Takehara J., Ikariya T., Noyori R., *J. Am. Chem. Soc.*, 1995, 117, 7562-7563.

Hieber W., *Anorg. Allg. Chem. Soc.*, 1932, 203, 165.

Hieber W., Becker E., *Chem. Ber.*, 1930, 63, 1405.

Hill E. W., Bradley J. S., *Inorganic Syntheses*, 1990, 27, 182–188

Hoffmann R., *Angew. Chem., Int. Ed. Engl.*, 1982, 21, 711.

Holz J., Monsees A., Jiao H., You J., Komarov I. V., Fischer C., Frauz K., Börner A., *J. Org. Chem.*, 2003, 68, 1701

Hugues F., Basset J. M., Ben Taarit Y., Choplin A., Primet M., Rojas D., Smith A. K., *American Chem. Soc.*, 1982, 104, 7020-70024

Hugues F., Smith A. K., Ben Taarit Y., Basset J. M., Commereuc D., Chauvin Y., *JCSChem. Commun.*, 1980, 68

Imamoto T., Watanabe J., Wada Y., Masuda H., Yamada H., Tsuruta H., Matsukawa S., Yamaguchi K., *J. Am. Chem. Soc.*, 1998, 120, 1635.

Ionescu A., Allouche A., Aycard J. P., Rajzmann M., Hutschka F., *J. Phys. Chem.*, 2002, 106, 9359–9366

Jang J. H., Lee J. G., Lee H., Xie Y., Schaefer H. F., *J. Phys. Chem. A.*, 1998, 102, 5298-5304.

Jiang Q., Jiang Y., Xiao D., Cao P., Zhang X., *Angew. Chem., Int. Ed. Engl.* 1998, 37, 1100

Johnson B. F. G., Bott A., *J. Chem. Soc. Dalton Trans.*, 1990, 2437.

Johnson B. F. G., *J. Chem. Soc. Commun.*, 1976, 703.

Johnson B. F. G., *J. Chem. Soc. Dalton Trans.*, 1997, 1472.

Jonas V., Thiel W., *J. Phys. Chem.*, 1995, 102, 8474.

Kagan H. B., Fiaud J. C., Hoornaert C., Meyer D., Poulin J. C., *Bull. Soc. Chim. Belg.*, 1979, 88, 923.

Kilbourn P. T., Reaburn V. A., Thompson D. T., *J. Chem. Soc. A.*, 1969, 1906

King R. B., Gimeno J., *Inorg. Chem.*, 1978, 17, 2390.

King R. B., Ragru Veer K. S., *Inorg. Chem.*, 1984, 23, 2482.

Latella B. A., O'Connor B. H., *J. Am. Ceram. Soc.*, 1997, 80, 2941–2944.

Legaditis P. O., Lough A.J. and Morris R. H., *J. Am. Chem. Soc.*, 2011, 133, 9662

Lentz D., Marschall R., *Organometallics*, 1991, 10, 1487.

Louër D. and Louër M., *Journal of Applied Crystallography*, 1972, 5, 271±275

Louër D. and Vargas R., *Journal of Applied Crystallography*, 1982, 15, 542±545

Luthi H. P., Siegbahn P. E. M., Almlof J., *J. Phys. Chem.*, 1985, 89, 2156.



- Mann B. E., *Chem. Commun.*, 1971, 1173
- Mann B. E., *J. Chem. Soc. Dalton Trans.*, 1997, 1457
- Manuel T. A., *Advan. Organometal. Chem.*, 1966, 5, 181.
- Marinetti A., Jus S., Genet J. P., *J. Organomet. Chem.*, 2001, 624, 162
- Markin E. M., Sugawara K., *J. Phys. Chem. A.*, 2000, 104, 1416.
- Masters C., Van Doorn J. A., De Boer J. J., *J. Chem. Soc. Chem. Commun.*, 1978, 1005.
- Mathey F., Mercier F., Robin F., Ricard L., *J. Organometallic Chem.*, 1998, 577, 117
- Meerwein H., *Chemiker-Zeitung*, 1920, 44, 693.
- Meyer N., Lough A. J., Morris R. H., *Chem. Eur. J.*, 2009, 15, 5605-5610
- Mond L., Langer C., *J. Chem. Soc.*, 1891, 59, 1090
- Mond L., Langer C., *Trans. Chem. Soc.* 1891, 59, 1090.
- Naud F., Spindler F., Reuggeberg C. J., Schmidt A. T. and Blaser H. U., *Org. Process Res. Dev.*, 2007, 11, 519
- Noyori R., Ohkuma T., Kitamura M., Takaya H., Sayo N., Kumobayashi H., Akutagawa S., *J. Am. Chem. Soc.*, 1987, 109, 5856.
- Ohkuma T., Ishii D., Takeno H., Noyori R., *J. Am. Chem. Soc.*, 2000, 122, 6510.
- Ojima I., Ed. In *Catalytic Asymmetric Synthesis*, Wiley-VCH, New York, 2000
- Paglia G., Buckley C. E., Rohl A. L., Hart R. D., Winter K., Studer A. J., Hunter B. A., Hanna J. V., *Chem. Mater.*, 2004, 16, 220–236.
- Pamies O., Bäckvall J.E., *Chem. Eur. J.*, 2001, 7, 5052-5058.
- Poliakoff M., Turner J. J., *J. Chem. Soc. A.*, 1971, 2403.
- Powell H. M., Ewens R. V. G., *J. Chem. Soc.*, 1939, 286
- Pye P. J., Rossen K., Reamer R. A., Volante R. P., Reider P. J., *Tetrahedron Lett.*, 1998, 39, 4441
- Richardson, D., *Stealth-Kampfflugzeuge: Täuschen und Tarnen in der Luft. Zürich: Dietikon.*, 2002

- Roberts P. J., Penfold B. R., Trotter J., *Inorg. Chem.*, 1970, 9, 2137
- Robin F., Mercier F., Ricard L., Mathey F., Spagnol M., *Chem. Eur. J.*, 1997, 3, 1365.
- Ryander P.N., Hydrogenation Methods, *Academic Press*, New York, 1990
- Samec J. S. M., Bäckvall J. E., Andersson P. G., Brandt P., *Chem. Soc. Rev.*, 2006, 35, 237-248.
- Schwarz J. A., Contescu C., Contescu A., *Chem. Rev.*, 1995, 95, 477–510.
- Shirley R., *In Accuracy in Powder Diffraction, Natl Bur. Stand. (US) Spec. Publ.*, 1980, 567, 361-382
- Silver J., *Chemistry of Iron.*, 1993
- Song X., Qu P., Yang H., He X., Qiu G., *J. of Central South Uni. of Tech.*, 2005, 12, 536-541
- Spogliarich R., Vidotto S., Farnetti E., Graziani M., Gulati N. V., *Tetrahedron: Asymmetry*, 1992, 1001.
- Stein E., Fujiwara F. Y., *J. Organometallic Chem.*, 1996, 525, 31-37.
- Sues P. E., Demmans K. Z., Morris R. H., *Dalton Transaction*, 2014, 43, 7650-7667
- Summers J. C., Ausen S. A., *J. Catal.*, 1978, 52, 445–452.
- Tachikawa M., Muetterties E. L., *Prog. Inorg. Chem.*, 1981, 28, 203-238.
- Tang W. and Zhang X., *Chem. Rev.*, 2003, 103, 3029-3069
- Törös S., Heil B., Kollar L., Marko L., *J. Organomet. Chem.*, 1980, 197, 85.
- Treichel P. M., Dean W. K., Douglas W. M., *Inorg. Chem.*, 1972, 11, 1609-1615.
- Trieichel P. M., Douglas W. M., Dean W. K., *Inorg. Chem.*, 1972, 11, 1615
- Trueba M., Trasatti S. P., *Eur. J. Inorg. Chem.*, 2005, 3393–3403
- Tsyganenko A. A., Mardilovich P. P., *J. Chem. Soc., Faraday Trans.*, 1996, 92, 4843–4852.
- Vijayendran K. K., Praneeth M. R., Ringenberg, and Thomas R. W., *Angew. Chem. Int. Ed.*, 2012, 51, 10228 – 10234

- Visser J. W., *Journal of Applied Crystallography*, 1969, 2, 89-95
- Wang N., Wang M., Lui T., Li P., Zhang T., Darensbourg M. Y., Sun L., *Inorg. Chem.*, 2008, 47, 6948-6955.
- Wang P. and Atwood J. D., *Organometallics.*, 1993, 12, 4247.
- Wefers K., *Alumina Chemicals: Science and Technology Handbook, The American Ceramic Society*, 1990, 13
- Wehrli B., Wieland E., Furrer G., *Aquat. Sci.*, 1990, 52, 1-31.
- Wei C. H., Dahl J. F., *J. Am. Chem. Soc.*, 1966, 88, 1821
- Werner P.E., Eriksson L. and Westdahl M., *Journal of Applied Crystallography*, 1985, 18, 367-370
- Werner, P. E., *Z. Kristallogr.*, 1964, 120, 375-387
- Wolverton C., Hass K. C., *Phys. Rev.*, 2000, 63, 1-16
- Yamanoi Y., Imamoto T., *J. Org. Chem.* 1999, 64, 2988
- Yasutake M., Gridnev I. D., Higashi N., Imamoto T., *Org. Lett.*, 2001, 3, 1701.
- Zassinovich G., Mestroni G., Gladiali S., *Chem. Rev.*, 1992, 92, 1051-1069
- Zhang X., Zhang F., Chan K., *Mater. Lett.*, 2004, 58, 2872-2877.

# EXPERIMENTAL

## 2.1 GENERAL TECHNIQUES AND METHODS

---

All reactions involving air-sensitive components are performed using Schlenk-techniques in inert atmosphere. Removing of the solvents and drying of the solid materials are performed under vacuum. Dried compounds are stored under argon atmosphere in Glove box. The solvents were analytical grade.

*Reagents:* Dyglyme, dichloromethane, butanol, ethanol, methanol, hexane, pentane, dppm, dppe, dppp, Fe(CO)<sub>5</sub>, Fe<sub>2</sub>(CO)<sub>9</sub>, Fe<sub>3</sub>(CO)<sub>12</sub>, Na<sub>2</sub>Fe(CO)<sub>4</sub>, Et<sub>3</sub>NO, AlO(OH) were obtained from Sigma Aldrich. Also acetophenone, 4'chloroacetophenone, 4'(triflouromethyl)acetophenone, 3-methoxyacetophenone, 3,3-dimethyl-2-butanone and propiophenone were provided from Sigma Aldrich.  $\gamma$ -Al<sub>2</sub>O<sub>3</sub>, *i*PrONa, 2-chloroacetophenone, pinacolone and cyclohexylmethyl ketone were ordered from Alfa Easar. Isopropanol and petroleum ether (30-60°C) were obtained from Merck. All other commercially available chemicals were obtained from chemical stores of technical university of Munich. Fe<sub>2</sub>(CO)<sub>4</sub>( $\mu$ -CO)( $\mu,\eta^2$ -dppm)<sub>2</sub> (**2**), Fe<sub>2</sub>(CO)<sub>4</sub>( $\mu$ -CO)<sub>3</sub>( $\mu,\eta^2$ -dppm) (**3**), Fe(CO)<sub>4</sub>( $\eta^1$ -dppm) (**4**) (Cartwright et al., 1986), Fe<sub>3</sub>(CO)<sub>8</sub>( $\mu$ -CO)<sub>2</sub>( $\mu,\eta^2$ -dppm) (**7**) (Adams et al., 2001), Fe<sub>3</sub>(CO)<sub>8</sub>( $\mu$ -CO)<sub>2</sub>( $\mu,\eta^2$ -dppe) (**8**) (Stein and Fujiwara, 1996) were synthesized according to literature procedures.

## 2.2 CHARACTERIZATION OF SUBSTANCES

---

### 2.2.1 Nuclear Magnetic Resonance Spectroscopy

NMR spectra were measured on Bruker Avance 360, Bruker AMX-400 and Bruker Avance 500c spectrometers. NMR multiplicities are abbreviated as follows: s = singlet, d = doublet, t = triplet, q = quartet, p = quintet, sept = septet, m = multiplet, br = broad signal. Coupling constants are given in Hz.

### 2.2.2 Elemental Analysis

Elemental analysis (C, H, Fe, P and S) was performed by the Microanalytical Laboratory of the technical university of Munich.

### 2.2.3 Mass Spectroscopy

Mass spectra were measured on MAT-90. It was used for the characterization using Fast Atom Bombardment technique (FAB, solvent: 4-nitrobenzylalcohol).

### 2.2.4 Gas Chromatography

A Hewlett-Packard HP 5970 mass spectrometer was used in connection with HP 5890 gas chromatograph for separation, identification and characterization of fluid reaction samples.

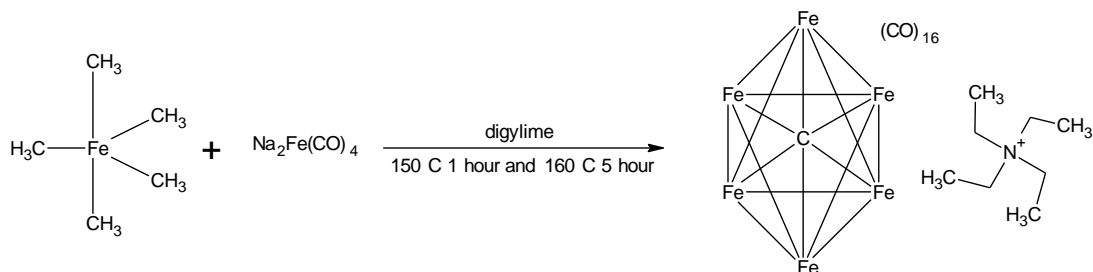
For chromatographic separations, a HP-1 column (50 m, 0.2 mm, 0.33  $\mu\text{m}$ ) was used with helium as carrier gas. Several different programmed temperature gradients (35  $^{\circ}\text{C}$  to 240  $^{\circ}\text{C}$ , heating rate between 15  $^{\circ}\text{C}/\text{min}$  and 35  $^{\circ}\text{C}/\text{min}$ ) were employed.

## 2.3 WORKING PROCEDURES

---

### 2.3.1 Synthesis of iron carbonyl cluster

#### 2.3.1.1 Synthesis of $[\text{Et}_4\text{N}]_2[\text{Fe}_6\text{C}(\text{CO})_{16}]$ (1)



In a one liter three-necked flask equipped with a serum cap, a stopper and a stopcock adaptor are placed 1 g (2,89 mmol)  $\text{Na}_2\text{Fe}(\text{CO})_4$  3/2 dioxane complex. First, diglyme (10 ml) and  $\text{Fe}(\text{CO})_5$  (2 ml) are added by means of syringe. The septum is replaced with a condenser and the solution is heated up to 150-155 $^{\circ}\text{C}$  for 5 hour, then the mixture is heated up to 160 $^{\circ}\text{C}$  for one hour (Tachikawa et al., 1981). On cooling of solution to room temperature, addition of hexane (70 ml) results in formation of an oily precipitate and purple supernatant. The supernatant is discarded and the solution is washed again with hexane (30 ml). The filtered oily precipitate is treated  $\text{Et}_4\text{NCl}$  and degassed water (50 ml) several times. The black-red precipitate is obtained after the separation of the water layer.

**$^{13}\text{C}$ -NMR:**  $[\text{Et}_4\text{N}]_2[\text{Fe}_6\text{C}(\text{CO})_{16}]$  (**1**) (400 MHz,  $d_6$ -Acetone, 25°C),  $\delta$  [ppm]: 7.68 (-CH<sub>3</sub>), 52.99 (-CH<sub>2</sub>-), 229.02 (-CO).

**Mass Spectroscopy:**  $[\text{Et}_4\text{N}]_2[\text{Fe}_6\text{C}(\text{CO})_{16}]$  (**1**) was measured and all of the decomposition products are shown in table 5.

Table 5 Mass-Spectrum analysis of  $[\text{Et}_4\text{N}]_2[\text{Fe}_6\text{C}(\text{CO})_{16}]$  (**1**).

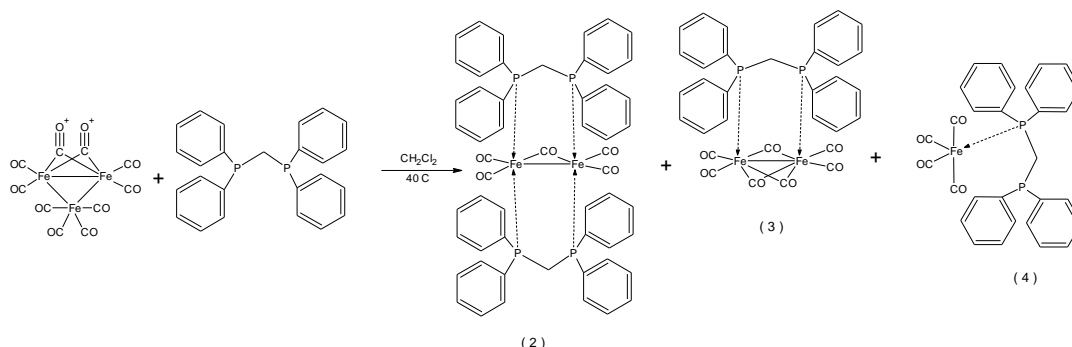
	m/z	Abundance %	Decomposition Product
<b><math>[\text{Fe}_6\text{C}(\text{CO})_{16}]^{-2}</math> (<b>1</b>) [M]: 796.2</b>	796.2	8.62	[M]
	768.2	12.64	[M-1CO]
	738.3	26.17	[M-2CO]
	710.4	14.50	[M-3CO]
	682.5	10.00	[M-4CO]
	654.7	12.30	[M-5CO]
	626.7	10.34	[M-6CO]
	598.8	6.74	[M-7CO]
	572.9	9.85	[M-8CO]
	544.9	13.32	[M-9CO]
517.0	8.35	[M-10CO]	

**Elemental analysis**  $[\text{Et}_4\text{N}]_2[\text{Fe}_6\text{C}(\text{CO})_{16}]$  (**1**), Mw: 926.4 g/mol

Elements	Calculated	Found
C	37.21 %	37.09 %
H	3.905 %	3.920 %
N	2.739 %	2.750 %
Fe	31.40 %	31.29

## 2.3.2 Synthesis of Iron Carbonyl Complexes

### 2.3.2.1 Synthesis of $\text{Fe}_2(\text{CO})_4(\mu\text{-CO})(\mu,\eta^2\text{-dppm})_2$ (**2**), $\text{Fe}_2(\text{CO})_4(\mu\text{-CO})_3(\mu,\eta^2\text{-dppm})$ (**3**) and $\text{Fe}(\text{CO})_4(\eta^1\text{-dppm})$ (**4**) (Cartwright et al., 1986)



Triiron dodecacarbonyl 2.00g (3.97 mmol) and 1,1-bis(diphenylphosphino)methane 3.06g (7.96 mmol) are dissolved in dichloromethane (70 ml) and are heated under reflux for one hour. The resulting deep red solution is reduced in volume and ethanol (10 ml) is added to the reaction mixture. On cooling this solution, brown solid is separated. After the filtration of the solvent the  $\text{Fe}_2(\text{CO})_4(\mu\text{-CO})(\mu,\eta^2\text{-dppm})_2$  (**2**) is obtained. Yield: 1.45 g (35 %). The remaining solution is reduced in volume using the Schlenk-line under argon atmosphere. On cooling, the orange precipitate of  $\text{Fe}(\text{CO})_4(\eta^1\text{-dppm})$  (**4**) is separated out. Yield: 0.62g (23%). The remaining solution is evaporated to dryness and  $\text{Fe}_2(\text{CO})_4(\mu\text{-CO})_3(\mu,\eta^2\text{-dppm})$  (**3**) is produced as a red solid. Yield: 0.28 g (13 %) (Cartwright et al., 1986).

**$^{13}\text{C}$ -NMR of  $\text{Fe}_2(\text{CO})_4(\mu\text{-CO})(\mu,\eta^2\text{-dppm})_2$  (**2**)** (400 MHz,  $\text{CDCl}_3$ ,  $25^\circ\text{C}$ ),  $\delta$  [ppm]: 19.84 (P- $\text{CH}_2$ -P), 58.29 (- $\text{CH}_2$ -OH), 132.16 – 127.86 (Ar-C), 224.65 and 203.30 (-CO).

**$^{13}\text{C}$ -NMR of  $\text{Fe}_2(\text{CO})_4(\mu\text{-CO})_3(\mu,\eta^2\text{-dppm})$  (**3**)** (500 MHz,  $d_6$ -Acetone,  $25^\circ\text{C}$ ),  $\delta$  [ppm]: 19.72 (P- $\text{CH}_2$ -P), 132.16 – 127.86 (Ar-C), 223.16 and 214.65 (-CO).

**$^{13}\text{C}$ -NMR of  $\text{Fe}(\text{CO})_4(\eta^1\text{-dppm})$  (**4**)** (400 MHz,  $d_6$ -Acetone,  $25^\circ\text{C}$ ),  $\delta$  [ppm]: 18.91 (P- $\text{CH}_2$ -P), 57.72 (- $\text{CH}_2$ -OH), 133.88 – 129.29 (Ar-C), 214.45 (-CO).

**Mass Spectroscopy:**  $\text{Fe}_2(\text{CO})_4(\mu\text{-CO})(\mu,\eta^2\text{-dppm})_2$  (**2**),  $\text{Fe}_2(\text{CO})_6(\mu\text{-CO})(\mu,\eta^2\text{-dppm})$  (**3**) and  $\text{Fe}(\text{CO})_4(\eta^1\text{-dppm})$  (**4**) was measured and all of the decomposition products are shown in table 6 and 7.

Table 6 Mass-Spectrum analysis of  $\text{Fe}_2(\text{CO})_4(\mu\text{-CO})(\mu,\eta^2\text{-dppm})_2$  (**2**) and  $\text{Fe}_2(\text{CO})_4(\mu\text{-CO})_3(\mu,\eta^2\text{-dppm})$  (**3**).

	m/z	Abundance %	Decomposition Product
<b><math>\text{Fe}_2(\text{CO})_5(\text{dppm})_2</math></b> <b>(2) [M]: 1020.34</b>	1020.1	9.91	[M]
	992.1	5.64	[M-1CO]
	964.2	30.62	[M-2CO]
	936.2	5.17	[M-3CO]
	880.2	20.60	[M-3CO-Fe]
	852.2	1.71	[M-4CO-Fe]
	824.3	1.17	[M-5CO-Fe]
<b><math>\text{Fe}_2(\text{CO})_7(\text{dppm})</math></b> <b>(3) [M]: 692.1</b>	692.1	5.05	[M]
	664.0	1.17	[M-CO]
	636.0	65.80	[M-2CO]
	608.0	39.32	[M-3CO]
	552.1	52.38	[M-3CO-Fe]
	524.1	52.29	[M-4CO-Fe]
	496.1	39.34	[M-5CO-Fe]
	468.1	51.27	[M-6CO-Fe]
	440.1	100.00	[M-7CO-Fe]



Table 7 Mass-Spectrum analysis of  $\text{Fe}(\text{CO})_4(\eta^1\text{-dppm})$  (**4**).

	m/z	Abundance %	Decomposition Product
<b><math>\text{Fe}(\text{CO})_4(\text{dppm})</math> (4) [M]: 552.3</b>	552.1	4.07	[M]
	524.1	14.06	[M-1CO]
	468.1	38.99	[M-3CO]
	440.1	55.35	[M-4CO]

**Elemental analysis**  $\text{Fe}_2(\text{CO})_4(\mu\text{-CO})(\mu,\eta^2\text{-dppm})_2$  (**2**), Mw: 1020.34 g/mol

Elements	Calculated	Found
C	64.73 %	64.31 %
H	4.35 %	4.13 %
P	12.14 %	12.39 %
Fe	10.94%	11.18%

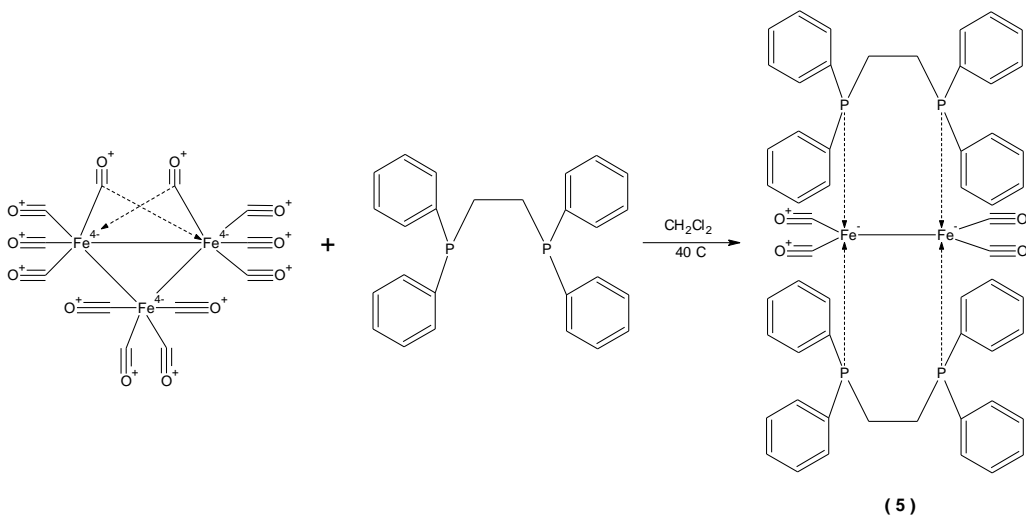
**Elemental analysis**  $\text{Fe}_2(\text{CO})_4(\mu\text{-CO})_3(\mu,\eta^2\text{-dppm})$  (**3**), Mw: 692.1 g/mol

Elements	Calculated	Found
C	55.53 %	55.86 %
H	3.20 %	3.38 %
P	8.95 %	9.35 %
Fe	16.14%	16.82 %

**Elemental analysis**  $\text{Fe}(\text{CO})_4(\eta^1\text{-dppm})$  (**4**), Mw: 552.3 g/mol

Elements	Calculated	Found
C	63.07 %	62.88 %
H	4.02 %	4.14 %
P	11.22%	11.07 %
Fe	10.11	10.61 %

### 2.3.2.2 Synthesis of $\text{Fe}_2(\text{CO})_4(\mu,\eta^2\text{-dppe})_2$ (**5**)



In a Schlenk flask, triiron dodecacarbonyl 2.00g (3.97 mmol) and 1,2-bis(diphenylphosphino)ethane 3.17g (7.96 mmol) are placed. After addition of the dichloromethane (70 ml), the mixture is heated under reflux for one hour. The resulting deep-green solution is reduced in volume and ethanol (10 ml) is added. With the help of separation caused by the ethanol,  $\text{Fe}_2(\text{CO})_4(\mu,\eta^2\text{-dppe})_2$  (**5**) is obtained as a green-grey solid.

Yield: 0.672 g (15 %).

$^{13}\text{C}$ -NMR of  $\text{Fe}_2(\text{CO})_4(\mu,\eta^2\text{-dppe})_2$  (**5**) (400 MHz,  $d_6$ -Acetone, 25°C),  $\delta$  [ppm]: 19.73 (P-CH<sub>2</sub>-C), 131.88-128.38 (Ar-C), 222.28 (-CO).

**Mass Spectroscopy:**  $\text{Fe}_2(\text{CO})_4(\mu, \eta^2\text{-dppe})_2$  (**5**) was measured and all of the decomposition products are shown in table 8.

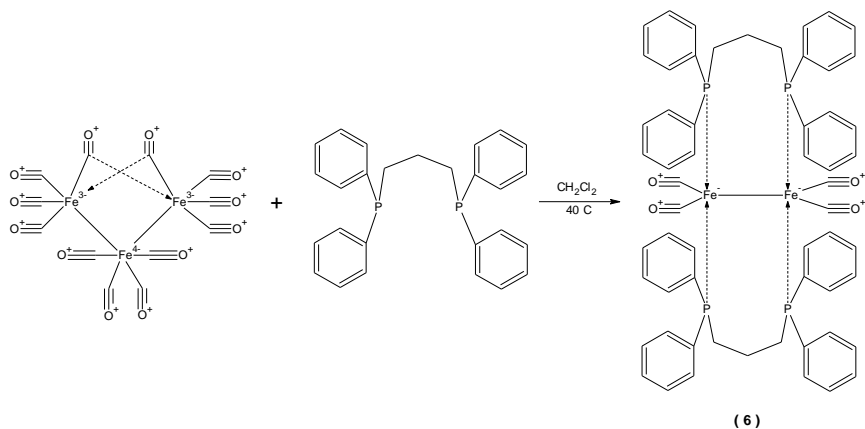
Table 8 Mass-Spectrum analysis of  $\text{Fe}_2(\text{CO})_4(\mu, \eta^2\text{-dppe})_2$  (**5**).

	m/z	Abundance %	Decomposition Product
<b><math>\text{Fe}_2(\text{CO})_4(\text{dppe})_2</math> (5) [M]: 1020.1</b>	1019.9	2.12	[M]
	621.9	6.27	[M-L]
	594.0	10.64	[M-L-CO]
	566.0	14.05	[M-L-2CO]
	538.0	16.87	[M-L-3CO]
	510.1	57.30	[M-L-4CO]
	454.1	100.00	[M-L-Fe-4CO]

**Elemental analysis**  $\text{Fe}_2(\text{CO})_4(\mu, \eta^2\text{-dppe})_2$  (**5**), Mw: 1020.34 g/mol

Elements	Calculated	Found
C	65.90 %	65.62 %
H	4.74 %	4.43 %
P	12.14 %	12.48 %
Fe	12.39%	11.25%

### 2.3.2.3 Synthesis of $\text{Fe}_2(\text{CO})_4(\mu, \eta^2\text{-dppp})_2$ (6)



$\text{Fe}_2(\text{CO})_4(\mu, \eta^2\text{-dppp})_2$  (6) is synthesized in the same procedure of compound 5. But instead of the 1,2-bis(diphenylphosphino)ethane the reaction is carried out using the compound 1,3-bis(diphenylphosphino)propane 3.27 g (7.96 mmol). The resulting deep-green solution is reduced in volume and washed with diethyl ether. After removing the excess solvent the grey product is obtained.

Yield: 0.58 g (13%).

$^{13}\text{C}$ -NMR of  $\text{Fe}_2(\text{CO})_4(\mu, \eta^2\text{-dppp})_2$  (6) (500 MHz,  $d_6$ -Acetone, 25°C),  $\delta$  [ppm]: 18.93 (P-CH<sub>2</sub>-), 19.67 (C-CH<sub>2</sub>-C), 132.66-128.89 (Ar-C), 219.08 (-CO).

**Mass Spectroscopy:**  $\text{Fe}_2(\text{CO})_4(\mu, \eta^2\text{-dppp})_2$  (6) was measured and all of the decomposition products are shown in table 9.

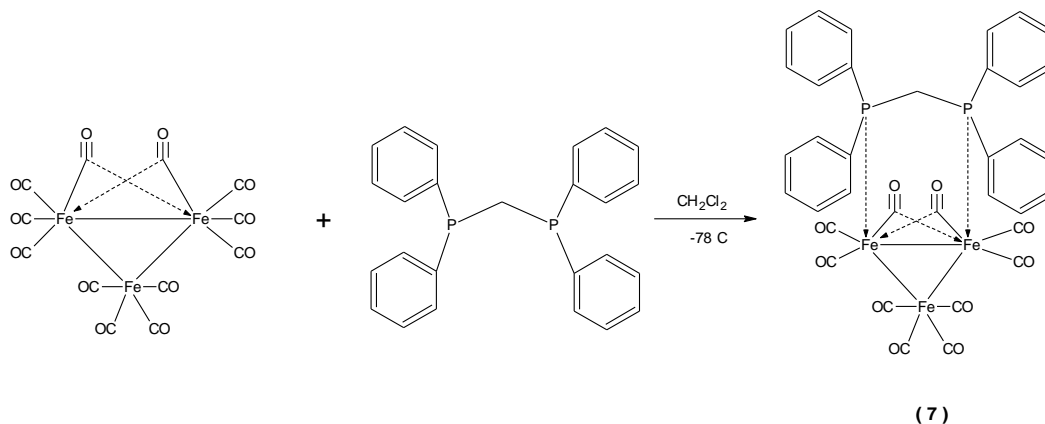
Table 9 Mass-Spectrum analysis of  $\text{Fe}_2(\text{CO})_4(\mu, \eta^2\text{-dppp})_2$  (6)

	m/z	Abundance %	Decomposition Product
<b><math>\text{Fe}_2(\text{CO})_4(\text{dppp})_2</math> (6) [M]: 1048.3</b>	1048.3	2.60	[M]
	636.4	11.21	[M-L]
	608.4	22.81	[M-L-1CO]
	580.5	11.98	[M-L-2CO]
	552.5	23.04	[M-L-3CO]
	524.6	39.97	[M-L-4CO]
	468.6	100.00	[M-4CO-L-Fe]

**Elemental analysis**  $\text{Fe}_2(\text{CO})_4(\mu, \eta^2\text{-dppp})_2$  (**6**), Mw: 1048.3 g/mol

Elements	Calculated	Found
C	66.43 %	66.12 %
H	5.0 %	4.87 %
P	11.82%	11.41%
Fe	10.65%	11.15

### 2.3.2.4 Synthesis of $\text{Fe}_3(\text{CO})_8(\mu\text{-CO})_2(\mu, \eta^2\text{-dppm})$ (**7**) (Adams et al., 2001)



Triiron dodecacarbonyl 1.00g (1.985 mmol) is placed in an argon purged schlenk-flask and is dissolved in  $\text{CH}_2\text{Cl}_2$  (300ml). The flask is cooled to  $-78^\circ\text{C}$  in a dry ice-acetone bath and the 1,1-bis(diphenylphosphino)methane 0.764g (1.985 mmol) is slowly added into the flask with stirring, followed by  $\text{Me}_3\text{NO}$  0.3g (4 mmol). The flask is removed from the solid  $\text{CO}_2$ -acetone bath and allowed to room temperature. The reaction is monitored by TLC. Four hours later all of the triiron dodecacarbonyl has been consumed in room temperature. The solvent is removed and the product purified by chromatography on silica, eluting with hexane-dichloromethane (3:1). The compound is obtained as a dark green solid (Adams et al., 2001).

Yield: 0.89 g (47 %).

$^{13}\text{C}$ -NMR of  $\text{Fe}_3(\text{CO})_8(\mu\text{-CO})_2(\mu,\eta^2\text{-dppm})$  (**7**) (400 MHz,  $d_6$ -Acetone,  $25^\circ\text{C}$ ),  $\delta$  [ppm]: 24.25, 23.43 (P-CH<sub>2</sub>-P), 165.75, 132.49-129.30 (Ar-C), 213.89 (-CO).

**Mass Spectroscopy:**  $\text{Fe}_3(\text{CO})_8(\mu\text{-CO})_2(\mu,\eta^2\text{-dppm})$  (**7**) was measured and all of the decomposition products are shown in table 10.

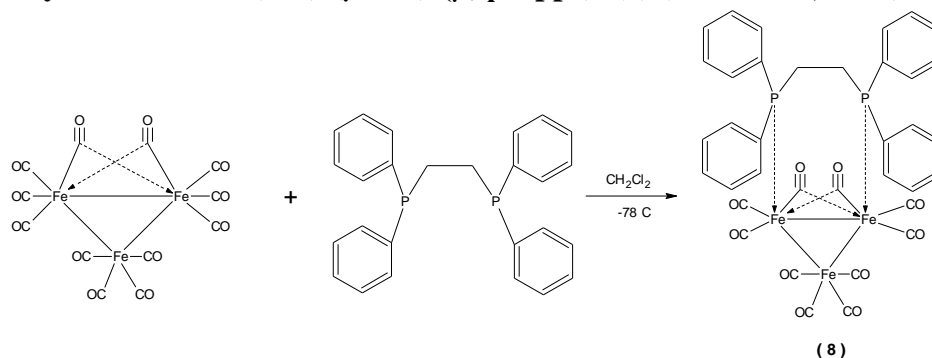
Table 10 Mass-Spectrum analysis of  $\text{Fe}_3(\text{CO})_8(\mu\text{-CO})_2(\mu,\eta^2\text{-dppm})$  (**7**).

	m/z	Abundance %	Decomposition Product
<b><math>\text{Fe}_3(\text{CO})_8(\mu\text{-CO})_2(\mu,\eta^2\text{-dppm})</math> (<b>7</b>) [M]: 832.02</b>	636.1	10.00	[M-7(CO)]
	608.1	4.14	[M-8(CO)]
	552.1	8.94	[M-8(CO)-Fe]
	524.2	6.98	[M-9(CO)-Fe]
	496.2	5.57	[M-10(CO)-Fe]
	440.2	8.23	[M-10(CO)-2Fe]

**Elemental analysis of  $\text{Fe}_3(\text{CO})_8(\mu\text{-CO})_2(\mu,\eta^2\text{-dppm})$  (**7**), Mw: 832.02 g/mol**

Elements	Calculated	Found
C	50.52 %	50.85 %
H	2.67 %	2.82 %
P	7.45%	7.10%
Fe	20.14%	19.52

### 2.3.2.5 Synthesis of $[\text{Fe}_3(\text{CO})_8(\mu\text{-CO})_2(\mu,\eta^2\text{-dppe})]$ (**8**) (Stein et al., 1996)



The synthesis of  $[\text{Fe}_3(\text{CO})_8(\mu\text{-CO})_2(\mu,\eta^2\text{-dppe})]$  (**8**) followed in the same procedure of compound 7. But instead of the 1,1-bis(diphenylphosphino)methane it is carried out using the compound 1,2-bis(diphenylphosphino)ethane 0.79g (1.985 mmol). The solvent is removed and the product purified by chromatography on silica column, eluting with petroleum ether (30-60°C)-dichloromethane (85:15). The compound was obtained as a dark violet solid (Stein et al., 1996).

Yield: 0.65 g (38.7 %).

$^{13}\text{C}$ -NMR of  $[\text{Fe}_3(\text{CO})_8(\mu\text{-CO})_2(\mu,\eta^2\text{-dppe})]$  (**8**) (500 MHz,  $\text{CDCl}_3$ , 25°C),  $\delta$  [ppm]: 27.70 and 21.96 (P- $\text{CH}_2$ -C), 166.74, 130.84–127.93 (Ar-C), 211.84(-CO).

**Mass Spectroscopy:**  $[\text{Fe}_3(\text{CO})_{10}(\mu,\eta^2\text{-dppe})]$  (**8**) was measured and all of the decomposition products are shown in table 11.

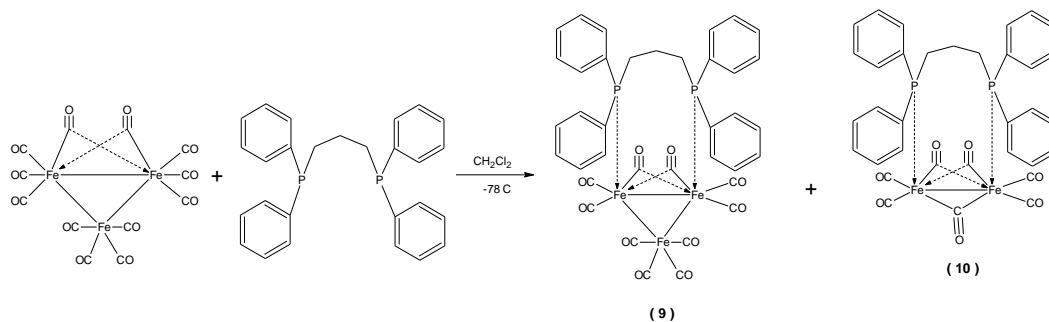
Table 11 Mass-Spectrum analysis of  $[\text{Fe}_3(\text{CO})_{10}(\mu,\eta^2\text{-dppe})]$  (**8**).

	m/z	Abundance %	Decomposition Product
<b><math>[\text{Fe}_3(\text{CO})_{10}(\text{dppe})]</math> (<b>8</b>) [M]: 846.05</b>	763.1	1.43	[M-3(CO)]
	650.2	12.18	[M-7(CO)]
	622.2	32.92	[M-8(CO)]
	594.3	18.83	[M-9(CO)]
	566.3	9.53	[M-10(CO)]
	510.3	1.59	[M-10(CO)-Fe]
	454.4	1.13	[M-10(CO)-2Fe]
	391.7	100.00	[M-L-2(CO)]
	147.4	91.82	Acetonitrile

**Elemental analysis**  $[\text{Fe}_3(\text{CO})_{10}(\mu, \eta^2\text{-dppe})]$  (**8**), Mw: 846.05 g/mol

Elements	Calculated	Found
C	51.11 %	51.39 %
H	2.86 %	2.96 %
P	7.32 %	7.57 %
Fe	19.80%	20.48 %

### 2.3.2.6 Synthesis of $[\text{Fe}_3(\text{CO})_8(\mu\text{-CO})_2(\mu, \eta^2\text{-dppp})]$ (**9**) and $[\text{Fe}_2(\text{CO})_4(\mu\text{-CO})_3(\mu, \eta^2\text{-dppp})]$ (**10**)



The synthesis of  $[\text{Fe}_3(\text{CO})_8(\mu\text{-CO})_2(\mu, \eta^2\text{-dppp})]$  (**9**) followed in the same procedure of compound **7**. But instead of the 1,1-bis(diphenylphosphino)methane it is carried out using the compound 1,3-bis(diphenylphosphino)propane 0.82g (1.985 mmol). The solvent is removed and the product purified by chromatography on silica, eluting with petroleum ether (30  $-60^\circ\text{C}$ )-dichloromethane (85:15). The compound (**9**) is obtained from the second band of column chromatography as a violet solid. Yield: 0.42 g (24.7 %). The third green band eluted on the column chromatography is identified as  $[\text{Fe}_2(\text{CO})_4(\mu\text{-CO})_3(\mu, \eta^2\text{-dppp})]$  (**10**). Yield: 0.42 g (32 %).

$^{13}\text{C}$ -NMR of  $[\text{Fe}_3(\text{CO})_8(\mu\text{-CO})_2(\mu, \eta^2\text{-dppp})]$  (**9**) (400 MHz,  $d_6$ -Acetone,  $25^\circ\text{C}$ ),  $\delta$  [ppm]: 30.23 (-P- $\text{CH}_2$ -), 20.66 (-C- $\text{CH}_2$ -C-), 132.53-128.74 (Ar-C), 213.76 (-CO).

**Mass Spectroscopy:**  $[\text{Fe}_3(\text{CO})_8(\mu\text{-CO})_2(\mu, \eta^2\text{-dppp})]$  (**9**) was measured and all of the decomposition products are shown in table 12.



**Elemental analysis**  $[\text{Fe}_3(\text{CO})_8(\mu\text{-CO})_2(\mu,\eta^2\text{-dppp})]$  (**9**), Mw: 846.05 g/mol

Elements	Calculated	Found
C	51.67 %	51.47 %
H	3.05 %	3.28 %
P	7.20 %	7.07 %
Fe	19.48 %	20.13 %

Table 12 Mass-Spectrum analysis of  $[\text{Fe}_3(\text{CO})_8(\mu\text{-CO})_2(\mu,\eta^2\text{-dppp})]$  (**9**).

	m/z	Abundance %	Decomposition Product
<b><math>[\text{Fe}_3(\text{CO})_8(\mu\text{-CO})_2(\mu,\eta^2\text{-dppp})]</math> (<b>9</b>) [M]: 860.07</b>	860.6	1.38	[M]
	748.8	1.21	[M-4(CO)]
	719.8	2.60	[M-5(CO)]
	692.2	4.17	[M-6(CO)]
	664.2	19.81	[M-7(CO)]
	636.3	60.96	[M-8(CO)]
	608.3	86.34	[M-9(CO)]
	552.4	70.88	[M-9(CO)-Fe]
	524.4	100.00	[M-10(CO)-Fe]
	468.4	97.78	[M-10(CO)-2Fe]

$^{13}\text{C}$ -NMR of  $[\text{Fe}_2(\text{CO})_4(\mu\text{-CO})_3(\mu,\eta^2\text{-dppp})]$  (**10**) ( 500 MHz,  $\text{CD}_2\text{Cl}_2$ ,  $25^\circ\text{C}$  ),  $\delta$  [ppm]: 28.93 (-P- $\text{CH}_2$ -), 23.00 (-C- $\text{CH}_2$ -C-), 132.71 - 128.82 ( Ar-C ), 213.88 ( -CO).

**Mass Spectroscopy:**  $[\text{Fe}_2(\text{CO})_4(\mu\text{-CO})_3(\mu,\eta^2\text{-dppp})]$  (**10**) was measured and all of the decomposition products are shown in table 13.

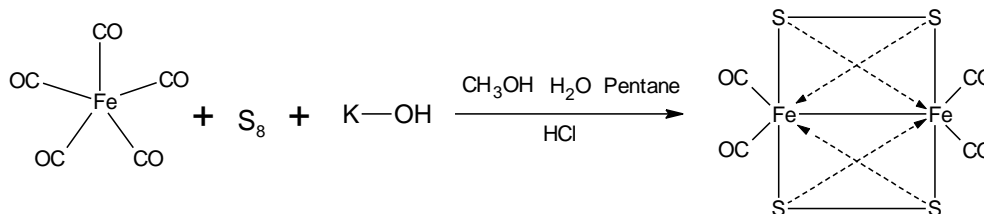
**Elemental analysis**  $[\text{Fe}_2(\text{CO})_4(\mu\text{-CO})_3(\mu,\eta^2\text{-dppp})]$  (**10**), Mw: 720.2 g/mol

Elements	Calculated	Found
C	56.70 %	56.52 %
H	3.64 %	3.92 %
P	8.24%	8.42 %
Fe	15.51 %	14.93 %

Table 13 Mass-Spectrum analysis of  $[\text{Fe}_2(\text{CO})_4(\mu\text{-CO})_3(\mu,\eta^2\text{-dppp})]$  (**10**).

	m/z	Abundance %	Decomposition Product
$[\text{Fe}_2(\text{CO})_4(\mu\text{-CO})_3(\mu,\eta^2\text{-dppp})_2]$ <b>(10) [M]: 720.20</b>	720.1	3.14	[M]
	692.2	2.29	[M-(CO)]
	664.2	3.52	[M-2(CO)]
	636.3	8.36	[M-3(CO)]
	608.2	10.73	[M-4(CO)]
	580.3	7.39	[M-5(CO)]
	552.4	10.16	[M-6(CO)]
	524.5	15.09	[M-7(CO)]
	468.4	22.99	[M-7(CO)-Fe]

### 2.3.2.7 Synthesis of $[\text{Fe}_2(\text{S}_4)(\text{CO})_4]$ (11)



Iron pentacarbonyl (5 ml) and a degassed solution of 50% aqueous KOH (20ml, 240 mmol) are added to a three-necked flask, to which is added dichloromethane (50 ml). After fifteen min, the solution is cooled to 0°C and sulphur 11.5g (36 mmol) is added in one portion. The mixture became very warm and instantly turned black. 15 min later, water (125 ml) and pentane (250 ml) are added and the mixture is carefully acidified with 25% HCl (100 ml). The mixture is filtered and the solid rinsed with pentane. The pentane layer is washed with water and dried over sodium sulphate. Evaporation of the pentane layer gives a red precipitate. Yield: 0.74 g (11 %).

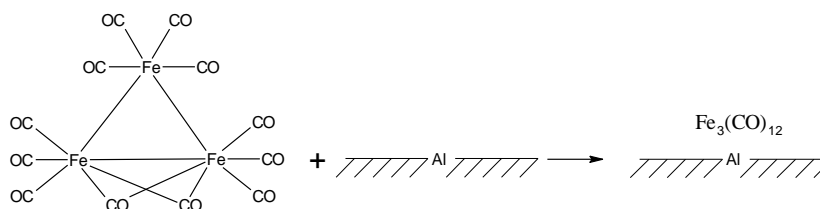
$^{13}\text{C}$ -NMR of  $[\text{Fe}_2(\text{S}_4)(\text{CO})_4]$  (11) (400 MHz,  $d_6$ -Acetone, 25°C), 213.43 (-CO).

**Elemental analysis**  $[\text{Fe}_2(\text{S}_4)(\text{CO})_4]$  (11), Mw: 408.021 g/mol

Elements	Calculated	Found
C	17.66 %	18.17 %
S	31.44%	31.56 %
Fe	27.37 %	28.28%

### 2.3.3 Obtainment of Supported Iron Carbonyl Clusters on Alumina

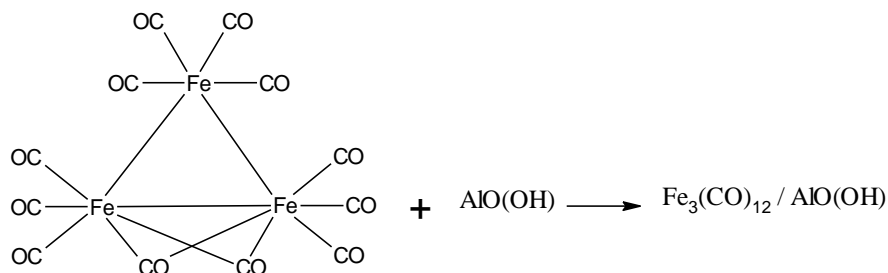
#### 2.3.3.1 Obtainment of physisorbed $\text{Fe}_3(\text{CO})_{12}$ on $\gamma\text{-Al}_2\text{O}_3$ (12)



The catalyst is prepared by impregnation of  $\gamma\text{-Al}_2\text{O}_3$  (100-200  $\text{m}^2 \text{g}^{-1}$ ) with  $\text{Fe}_3(\text{CO})_{12}$ . In a schlenk flask,  $\text{Fe}_3(\text{CO})_{12}$  (0.20 mmol) and  $\gamma\text{-Al}_2\text{O}_3$  (2.0 g) are placed. Hexane (30

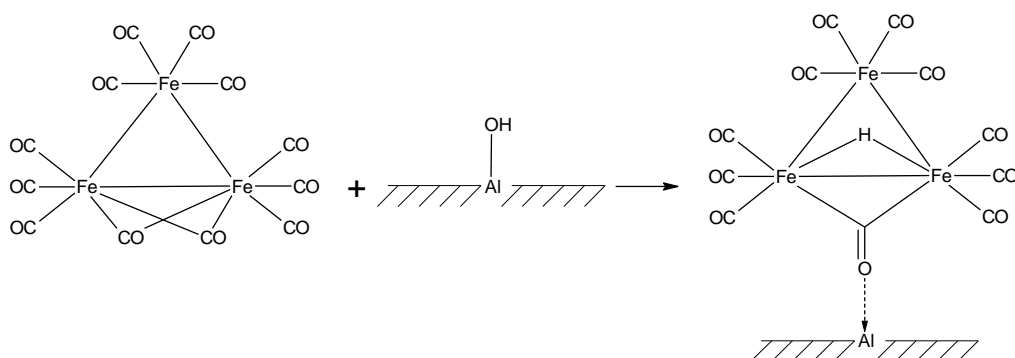
ml) is added in the mixture and  $\text{Fe}_3(\text{CO})_{12}$  and  $\gamma\text{-Al}_2\text{O}_3$  and hexane is mixed for several hours at room temperature. When the  $\gamma\text{-Al}_2\text{O}_3$  without any pretreatment is stirred with a hexane solution of triiron dodecacarbonyl, only a very slight decolouration of the solution occurred. After the evaporation of the solvent, all of the  $\text{Fe}_3(\text{CO})_{12}$  transferred onto the gamma alumina. The 2%  $\text{Fe}_3(\text{CO})_{12}$  containing light green-coloured alumina was obtained.

### 2.3.3.2 Obtainment of physisorbed $\text{Fe}_3(\text{CO})_{12}$ on $\text{AlO}(\text{OH})$ (13)



The catalyst is prepared by impregnation of  $\text{AlO}(\text{OH})$  with  $\text{Fe}_3(\text{CO})_{12}$ . In a schlenk flask,  $\text{Fe}_3(\text{CO})_{12}$  (0.20 mmol) and  $\text{AlO}(\text{OH})$  (2.0 g) are placed. Hexane (30 ml) is added in the mixture and is mixed for several hours at room temperature. After the evaporation of the solvent, all of the  $\text{Fe}_3(\text{CO})_{12}$  transferred onto the  $\text{AlO}(\text{OH})$ . The 2%  $\text{Fe}_3(\text{CO})_{12}$  containing light green-coloured alumina was obtained.

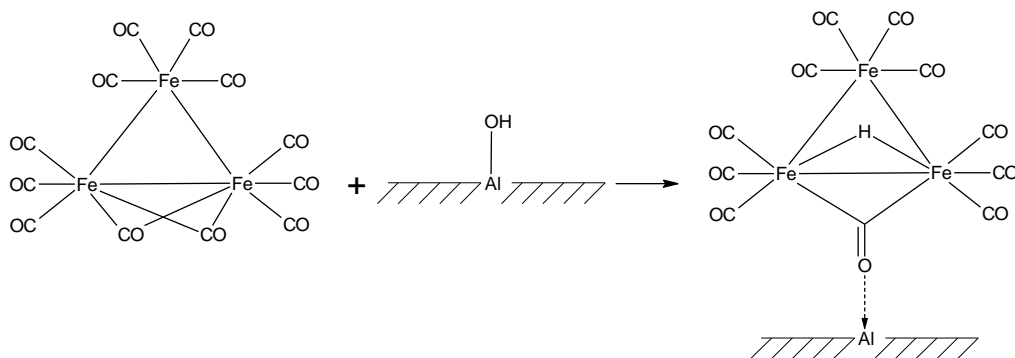
### 2.3.3.3 Obtainment of chemisorbed $\text{Fe}_3(\text{CO})_{12}$ on $\gamma\text{-Al}_2\text{O}_3$ (Pre-treatment 1) (14) (Hugues et al., 1982)



The catalyst is prepared by impregnation of  $\gamma\text{-Al}_2\text{O}_3$  with  $\text{Fe}_3(\text{CO})_{12}$ . Before adsorption of the iron carbonyl cluster, the  $\gamma\text{-Al}_2\text{O}_3$  is treated in the following way: the support is heated up to  $180^\circ\text{C}$  for one hour to remove water and is heated slowly under vacuum ( $10^{-4}$  torr) up to  $500^\circ\text{C}$  for 14 hours. The pre-treated  $\gamma\text{-Al}_2\text{O}_3$  (2.0 g) and  $\text{Fe}_3(\text{CO})_{12}$  (0.20 mmol) are placed in a schlenk flask. Hexane (30 ml) is added in

the mixture and is mixed for 10 hours at room temperature. When the  $\gamma\text{-Al}_2\text{O}_3$  with the pre-treatment is mixed with triiron dodecacarbonyl in hexane, the solution is completely decolorized after around 10 hours of stirring. The 2%  $\text{Fe}_3(\text{CO})_{12}$  containing light orange-coloured alumina can be washed several times with hexane till no extraction of the cluster was obtained (Hugues et al., 1982).

**2.3.3.4 Obtainment of chemisorbed  $\text{Fe}_3(\text{CO})_{12}$  on  $\gamma\text{-Al}_2\text{O}_3$  (Pre-treatment 2)  
(15) (Hugues et al., 1982)**



The catalyst is prepared by impregnation of  $\gamma\text{-Al}_2\text{O}_3$  with  $\text{Fe}_3(\text{CO})_{12}$ . Before adsorption of the iron carbonyl cluster, the  $\gamma\text{-Al}_2\text{O}_3$  is heated up to  $180^\circ\text{C}$  for one hour to remove water and is heated to calcine under oxygen pressure up to  $500^\circ\text{C}$  for 14 hours. After calcination with the oxygen, support is heated slowly (4 K/min) under vacuum ( $10^{-4}$  torr) up to  $500^\circ\text{C}$  for 2 hours. The pre-treated  $\gamma\text{-Al}_2\text{O}_3$  (2.0 g) and  $\text{Fe}_3(\text{CO})_{12}$  (0.20 mmol) are placed in a schlenk flask. Hexane (30 ml) is added in the mixture and is mixed for 10 hours at room temperature. When the  $\gamma\text{-Al}_2\text{O}_3$  with the pre-treatment is mixed with triiron dodecacarbonyl in hexane, the solution is completely decolorized after around 10 hours of stirring. The 2%  $\text{Fe}_3(\text{CO})_{12}$  containing light pink-coloured alumina can be washed several times with hexane till no extraction of the cluster can be occurred (Hugues et al., 1982).

**2.3.3.5 Obtainment of physisorbed  $\text{Fe}_2(\text{CO})_4(\mu\text{-CO})(\mu,\eta^2\text{-dppm})_2$  on  $\gamma\text{-Al}_2\text{O}_3$  (Pretreatment 2) (16)**



The synthesis of physisorbed  $\text{Fe}_2(\text{CO})_4(\mu\text{-CO})(\mu,\eta^2\text{-dppm})_2$  on  $\gamma\text{-Al}_2\text{O}_3$  (pre-treatment 2) followed in the same procedure of catalyst 15. Instead of the triiron dodecacarbonyl, it is carried out using the compound  $\text{Fe}_2(\text{CO})_4(\mu\text{-CO})(\mu,\eta^2\text{-dppm})_2$  (0.20 mmol). When the  $\gamma\text{-Al}_2\text{O}_3$  with the pre-treatment is mixed with  $\text{Fe}_2(\text{CO})_4(\mu\text{-CO})(\mu,\eta^2\text{-dppm})_2$  in hexane (20ml) and acetone (4ml), the colour of the solution was slightly decolorized after around 10 hours of stirring. The 2%  $\text{Fe}_2(\text{CO})_4(\mu\text{-CO})(\mu,\eta^2\text{-dppm})_2$  containing light light orange-red coloured alumina was obtained.

**2.3.3.6 Obtainment of physisorbed  $\text{Fe}_2(\text{CO})_7(\mu,\eta^2\text{-dppm})$  on  $\gamma\text{-Al}_2\text{O}_3$  (Pretreatment 2) (17)**



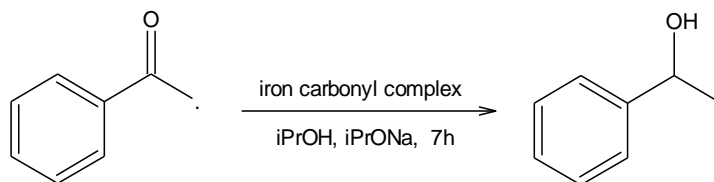
The synthesis of compound 17 followed in the same procedure. But instead of the  $\text{Fe}_2(\text{CO})_4(\mu\text{-CO})(\mu,\eta^2\text{-dppm})_2$  it was carried out using the compound  $\text{Fe}_2(\text{CO})_7(\mu,\eta^2\text{-dppm})$  (0.20 mmol). When the  $\gamma\text{-Al}_2\text{O}_3$  with the pre-treatment was mixed with  $\text{Fe}_2(\text{CO})_7(\mu,\eta^2\text{-dppm})$  in hexane (20 ml) and acetone (5ml), the colour of the solution wasn't changed after around 10 hours of stirring. The light light orange-red coloured alumina was obtained.

**2.3.3.7 Obtainment of physisorbed  $\text{Fe}(\text{CO})_4(\text{dppm})$  on  $\gamma\text{-Al}_2\text{O}_3$  (Pre-treatment 2) (18)**



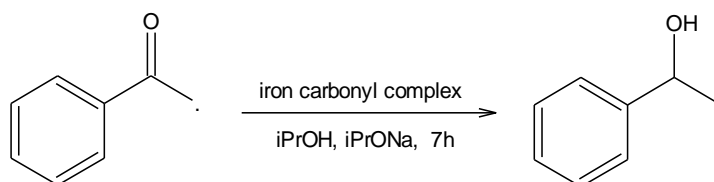
The synthesis of compound 17 followed in the same procedure. But instead of the  $\text{Fe}_2(\text{CO})_4(\mu\text{-CO})(\mu,\eta^2\text{-dppm})_2$  it was carried out using the compound  $\text{Fe}(\text{CO})_4(\text{dppm})$  (0.20 mmol). When the  $\gamma\text{-Al}_2\text{O}_3$  with the pre-treatment was mixed with  $\text{Fe}(\text{CO})_4(\text{dppm})$  in hexane, the colour of the solution was not changed after around 10 hours of stirring. The 2%  $\text{Fe}(\text{CO})_4(\text{dppm})$  containing light yellow-coloured alumina was occurred.

### 2.3.4 Experimental of Transfer Hydrogenation



Solutions of the catalysts **2-11** and iron carbonyl clusters were prepared in isopropanol with sodium isopropoxide. In a rubber vial (25 mL), the catalyst (0,025 mmol) was placed with isopropanol (12.5mmol). The system was treated with sodium 2-propylate (0,025-0,5 mmol). After addition of ketone (2,5 mmol), the reaction mixture was stirred for 7 h at 85°C. The solution was cooled to room temperature. The conversion was measured by GC without further purification.

### 2.3.5 Experimental of Heterogeneous Catalysis



Mixture of the catalysts **12-18** and ketone were placed in a stainless steel Parr pressure Reactor in a glove-box. The reactor was pressurized with 3 atm, 10 atm, 20 atm 35 atm and 50 atm of H<sub>2</sub>, placed in an oil bath maintained at 25 °C, 50 °C, 100 °C, 150 °C and 200 °C, and allowed to stir for 5 hours. The mixture was cooled to room temperature. The conversion was measured by GC without further purification.

## 2.4 REFERENCES

---

- Adams H., Agostinho S. C. M., Chomka K., Mann B. E., Smith S., Squires C., Spey S. E., *Can. J. Chem.*, 2001, 79, 760-774
- Cartwright S., Clucas J. A., Dawson R. H., Foster D. F., Harding M. M., Smith A. K., *J. Organomet. Chem.*, 1986, 302, 403-412
- Stein E., Fujiwara F. Y., *J. Organometallic Chem.*, 1996, 525, 31-37
- Tachikawa M., Muetterties E. L., *Prog. Inorg. Chem.*, 1981, 28, 203-238.
- Hugues F., Basset J. M., Ben Taarit Y., Choplin A., Primet M., Rojas D., Smith A. K., *American Chem. Soc.*, 1982, 104, 7020-70024



# RESULTS AND DISCUSSION

## 3.1 SYNTHESIS

---

In this study, eleven iron carbonyl diphosphine complexes were synthesized. For this purpose, firstly  $[\text{Fe}_6\text{C}(\text{CO})_{16}]^{-2}$  (**1**) was synthesized by the reaction of  $\text{Fe}(\text{CO})_5$  with a metal carbonyl anions, contains an octahedral  $\text{Fe}_6\text{C}$  core (Churchill et al., 1971). Initially from the reactions of triiron dodecacarbonyl  $[\text{Fe}_3(\text{CO})_{12}]$  with bidentate phosphines 1,1-bis(diphenylphosphino)methane (dppm), 1,2-bis(diphenylphosphino)ethane (dppe), 1,3-bis(diphenylphosphino)propane (dppp) were synthesized  $\text{Fe}_2(\text{CO})_4(\mu\text{-CO})(\mu\text{-dppm})_2$  (**2**),  $\text{Fe}_2(\text{CO})_4(\mu\text{-CO})_3(\mu\text{-dppm})$  (**3**), in addition to  $\text{Fe}(\text{CO})_4(\mu\text{-dppm})$  (**4**). The new diphosphine derivatives of dinuclear iron complexes, which are  $\text{Fe}_2(\text{CO})_4(\mu\text{-dppe})_2$  (**5**),  $\text{Fe}_2(\text{CO})_4(\mu\text{-dppp})_2$  (**6**) and  $\text{Fe}_2(\text{CO})_4(\mu\text{-CO})_3(\mu\text{-dppp})$  (**10**), have been isolated and spectroscopically characterised. From the reactions of triiron dodecacarbonyl with bidentate phosphines dppm, dppe, dppp using triethylamine N-oxide as a decarbonylating agent were obtained  $[\text{Fe}_3(\text{CO})_8(\mu\text{-CO})_2(\mu,\eta^2\text{-diphosphine})]$  (**7-9**) and  $[\text{Fe}_3(\text{CO})_8(\mu\text{-CO})_2(\mu,\eta^2\text{-dppp})]$  (**9**) was isolated as a new compound.  $\text{Fe}_2(\text{S}_4)(\text{CO})_4$  (**11**) was prepared by the help of potassium hydroxide from the reaction of iron pentacarbonyl with sulphur. Structures of the compounds (**1-10**) were characterized with the help of IR,  $^{31}\text{P}$ -NMR,  $^{13}\text{C}$ -NMR, X-ray powder, elemental analysis and MS spectroscopic data.

## 3.2 ELEMENTAL ANALYSIS OF THE SYNTHESIZED COMPOUNDS

---

Elemental analysis results of the synthesized compounds are given in table 14. Calculated elemental analysis and the results were found to be consistent with each other. In addition calculated and found elemental analysis of iron carbonyl cluster complexes were determined in very close expected value of stoichiometric ratio.

A maximum deviation of 0.4% between expected and found values for elemental analysis is accepted. In our compound,  $\text{Fe}(\text{CO})_4(\text{dppm})$  (**4**), a deviation of 4.71% as a maximum for iron was determined. 2.05-4.71% deviation in the Fe content of the other compounds was also found. The deviation in carbon content of all of compounds is also between 0.30 - 0.94%.

Table 14 Elemental analysis of iron carbonyl cluster complexes

Comp.	Colour	Elemental Analyse (%) Found (Calculated.)			
		C	H	Fe	P
2	Brown	64.31 (64.73)	4.13 (4.35)	11.17 (10.94)	12.29 (12.14)
3	Red	56.06 (55.53)	3.38 (3.2)	16.14 (16.82)	9.35 (8.95)
4	Yellow	62.88 (63.07)	4.14 (4.02)	10.61 (10.11)	11.07 (11.22)
5	Green	65.42 (65.9)	4.43 (4.74)	11.25 (10.94)	12.48 (12.14)
6	Black-grey	65.82 (66.43)	4.87 (5.0)	11.15 (10.65)	11.42 (11.82)
7	Violet	50.85 (50.52)	2.67 (2.82)	19.52 (20.14)	7.45 (7.1)
8	Violet	51.39 (51.11)	2.96 (2.86)	20.48 (19.8)	7.57 (7.32)
9	Violet	51.47 (51.67)	3.28 (3.05)	20.13 (19.48)	7.07(7.2)
10	Black-green	56.52 (56.7)	3.92 (3.64)	14.93 (15.51)	8.42 (8.6)

These results show that there should have an impurity in our compounds. After investigation of the iron precursor and ligands, we found a 7.21% deviation for iron from the elemental analysis of  $\text{Fe}_3(\text{CO})_{12}$ . This result shows us, that the deviation of elemental analysis comes from the iron precursor. As we understand from the results, the source of this deviation was not based on impurities. On the contrary of impurities, it is caused by error of  $\text{Fe}_3(\text{CO})_{12}$  content.

### 3.3 $^{13}\text{C}$ -NMR AND $^{31}\text{P}$ -NMR SPECTRA

The  $^{13}\text{C}$ -NMR data of compounds (1-11) were recorded with the help of Bruker AMX-400 and Bruker Avance 500c spectrometers (Table 15). In all of the iron carbonyls (**1-11**), the characteristic  $-\text{CO}$  carbons peaks were detected between at 229.02 and 203.3 ppm. The aliphatic carbons (P- $\text{CH}_2$ -P) of dpmm containing complexes were observed at 19.84 (**2**), 19.72 (**3**), 18.91(**4**), 24.25 and 23.43 (**7**),

respectively. The aliphatic carbons (P-CH<sub>2</sub>-C) of dppe and dppp containing complexes were detected at 19.73(**5**), 19.93(**6**), 23.00(**10**), 22.7, 21.96 (**8**) and 20.66(**9**). In dppp containing iron carbonyl cluster complexes, the aliphatic carbons (C-CH<sub>2</sub>-C) were observed at 29.67(**6**), 28.42(**10**) and 30.23(**9**). The signals of the aromatic carbons were detected in the expected region, and equal to the number in the proposed structures of compounds (2-11). The <sup>13</sup>C-NMR spectra of complexes, upfield chemical shifts were detected for the iron carbonyls carbon (-CO).

Table 15 <sup>13</sup>C-NMR spectral data. Chemical shifts (δ) are reported in ppm.

Comp.	CO	P-CH <sub>2</sub> -P	P-CH <sub>2</sub> -C	C-CH <sub>2</sub> -C	N-CH <sub>2</sub>	CH <sub>2</sub> -CH <sub>3</sub>
1	229.02	-	-	-	52.99	7.68
2	224.65, 203.3	19.84	-	-	-	-
3	223.16, 214.16	19.72	-	-	-	-
4	214.45	18.91	-	-	-	-
5	222.28	-	19.73	-	-	-
6	219.08	-	19.93	29.67	-	-
7	213.89	24.25, 23.43	-	-	-	-
8	211.84	-	22.7, 21.96	-	-	-
9	213.76	-	20.66	30.23	-	-
10	213.88	-	23.00	28.42	-	-
11	213.43	-	-	-	-	-

The <sup>31</sup>P-NMR spectra of iron carbonyl dpmm complexes (**2-4** and **7**), iron carbonyl dppe complexes (**5** and **8**), and iron carbonyl dppp complexes (**6**, **9** and **10**) show two singlet in expected area. The <sup>31</sup>P-NMR spectra of diphosphine complexes proved the fluxionality of iron carbonyl cluster complexes in a solution as in the bridge opening – bridge closing mechanism.

### 3.4 FT-IR SPECTRA

Selected IR data for the iron carbonyl cluster diphosphine complexes are listed in table 16. In metal carbonyl clusters, characteristic  $\nu(\text{C}=\text{O})$  vibrations were observed in between  $2120\text{-}1850\text{cm}^{-1}$  for terminal carbon monoxide and in between  $1850\text{-}1720\text{cm}^{-1}$  for  $\mu$ -bridging carbon monoxide. Phosphorus compounds with phenyl groups at phosphorus are marked by medium to strong intensity in between  $1480\text{-}1420\text{cm}^{-1}$  and in between  $1010\text{-}990\text{cm}^{-1}$ .

Table 16 IR spectra ( $4000\text{-}550\text{ cm}^{-1}$ ) of compounds (1-10)

Comp	$\nu(\text{CO})_{\text{terminal}}$	$\nu(\text{CO})_{\text{bridging}}$	$\nu(\text{P-C})_{\text{arom.}}$	$\nu(\text{P-C})_{\text{alip.}}$
1	2035w, 1924s	1760m, 1744m	-	-
2	2042w, 1993w, 1973w, 1955m, 1904s, 1875s, 1860s	1763w	1434m	1093m
3	2040s, 1989w, 1974s, 1940s, 1919s	1763s	1435m	1095m
4	2045s, 1973s, 1938s, 1918s	-	1437m	1095m
5	2047m, 1974m, 1924s, 1967s	-	1434s	1096m
6	2046s, 1973s, 1920s, 1904, 1877s, 1864s	-	1433s	1096m
7	2061s, 2042m, 2004w, 1975s, 1937s, 1903s	1760w, 1730m	1434s	1089s
8	2047s, 1976m, 1921s, 1865s	-	1434s	1095s
9	2046m, 1974s, 1916s, 1906s, 1879s	-	1435m	1097m
10	2046s, 2005m, 1972s, 1917s, 1879s	1777m, 1721m	1434s	1096s

Note: w, weak; m, medium; s, strong.

In the iron carbonyl cluster bis(diphenylphosphine) complexes (**2-10**), the aliphatic  $\nu(\text{P-C})$  was detected by one single band of medium to strong intensity in between  $1097\text{-}1086\text{cm}^{-1}$  and the aromatic  $\nu(\text{P-C})$  was detected by one single band of medium to strong intensity in between  $1437\text{-}1433\text{cm}^{-1}$ . The aliphatic  $\nu(\text{P-C})$  stretching vibrations of iron carbonyl cluster complexes were observed  $78\text{-}87\text{cm}^{-1}$  shifted to the right according to the aliphatic  $\nu(\text{P-C})$  stretching vibrations of the free ligands. These shifted aliphatic  $\nu(\text{P-C})$  stretching vibrations prove that iron carbonyl cluster attached to the diphosphine ligands as expected.

In iron carbonyl cluster diphosphine complexes (**1-10**), characteristic  $\nu(\text{C=O})$  vibrations were observed in between  $2061\text{-}1850\text{cm}^{-1}$  for terminal carbon monoxide and in between  $1850\text{-}1720\text{cm}^{-1}$  for  $\mu$ -bridging carbon monoxide. The FT-IR spectra of the **1**, **2**, **3**, **7**, and **10** exhibit  $\mu$ -bridging  $\nu(\text{CO})$  stretching vibration. Nevertheless the IR spectra of **4**, **5**, **6**, **8**, and **9** show any  $\mu$ -bridging  $\nu(\text{CO})$  stretching vibration in their solid state.

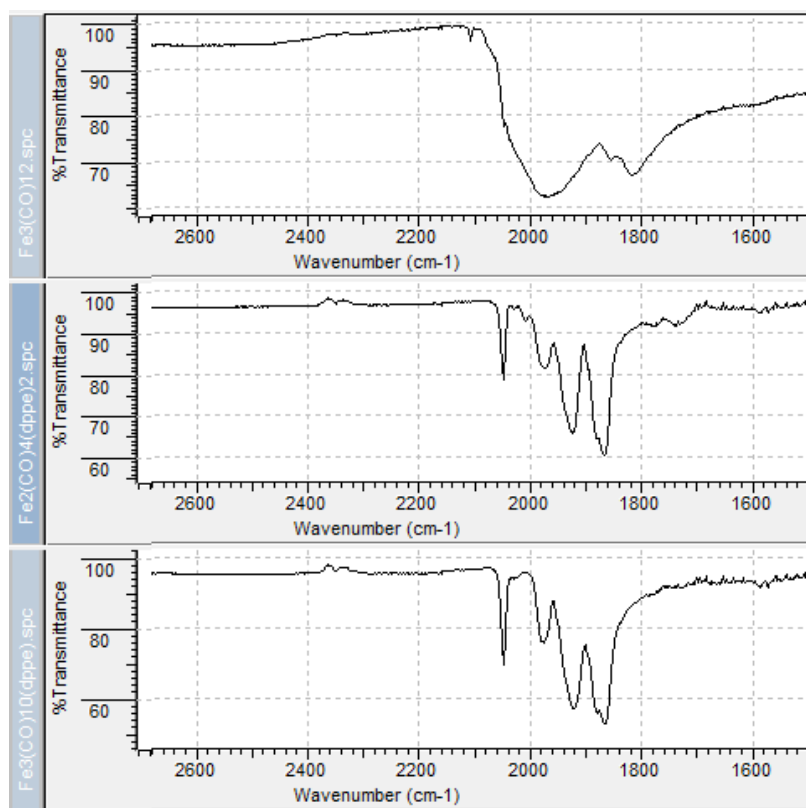


Figure 25  $\nu(\text{CO})$  stretching vibration a)  $\text{Fe}_3(\text{CO})_{12}$ , b)  $\text{Fe}_2(\text{CO})_4(\text{dppe})_2$ , and  $\text{Fe}_3(\text{CO})_{10}(\text{dppe})$

The FT-IR spectra of triiron dodecacarbonyl and its dppe complexes are compared in figure 25. When the carbon monoxide stretching vibrations of iron carbonyl clusters and their complexes are compared with each other, the four peaks of iron carbonyl cluster dppe complexes and two broad peaks of iron carbonyl were observed.  $\nu(\text{CO})$  characteristic stretching vibration of iron carbonyl clusters and the  $\nu(\text{CO})$  stretching vibrations of metal carbonyl phosphine offer the additional information about the formation of the iron carbonyl cluster phosphine complexes.

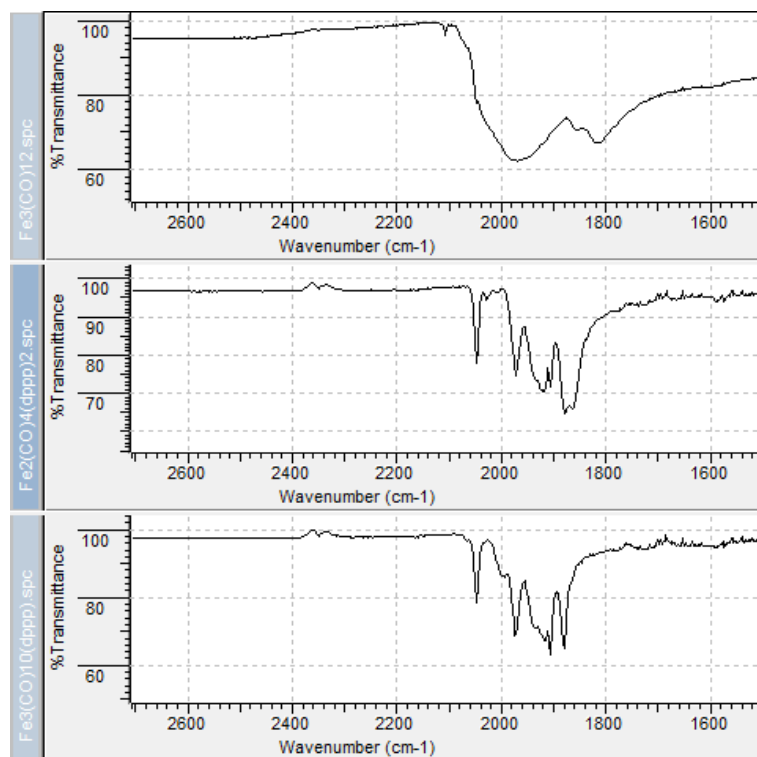


Figure 26  $\nu(\text{CO})$  stretching vibration a)  $\text{Fe}_3(\text{CO})_{12}$ , b)  $\text{Fe}_2(\text{CO})_4(\text{dppe})_2$ , and  $\text{Fe}_3(\text{CO})_{10}(\text{dppe})$

The FT-IR spectra of triiron dodecacarbonyl and its dppe complexes are compared too in figure 26. The carbon monoxide stretching vibrations of iron carbonyl clusters and their complexes are compared with each other and the four peaks of iron carbonyl cluster dppe complexes as iron carbonyl cluster dppe complexes and two broad peaks of iron carbonyl were detected. This results show, iron carbonyl cluster diphosphine complexes formed from the reaction of triiron dodecacarbonyl and dppe ligand. Furthermore, these IR-spectra of iron carbonyl dppe complexes prove that there isn't any unreacted iron carbonyl, dppe ligand and any another complexes.

### 3.5 X-RAY POWDER DIFFRACTIONS

To characterize of the synthesized iron carbonyl complexes were used powder X-ray diffraction in this study. As a scan type, 2Theta:Omega was used for all of the experiments, the scan mode and diffraction were decided as a transmission. The purpose of this section was to confirm the published structure and was to characterize of novel compounds with the help of 30 min X-ray scans. The diffraction patterns recorded by x-ray measurements are shown in tables 17-26 for the iron carbonyl complexes, respectively. All the patterns were fitted with a calculated structural profile using the refinement program WinXPOW.

#### 3.5.1 The Powder X-ray Structure of $[\text{Et}_4\text{N}]_2[\text{Fe}_6\text{C}(\text{CO})_{16}]$ (1)

This section describes the space group and the crystal system of  $[\text{Et}_4\text{N}]_2[\text{Fe}_6\text{C}(\text{CO})_{16}]$  (1). This powder diffraction patterns were isolated from experimental data presented in table 17. The diffraction pattern of it was fitted using Louër solution. By the help of the Louër solution, space group was obtained as ‘P 21 2 2 (-c, b, a)’ and the crystal system was defined as ‘orthorhombic’. The details of the diffraction data given in table 17 and the crystal structure of it was described by previous researchers.

Table 17 The result of the Louër solution for  $[\text{Et}_4\text{N}]_2[\text{Fe}_6\text{C}(\text{CO})_{16}]$  (1)

$[\text{Et}_4\text{N}]_2[\text{Fe}_6\text{C}(\text{CO})_{16}]$ (1)	
<b>Crystal System</b>	Orthorhombic
<b>Space Group</b>	P 21 2 2 (-c, b, a)
<b>a (Å)</b>	13.21 (8) Å
<b>b (Å)</b>	9.83 (6) Å
<b>c (Å)</b>	9.52 (5) Å
<b>Unind.</b>	2
<b>Zshift (R-factor)</b>	-0,095

A total of 6 peaks and 51 calculated peaks were refined, which included two errors by the Louër solution. The orthorhombic form of  $[\text{Et}_4\text{N}]_2[\text{Fe}_6\text{C}(\text{CO})_{16}]$  (1) was described within an input file to be refined.

### 3.5.2 The Powder X-ray Structure of $\text{Fe}_2(\text{CO})_4(\mu\text{-CO})(\mu,\eta^2\text{-dppm})_2$ (2)

The space group and the crystal system of  $[\text{Fe}_2(\text{CO})_4(\mu\text{-CO})(\mu,\eta^2\text{-dppm})_2]$  (2) will be described in detail according to the powder XRD experimental data. These XRD powder parameters are presented in table 18. The diffraction pattern of it was fitted using Visser solution. With the help of the using solution, space group was detected as ‘P 2’ and the crystal system was defined as ‘monoclinic’ structure. The details of the diffraction data were given in table 18.

Table 18 The result of the Visser solution for  $\text{Fe}_2(\text{CO})_4(\mu\text{-CO})(\mu,\eta^2\text{-dppm})_2$  (2)

$\text{Fe}_2(\text{CO})_4(\mu\text{-CO})(\mu,\eta^2\text{-dppm})_2$ (2)	
<b>Crystal System</b>	Orthorhombic
<b>Space Group</b>	P 2
<b>a (Å)</b>	9.91 (7) Å
<b>b (Å)</b>	2.795 (20) Å
<b>c (Å)</b>	14.33 (19) Å
<b>Unind.</b>	1
<b>Zshift (R-factor)</b>	-0,154

All 14 peaks were obtained from the experimental data's and 206 peaks were calculated with one error by the Visser solution. The monoclinic form of  $\text{Fe}_2(\text{CO})_4(\mu\text{-CO})(\mu,\eta^2\text{-dppm})_2$  (2) was described within an input file to be refined.

### 3.5.3 The Powder X-ray Structure of $\text{Fe}_2(\text{CO})_4(\mu\text{-CO})_3(\mu,\eta^2\text{-dppm})$ (3)

In this section, the space group and the crystal system of binucleic complex,  $\text{Fe}_2(\text{CO})_4(\mu\text{-CO})_3(\mu,\eta^2\text{-dppm})$  (3), will be explained. These XRD powder parameters were detected from experimental data, which is presented in table 19. The diffraction pattern of it was fitted using Louër solution. By the help of the Louër solution, space group was obtained as ‘P 2’ and the crystal system was defined as ‘monoclinic’ structure. The details of the diffraction data were given in table 19.



Table 19 The Louër solution for  $\text{Fe}_2(\text{CO})_4(\mu\text{-CO})_3(\mu,\eta^2\text{-dppm})$  (3)

<b><math>\text{Fe}_2(\text{CO})_4(\mu\text{-CO})_3(\mu,\eta^2\text{-dppm})</math> (3)</b>	
<b>Crystal System</b>	Monoclinic
<b>Space Group</b>	P 2
<b>a (Å)</b>	8.9 (29) Å
<b>b (Å)</b>	9.0 (29) Å
<b>c (Å)</b>	9.3 (30) Å
<b>Unind.</b>	2
<b>Zshift (R-factor)</b>	-0,012

Totally, 13 peaks and 305 calculated peaks were detected from the diffraction of  $\text{Fe}_2(\text{CO})_4(\mu\text{-CO})_3(\mu,\eta^2\text{-dppm})$  (3), which included one error by the Louër solution. The monoclinic form of this complex was described within an input file to be refined.

### 3.5.4 The Powder X-ray Structure of $\text{Fe}(\text{CO})_4(\eta^1\text{-dppm})$ (4)

The space group and the crystal system of the  $\text{Fe}(\text{CO})_4(\eta^1\text{-dppm})$  (4) complex will be described here. The XRD powder parameters of mono iron dppm complex were obtained from experimental data and these results are presented in table 20.

Table 20 The result of the Louër solution for  $\text{Fe}(\text{CO})_4(\eta^1\text{-dppm})$  (4)

<b><math>\text{Fe}(\text{CO})_4(\eta^1\text{-dppm})</math> (4)</b>	
<b>Crystal System</b>	Monoclinic
<b>Space Group</b>	P 2
<b>a (Å)</b>	10.79 (7) Å
<b>b (Å)</b>	4.85 (3) Å
<b>c (Å)</b>	12.39 (8) Å
<b>Unind.</b>	4
<b>Zshift (R-factor)</b>	-0,079

The diffraction pattern of mono iron carbonyl dpmm complex was fitted using Louër solution. By the help of this calculation, space group was detected as ‘P 2’ and the crystal system was defined as ‘monoclinic’. The details of the diffraction data were given in table 20.

In all of 15 peaks were detected and 314 peaks were calculated, which included four errors by the Louër solution. The monoclinic form of  $\text{Fe}(\text{CO})_4(\eta^1\text{-dpmm})$  (**4**) was described within an input file to be refined.

### 3.5.5 The Powder X-ray Structure of $\text{Fe}_2(\text{CO})_4(\mu,\eta^2\text{-dppe})_2$ (**5**)

In this section, the space group and the crystal system of  $\text{Fe}_2(\text{CO})_4(\mu,\eta^2\text{-dppe})_2$  (**5**) will be discussed in detail. The parameters of the powder X-ray diffraction were detected from experimental data, which are shown in table 21. The diffraction pattern of it was fitted using Werner solution. By the help of the calculation, space group was calculated as ‘P 2’ and the crystal system was determined as ‘monoclinic’, which is same as all bimetallic iron carbonyl cluster complexes. The details of the powder X-ray diffraction results were given in table 21.

Table 21 The Werner solution for  $\text{Fe}_2(\text{CO})_4(\mu,\eta^2\text{-dppe})_2$  (**5**)

<b><math>\text{Fe}_2(\text{CO})_4(\mu,\eta^2\text{-dppe})_2</math> (<b>5</b>)</b>	
<b>Crystal System</b>	Monoclinic
<b>Space Group</b>	P 2
<b>a (Å)</b>	12.56 Å
<b>b (Å)</b>	10.59 Å
<b>c (Å)</b>	15.05 Å
<b>Unind.</b>	2
<b>Zshift (R-factor)</b>	0,023

Totally, 15 peaks were detected and 547 calculated peaks were obtained from the diffraction of  $\text{Fe}_2(\text{CO})_4(\mu,\eta^2\text{-dppe})_2$  (**5**), which included two errors by the Werner solution. The monoclinic form of  $\text{Fe}_2(\text{CO})_4(\mu,\eta^2\text{-dppe})_2$  (**5**) was described within an input file to be refined.

### 3.5.6 The Powder X-ray Structure of $\text{Fe}_2(\text{CO})_4(\mu, \eta^2\text{-dppp})_2$ (6)

In this section, the crystal system and the space group of  $\text{Fe}_2(\text{CO})_4(\mu, \eta^2\text{-dppp})_2$  (6) will be discussed in detail. The powder XRD parameters were detected from experimental data, and they are shown in the following table 22. The diffraction pattern of it was collected with the help of Werner solution. The space group was calculated as 'P 2' and the crystal system was determined as 'monoclinic'. The space group of  $\text{Fe}_2(\text{CO})_4(\mu, \eta^2\text{-dppp})_2$  (6) is same as  $\text{Fe}_2(\text{CO})_5(\mu, \eta^2\text{-dppm})_2$  (2) and  $\text{Fe}_2(\text{CO})_4(\mu, \eta^2\text{-dppe})_2$  (5). The details of the diffraction data were given in table 22.

Table 22 The Werner solution of  $\text{Fe}_2(\text{CO})_4(\mu, \eta^2\text{-dppp})_2$  (6)

<b><math>\text{Fe}_2(\text{CO})_4(\mu, \eta^2\text{-dppp})_2</math> (6)</b>	
<b>Crystal System</b>	Monoclinic
<b>Space Group</b>	P 2
<b>a (Å)</b>	8.6 (7) Å
<b>b (Å)</b>	8.5 (7) Å
<b>c (Å)</b>	9.6 (8) Å
<b>Unind.</b>	2
<b>Zshift (R-factor)</b>	-0,061

Totally, 9 peaks were obtained from the experimental diffraction of  $\text{Fe}_2(\text{CO})_4(\mu, \eta^2\text{-dppp})_2$  (6) and 104 peaks were determined with two errors by the Werner solution. The monoclinic form of  $\text{Fe}_2(\text{CO})_4(\mu, \eta^2\text{-dppp})_2$  (6) was described within an input file to be refined.

### 3.5.7 The Powder X-ray Structure of $\text{Fe}_3(\text{CO})_8(\mu\text{-CO})_2(\mu, \eta^2\text{-dppm})$ (7)

The space group and the crystal system of  $[\text{Fe}_3(\text{CO})_8(\mu\text{-CO})_2(\mu, \eta^2\text{-dppm})]$  (7) will be explained as detail in this section. The powder X-ray diffraction parameters were obtained from experimental data's and the data's are presented in following table 23. The diffraction pattern of trinucleic iron diphosphine complex was calculated using Werner solution. By the help of the using solution, space group was detected as 'P c'

and the crystal system was defined as ‘orthorhombic’. The details of the diffraction data were given in table 23.

Table 23 The result of the Werner calculation for  $\text{Fe}_3(\text{CO})_8(\mu\text{-CO})_2(\mu,\eta^2\text{-dppm})$  (7)

$\text{Fe}_3(\text{CO})_8(\mu\text{-CO})_2(\mu,\eta^2\text{-dppm})$ (6)	
<b>Crystal System</b>	Orthorhombic
<b>Space Group</b>	P c
<b>a (Å)</b>	8.66 Å
<b>b (Å)</b>	10.40 Å
<b>c (Å)</b>	12.09 Å
<b>Unind.</b>	2
<b>Zshift (R-factor)</b>	0,010

Fifteen peaks were refined and 481 peaks calculated using Werner solution, which included two errors. The orthorhombic form of  $\text{Fe}_3(\text{CO})_8(\mu\text{-CO})_2(\mu,\eta^2\text{-dppm})$  (7) was described within an input file to be refined.

### 3.5.8 The Powder X-ray Structure of $\text{Fe}_3(\text{CO})_8(\mu\text{-CO})_2(\mu,\eta^2\text{-dppe})$ (8)

The crystal system and the space group of  $\text{Fe}_3(\text{CO})_8(\mu\text{-CO})_2(\mu,\eta^2\text{-dppe})$  (8) will be dealt in this section. The parameters of the X-ray powder diffraction were obtained from experimental data, and the results are shown in the following table 24.

Table 24 The result of Werner solution for  $\text{Fe}_3(\text{CO})_8(\mu\text{-CO})_2(\mu,\eta^2\text{-dppe})$  (8)

$\text{Fe}_3(\text{CO})_8(\mu\text{-CO})_2(\mu,\eta^2\text{-dppe})$ (8)	
<b>Crystal System</b>	Orthorhombic
<b>Space Group</b>	P 2 2 2
<b>a (Å)</b>	9.14 (18) Å
<b>b (Å)</b>	8.53 (17) Å
<b>c (Å)</b>	7.35 (13) Å
<b>Unind.</b>	2
<b>Zshift (R-factor)</b>	-0,022

The diffraction pattern of iron complex was collected using Werner solution and the space group was calculated as ‘P 2 2 2’ and the crystal system was determined as ‘orthorhombic’. The details of the diffraction data were given in table 24.

Seven peaks were detected and 165 peaks were calculated using Werner solution from the diffraction of  $\text{Fe}_3(\text{CO})_8(\mu\text{-CO})_2(\mu,\eta^2\text{-dppe})$  (**8**), which included two errors. The orthorhombic form of  $\text{Fe}_3(\text{CO})_8(\mu\text{-CO})_2(\mu,\eta^2\text{-dppe})$  (**8**) was described within an input file to be refined.

### 3.5.9 The Powder X-ray Structure of $\text{Fe}_3(\text{CO})_8(\mu\text{-CO})_2(\mu,\eta^2\text{-dppp})$ (**9**)

In this section, the crystal system and the space group of  $\text{Fe}_3(\text{CO})_8(\mu\text{-CO})_2(\mu,\eta^2\text{-dppp})$  (**9**) will be discussed in detail. The parameters of the powder X-ray diffraction were obtained from experimental data, which shown in the following table 25. The diffraction pattern of trinucleic iron dppp complex was collected and calculated with the help of Werner solution. The space group was defined as ‘P c m 21 (b, a, -c)’ and the crystal system was determined ‘orthorhombic’ as the other trinucleic dppm and dppe complexes. The details of the diffraction data were given in table 25.

Table 25 The result of the Werner solution for  $\text{Fe}_3(\text{CO})_8(\mu\text{-CO})_2(\mu,\eta^2\text{-dppp})$  (**9**)

$\text{Fe}_3(\text{CO})_8(\mu\text{-CO})_2(\mu,\eta^2\text{-dppp})$ ( <b>9</b> )	
<b>Crystal System</b>	Orthorhombic
<b>Space Group</b>	P c m 21 (b, a, -c)
<b>a (Å)</b>	14.59 (23) Å
<b>b (Å)</b>	11.15 (17) Å
<b>c (Å)</b>	10.57 (16) Å
<b>Unind.</b>	1
<b>Zshift (R-factor)</b>	-0,005

A total of 10 peaks were obtained and 441 peaks were calculated with the help of Werner solution from the diffraction of  $\text{Fe}_3(\text{CO})_8(\mu\text{-CO})_2(\mu,\eta^2\text{-dppp})$  (**9**), which included one error. The monoclinic form of  $\text{Fe}_3(\text{CO})_8(\mu\text{-CO})_2(\mu,\eta^2\text{-dppp})$  (**9**) was described within an input file to be refined.

### 3.5.10 The Powder X-ray Structure of $\text{Fe}_2(\text{CO})_4(\mu\text{-CO})_3(\mu,\eta^2\text{-dppp})$ (10)

The crystal system and the space group of  $\text{Fe}_2(\text{CO})_4(\mu\text{-CO})_3(\mu,\eta^2\text{-dppp})$  (10) will be discussed in this section. The parameters of the X-ray powder diffraction were obtained from experimental data, and the results are exhibited in the table 26. The diffraction pattern of iron complex was collected with the help of Louër solution. The space group was calculated as ‘P 2 2 2’ and the crystal system was determined as ‘monoclinic’. The details of the diffraction data were given in table 26.

Table 26 The Louër calculation of  $\text{Fe}_2(\text{CO})_4(\mu\text{-CO})_3(\mu,\eta^2\text{-dppp})$  (10)

$\text{Fe}_2(\text{CO})_4(\mu\text{-CO})_3(\mu,\eta^2\text{-dppp})$ (10)	
<b>Crystal System</b>	Orthorhombic
<b>Space Group</b>	P 2 2 2
<b>a (Å)</b>	14.25 (3) Å
<b>b (Å)</b>	12.84 (3) Å
<b>c (Å)</b>	10.93 (3) Å
<b>Unind.</b>	2
<b>Zshift (R-factor)</b>	0,080

Sixteen peaks were detected and 495 peaks were calculated using Louër solution from the diffraction of  $\text{Fe}_2(\text{CO})_4(\mu\text{-CO})_3(\mu,\eta^2\text{-dppp})$  (10), which included two errors. The orthorhombic form of  $\text{Fe}_2(\text{CO})_4(\mu\text{-CO})_3(\mu,\eta^2\text{-dppp})$  (10) was described within an input file to be refined.

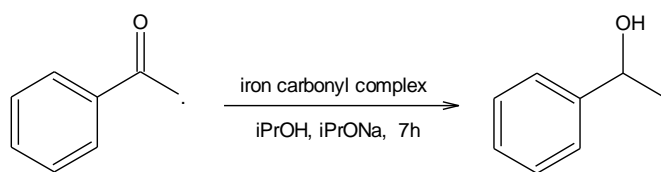
### 3.6 APPLICATION OF TRANSFER HYDROGENATION

In the homogeneous catalyst, the catalytic reduction of ketones by use of the transition metals and their complexes take an important role for the produce of alcohols for use in the pharmaceutical, fragrances, agrochemicals and flavours industry (Meyer, 2009). For this reason, iron carbonyls complexes were synthesized from the reaction between iron carbonyls and dppx ligands and were characterized by the help of spectroscopic techniques. The catalytic behaviour of synthesized iron carbonyl complexes was examined to obtain alcohol from ketones in the transfer hydrogenation. In addition, the effect of coordinating ligands on the catalyst stability and functionality is investigated. We researched the effect of catalyst, ligands, base, amount of hydrogen source and solvent to optimize the catalytic reaction.

The  $\text{Fe}(\text{CO})_5$ ,  $\text{Fe}_2(\text{CO})_9$ ,  $\text{Fe}_3(\text{CO})_{12}$ ,  $(\text{Et}_4\text{N})_2[\text{Fe}_6\text{C}(\text{CO})_{16}]$  and their complexes (**2–11**), were investigated for their ability to serve as catalysts for the  $>\text{C}=\text{O}$  reduction of acetophenone under the conditions of transfer hydrogenation. In order to examine the factors influencing the catalytic performance, the reaction parameters (temperature, reaction time, and catalysts) were determined by GC without further purification.

#### 3.6.1 Optimization of Iron-Catalysed Transfer Hydrogenation of Ketone

The reduction of acetophenone to 1-phenylethanol was chosen as a model reaction to explore the catalytic behaviours of iron complexes using isopropanol as the hydrogen source in the presence of *i*PrONa as base. Isopropanol-based transfer hydrogenation of ketone was examined with iron contained catalysts. Ketone, base, catalyst and solvent ratio was optimized by varying the relative molar equivalents.



Scheme 21 Carbonyl hydrogen transfer reduction

##### 3.6.1.1 Optimization of Base Concentration

Different amount of base were examined to determine influence of sodium isopropoxide in transfer hydrogenation. In this reason, the catalyst and the base amount were chosen in ratio of 1÷1, 1÷2, 1÷5, 1÷10, 1÷20, and 1÷25.  $\text{Fe}_3(\text{CO})_{12}$  and

$\text{Fe}_2(\text{CO})_4(\mu\text{-CO})(\mu,\eta^2\text{-dppm})_2$  (**2**) clusters were used as the catalyst to optimize base concentration. The reactions were monitored over time by GC analysis, and the conversions of acetophenone were calculated as it is shown in the following table 27 and 28.

Table 27 Influence of base in the  $\text{Fe}_3(\text{CO})_{12}$ -catalyzed transfer hydrogenation of acetophenone

<b>Number of equivalents</b>					
<b>Entry</b>	<b><math>\text{Fe}_3(\text{CO})_{12}</math></b>	<b>iPrONa</b>	<b>iPrOH</b>	<b>Conversion %</b>	<b>Selectivity %</b>
<b>1</b>	-	1	500	39,6	49,7
<b>2</b>	-	2	500	41,8	45,8
<b>3</b>	-	5	500	52,7	76,3
<b>4</b>	-	25	500	90,2	73,8
<b>5</b>	1	1	500	20,1	<1
<b>6</b>	1	2	500	20,6	<1
<b>7</b>	1	5	500	30,3	24
<b>8</b>	1	25	500	91,7	89,9

(i) Reaction condition: the catalyst (0,025mmol), ketone (2,5 mmol), isopropanol (12,5mmol), 7 hour, 82°C.

From the result of transfer hydrogenation experiments using  $\text{Fe}_3(\text{CO})_{12}$  as a catalyst, increase of the base concentration increases the conversion of acetophenone and selectivity. The catalytic activity of iron carbonyl was obtained from the ratio of 1÷25.  $\text{Fe}_3(\text{CO})_{12}$  did not show any catalytic activity in other ratio. Additionally, triiron dodecacarbonyl decreases the conversation of acetophenone and selectivity.



Table 28 Influence of base in the  $\text{Fe}_2(\text{CO})_4(\mu\text{-CO})(\mu,\eta^2\text{-dppm})_2$  (2)-catalyzed transfer hydrogenation of acetophenone

<b>Number of equivalents</b>					
<b>Entry</b>	<b><math>\text{Fe}_2(\text{CO})_5(\text{dppm})_2</math></b>	<b>iPrONa</b>	<b>iPrOH</b>	<b>Conversion %</b>	<b>Selectivity %</b>
1	-	1	500	39,6	49,7
2	-	5	500	52,7	76,3
13	-	10	500	85,7	58,8
14	-	20	500	90,6	67,6
15	1	1	500	55,5	59,6
16	1	5	500	77,8	46,5
17	1	10	500	86,2	56,4
18	1	20	500	91,7	89,9

(i) Reaction condition: the catalyst (0,025mmol), ketone (2,5 mmol), isopropanol (12,5mmol), 7 hour, 82°C.

From the result of transfer hydrogenation experiments using  $\text{Fe}_2(\text{CO})_4(\mu\text{-CO})(\mu,\eta^2\text{-dppm})_2$  (2) as a catalyst, increase of base concentration increases the conversion of acetophenone and selectivity too. The conversion of acetophenone was obtained 85,7 % in entry 13 and 90,6 % in entry 14. Increasing of the base concentration does not play any reasonable role in transfer hydrogenation after the ratio of 1÷10. The best catalytic activity of iron carbonyl bisphosphine cluster was obtained from the ratio of 1÷5 (Catalyst-Base).  $\text{Fe}_2(\text{CO})_4(\mu\text{-CO})(\mu,\eta^2\text{-dppm})_2$  (2) shown poor catalytic activity in ratio 1÷10 and 1÷20.

As a result, triiron dodecacarbonyl did not show catalytic activity in reduction of acetophenone using isopropanol as a hydrogen source. On the contrary of  $\text{Fe}_3(\text{CO})_{12}$ ,  $\text{Fe}_2(\text{CO})_4(\mu\text{-CO})(\mu,\eta^2\text{-dppm})_2$  (2) observed good catalytic activity in every ratio of catalyst-base.

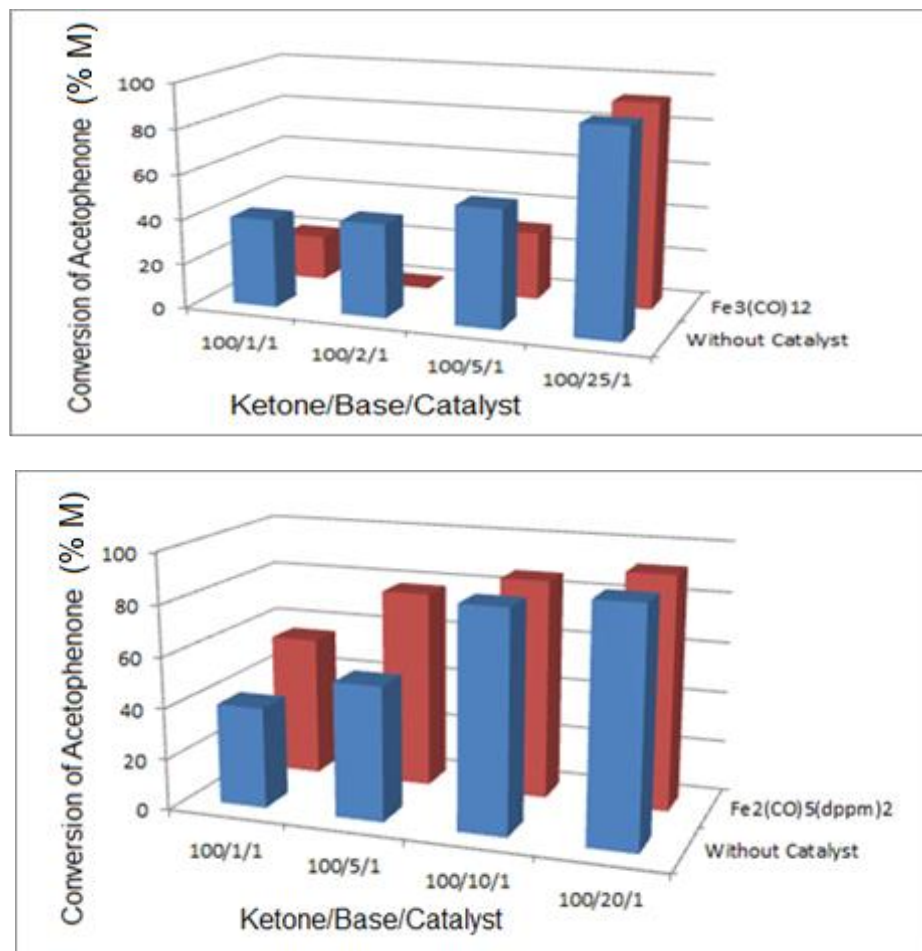


Diagram 3 Comparison of base amount and Fe<sub>3</sub>(CO)<sub>12</sub> and Fe<sub>2</sub>(CO)<sub>5</sub>(dppm)<sub>2</sub>(2) (ketone/base/catalyst (molar equivalent))

The reduction of acetophenone was resulted better without iron carbonyl such as Fe(CO)<sub>5</sub>, Fe<sub>2</sub>(CO)<sub>9</sub> and Fe<sub>3</sub>(CO)<sub>12</sub>. The entry 5, 7, 22, 23, 24 and 25 (Table 29) show the activity of iron carbonyl clusters, that they decrease the conversion of the acetophenone and reaction selectivity.

High conversions were obtained, when Fe<sub>2</sub>(CO)<sub>4</sub>(μ-CO)(μ,η<sup>2</sup>-dppm)<sub>2</sub> (**2**) and [Fe<sub>6</sub>C(CO)<sub>16</sub>]<sup>2-</sup> (**1**) were used as a catalyst. Entries 15, 16, 17, 18, 26 and 27 show us, that the Fe<sub>2</sub>(CO)<sub>4</sub>(μ-CO)(μ,η<sup>2</sup>-dppm)<sub>2</sub> (**2**) and [Fe<sub>6</sub>C(CO)<sub>16</sub>]<sup>2-</sup> (**1**) complexes increase the conversion of acetophenone. We found, that the best activity for the Fe<sub>2</sub>(CO)<sub>4</sub>(μ-CO)(μ,η<sup>2</sup>-dppm)<sub>2</sub>(**2**) complex was obtained from the ratio of 100:5:1 (Ketone:Base:Catalyst). In this ratio, the complex shows excellent activity.

Table 29 Influence of base amount with different iron carbonyl complexes in transfer hydrogenation of acetophenone

<b>Number of equivalents</b>					
<b>Entry</b>	<b>Catalyst</b>	<b><i>i</i>PrONa</b>	<b><i>i</i>PrOH</b>	<b>Conversion %</b>	<b>Selectivity %</b>
22	Fe(CO) <sub>5</sub>	1	500	10,5	≤1
23	Fe(CO) <sub>5</sub>	5	500	11,2	≤1
24	Fe <sub>2</sub> (CO) <sub>9</sub>	1	500	9,3	≤1
25	Fe <sub>2</sub> (CO) <sub>9</sub>	5	500	49,3	11,5
5	Fe <sub>3</sub> (CO) <sub>12</sub>	1	500	20,1	≤1
7	Fe <sub>3</sub> (CO) <sub>12</sub>	5	500	30,3	24,0
26	[Fe <sub>6</sub> C(CO) <sub>16</sub> ] <sup>2-</sup>	1	500	37,5	31,0
27	[Fe <sub>6</sub> C(CO) <sub>16</sub> ] <sup>2-</sup>	5	500	70,9	54,3
15	Fe <sub>2</sub> (CO) <sub>5</sub> (dppm) <sub>2</sub>	1	500	55,5	59,6
16	Fe <sub>2</sub> (CO) <sub>5</sub> (dppm) <sub>2</sub>	5	500	77,8	46,5

(i) Reaction condition: the catalyst (0,025mmol), ketone (2,5 mmol), isopropanol (12,5mmol), 7 hour, 82°C.

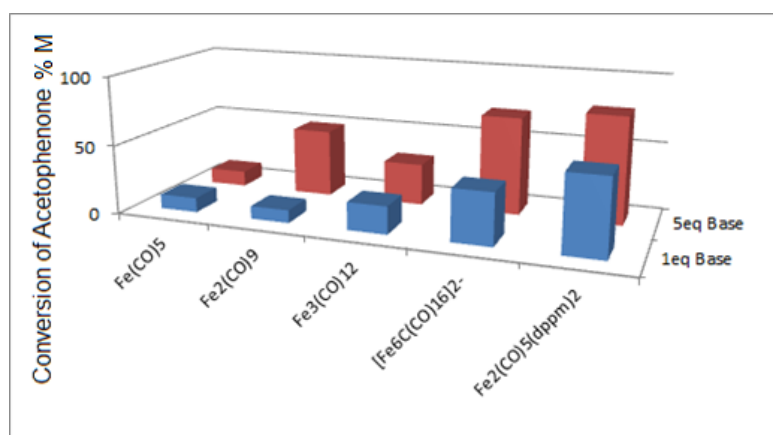


Diagram 4 Comparison of base amount and iron carbonyl complexes (ketone/base/catalyst (molar equivalent))

### 3.6.1.2 Choosing the Well Solvent of Transfer Hydrogenation

The reduction of acetophenone to 1-phenylethanol was chosen as a model reaction to optimize the influence of solvents using isopropanol as the hydrogen source in the presence of *i*PrONa as base. Seven different solvents were compared with each other to find a best solvent for reduction of acetophenone. The best results were obtained from isopropanol as a pure solvent and hydrogen source. The reactions were monitored over time by GC analysis, and the conversion of acetophenone was determined calculated as it is shown in the following table 30.

Table 30 Influence of solvent in transfer hydrogenation of acetophenone

Number of equivalents						
Entry	Catalyst	<i>i</i> PrONa	<i>i</i> PrOH / Solvent		Con. %	Selec. %
2	-	5	<i>i</i> PrOH	<i>i</i> PrOH	52,7	76,3
16	Fe <sub>2</sub> (CO) <sub>5</sub> (dppm) <sub>2</sub>	5	<i>i</i> PrOH	<i>i</i> PrOH	77,8	46,5
38	-	5	<i>i</i> PrOH	DMF	22,3	≤1
39	Fe <sub>2</sub> (CO) <sub>5</sub> (dppm) <sub>2</sub>	5	<i>i</i> PrOH	DMF	19,5	≤1
40	-	5	<i>i</i> PrOH	Acetonitrile	69,3	18,1
41	Fe <sub>2</sub> (CO) <sub>5</sub> (dppm) <sub>2</sub>	5	<i>i</i> PrOH	Acetonitrile	35,1	12,4
42	-	5	<i>i</i> PrOH	Diglyme	70,0	23,4
43	Fe <sub>2</sub> (CO) <sub>5</sub> (dppm) <sub>2</sub>	5	<i>i</i> PrOH	Diglyme	39,4	12,0
44	-	5	<i>i</i> PrOH	Acetone	50,3	3,7
45	Fe <sub>2</sub> (CO) <sub>5</sub> (dppm) <sub>2</sub>	5	<i>i</i> PrOH	Acetone	41,0	≤1
46	-	5	<i>i</i> PrOH	THF	71,1	25,9
47	Fe <sub>2</sub> (CO) <sub>5</sub> (dppm) <sub>2</sub>	5	<i>i</i> PrOH	THF	50,5	18,2
48	-	5	<i>i</i> PrOH	DCM	37,1	6,1
49	Fe <sub>2</sub> (CO) <sub>5</sub> (dppm) <sub>2</sub>	5	<i>i</i> PrOH	DCM	37,8	≤1

(i) Reaction condition: the catalyst (0,025mmol), ketone (2,5 mmol), sodium isopropylate (0,125mmol), isopropanol (2,5mmol), solvent (10mmol), 7 hour, 82°C.

DMF, acetonitrile, diglyme, acetone, THF decrease the catalytic activity of  $\text{Fe}_2(\text{CO})_4(\mu\text{-CO})(\mu,\eta^2\text{-dppm})_2$  (**2**). The lowest catalytic activity of iron carbonyl bisphosphine cluster was determined in solution of isopropanol and DCM. Dichloromethane as a solvent increases the conversion of acetophenone just 0.7 percent. Entry 48 and 49 show the catalytic activity of  $\text{Fe}_2(\text{CO})_4(\mu\text{-CO})(\mu,\eta^2\text{-dppm})_2$  (**2**) in DCM. The high conversions were obtained, when isopropanol were used as a solvent too. The entry 2 and 16 show, that the  $\text{Fe}_2(\text{CO})_4(\mu\text{-CO})(\mu,\eta^2\text{-dppm})_2$  (**2**) cluster have activity for the reduction of acetophenone. We found, that the best activity for the  $\text{Fe}_2(\text{CO})_4(\mu\text{-CO})(\mu,\eta^2\text{-dppm})_2$  (**2**) was obtained from the isopropanol, and the complex shows significant catalytic activity in isopropanol.

### 3.6.1.3 Optimization of Solvent Concentration

To optimize the influence of isopropanol concentration in reduction of acetophenone, different concentrations of the isopropanol were examined. In this reason, the catalyst and the solvent concentration were chosen in ratio of 1÷100, 1÷500, 1÷1000, and 1÷2000 for  $\text{Fe}_3(\text{CO})_{12}$  (Catalyst-Solvent). Also, the catalyst and the solvent concentration were chosen in ratio of 1÷100, 1÷500, and 1÷1000 for  $\text{Fe}_2(\text{CO})_4(\mu\text{-CO})(\mu,\eta^2\text{-dppm})_2$  (**2**) (Catalyst-Solvent). The reactions were monitored over time by GC analysis, and the conversion of acetophenone was calculated as it is shown in the following table 31 and 32.

Table 31 Influence of solvent in the  $\text{Fe}_3(\text{CO})_{12}$ -catalyzed transfer hydrogenation of acetophenone

<b>Number of equivalents</b>					
<b>Entry</b>	<b><math>\text{Fe}_3(\text{CO})_{12}</math></b>	<b>iPrONa</b>	<b>iPrOH</b>	<b>Conversion%</b>	<b>Selectivity%</b>
<b>9</b>	1	5	100	33,8	<1
<b>10</b>	1	5	500	30,3	24
<b>11</b>	1	5	1000	14,2	13,7
<b>12</b>	1	5	2000	11,3	<1

(i) Reaction condition: the catalyst (0,025mmol), ketone (2,5 mmol), sodium isopropylate (0,125mmol), 7 hour, 82°C.

Table 32 Influence of base and solvent in the  $\text{Fe}_2(\text{CO})_4(\mu\text{-CO})(\mu,\eta^2\text{-dppm})_2$  (**2**)-catalyzed transfer hydrogenation of acetophenone

<b>Number of equivalents</b>					
<b>Entry</b>	<b><math>\text{Fe}_2(\text{CO})_5(\text{dppm})_2</math></b>	<b>iPrONa</b>	<b>iPrOH</b>	<b>Conversion%</b>	<b>Selectivity%</b>
<b>19</b>	1	5	100	40,7	7,1
<b>20</b>	1	5	500	77,8	46,5
<b>21</b>	1	5	1000	29,1	16,3

(i) Reaction condition: the catalyst (0,025mmol), ketone (2,5 mmol), sodium isopropylate (0,125mmol), 7 hour, 82°C.

We obtained the best activity and chemoselectivity from 1 mmol ketone, 5% base, 1% catalyst and 5 mmol solvent (100:25:1:500). The results show, that the catalyst is more effective in ratio of 1÷5 (ketone/isopropanol). Triiron dodecacarbonyl and  $\text{Fe}_2(\text{CO})_4(\mu\text{-CO})(\mu,\eta^2\text{-dppm})_2$  (**2**) as a catalysts in transfer hydrogenation show different activity. Although the increase of solvent volume reduces the conversion, when triiron dodecacarbonyl is used as the catalyst; the increase of solvent volume raised conversion at first, when  $\text{Fe}_2(\text{CO})_4(\mu\text{-CO})(\mu,\eta^2\text{-dppm})_2$  (**2**) is used as a catalyst. The optimum solvent concentration was determined in ratio of 1÷5 (ketone/solvent) with using  $\text{Fe}_2(\text{CO})_4(\mu\text{-CO})(\mu,\eta^2\text{-dppm})_2$  as a catalyst.

### 3.6.2 Different Iron Carbonyl Precursors

In our research, we focused on identifying the catalytic feature of iron carbonyl cluster complexes, which contains 1,1-Bis(diphenylphosphino)methane, 1,2-Bis(diphenylphosphino)ethane and 1,3-Bis(diphenylphosphino)propane as ligands. The iron carbonyl cluster complexes show significant catalytic activity in reduction of acetophenone to 1-phenylethanol (Table 33). We decided to examine the catalytic activity of the mono-nuclear, bi-nuclear and tri-nuclear complexes in transfer hydrogenation. The reactions were monitored over time by GC analysis, and the conversion of acetophenone was determined.

Table 33 Influence of the iron carbonyl complexes in transfer hydrogenation of acetophenone

<b>Number of equivalents</b>					
<b>Entry</b>	<b>Catalyst</b>	<b><i>i</i>PrONa</b>	<b><i>i</i>PrOH</b>	<b>Conversion %</b>	<b>Selectivity %</b>
16	Fe <sub>2</sub> (CO) <sub>5</sub> (dppm) <sub>2</sub>	5	500	77,8	46,5
28	Fe <sub>2</sub> (CO) <sub>7</sub> (dppm)	5	500	51,2	60,9
29	Fe(CO) <sub>4</sub> (dppm)	5	500	64,2	58,7
30	Fe <sub>2</sub> (CO) <sub>4</sub> (dppe) <sub>2</sub>	5	500	75,5	36,8
31	Fe <sub>2</sub> (CO) <sub>4</sub> (dppp) <sub>2</sub>	5	500	78,3	40,7
32	Fe <sub>2</sub> (CO) <sub>7</sub> (dppp)	5	500	63,1	50,7
33	Fe <sub>3</sub> (CO) <sub>10</sub> (dppm)	5	500	59,1	32,6
34	Fe <sub>3</sub> (CO) <sub>10</sub> (dppe)	5	500	60,5	34,9
35	Fe <sub>3</sub> (CO) <sub>10</sub> (dppp)	5	500	60,9	40,5
36	Fe <sub>2</sub> (S) <sub>4</sub> (CO) <sub>4</sub>	5	500	5,1	≤1

(i) Reaction condition: the catalyst (0,025mmol), ketone (2,5 mmol), sodium isopropylate (0,125mmol), isopropanol (12,5mmol), 7 hour, 82°C.

Fe<sub>2</sub>(CO)<sub>7</sub>(dppm)(**3**) as a catalyst did not show any activity in reduction, and the use of complex decreases the conversion of acetophenone 1,5 percent. The best conversions were obtained when tetradentate bisphosphine ligand containing bi nuclear iron cluster complexes (**2**, **5**, and **6**) were used as the catalysts. Tetradentate ligands increase the catalytic activity and selectivity of iron carbonyl clusters. Fe<sub>2</sub>(S)<sub>4</sub>(CO)<sub>4</sub> take a role as an inhibitor of reduction of acetophenone.

In our another study, Fe(CO)<sub>5</sub>, Fe<sub>2</sub>(CO)<sub>9</sub>, Fe<sub>3</sub>(CO)<sub>12</sub> and [Et<sub>4</sub>N]<sub>2</sub>[Fe<sub>6</sub>C(CO)<sub>16</sub>] were compared with each other. The highest conversion and selectivity was obtained using

the  $[\text{Et}_4\text{N}]_2[\text{Fe}_6\text{C}(\text{CO})_{16}]$  compound as a catalyst.  $\text{Fe}(\text{CO})_5$ ,  $\text{Fe}_2(\text{CO})_9$  and  $\text{Fe}_3(\text{CO})_{12}$  indicated no catalytic activity in transfer hydrogenation with the equivalent 100:5:1:500 (ketone:base:catalyst:solvent) (Table 34). The experiments shown to us that iron carbonyl clusters,  $\text{Fe}(\text{CO})_5$ ,  $\text{Fe}_2(\text{CO})_9$ ,  $\text{Fe}_3(\text{CO})_{12}$ , aren't effective as a catalyst without ligand in transfer hydrogenation of ketone.

Table 34 Influence of the iron carbonyl clusters in transfer hydrogenation of acetophenone

<b>Number of equivalents</b>					
<b>Entry</b>	<b>Catalyst</b>	<b><i>i</i>PrONa</b>	<b><i>i</i>PrOH</b>	<b>Conversion %</b>	<b>Selectivity %</b>
23	$\text{Fe}(\text{CO})_5$	5	500	11,2	$\leq 1$
25	$\text{Fe}_2(\text{CO})_9$	5	500	49,3	11,5
7	$\text{Fe}_3(\text{CO})_{12}$	5	500	30,3	24,0
27	$[\text{Fe}_6\text{C}(\text{CO})_{16}]^{2-}$	5	500	70,9	54,3
16	$\text{Fe}_2(\text{CO})_5(\text{dppm})_2$	5	500	77,8	46,5

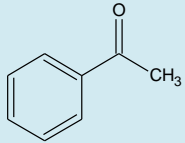
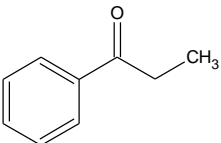
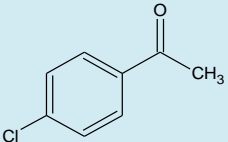
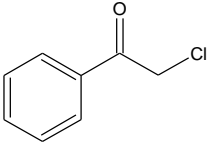
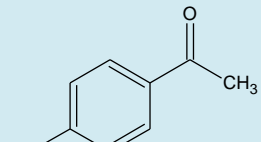
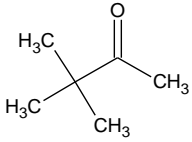
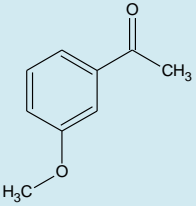
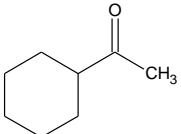
(i) Reaction condition: the catalyst (0,025mmol), ketone (2,5 mmol), sodium isopropylate (0,125mmol), isopropanol (12,5mmol), 7 hour, 82°C.

### 3.6.3 Substrate scope

With the optimized conditions in hand, the reductions of a wide range of ketones using the catalytic system of  $\text{Fe}_2(\text{CO})_4(\mu\text{-CO})(\mu, \eta^2\text{-dppm})_2$  (**2**) were examined. For this reason, we were using eight different substrates, which are acetophenone, 4'-Chloroacetophenone, 2-Chloroacetophenone, 4'(Trifluoromethyl)acetophenone, Pinacolone, 3-Methoxy- acetophenone and Cyclohexylethanone. The reactions were monitored over time by GC analysis, and the conversion of acetophenone was calculated. The catalytic activities and selectivities are shown in following table 35.



Table 35 Influence of the iron carbonyl clusters in transfer hydrogenation of acetophenone

Entry	Ketone	Conversion %	Selectivity %
16		77,8	46,5
50		43,5	65,9
51		60,9	37,7
52		30,3	≤1
53		64,9	5,9
54		3,4	97,3
55		53,9	99,2
56		27,8	≤1

(i) Reaction condition: the catalyst (0,025mmol), ketone (2,5 mmol), sodium isopropylate (0,125mmol), isopropanol (12,5mmol), 7 hour, 82°C.

As shown in table 35, these ketones were transformed to the corresponding secondary alcohols under the optimized reaction conditions for acetophenone. The steric and electronic properties of substrates affected considerably on the conversion and also on the selectivity. The more electron-rich the substrates are the slower the reaction with the catalyst system iron carbonyl bisphosphine clusters. The electronic properties of the substituents had an insignificant impact on the selectivity. Substituents change the electronegativity of  $\alpha$ -carbon atom.

The results show, that the best conversion was obtained from acetophenone and the best chemoselectivity was obtained from 3-Methoxyacetophenone. 3-Methoxyacetophenone was hydrogenated in good yield and selectivity. The chloro substituent in the  $\alpha$  position to the carbonyl group, trifloro substituent in para position of benzene and saturated aliphatic ketone proved to be problematic and deactivated the catalyst (Table 35, entry 52, 53, 54 and 56). Aromatic ketones are more challenging substrates than aliphatic ketones.

### 3.7 KINETIC INVESTIGATIONS OF TRANSFER HYDROGENATION

---

The reduction of acetophenone in isopropanol catalysed by  $\text{Fe}_2(\text{CO})_5(\text{dppm})_2$  (**2**) was chosen as a model system for the kinetic analysis. The concentration effects of acetophenone and 2-propanol were examined, and the formation of 1-phenylethanol over time was plotted for different acetophenone concentrations under otherwise identical reaction conditions. In the following diagram 5, the product concentration, obtained from the reduction of acetophenone, was examined using different time scales.

To help understand the reaction mechanism, the data from experiments was used to determine the rate constants for the steps of the reaction in above section.

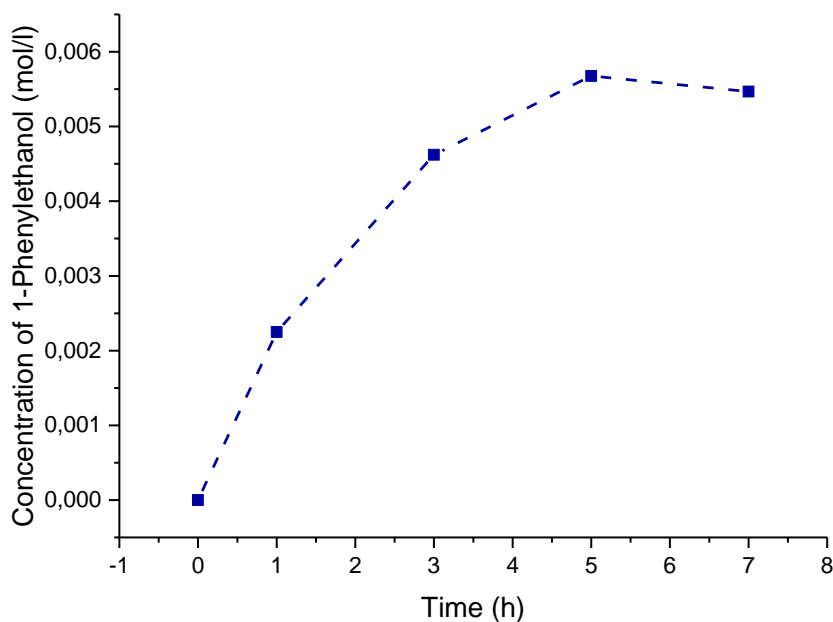


Diagram 5 Representative plot of a typical reaction profile for the transfer hydrogenation of acetophenone

The influence of different hydrogen source concentrations on the conversion of acetophenone was examined. It was expected that the reaction rate would be directly proportional to the concentration of the hydrogen donor (Diagram 6). This highest effect was obtained in 1:5 ratio of acetophenone to isopropanol.

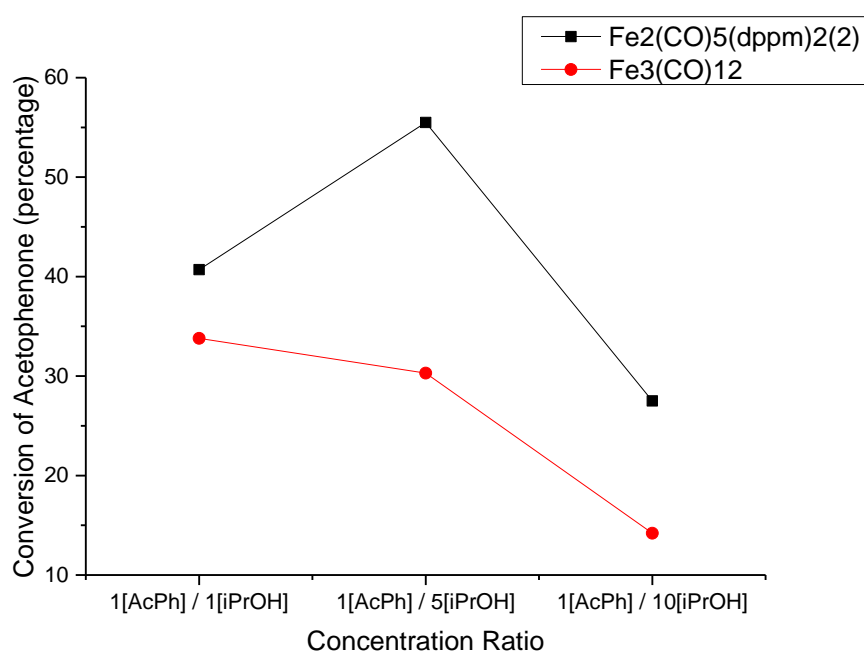
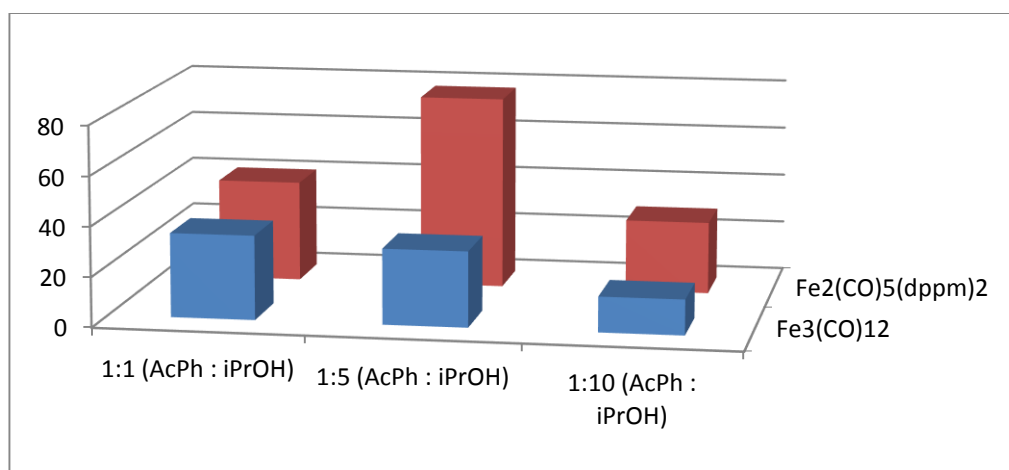


Diagram 6 Conversion of Acetophenone vs. Concentration ratio of acetophenone/isopropanol in the transfer hydrogenation.

A series of experiments was carried out to study the influence of the sodium isopropoxide concentration on the conversion of acetophenone in the transfer hydrogenation. Plotting the conversion of acetophenone versus the *iPrONa* concentration revealed (Diagram 7) that the effect increases at higher concentrations and seems to be saturated at 5:1 (AcPh : *iPrONa*).

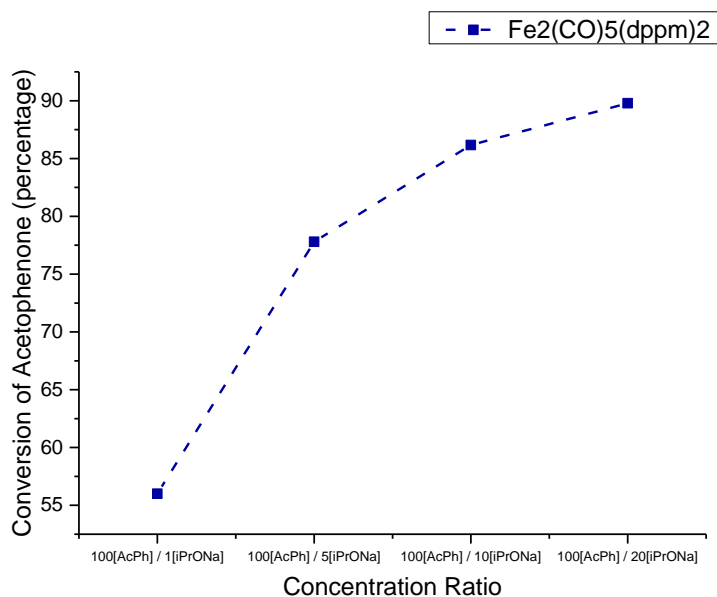
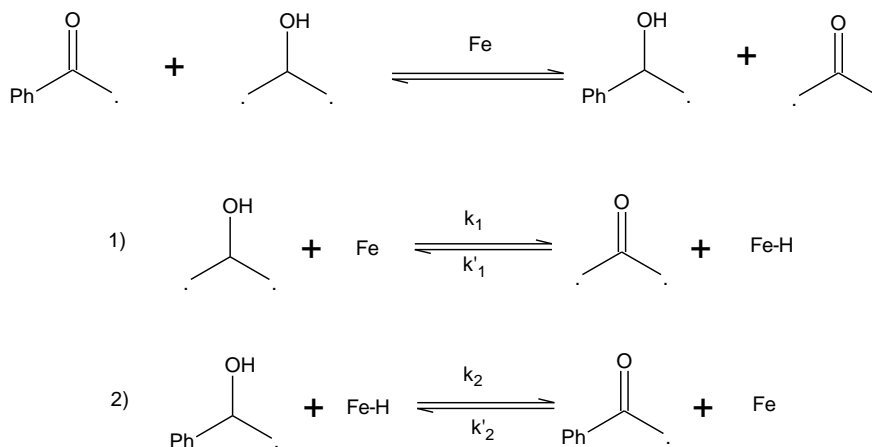


Diagram 7 Conversion of Acetophenone vs. concentration rate of acetophenone/sodium isopropylate in the transfer hydrogenation

### 3.7.1 Determination of the Rate of Reaction

To help understand the reaction mechanism, the data from experiments was used to determine the rate of reaction. In the above section, the concentration vs time plots and conversion vs concentration rate plots observed that each compounds has its own rate of change in concentration. The reactants, consumed in the reaction, have a negative slope. Products, formed in the reaction, have a positive slope.



Scheme 22 The representation of the whole process and of the two steps

The interference by acetophenone on the activation of the catalyst is an unexpected outcome; ketones are poor ligands and are unlikely to prevent the isopropoxide from coordinating to the iron and activating the catalyst (Mikhailine et al., 2012). The whole reaction could be separated into two steps; one of these steps is the activating of isopropanol (Scheme 22). The first step is the reaction between the iron catalyst and isopropanol to form the iron hydride and the second step is the reaction of hydrogenated iron and acetophenone to form the product and to regenerate the iron-catalyst. Iron carbonyls may react reversibly with base to give other precursors. The equilibria were not accounted for in the model since the concentrations of base and isopropanol stay approximately constant throughout the reaction. The varying concentrations of acetophenone and 1-phenylethanol were compared.

**Reaction Rates** The initial rate of isopropanol can be represented in terms of the concentrations.

$$\text{Initial rate} = \frac{\Delta[A]}{\Delta t}$$

$$\text{Initial rate} = \frac{[\text{AcPh}] \text{ at time } t_2 - [\text{AcPh}] \text{ at time } t_1}{t_2 - t_1}$$

Entry	Initial Rate (mole.L <sup>-1</sup> .sec <sup>-1</sup> )	Initial Conc. of <i>i</i> PrOH (mole/L)
1	2,614*10 <sup>-7</sup>	0,5
2	2,862*10 <sup>-7</sup>	10

From the following equation, reaction stoichiometry and reaction constant can be calculated.

$$\frac{\text{Initial rate } r_1}{\text{Initial rate } r_2} = \frac{k[iPrOH]_1^b}{k[iPrOH]_2^b}$$

$$\frac{2,614 * 10^{-7}}{2,862 * 10^{-7}} = \frac{k[0,5]_1^b}{k[10]_2^b}$$

$$b = 0,0267 \sim 0$$

These initial rates were calculated from the experimental results for in the model since the concentrations of isopropanol stay approximately constant throughout the

reaction. The initial rate of Acetophenone can be represented in terms of the concentrations.

Entry	Initial Rate (mole.L <sup>-1</sup> .sec <sup>-1</sup> )	Initial Conc. of AcPh (mole/L)
3	3,152*10 <sup>-7</sup>	1,9
4	4,503*10 <sup>-7</sup>	2,7

$$\frac{\text{Initial rate } r_3}{\text{Initial rate } r_4} = \frac{k[\text{AcPh}]_3^a}{k[\text{AcPh}]_4^a}$$

$$\frac{3,152 * 10^{-7}}{4,503 * 10^{-7}} = \frac{k[1,908]_3^a}{k[2,74]_4^a}$$

$$a = 0,9859 \sim 1$$

The reaction order is defined, to which its concentration term in the rate equation is raised. For the rate equation of our model reaction  $r = k [\text{AcPh}]^a [\text{iPrOH}]^b$ , the reaction order is  $a$  for substance Acetophenone,  $b$  for substance isopropanol. The *overall* reaction order is the sum of  $a=1$  and  $b=0$ . Therefore, the overall reaction order was determined as first order reaction.

**First Order Reaction Rate:** A first-order reaction depends on the concentration of only one reactant. The rate law for a reaction that is first order with respect to a reactant Acetophenone is

$$r = k[\text{AcPh}]_2^1 = -\frac{d[\text{AcPh}]}{dt}$$

$$k(dt) = -\frac{d[\text{AcPh}]}{[\text{AcPh}]}$$

$$\int_{t:0}^t k(dt) = - \int_{[\text{AcPh}]_0}^{[\text{AcPh}]} \frac{d[\text{AcPh}]}{[\text{AcPh}]}$$

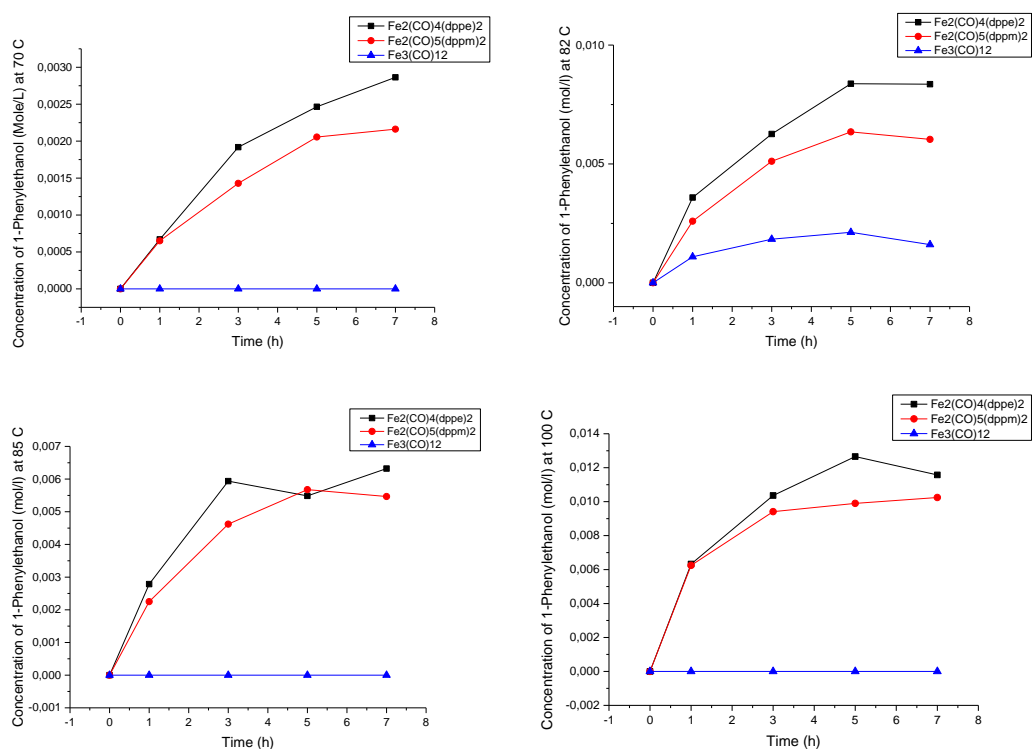
$$[\text{AcPh}] = [\text{AcPh}]_0 e^{-kt}$$

At the beginning of the reaction, the concentration of acetone and 1-phenylethanol was zero. Equations predict that the observed order in acetophenone and isopropanol depends on their relative concentrations. The rate of acetophenone can be identified

as having  $rate=k_2[AcPh]$  where the transfer of the hydride from the metal to the substrate becomes the rate determining step. On the other side, the rate of isopropanol can be determined as having  $rate=k_1[iPrOH]^0$ . The rate constants for the two reversible steps can also be determined. Since the transfer hydrogenation in isopropanol is an equilibrium reaction, the full rate explanation needs to be considered.

### 3.7.2 Different iron carbonyl precursors

We focused on the identification of the catalytic properties of iron carbonyl complexes with 1,1-Bis(diphenylphosphino)methane, 1,2-Bis(diphenylphosphino)ethane as ligands and without ligand. They showed catalytic activity (Diagram 8).



\*Diagram 8 Comparison of different iron carbonyl sources in the transfer hydrogenation of acetophenone (Concentration of 1-Phenylethanol (mol/l) vs time (h))



### 3.7.3 Temperature Dependence

Catalytic hydrogenation reaction was conducted at various temperatures between 343.15 and 373.15 K in order to obtain the reaction profiles. The maximum rates of catalytic reactions are resulting from the combined effect of different rate constants.

Temperature (K)	Rate Constant ( $M^{-1}sec^{-1}$ )
343,15	$1,2 \cdot 10^{-5}$
355,15	$2,1 \cdot 10^{-5}$
358,15	$2,45 \cdot 10^{-5}$
373,15	$4,4 \cdot 10^{-5}$

The activation energies of the catalytic steps are in a similar range, thus allowing the system to be driven by the thermodynamic equilibrium. The maximum energy point in the catalytic cycle is the reaction of acetophenone with the Fe-H, but the free energy that is required to get to this transition state is smaller than the energy, which needed to activate Fe by reaction with *i*-PrOH ( $E_A = 46.136$  kJ).

### 3.7.4 Calculation of $E_a$ using Arrhenius Equation

In 1889, Arrhenius rate constant ( $k$ ) was graphed versus temperature by Svante. Arrhenius,  $\ln k$  versus the inverse temperature ( $1/T$ ) was obtained as a straight-line graph. As temperature increases, liquid substances velocity also increases. The kinetic energy of a molecule is directly proportional to the velocity of the molecules. Therefore, when temperature increases, kinetic energy also increases. As temperature increases, more molecules have higher kinetic energy, and thus the fraction of molecules that have high enough kinetic energy to overcome the energy barrier also increases.

The fraction of molecules with energy equal to or greater than  $E_a$  is given by the exponential term  $e^{-E_a/RT}$  in the Arrhenius equation:

$$k = A e^{-E_a/RT}$$

- $k$  is the rate constant
- $E_a$  is the activation energy
- $R$  is the gas constant
- $T$  is temperature in Kelvin
- $A$  is frequency factor constant

Frequency factor is also known as Arrhenius factor. It indicates the rate of collision and the fraction of collisions with the proper orientation for the reaction to occur.

Taking the natural log of both sides of equation yields the following:

$$\ln k = \ln A - \frac{E_a}{RT}$$

The above equation has the linear form. Graphing  $\ln(k)$  vs  $1/T$  yields a straight line with a slope of  $-E_a/R$ .

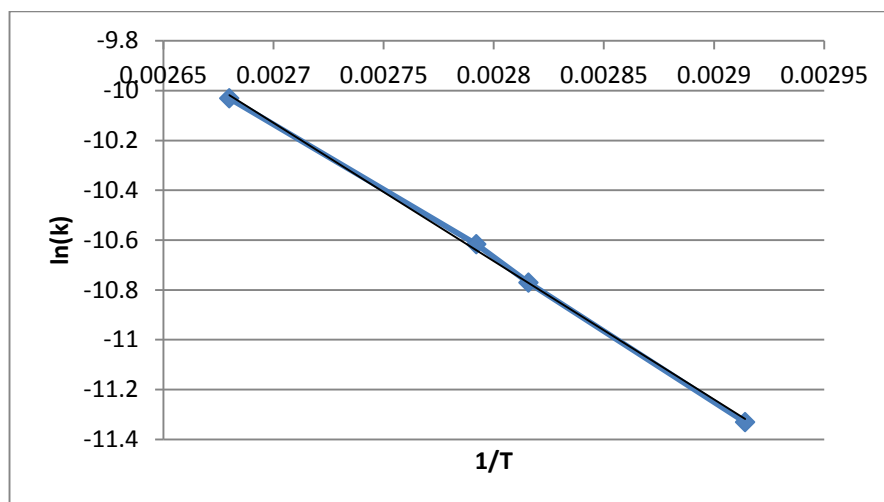


Diagram 9 Simulated reaction profiles using the proposed model

The activation energy can be calculated directly given two known temperatures and a rate constant at each temperature. Two different temperatures  $T_1$  and  $T_2$ , reaction rate constants  $k_1$  and  $k_2$ :

$$\ln k_1 = \ln A - \frac{E_a}{RT_1}$$

$$\ln k_2 = \ln A - \frac{E_a}{RT_2}$$

Subtract  $\ln(k_2)$  from  $\ln(k_1)$ :

$$\ln k_1 - \ln k_2 = \left( \ln A - \frac{E_a}{RT_1} \right) - \left( \ln A - \frac{E_a}{RT_2} \right)$$

After rearrangement:

$$\ln \left( \frac{k_1}{k_2} \right) = \frac{E_a}{R} \left( \frac{1}{T_2} - \frac{1}{T_1} \right)$$

Application of the model system:

$$\ln \left( \frac{4,4 * 10^{-5}}{1,2 * 10^{-5}} \right) = \frac{E_a}{8,314} \left( \frac{1}{343,15} - \frac{1}{373,15} \right)$$

$$E_a = 46136 \text{ J/mol}$$

The concentrations of the reagents were determined from the experiments (Table 36). Arrhenius energy for the process of converting *i*PrOH and acetophenone to acetone and 1-phenylethanol was obtained from the activation parameters.

Table 36 Calculation of experimental data's

T(K)	AcPh	Rate C.	ln(k)	Slope	Intercept	E <sub>a</sub> : kj	Arrh. Fact. (s <sup>-1</sup> )
343,15	0,0203	0,000012	-11,33	-5549,276	4,853	46,136	175.221
355,15	0,0162	0,000021	-10,77				
358,15	0,0148	0,000024	-10,61				
373,15	0,0089	0,000044	-10,03				

### 3.8 STABILITY OF CATALYSTS IN TRANSFER HYDROGENATION

First results of our studies with respect to the stability of iron carbonyl cluster complexes are discussed in this section. By means of using  $\text{Fe}_2(\text{CO})_5(\text{dppm})_2$ , the stability of iron carbonyl cluster complexes are examined. The data saves as a result from the reduction of acetophenone with the help of using  $\text{Fe}_2(\text{CO})_5(\text{dppm})_2$  when examine the stability with optimized ratio under inert atmosphere.

The catalyst with isopropanol was pretreated with sodium isopropoxide. After addition of acetophenone, the reaction mixture was stirred for 7 h at 85°C. The solution was cooled to room temperature. The conversion was measured by GC without further purification. As a result of GC analysis, acetophenone and sodium isopropoxide was added as much as amount of converted acetophenone on the reaction mixture. The conversion was measured as it is shown in the following table 37.

Table 37 Influence of the iron carbonyl clusters in transfer hydrogenation of acetophenone

Entry	Catalyst	Conversion %	Selectivity %
16	$\text{Fe}_2(\text{CO})_5(\text{dppm})_2$	77,8	46,5
57	$\text{Fe}_2(\text{CO})_5(\text{dppm})_2$	72,4	54,2

(i) Reaction condition: the catalyst (0,025mmol), ketone (2,5 mmol), isopropanol (12,5mmol), 7 hour, 82°C.

The results show that catalyst is still active after first reduction reaction, even if the conversion of acetophenone decreased 5.4 percent. Nevertheless, the selectivity of  $\text{Fe}_2(\text{CO})_5(\text{dppm})_2$  increased in rate of 7.7 percent. Just small part of iron carbonyl cluster catalyst in transfer hydrogenation decomposes to iron(III)oxide.

Iron carbonyl cluster complex,  $\text{Fe}_2(\text{CO})_5(\text{dppm})_2$ , is pretty much stable for asymmetric transfer hydrogenation. Presumably the added sodium isopropoxide, which is used as a base, increase the selectivity of iron carbonyl cluster complex in reaction 57.

### 3.9 THE EFFECT OF DIPHOSPHINE COMPLEXES ON THE CATALYST STABILITY AND FUNCTIONALITY

---

The effect of ligand parameters upon the ligand-metal and ligand-substrate interactions takes an important part of development of catalyst. The steric and electronic consequences of the phosphorus ligands to iron-phosphine bonding and reactivity have improved the catalytic activity of iron-phosphine complexes.

#### 3.9.1 Ligand Parameters

The electronic parameters of phosphorus ligands have been studied using a variety of methods in metal-phosphorus bonding in individual complexes and in some catalytic reactions. One of these approaches is to use mixed ligand complexes and examine the influence of the other ligands upon electronic changes at the metal centre caused by the phosphine ligand (Gillespie et al., 2012).

Coordination of a ligand to a metal centre can be defined as the donation of electrons from the ligand to the metal. This is the fundamental property of the donor-acceptor model of coordination. By the help of this method, the electronic-donating request of the phosphine can be detected. However, it is important to consider the electronic properties of diphosphines,  $\sigma$ -donation and  $\pi$ -acidity. The  $\sigma$ -donation determined as the electron donation of the phosphorus lone pair towards empty metal orbitals. Also, the  $\pi$ -acidity is defined as an acceptance of electron density from filled orbitals of metal to empty orbitals of ligand (Figure 27).

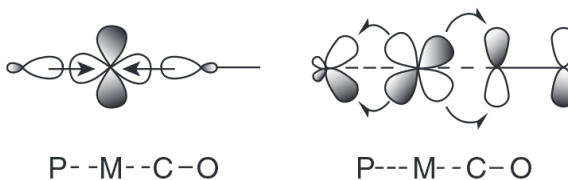


Figure 27  $\sigma$ -donation (left) and  $\pi$ -back donation (right) contributions

The influence of  $\sigma$ -donation and  $\pi$ -back-donation in iron mixed ligand complexes can be differentiated on the basis of the symmetry of the orbitals. Carbon monoxide bonds to transition metals are using  $\pi$  back-bonding. Carbonyl ligand is powerful  $\pi$ -acceptor ligand and excellent ligand for stabilizing electron-rich low-valence metal centres. The stretching frequencies of coordinated ligands, as carbon monoxide and

diphosphines, in transition metal complexes has become the most common parameter to examine the electronic effect of phosphorus ligand on iron metal (Tolman, 1970).

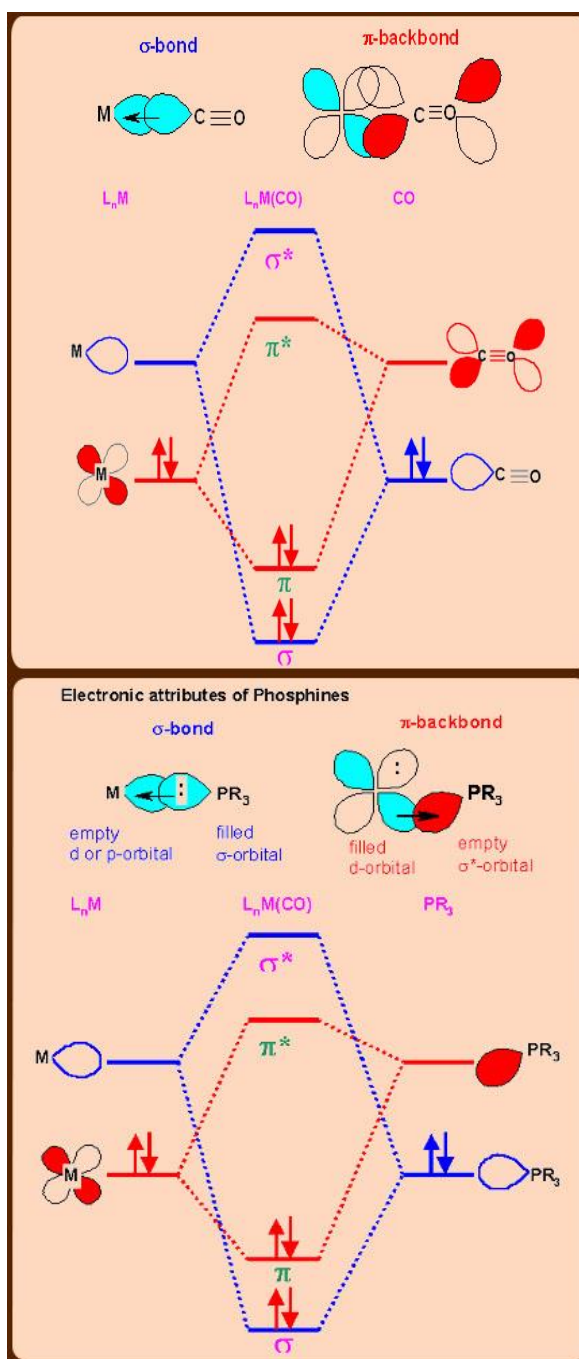


Figure 28 Molecular orbital theory of phosphine and carbonyl ligands

Based on IR stretching frequencies, the following ligands can be ranked from best  $\pi$ -acceptor to worst:  $\text{NO}^+ > \text{CO} > \text{PF}_3 > \text{RNC} > \text{PCl}_3 > \text{P(OR)}_3 > \text{PR}_3 > \text{RCN} > \text{NH}_3$ . In the infrared spectroscopy of metal carbonyl clusters, characteristic  $\nu(\text{C}=\text{O})$  vibrations were observed in between  $2120\text{-}1850\text{cm}^{-1}$  for terminal carbon monoxide and in

between 1850-1720 $\text{cm}^{-1}$  for  $\mu$ -bridging carbon monoxide. Phosphorus compounds with phenyl groups at phosphorus are marked by medium to strong intensity in between 1480-1420 $\text{cm}^{-1}$  and in between 1010-990 $\text{cm}^{-1}$ . In the phosphines and carbonyl ligands containing metal complex, the  $\nu(\text{CO})$  stretching frequencies would reveal the  $\sigma$ -donor or  $\pi$ -acceptor abilities.

When the phosphines employed are strong  $\sigma$ -donors, more electron density would move from  $\text{M}-\pi^*(\text{CO})$ . As a result, a decrease in the  $\nu(\text{CO})$  is observed. On the contrary, when the phosphine is a poor  $\sigma$ -donor but strong  $\pi$ -acceptor, phosphine competes with CO for back bonding. As the result in less decrease in  $\nu(\text{CO})$  frequency can be observed.

The  $\sigma$  bonding Fe-P interactions are the less stable than powerful  $\pi$ -bonding Fe-CO interactions. Therefore, iron carbonyl phosphine ligands are more active in catalytic reduction when the iron phosphine mixed ligand complexes are compared with iron carbonyl clusters.

### **3.9.2 Steric factors in phosphines (Tolman's cone angle)**

Cone angle is very important in examining the steric features of phosphines and their coordination behaviour. Another important point is the steric effect of phosphine ligands. This effect can be tuned by changing R group unlike in the case of carbonyls. Steric effect is a great advantage in transition metal chemistry. Low coordination states are as important as low oxidation states to stabilize metals. This condition increases catalytic activity of the metal center, so that is important step in the catalysis. The steric effects of phosphines can be defined by the help of Tolman's cone angle.

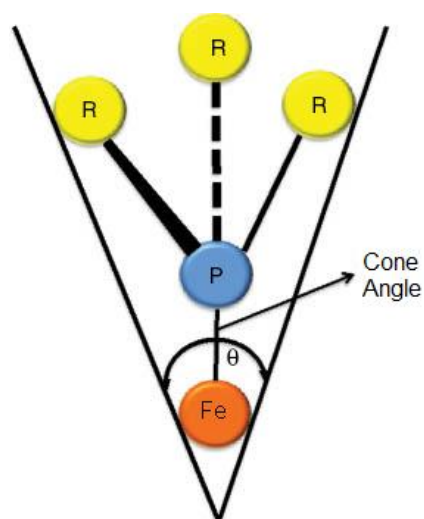


Figure 29 Tolman's cone angle for  $M-PR_3$

Carbonyl ligand and iron metal interaction can form linear geometry. In contrast of carbonyl ligand, dppm, dppe, and dppp ligands connect to the iron metal with a cone angle. The cone angle of the dppm, dppe, and dppp are defined  $121^\circ$ ,  $125^\circ$ , and  $127^\circ$  respectively. The concept of cone angle is of importance in catalysis because the size of the ligand affects the reactivity of metal center.



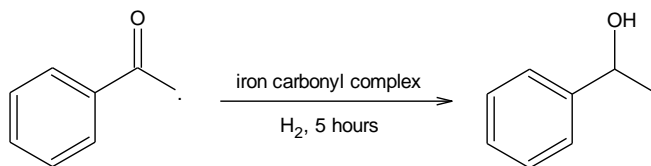
### 3.10 APPLICATION OF HETEROGENEOUS CATALYSIS

---

The supported  $\text{Fe}_3(\text{CO})_{12}$  and its complexes on alumina (12–18), were examined for their ability to serve as catalysts for the  $>\text{C}=\text{O}$  reduction of acetophenone under hydrogen pressure. In order to examine the factors influencing the catalytic performance, the reaction parameters (temperature, reaction time, catalysts) were measured by GC without further purification.

#### 3.10.1 Optimization of Iron Supported on Alumina-Catalysed Hydrogenation of Ketone

The reduction of acetophenone to 1-phenylethanol was chosen as a model reaction to explore the catalytic behaviours of iron carbonyl supported  $\gamma\text{-Al}_2\text{O}_3$  or  $\text{AlO}(\text{OH})$  using dihydrogen as the hydrogen source. Dihydrogen-based direct hydrogenation of ketone was examined with iron contained catalysts. Ketone, catalyst and dihydrogen ratio was optimized by varying the relative molar equivalents.



Scheme 23 Carbonyl hydrogenation

##### 3.10.1.1 Optimisation of Dihydrogen Pressure

Different pressures of hydrogen were examined to optimize of its influence in reduction of acetophenone with using  $\text{HFe}_3(\text{CO})_{11}/\gamma\text{-Al}_2\text{O}_3$  (**14**) as catalyst. In this reason, the hydrogen pressures were chosen in rate 3 atm, 10 atm, 20 atm 35 atm and 50 atm. The reactions were monitored over time by GC analysis. The conversion of acetophenone was obtained between 0-1 percent from all different pressure of dihydrogen.

##### 3.10.1.2 Optimisation of Catalyst Concentration

Different amount of catalysts were examined to determine their influences in direct hydrogenation. In this reason, the catalyst and the ketone amount were chosen in ratio of 1-10, 1-20, 1-50, 1-100, and 1-200.  $\text{HFe}_3(\text{CO})_{11}/\gamma\text{-Al}_2\text{O}_3$  (**14**) clusters were used as the catalyst to optimize catalyst concentration. The reactions were monitored over

time by GC analysis. From the result of direct hydrogenation, the catalyst concentration don't influence to the conversion of acetophenone and selectivity.

### **3.10.1.3 Optimisation of Temperature**

To find optimum temperature, the direct hydrogenation reactions were examined in 25 °C, 50 °C, 100 °C, 150 °C and 200 °C. The reactions were monitored over time by GC analysis, and  $\text{HFe}_3(\text{CO})_{11}/\gamma\text{-Al}_2\text{O}_3$  (**14**) as a catalyst did not show any activity in reduction of acetophenone. These results show, that  $\text{HFe}_3(\text{CO})_{11}/\gamma\text{-Al}_2\text{O}_3$  (**14**) is not right catalyst for hydrogenation of acetophenone.

### **3.10.2 Different Iron Carbonyl Precursors**

In our research, we focused on identifying the catalytic feature of iron carbonyl cluster complexes on  $\gamma\text{-Al}_2\text{O}_3$ .  $\text{HFe}_3(\text{CO})_{11}/\gamma\text{-Al}_2\text{O}_3$  (**14**) complex did not show catalytic activity in reduction of acetophenone to 1-phenylethanol. We decided to examine the catalytic activity of the physisorbed and chemisorbed iron carbonyl clusters on  $\gamma\text{-Al}_2\text{O}_3$  or  $\text{AlO}(\text{OH})$  in direct hydrogenation. The reactions were monitored over time by GC analysis, and the conversion of acetophenone was determined between 0-1 percent conversions. Iron carbonyls supported on  $\gamma\text{-Al}_2\text{O}_3$  or  $\text{AlO}(\text{OH})$  cannot use as catalyst in direct hydrogenation of acetophenone to 1-phenylethanol.

### 3.11 REFERENCES

---

- Adams H., Agostinho S. C. M., Chomka K., Mann B. E., Smith S., Squires C., Spey S. E., *Can. J. Chem.*, 2001, 79, 760-774
- Cartwright S., Clucas J. A., Dawson R. H., Foster D. F., Harding M. M., Smith A. K., *J. OrganometChem.*, 1986, 302, 403-412.
- Gillespie J. A., Zuidema E., van Leeuwen P. W. N., Kamer P. C. J., *John Willey & Sons*, 2012, First Edition
- Hull A. W., *Phys. Rev.*, 1917, 9, 84
- Kohlbeck & H6rl, 1976
- Stein E., Fujiwara F. Y., *J. Organometallic Chem.*, 1996, 525, 31-37
- Tolman C. A., *J. Am. Chem. Soc.*, 1970, 92, 2953

# SUMMARY AND CONCLUSION

In the presented work the synthesis of well-defined, uniform iron carbonyl based complexes incorporating diphosphine ligands was performed and their performance as homogeneous catalysts evaluated. Iron carbonyls supported on  $\gamma$ -Al<sub>2</sub>O<sub>3</sub> were obtained and their performance as heterogeneous catalysts quantified. In the following achieved results and gained insights are summarized.

In this study, six iron carbonyl diphosphine complexes were synthesized, which are [Fe<sub>6</sub>C(CO)<sub>16</sub>]<sup>-2</sup>(**1**), Fe<sub>2</sub>(CO)<sub>4</sub>( $\mu$ -CO)( $\mu$ -dppm)<sub>2</sub>(**2**), Fe<sub>2</sub>(CO)<sub>4</sub>( $\mu$ -CO)<sub>3</sub>( $\mu$ -dppm)(**3**), Fe(CO)<sub>4</sub>( $\mu$ -dppm)(**4**), [Fe<sub>3</sub>(CO)<sub>8</sub>( $\mu$ -CO)<sub>2</sub>( $\mu$ , $\eta^2$ -dppm)](**7**), [Fe<sub>3</sub>(CO)<sub>8</sub>( $\mu$ -CO)<sub>2</sub>( $\mu$ , $\eta^2$ -dppe)](**8**). The four new diphosphine derivatives of iron complexes, which are Fe<sub>2</sub>(CO)<sub>4</sub>( $\mu$ -dppe)<sub>2</sub>(**5**), Fe<sub>2</sub>(CO)<sub>4</sub>( $\mu$ -dppp)<sub>2</sub>(**6**) [Fe<sub>3</sub>(CO)<sub>8</sub>( $\mu$ -CO)<sub>2</sub>( $\mu$ , $\eta^2$ -dppp)](**9**) and Fe<sub>2</sub>(CO)<sub>4</sub>( $\mu$ -CO)<sub>3</sub>( $\mu$ -dppp)(**10**), have been isolated and spectroscopically characterised. Fe<sub>2</sub>(S<sub>4</sub>)(CO)<sub>4</sub>(**11**) was prepared to compare ligand effect on catalysis.

## 4.1 Transfer Hydrogenation of Ketones

---

The main focus of the transfer hydrogenation experiments was the investigation of the effect of iron carbonyl complexes and selectivity of catalysts and supported iron clusters.

Iron carbonyl complexes were synthesized from the reaction between iron carbonyls and bisphosphine ligands. The Fe(CO)<sub>5</sub>, Fe<sub>2</sub>(CO)<sub>9</sub>, Fe<sub>3</sub>(CO)<sub>12</sub>, (Et<sub>4</sub>N)<sub>2</sub>[Fe<sub>6</sub>C(CO)<sub>16</sub>] and their complexes (**2–11**), were examined for their ability to serve as catalysts for the >C=O reduction of acetophenone under the conditions of transfer hydrogenation. In addition, the effect of coordinating ligands on the catalyst stability and functionality is investigated.

The catalytic behaviour of synthesized iron carbonyl complexes was examined to obtain alcohol from ketones in the transfer hydrogenation. Fe(CO)<sub>5</sub>, Fe<sub>2</sub>(CO)<sub>9</sub>, Fe<sub>3</sub>(CO)<sub>12</sub> and [Et<sub>4</sub>N]<sub>2</sub>[Fe<sub>6</sub>C(CO)<sub>16</sub>] were compared with each other and single catalytic activity was obtained using the [Et<sub>4</sub>N]<sub>2</sub>[Fe<sub>6</sub>C(CO)<sub>16</sub>] compound. Iron carbonyl clusters such as Fe(CO)<sub>5</sub>, Fe<sub>2</sub>(CO)<sub>9</sub>, Fe<sub>3</sub>(CO)<sub>12</sub> aren't effective as a catalyst in transfer hydrogenation of ketone. Fe<sub>2</sub>(CO)<sub>7</sub>(dppm)(**3**) did not show any activity in reduction. The best conversions were obtained when tetradentate bisphosphine ligand

containing bi nuclear iron cluster complexes (**2**, **5**, and **6**) were used as the catalysts. But  $\text{Fe}_2(\text{S})_4(\text{CO})_4$  take a role as an inhibitor of conversion of acetophenone. Dppx ligands are worse  $\pi$ -acceptor than C=O ligands. Therefore iron carbonyl phosphine complexes are better hydrogen transporter than just carbonyl ligand containing iron catalysts.

From the experiments using different ketones, the best conversion was obtained from acetophenone and the best chemoselectivity was obtained from 3-Methoxyacetophenone. 3-Methoxyacetophenone was hydrogenated in good yield and selectivity. The chloro substituent in the  $\alpha$  position to the carbonyl group, trifloro substituent in para position of benzene and saturated aliphatic ketone proved to be problematic and deactivated the catalyst. Aromatic ketones are more challenging substrates than aliphatic ketones. Also the changing of the electronegativity of  $>\text{C}=\text{O}$  bond changes the conversion and selectivity. The effect of coordinating ligands on the catalyst stability and functionality is investigated.

The reaction order of transfer hydrogenation of acetophenone is defined, to which its concentration term in the rate equation is raised. For the rate equation of our model reaction  $r = k [\text{AcPh}]^a [\text{iPrOH}]^b$ , the reaction order is  $a$  for substance Acetophenone,  $b$  for substance isopropanol. The *overall* reaction order is the sum of  $a=1$  and  $b=0$ . Therefore, the overall reaction order was determined as first order reaction. The activation energy of transfer hydrogenation of acetophenone was found 46,136 kJ.

## 4.2 Heterogeneous Catalysis

---

The reduction of ketone to alcohol was chosen to explore the catalytic behaviours of iron carbonyls supported  $\gamma\text{-Al}_2\text{O}_3$  or  $\text{AlO}(\text{OH})$  using dihydrogen as the hydrogen source. The  $\text{Fe}_3(\text{CO})_{12}$  and iron carbonyl complexes supported on alumina (12–18), were examined for their ability to serve as catalysts for the  $>\text{C}=\text{O}$  reduction of acetophenone under hydrogen pressure.

Different pressures of hydrogen were examined to optimize of its influence in reduction of acetophenone. In this reason, the hydrogen pressures were chosen in rate 3 atm, 10 atm, 20 atm 35 atm and 50 atm. To find optimum temperature, the direct hydrogenation reactions were examined in 25 °C, 50 °C, 100 °C, 150 °C and 200 °C.  $\text{HF}_3(\text{CO})_{11}/\gamma\text{-Al}_2\text{O}_3$  clusters were used as the catalyst to optimize catalyst

concentration. All catalysts are inactive in direct hydrogenation of ketone. The conversion of acetophenone in heterogeneous catalysis was obtained less than 1 percent.

## **APPENDIX**

**APPENDIX 1 MASS SPECTRA**

**APPENDIX 2 <sup>13</sup>C-NMR SPECTRA**

**APPENDIX 3 <sup>31</sup>P-NMR SPECTRA**

**APPENDIX 4 FTIR SPECTRA**

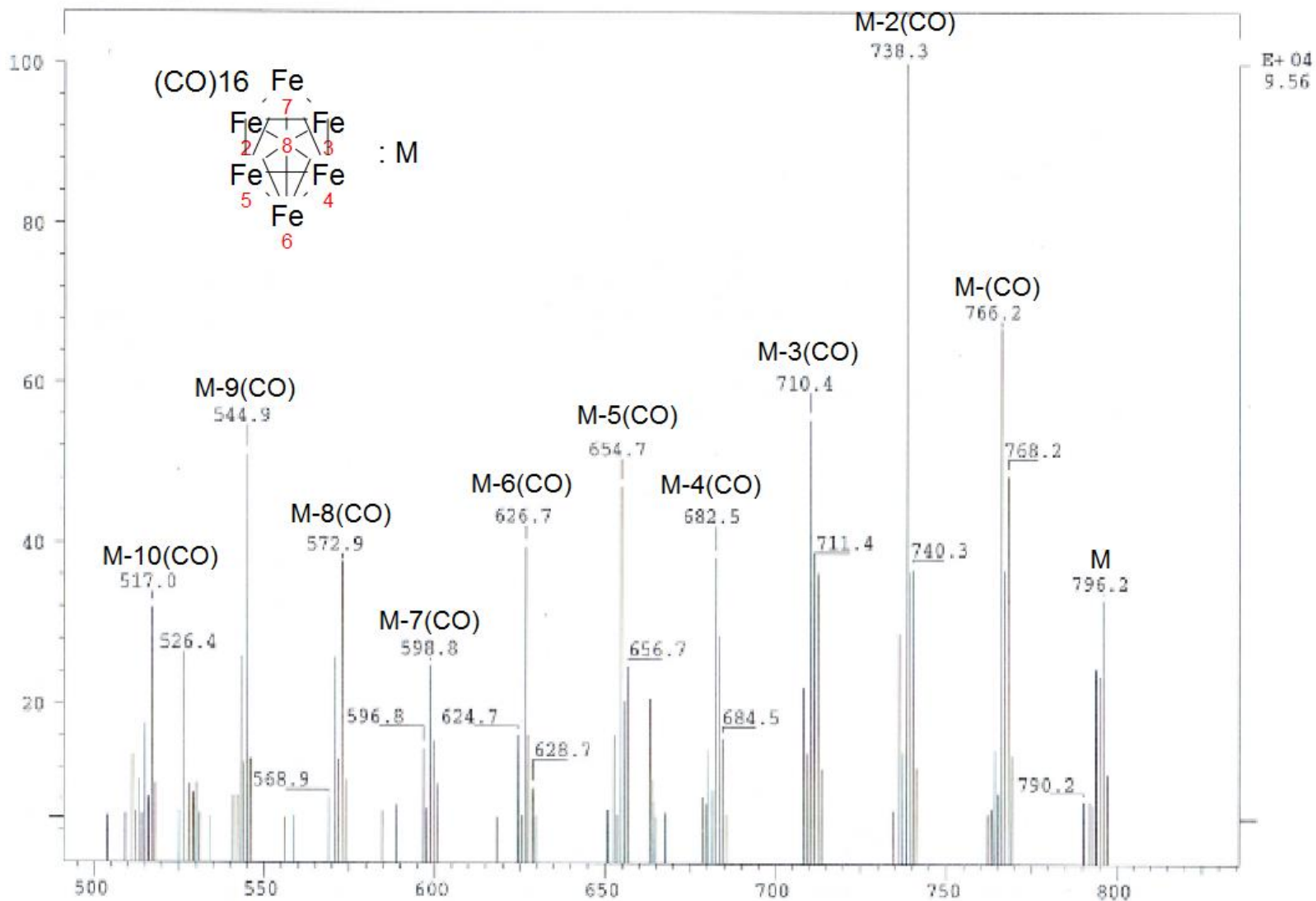
**APPENDIX 5 X-RAY POWDER DIFFRACTIONS**





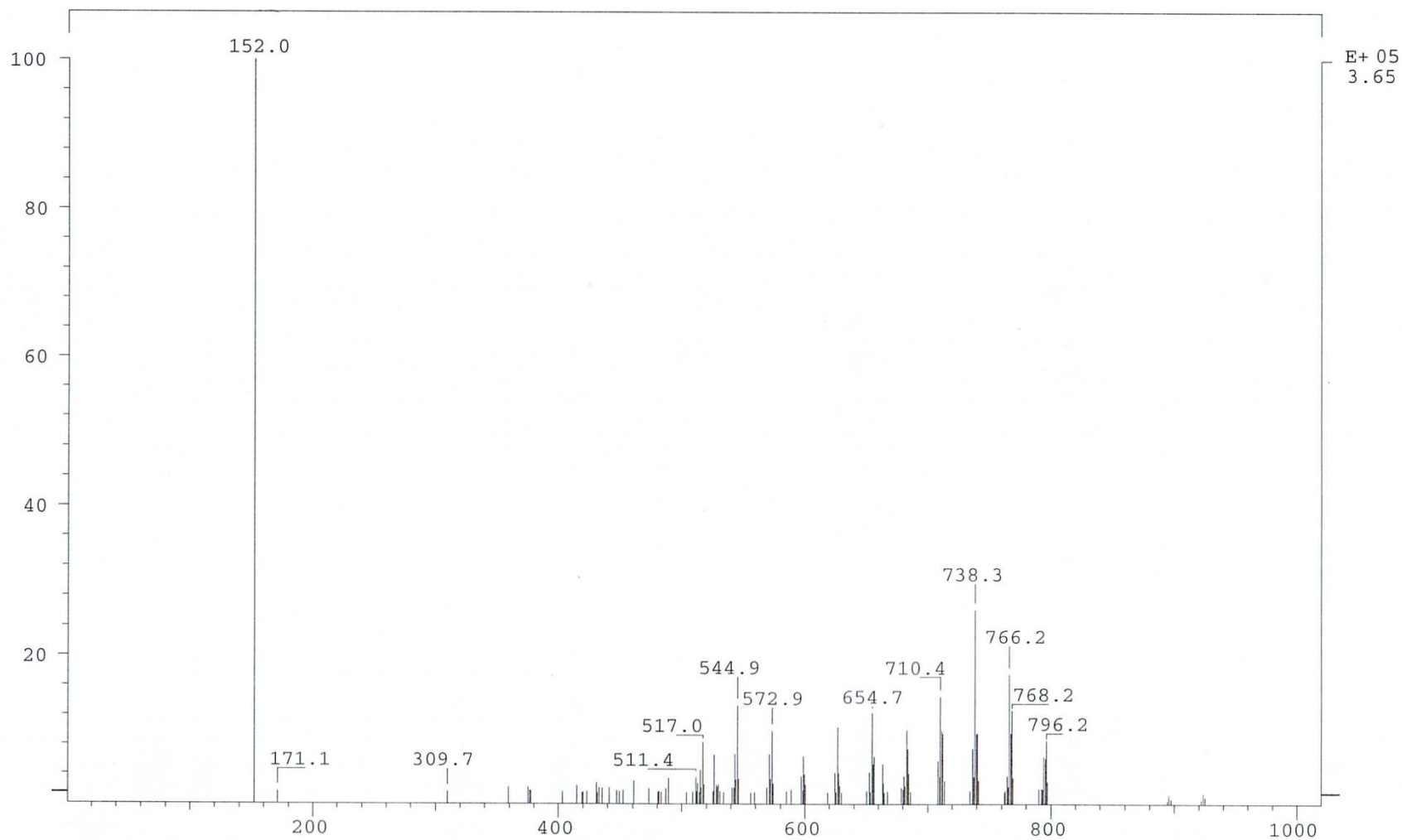
# APPENDIX 1 MASS SPECTRA

## Mass Spectrum of [Et<sub>4</sub>N]<sub>2</sub>[Fe<sub>6</sub>C(CO)<sub>16</sub>] (1)



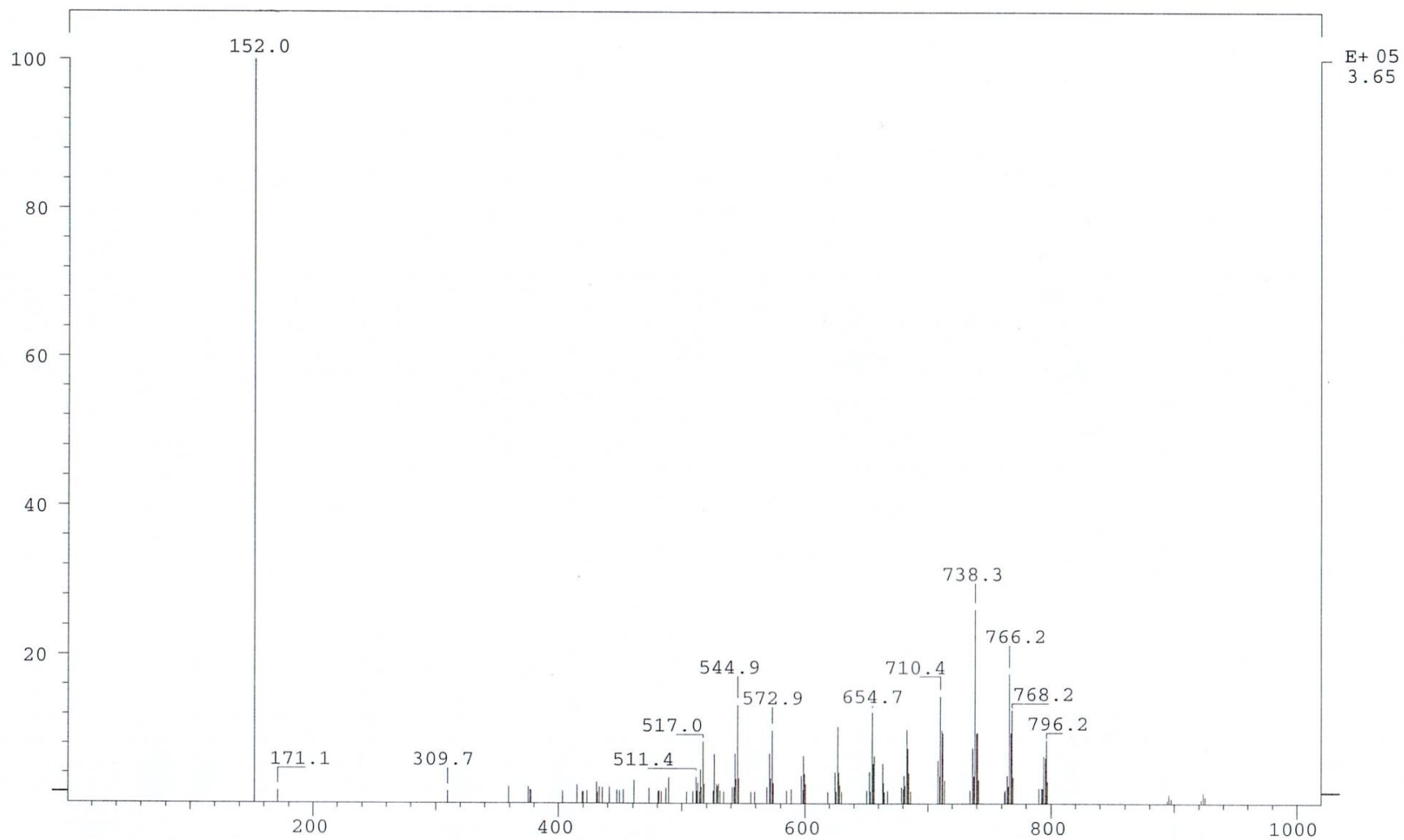
# APPENDIX 1 MASS SPECTRA

## Mass Spectrum of $[\text{Et}_4\text{N}]_2[\text{Fe}_6\text{C}(\text{CO})_{16}]$ (1)



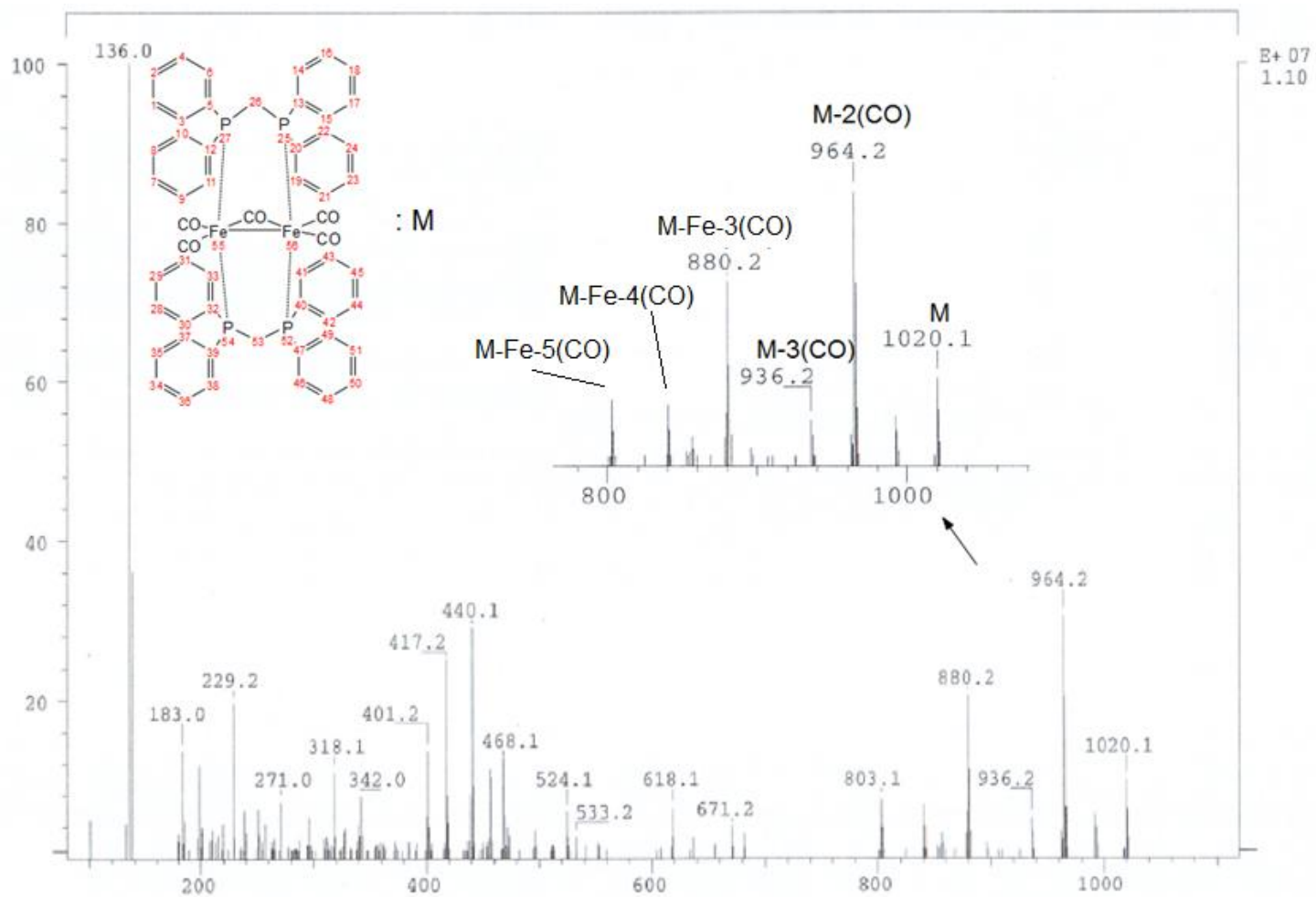
## APPENDIX 1 MASS SPECTRA

### Mass Spectrum of $[\text{Et}_4\text{N}]_2[\text{Fe}_6\text{C}(\text{CO})_{16}]$ (1)



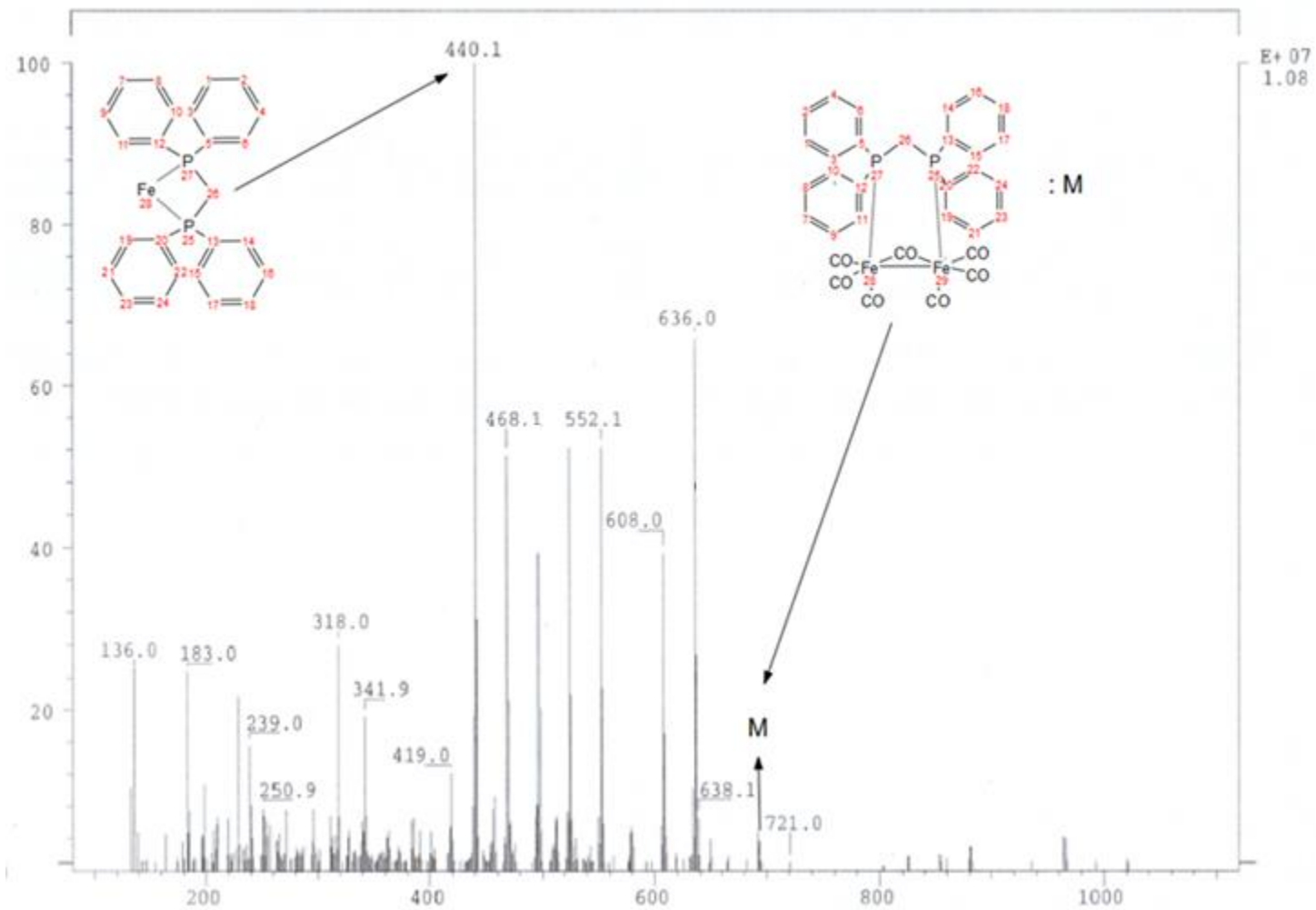
## APPENDIX 1 MASS SPECTRA

### Mass Spectrum of $[\text{Fe}_2(\text{CO})_4(\mu\text{-CO})(\mu,\eta^2\text{-dppm})_2]$ (2)



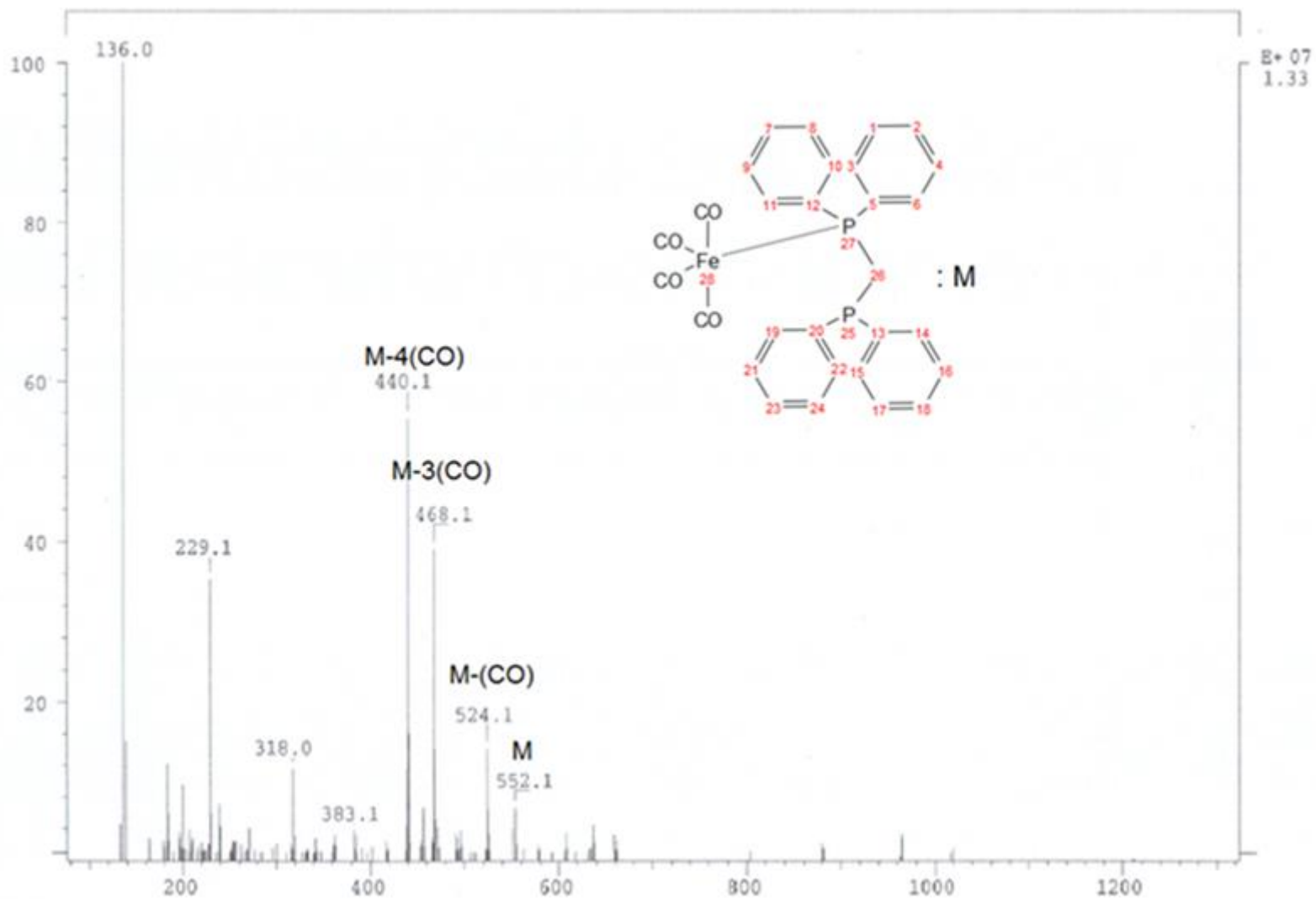
## APPENDIX 1 MASS SPECTRA

### Mass Spectrum of $[\text{Fe}_2(\text{CO})_4(\mu\text{-CO})_3(\mu,\eta^2\text{-dppm})]$ (3)



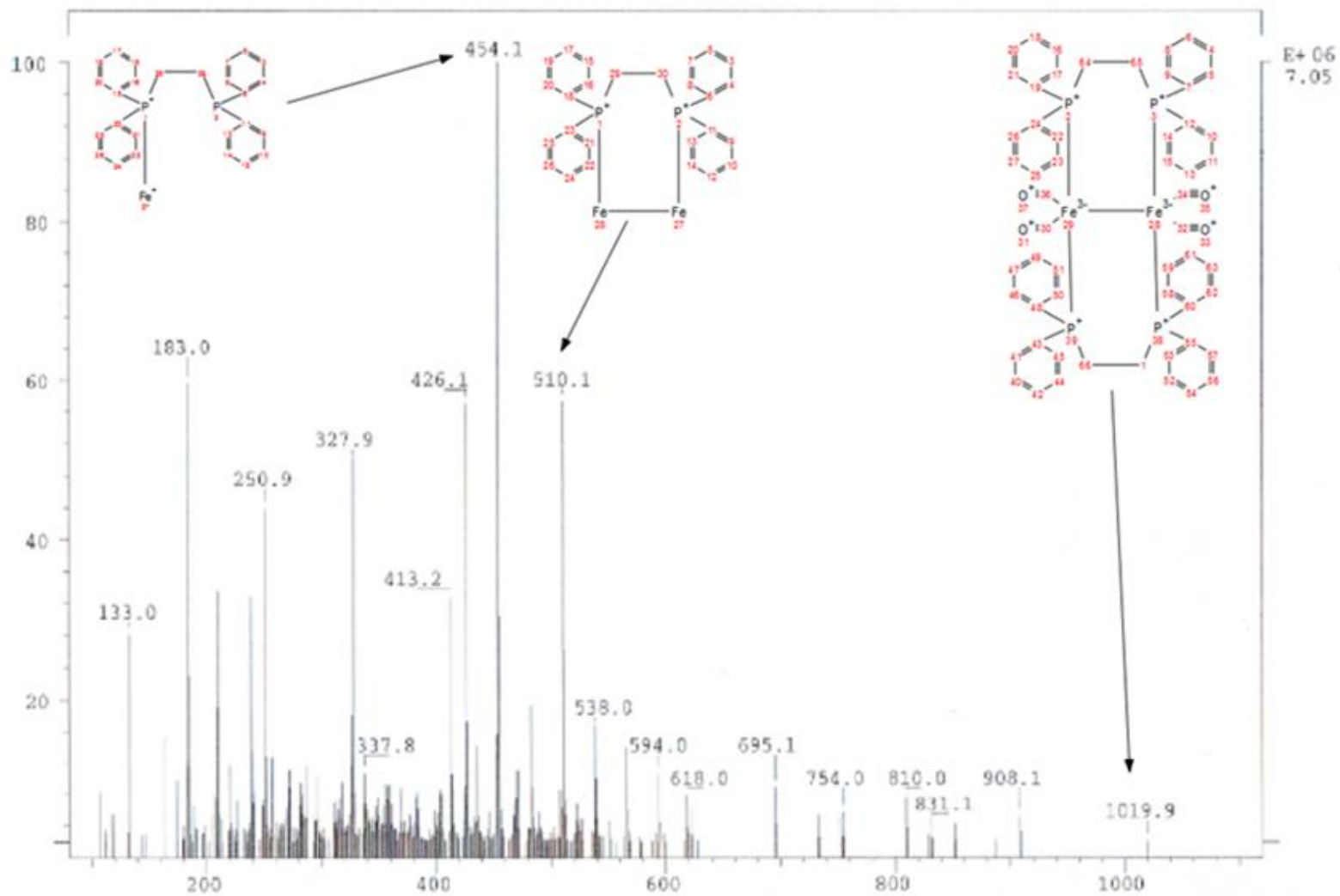
## APPENDIX 1 MASS SPECTRA

### Mass Spectrum of $[\text{Fe}(\text{CO})_4(\text{dppm})]$ (4)



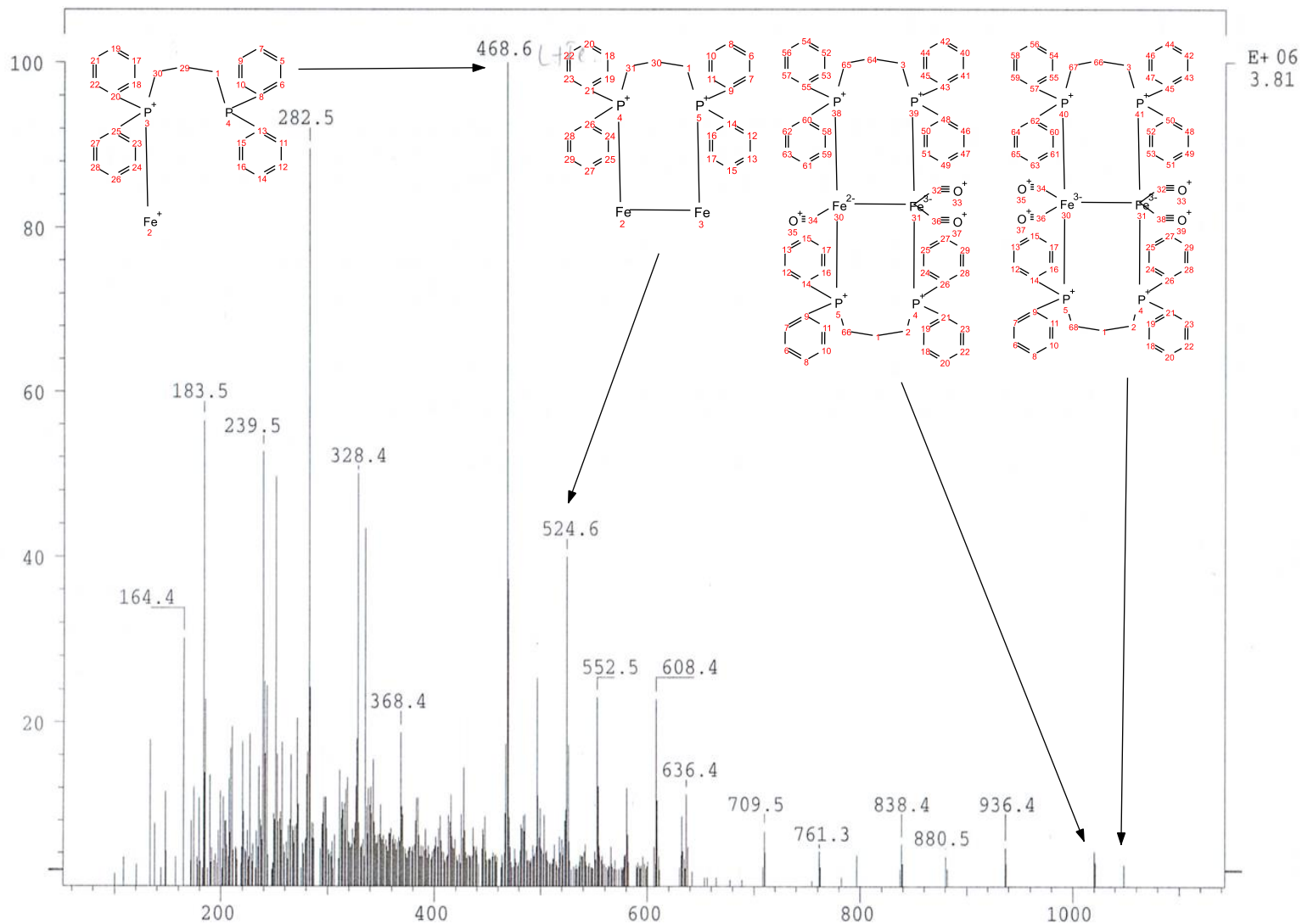
## APPENDIX 1 MASS SPECTRA

### Mass Spectrum of $[\text{Fe}_2(\text{CO})(\mu, \eta^2\text{-dppe})_2]$ (5)



# APPENDIX 1 MASS SPECTRA

## Mass Spectrum of $[\text{Fe}_2(\text{CO})_4(\mu, \eta^2\text{-dppp})_2]$ (6)

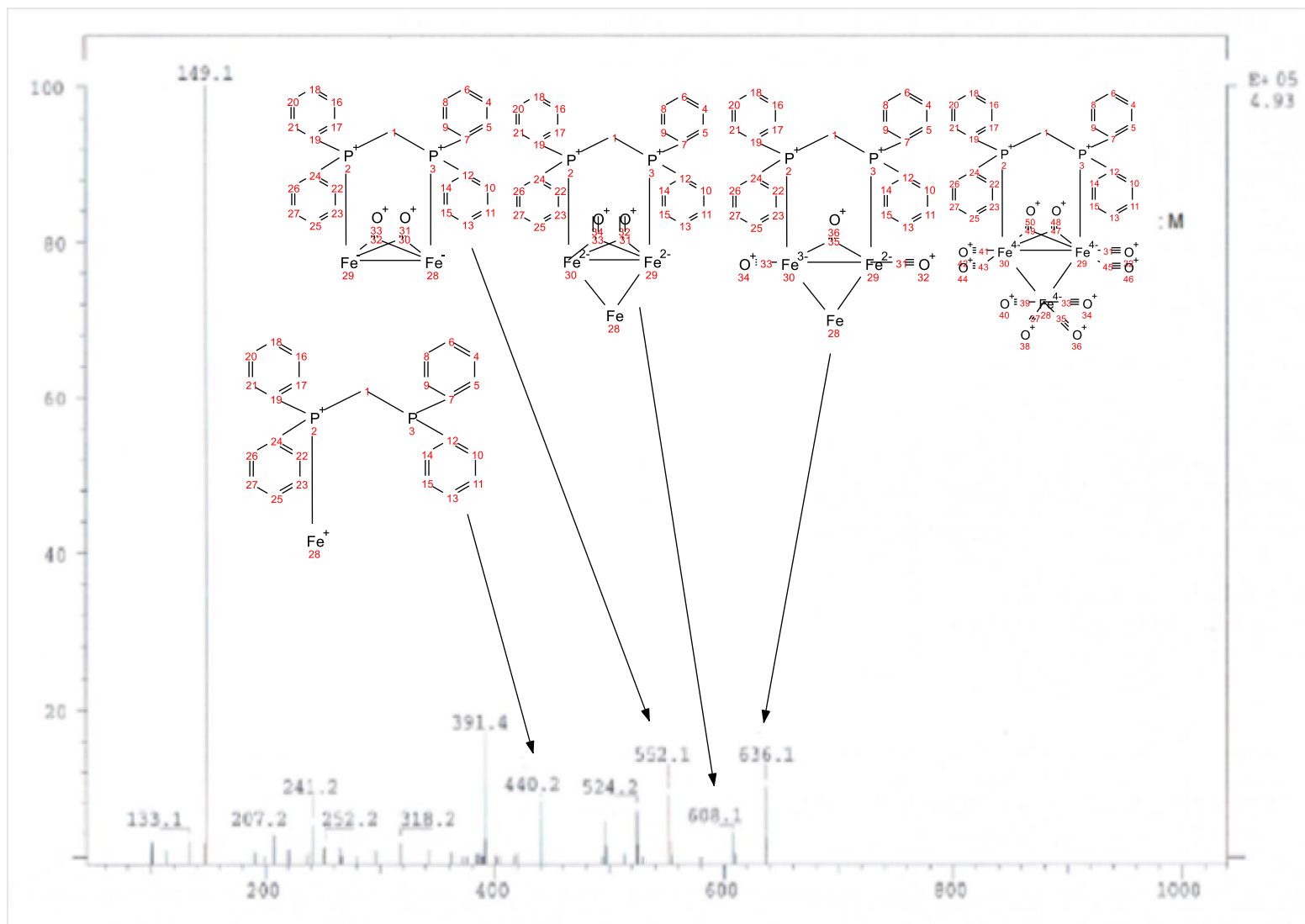


E+ 06  
3.81



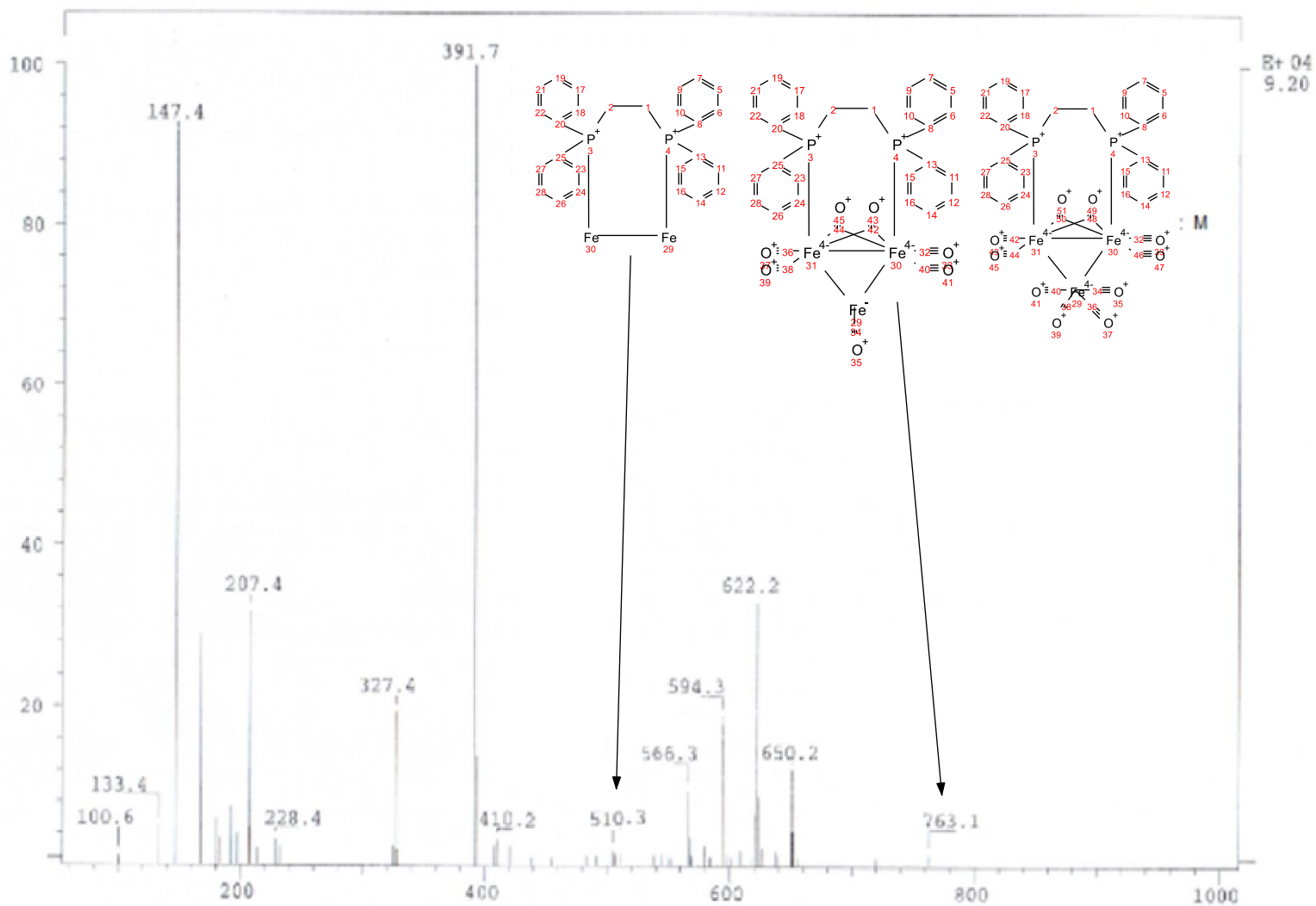
# APPENDIX 1 MASS SPECTRA

## Mass Spectrum of $[\text{Fe}_3(\text{CO})_8(\mu\text{-CO})_2(\mu,\eta^2\text{-dppm})]$ (7)



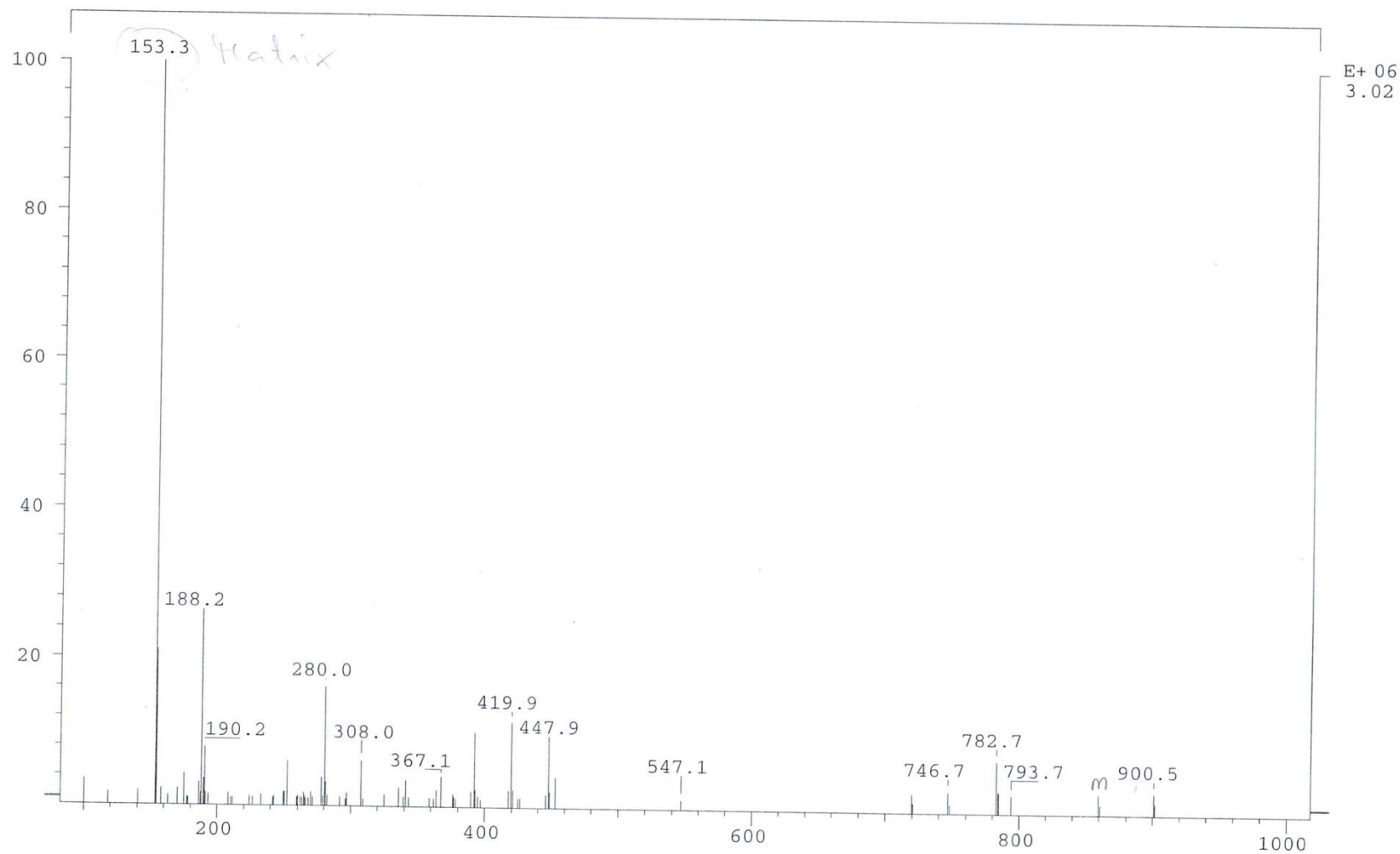
# APPENDIX 1 MASS SPECTRA

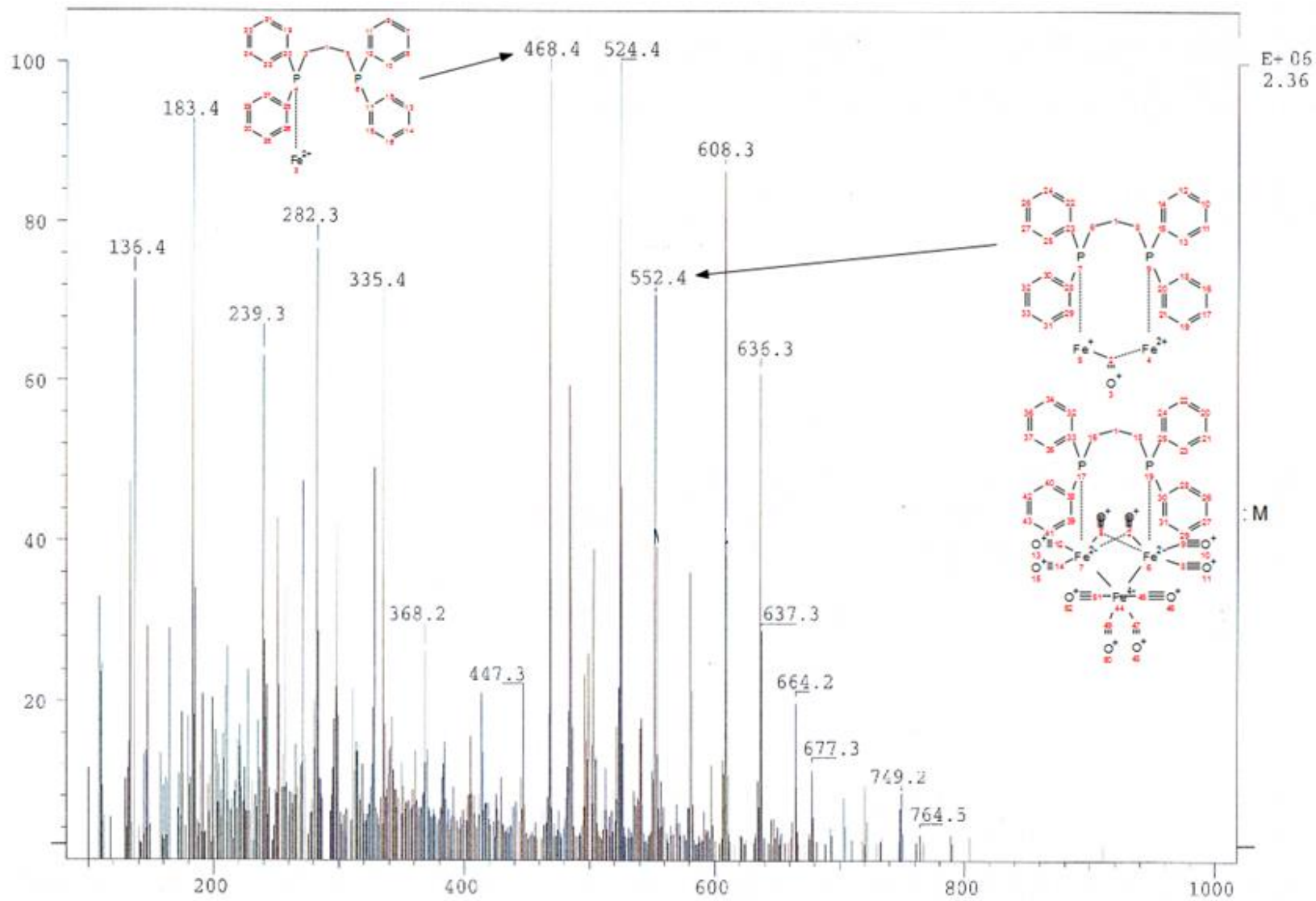
## Mass Spectrum of $[\text{Fe}_3(\text{CO})_8(\mu\text{-CO})_2(\mu,\eta^2\text{-dppe})]$ (8)



## APPENDIX 1 MASS SPECTRA

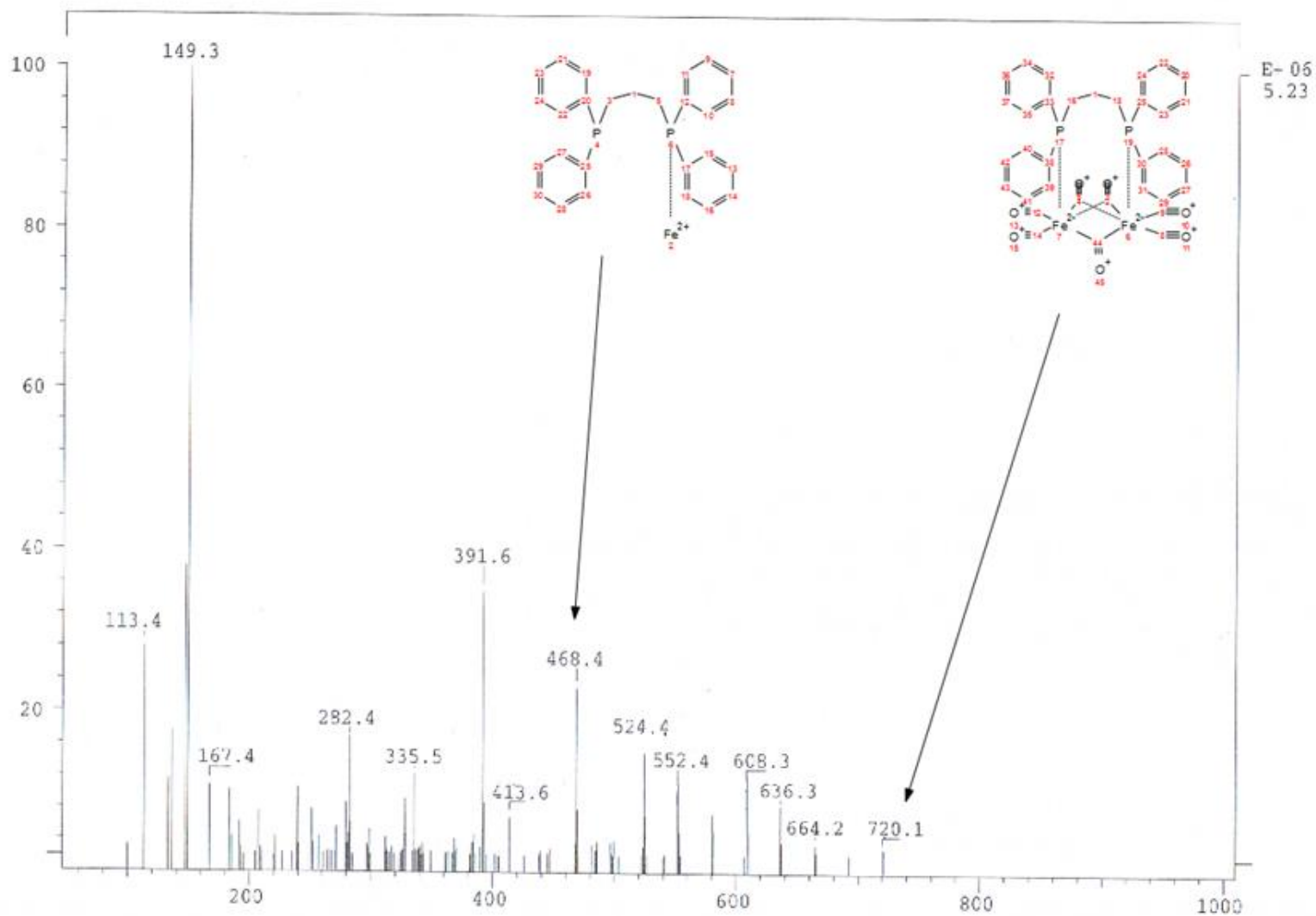
### Mass Spectrum of $[\text{Fe}_3(\text{CO})_4(\mu\text{-CO})_2(\mu,\eta^2\text{-dppp})]$ (9)





## APPENDIX 1 MASS SPECTRA

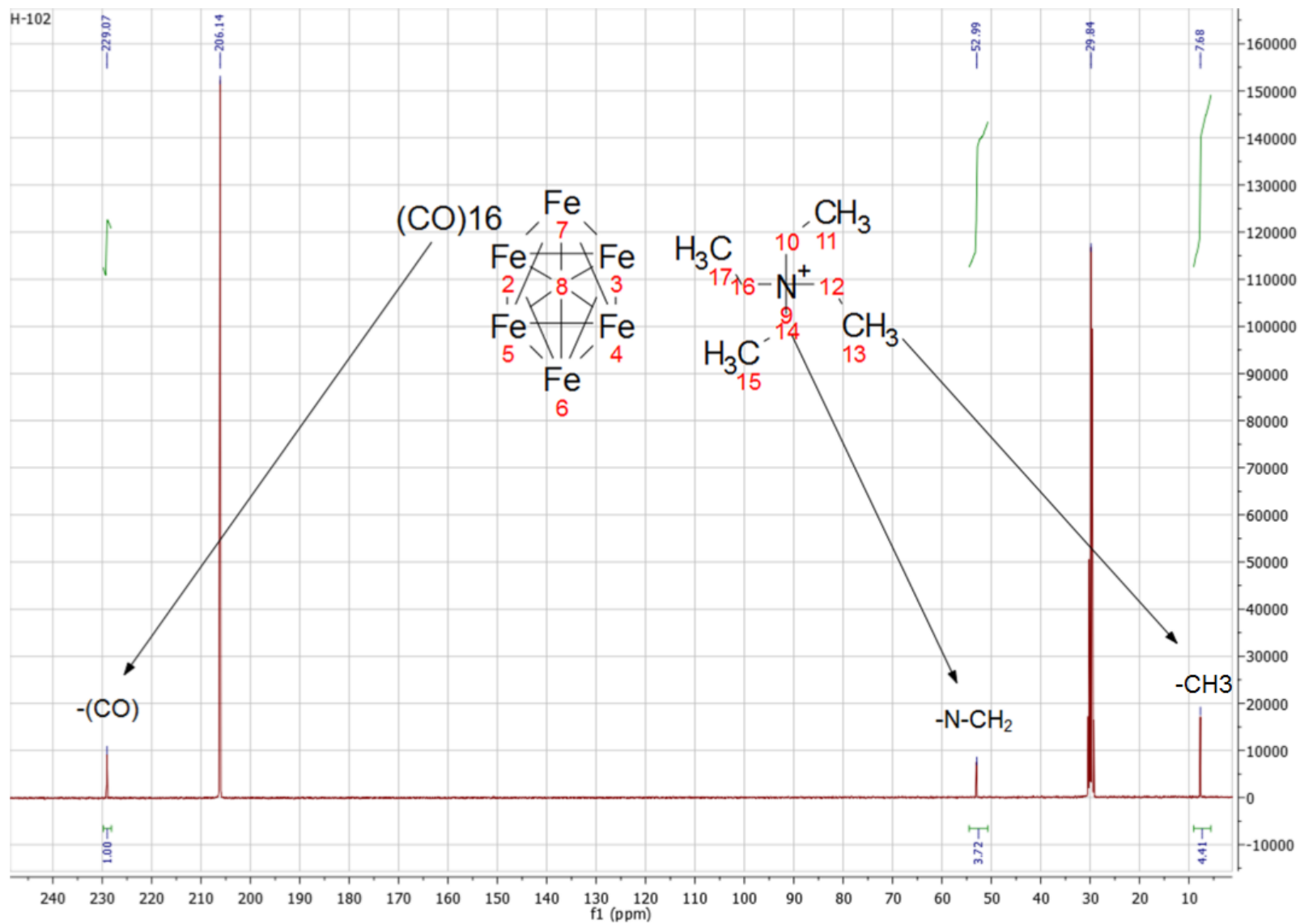
### Mass Spectrum of $[\text{Fe}_2(\text{CO})_4(\mu\text{-CO})_3(\mu,\eta^2\text{-dppp})]$ (10)



E-06  
5.23

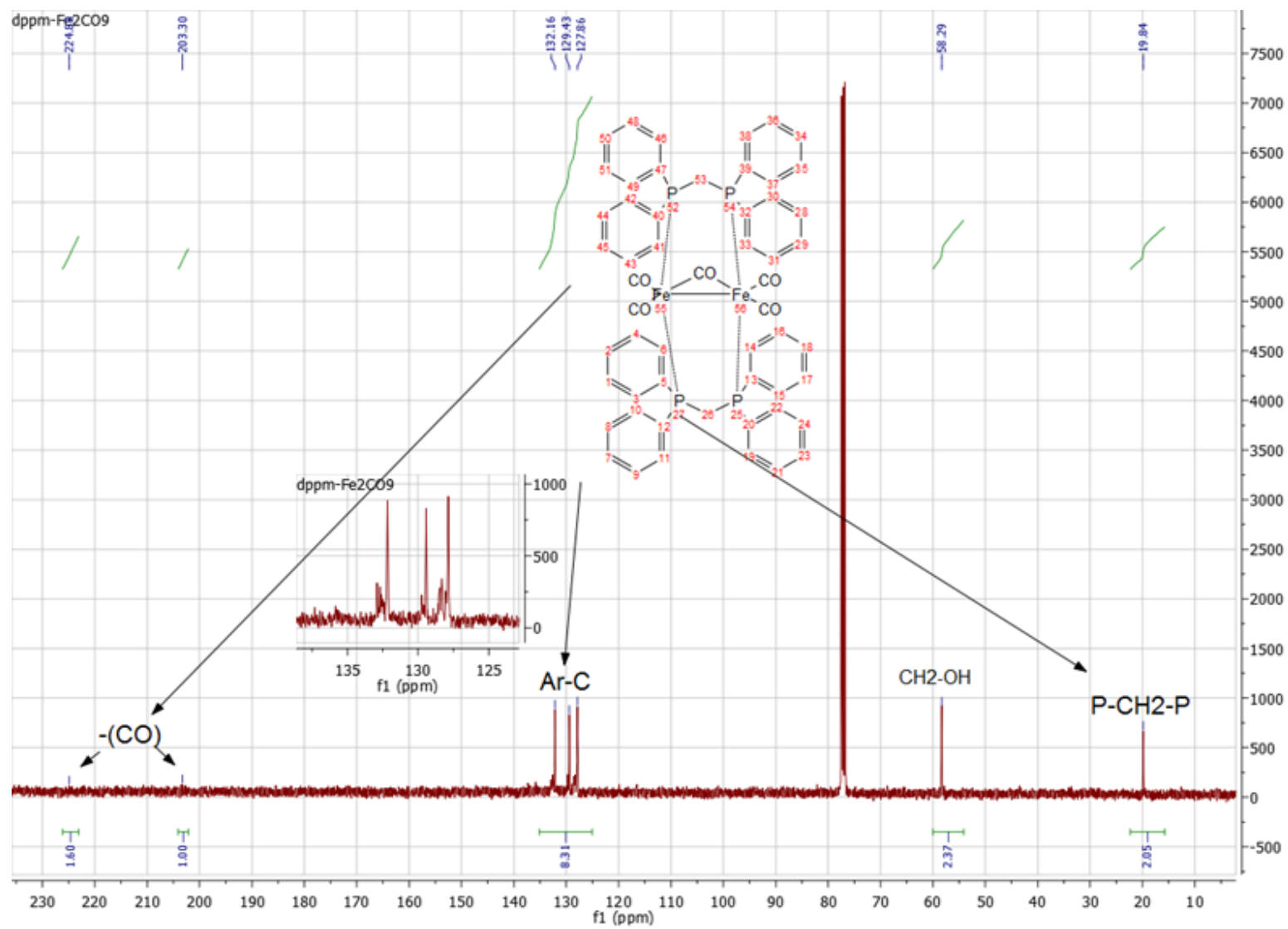
## APPENDIX 2 $^{13}\text{C}$ -NMR SPECTRA

### $^{13}\text{C}$ -NMR Spectrum of $[\text{Et}_4\text{N}]_2[\text{Fe}_6\text{C}(\text{CO})_{16}]$ (1)



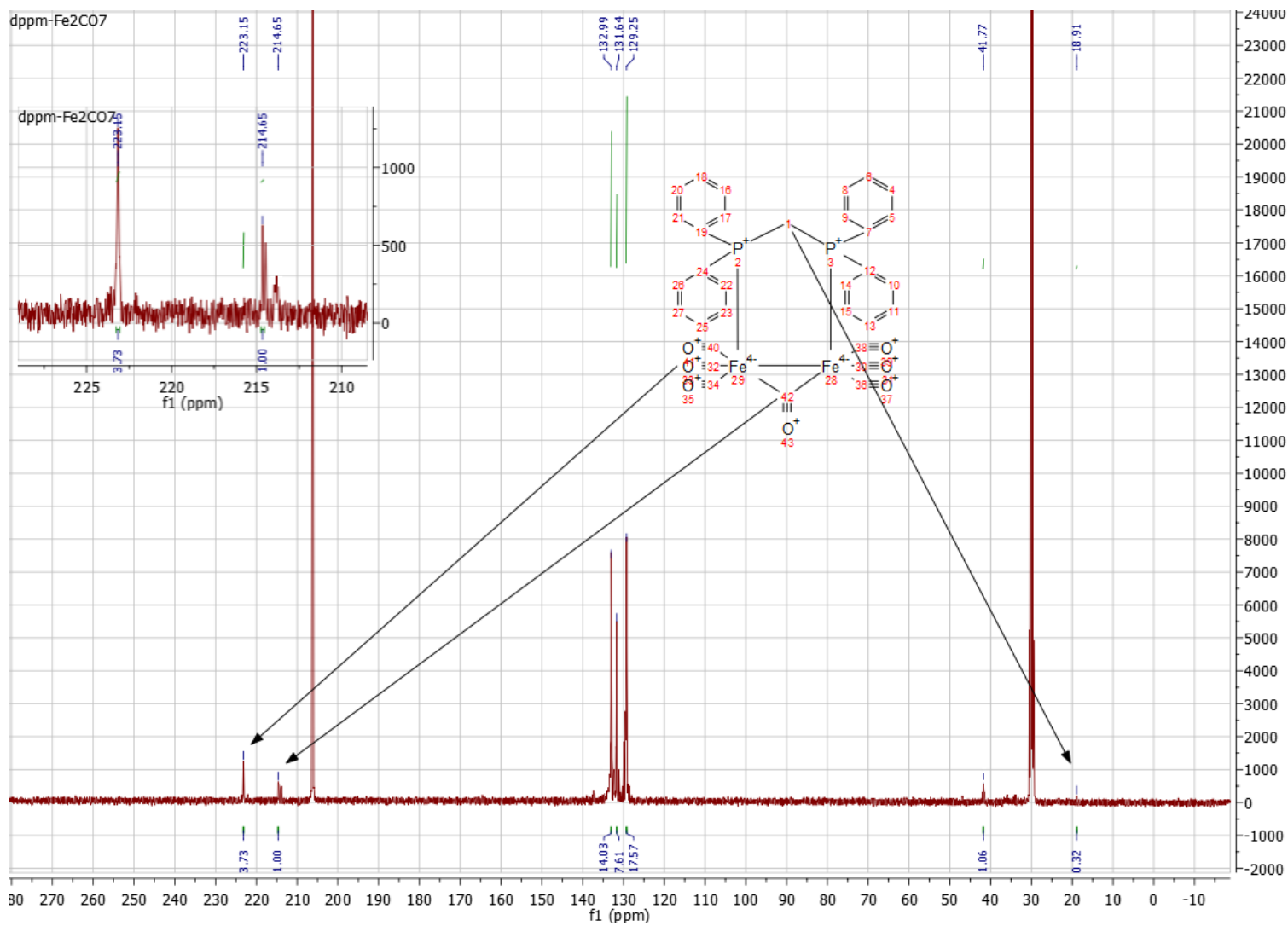
## APPENDIX 2 SPECTRA

### $^{13}\text{C}$ -NMR Spectrum of $[\text{Fe}_2(\text{CO})_4(\mu\text{-CO})(\mu,\eta^2\text{-dppm})_2]$ (2)



## APPENDIX 2 $^{13}\text{C}$ -NMR SPECTRA

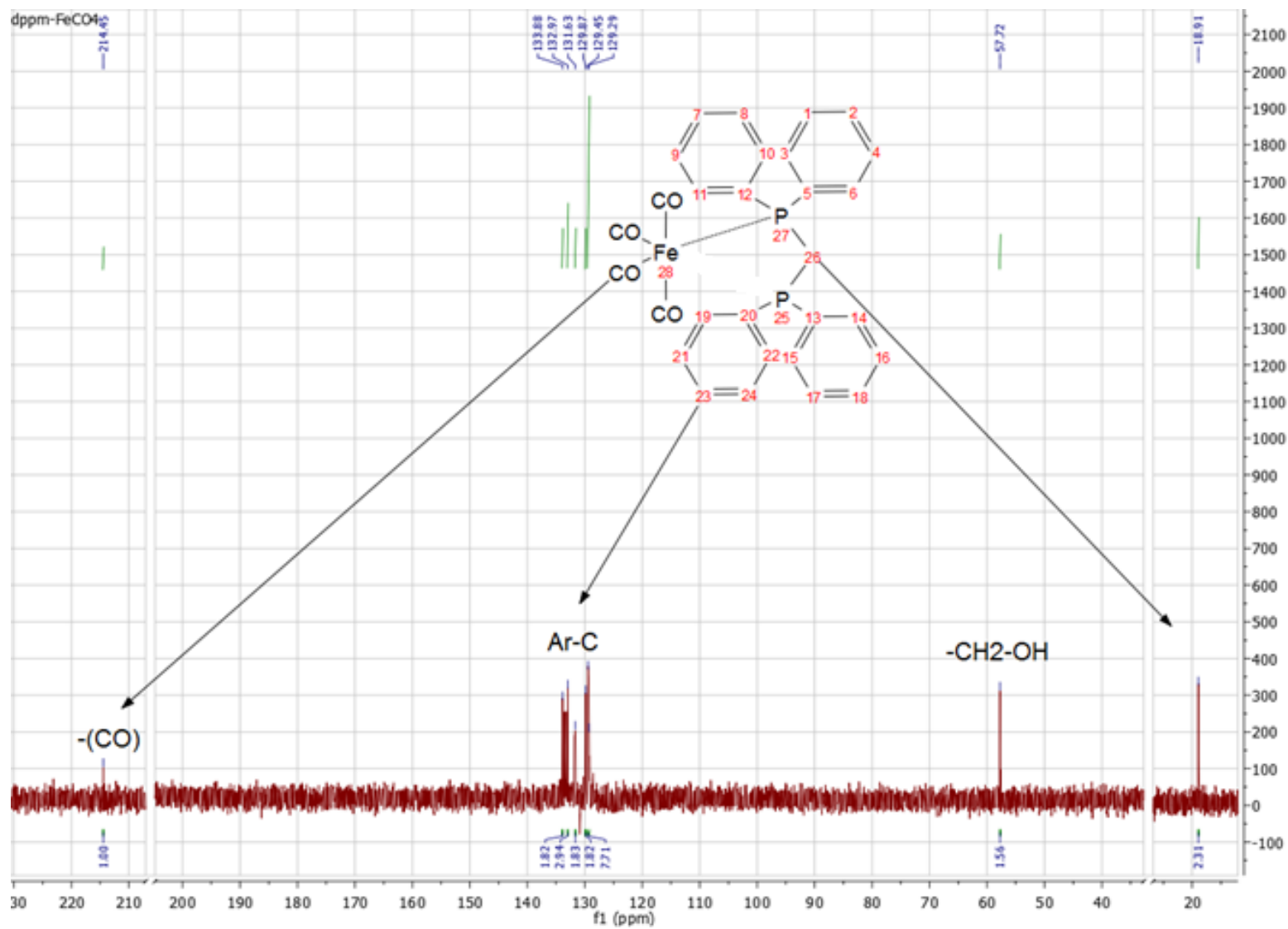
### $^{13}\text{C}$ -NMR Spectrum of $[\text{Fe}_2(\text{CO})_4(\mu\text{-CO})_3(\mu,\eta^2\text{-dppm})]$ (3)





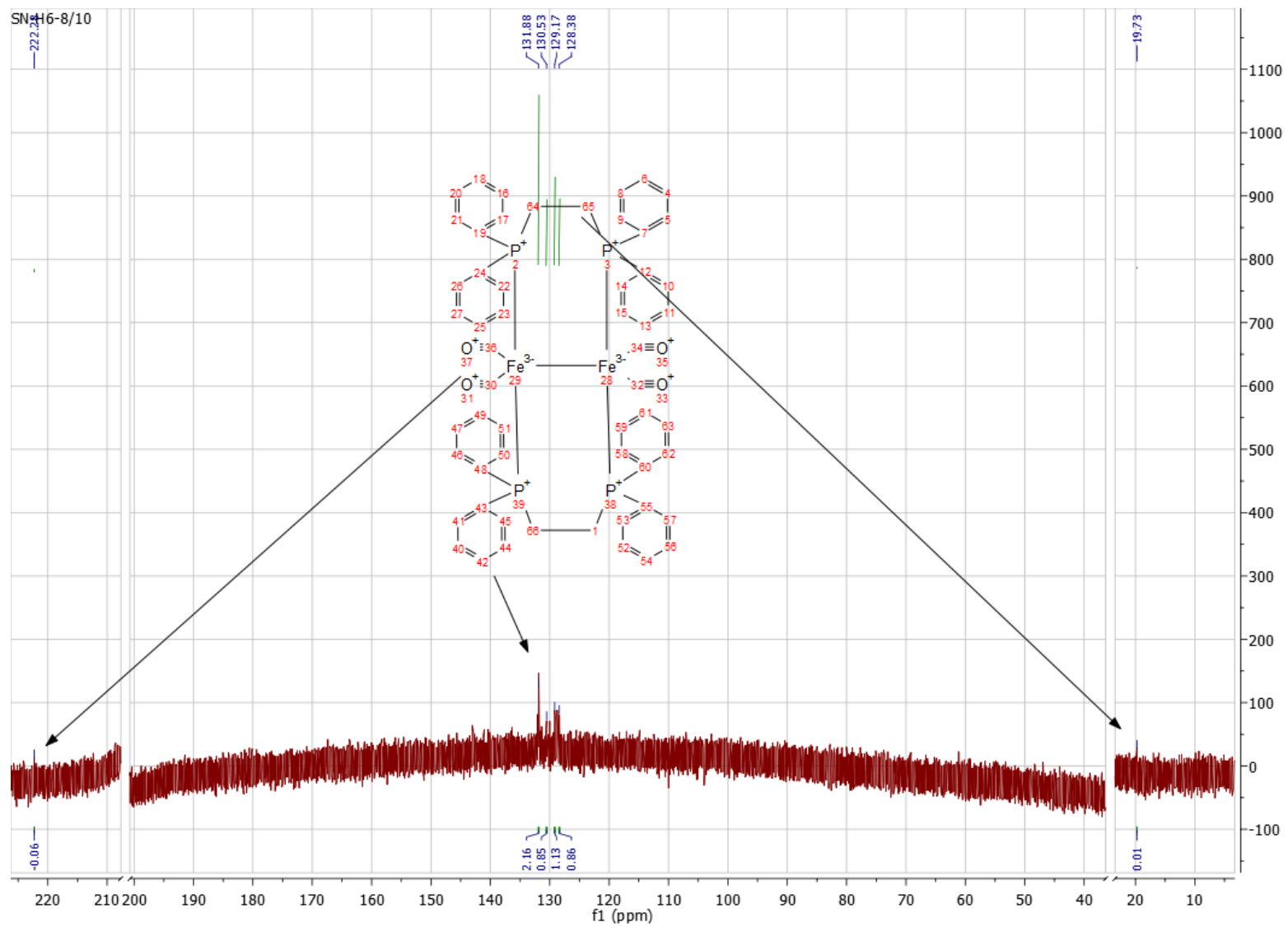
## APPENDIX 2 $^{13}\text{C}$ -NMR SPECTRA

### $^{13}\text{C}$ -NMR Spectrum of $[\text{Fe}(\text{CO})_4(\text{dppm})]$ (4)



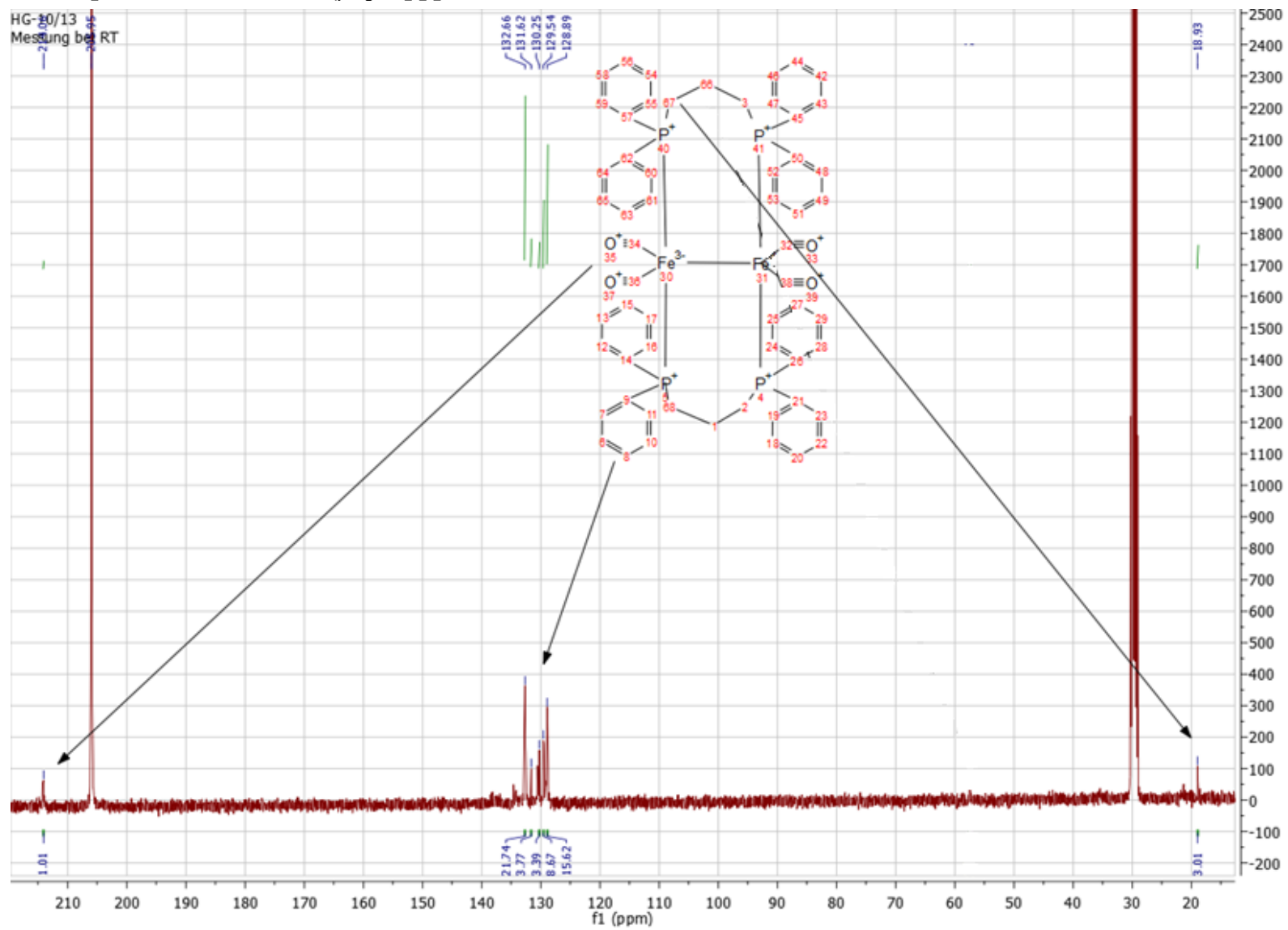
## APPENDIX 2 $^{13}\text{C}$ -NMR SPECTRA

### $^{13}\text{C}$ -NMR Spectrum of $[\text{Fe}_2(\text{CO})_4(\mu, \eta^2\text{-dppe})_2]$ (5)



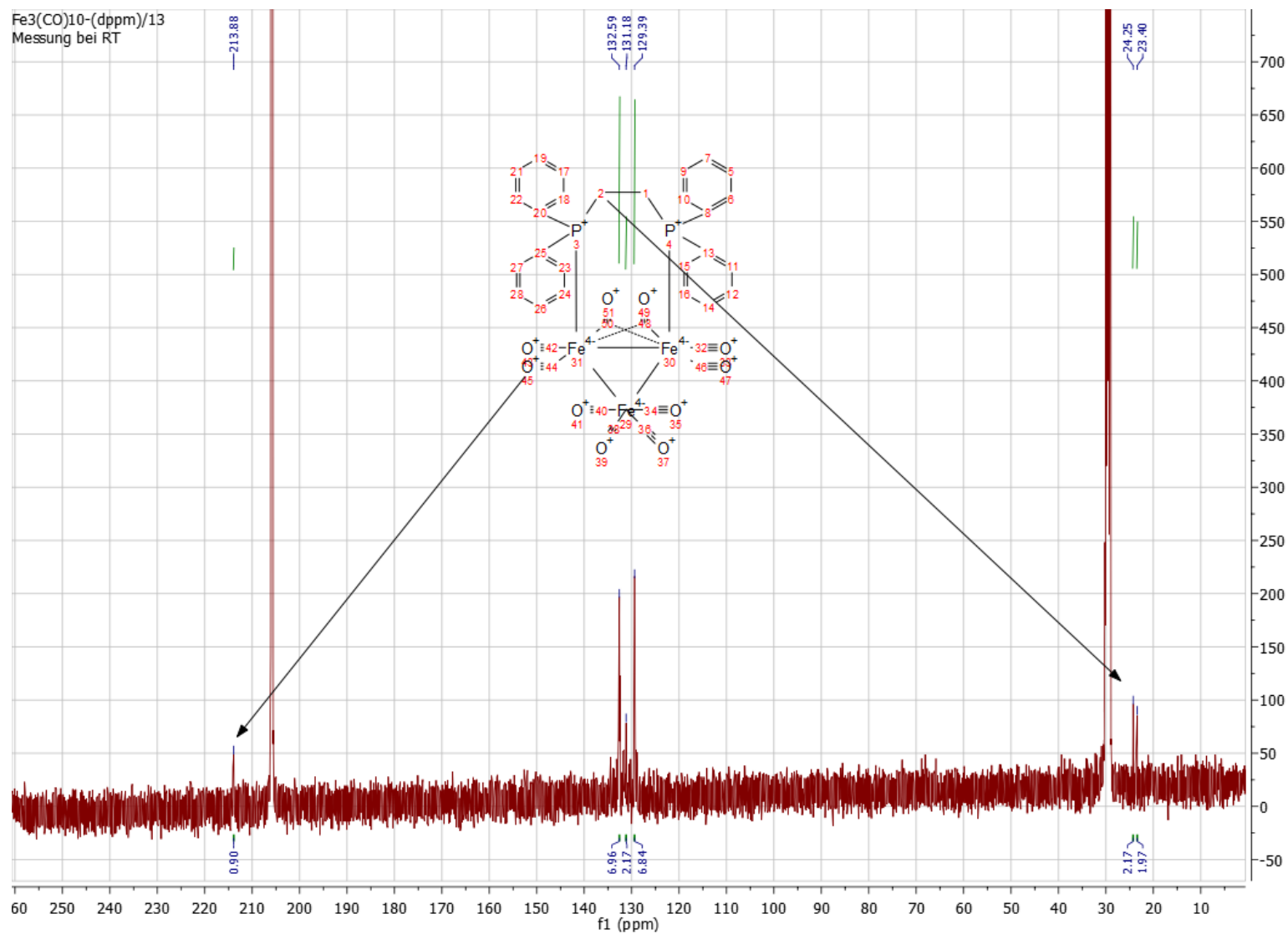
## APPENDIX 2 $^{13}\text{C}$ -NMR SPECTRA

### $^{13}\text{C}$ -NMR Spectrum of $[\text{Fe}_2(\text{CO})_4(\mu, \eta^2\text{-dppp})_2]$ (6)



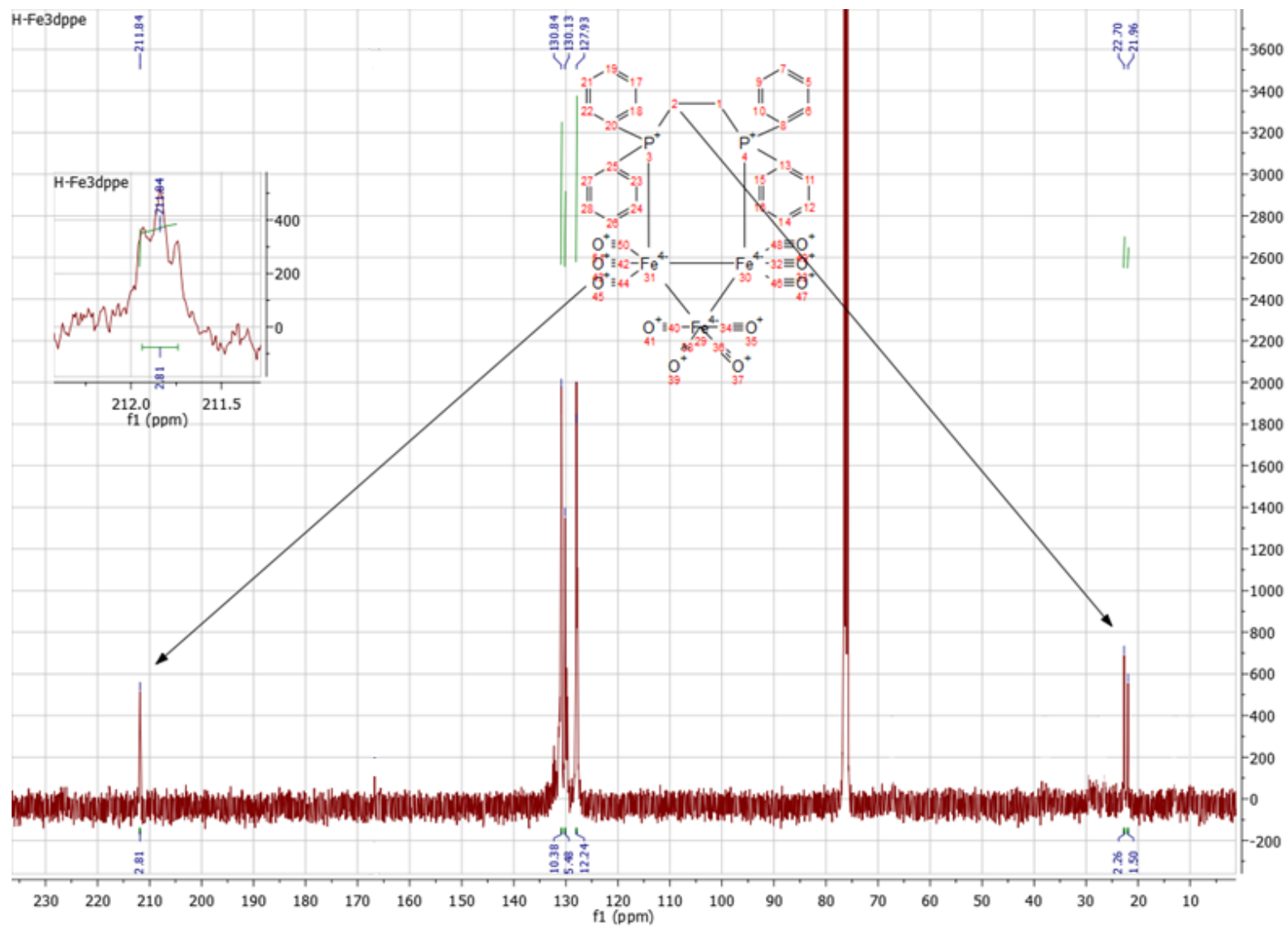
## APPENDIX 2 $^{13}\text{C}$ -NMR SPECTRA

### $^{13}\text{C}$ -NMR Spectrum of $[\text{Fe}_3(\text{CO})_8(\mu\text{-CO})_2(\mu,\eta^2\text{-dppm})]$ (7)



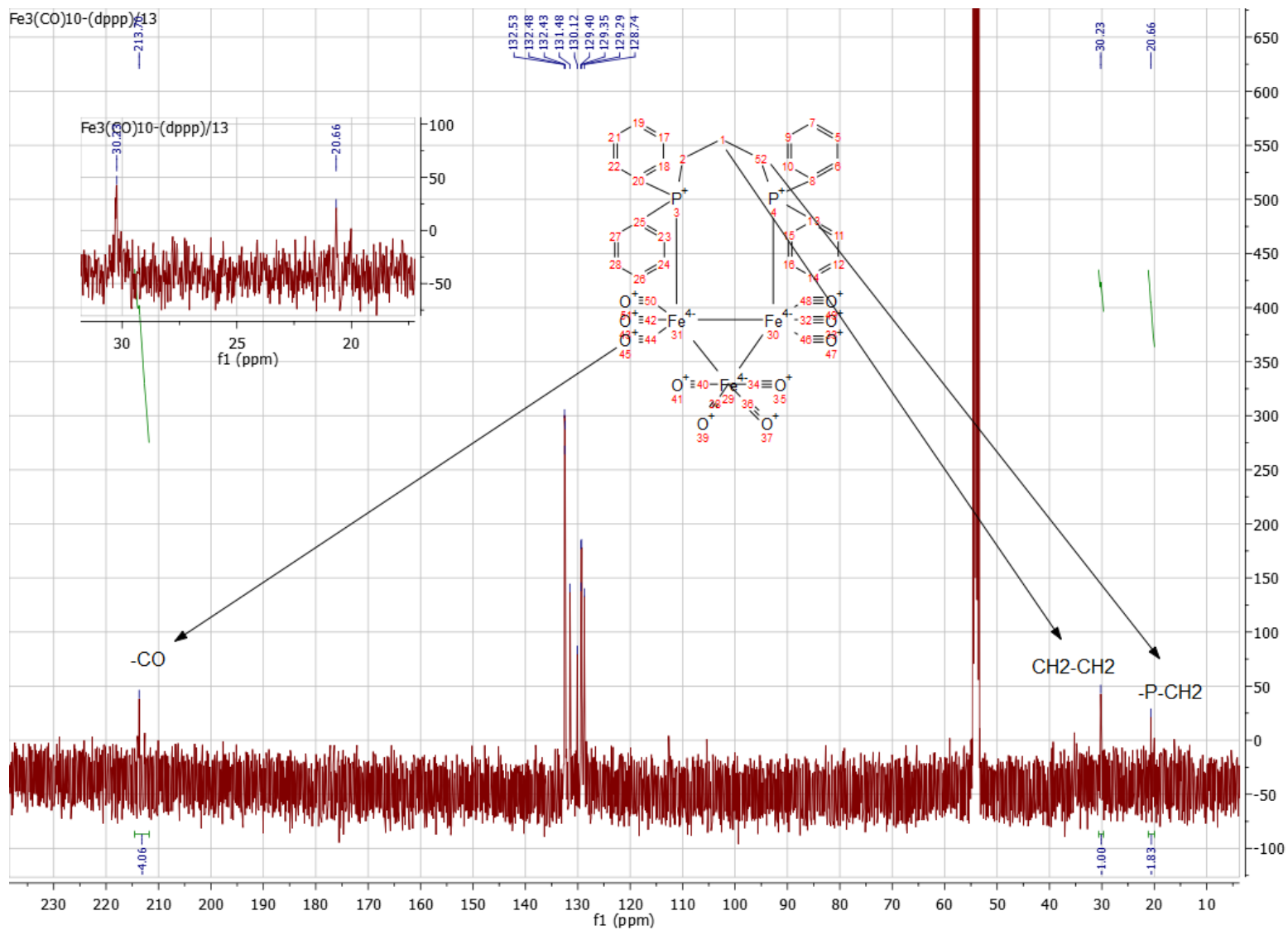
## APPENDIX 2 $^{13}\text{C}$ -NMR SPECTRA

### $^{13}\text{C}$ -NMR Spectrum of $[\text{Fe}_3(\text{CO})_8(\mu\text{-CO})_2(\mu,\eta^2\text{-dppe})]$ (8)



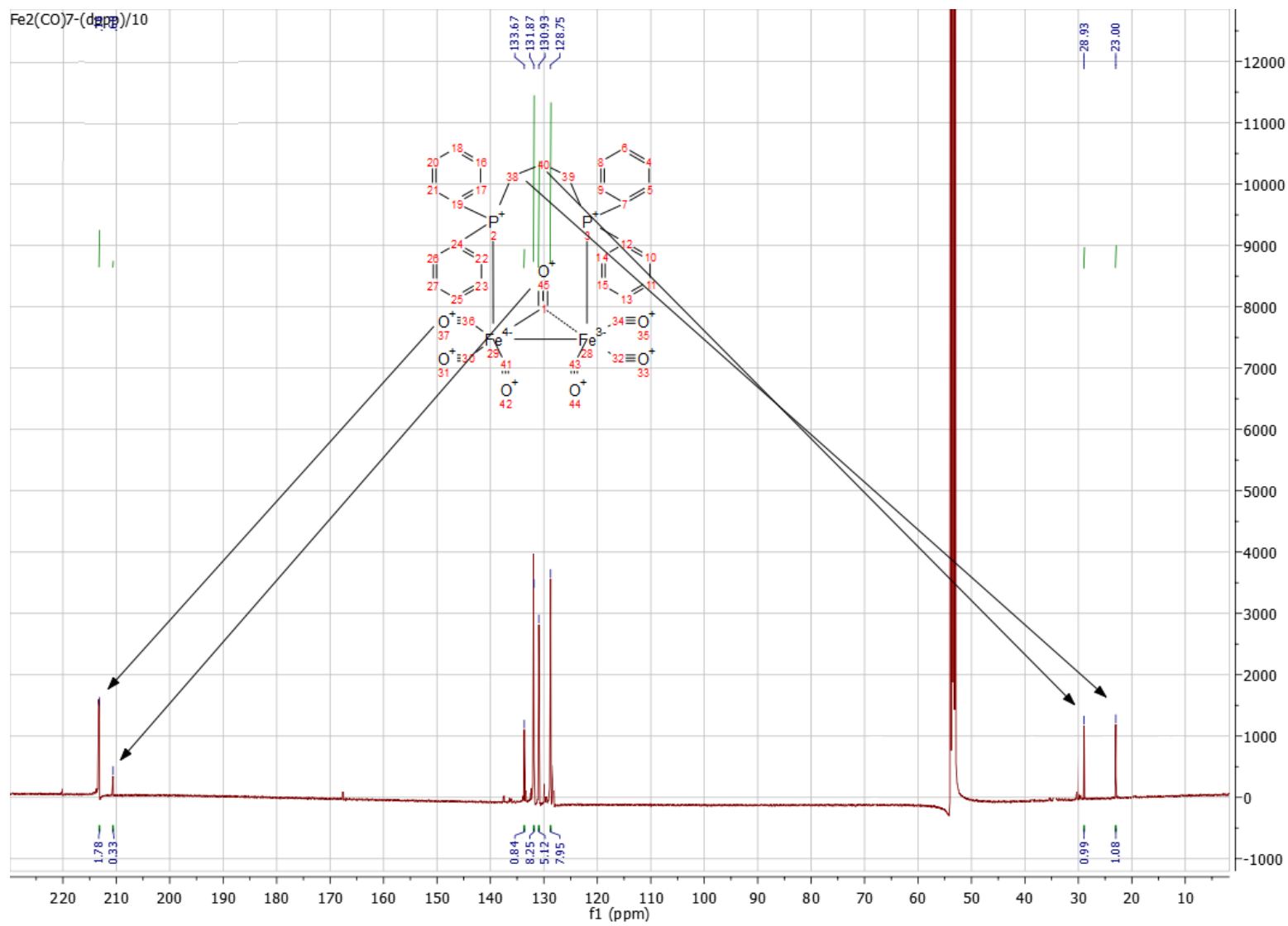
## APPENDIX 2 $^{13}\text{C}$ -NMR SPECTRA

### $^{13}\text{C}$ -NMR Spectrum of $[\text{Fe}_3(\text{CO})_8(\mu\text{-CO})_2(\mu,\eta^2\text{-dppp})]$ (9)



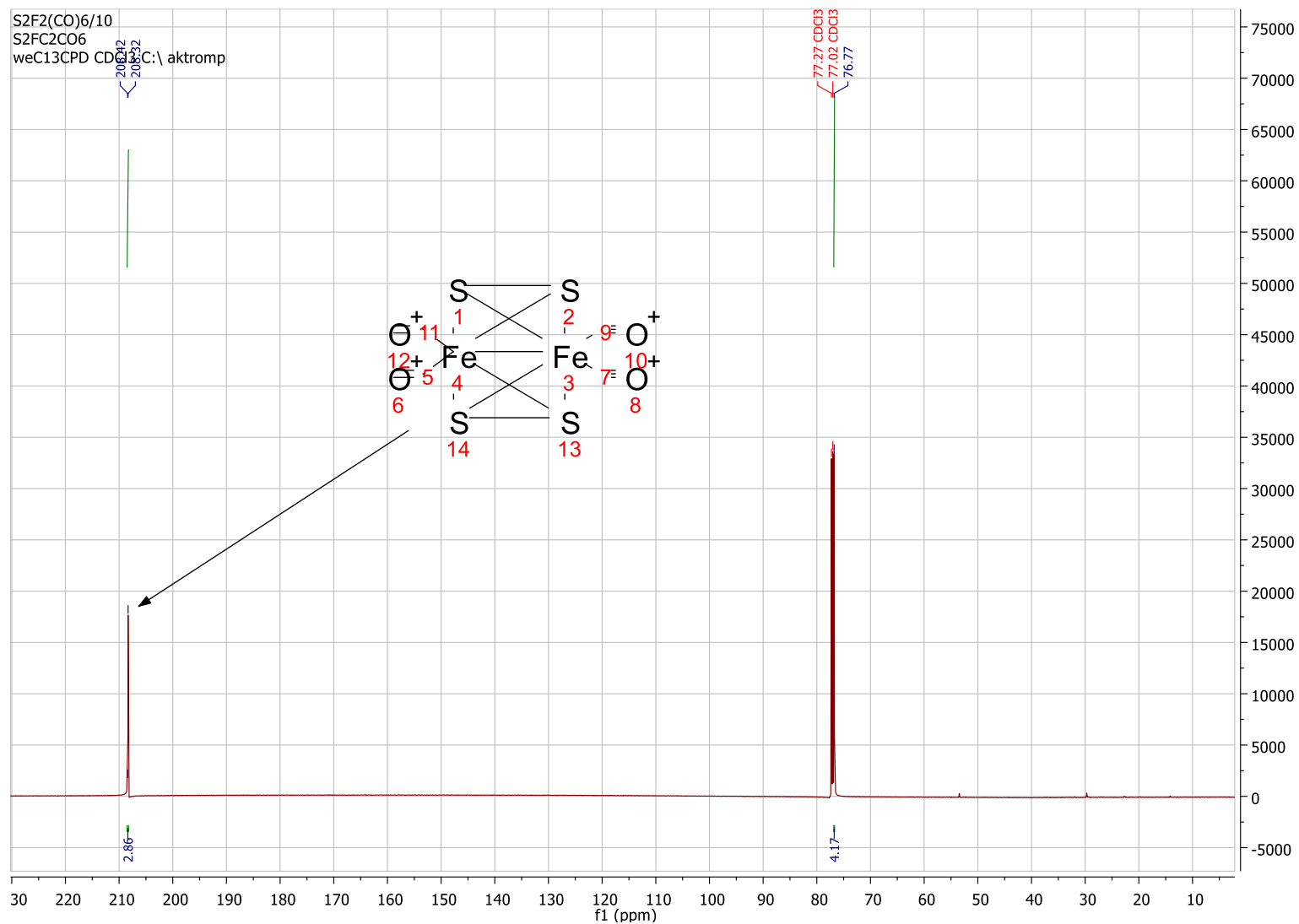
## APPENDIX 2 $^{13}\text{C}$ -NMR SPECTRA

### $^{13}\text{C}$ -NMR Spectrum of $[\text{Fe}_2(\text{CO})_4(\mu\text{-CO})_3(\mu,\eta^2\text{-dppp})]$ (10)



## APPENDIX 2 $^{13}\text{C}$ -NMR SPECTRA

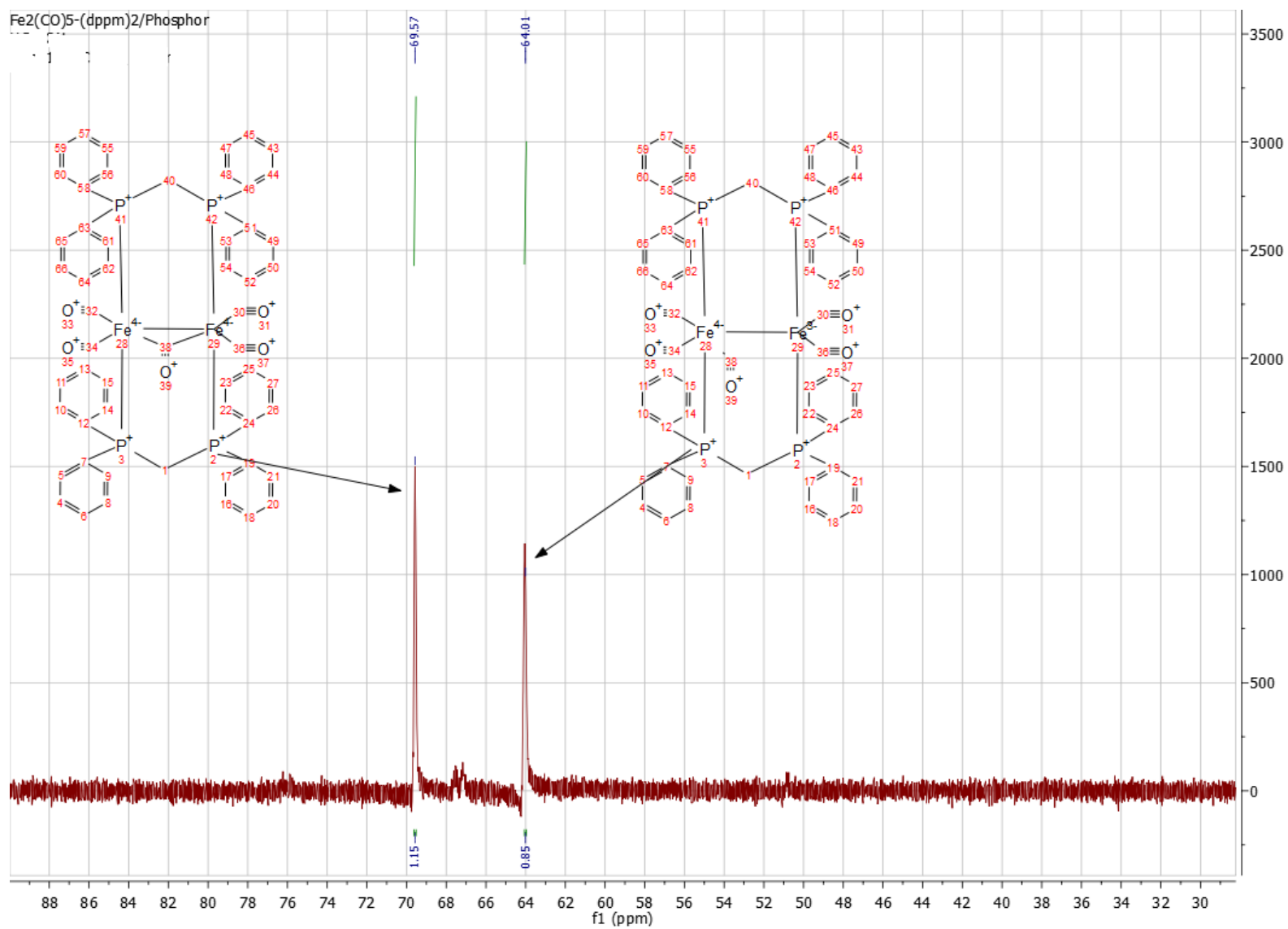
### $^{13}\text{C}$ -NMR Spectrum of $[\text{Fe}_2(\text{S}_4)(\text{CO})_4]$ (11)





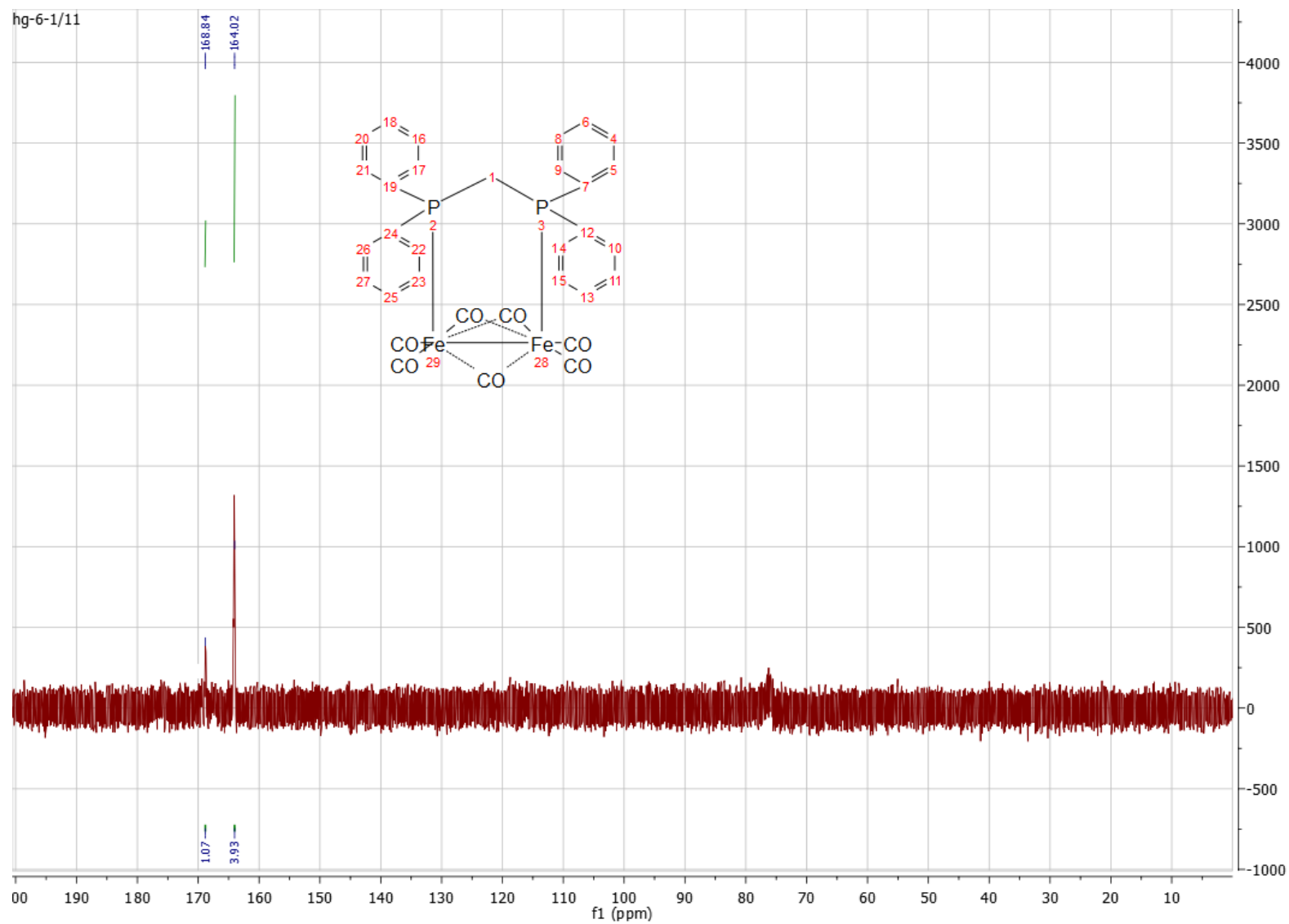
## APPENDIX 3 $^{31}\text{P}$ -NMR SPECTRA

### $^{31}\text{P}$ -NMR Spectrum of $[\text{Fe}_2(\text{CO})_4(\mu\text{-CO})(\mu,\eta^2\text{-dppm})_2]$ (2)



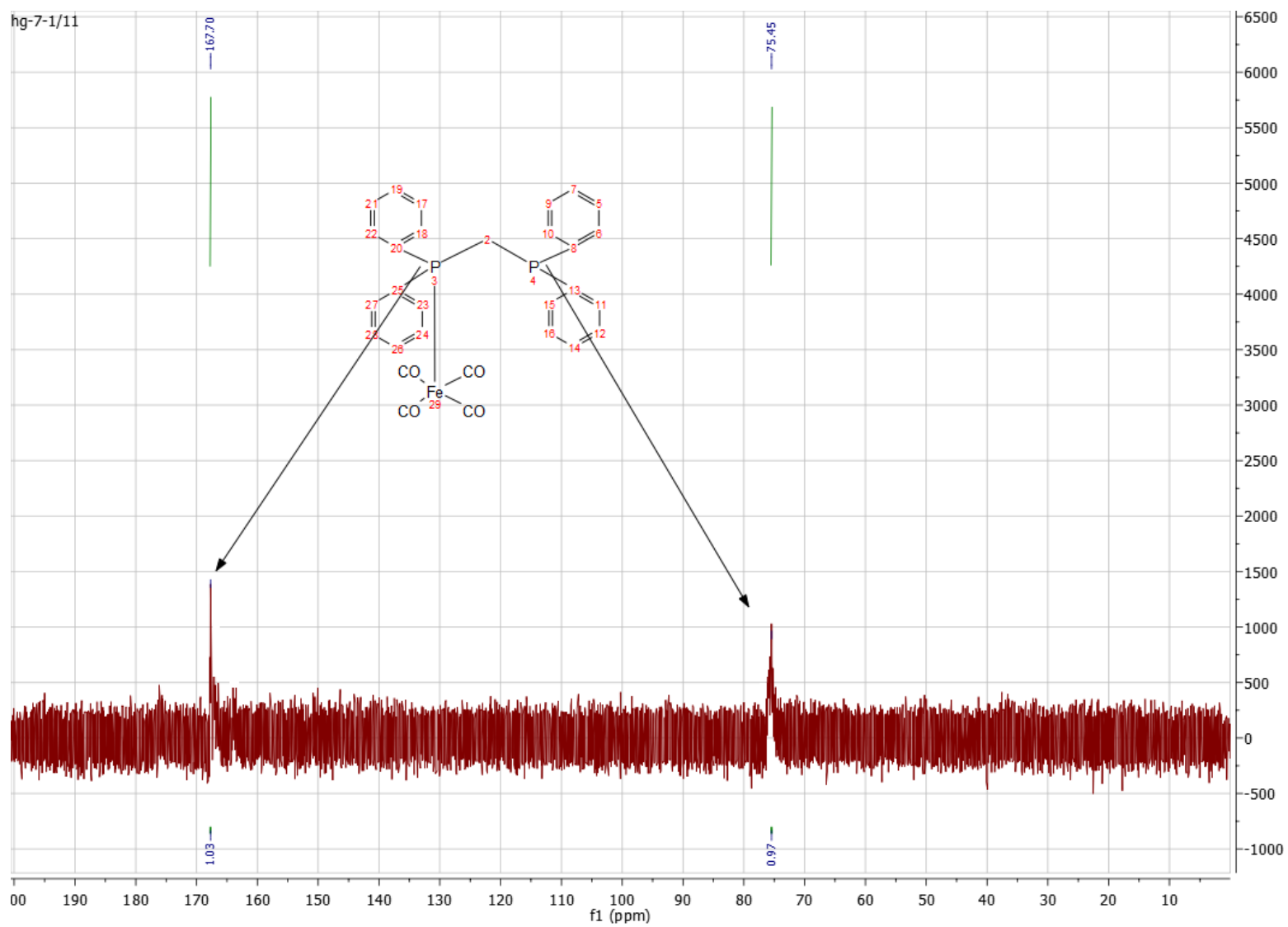
## APPENDIX 3 $^{31}\text{P}$ -NMR SPECTRA

### $^{31}\text{P}$ -NMR Spectrum of $[\text{Fe}_2(\text{CO})_4(\mu\text{-CO})_3(\mu,\eta^2\text{-dppm})]$ (3)



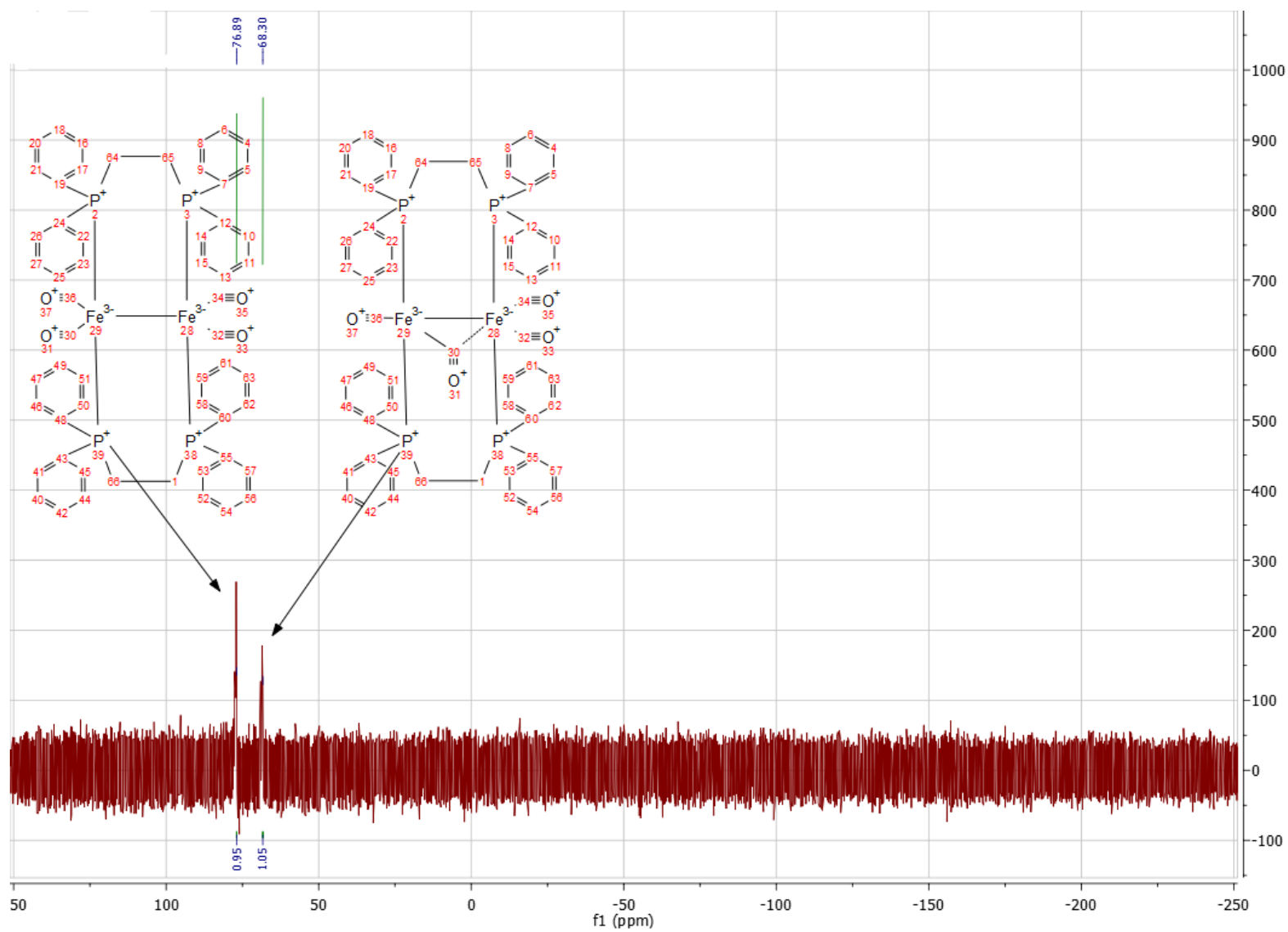
## APPENDIX 3 $^{31}\text{P}$ -NMR SPECTRA

### $^{31}\text{P}$ -NMR Spectrum of $[\text{Fe}(\text{CO})_4(\text{dppm})]$ (4)



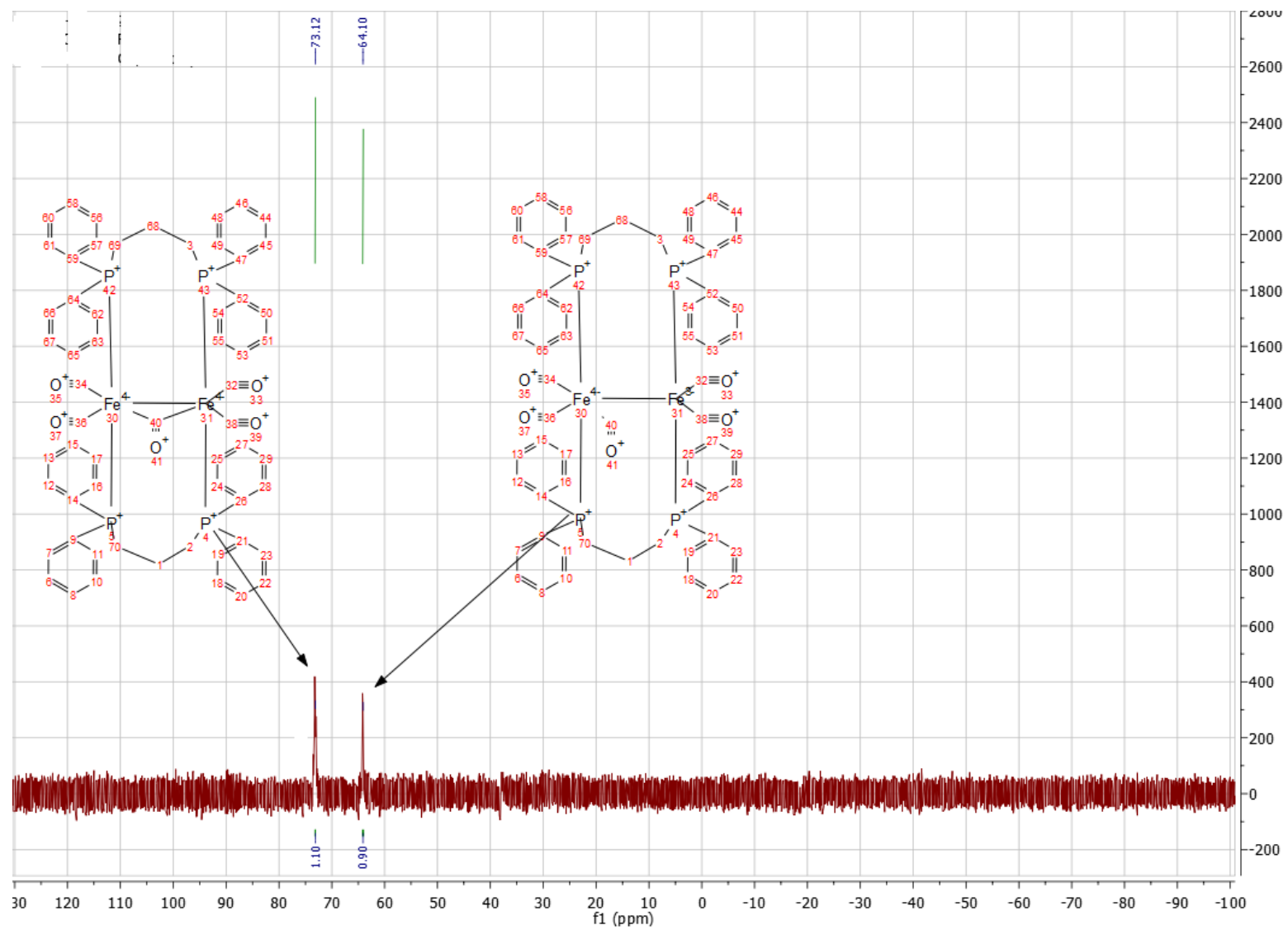
## APPENDIX 3 $^{31}\text{P}$ -NMR SPECTRA

### $^{31}\text{P}$ -NMR Spectrum of $[\text{Fe}_2(\text{CO})_4(\mu, \eta^2\text{-dppe})_2]$ (5)



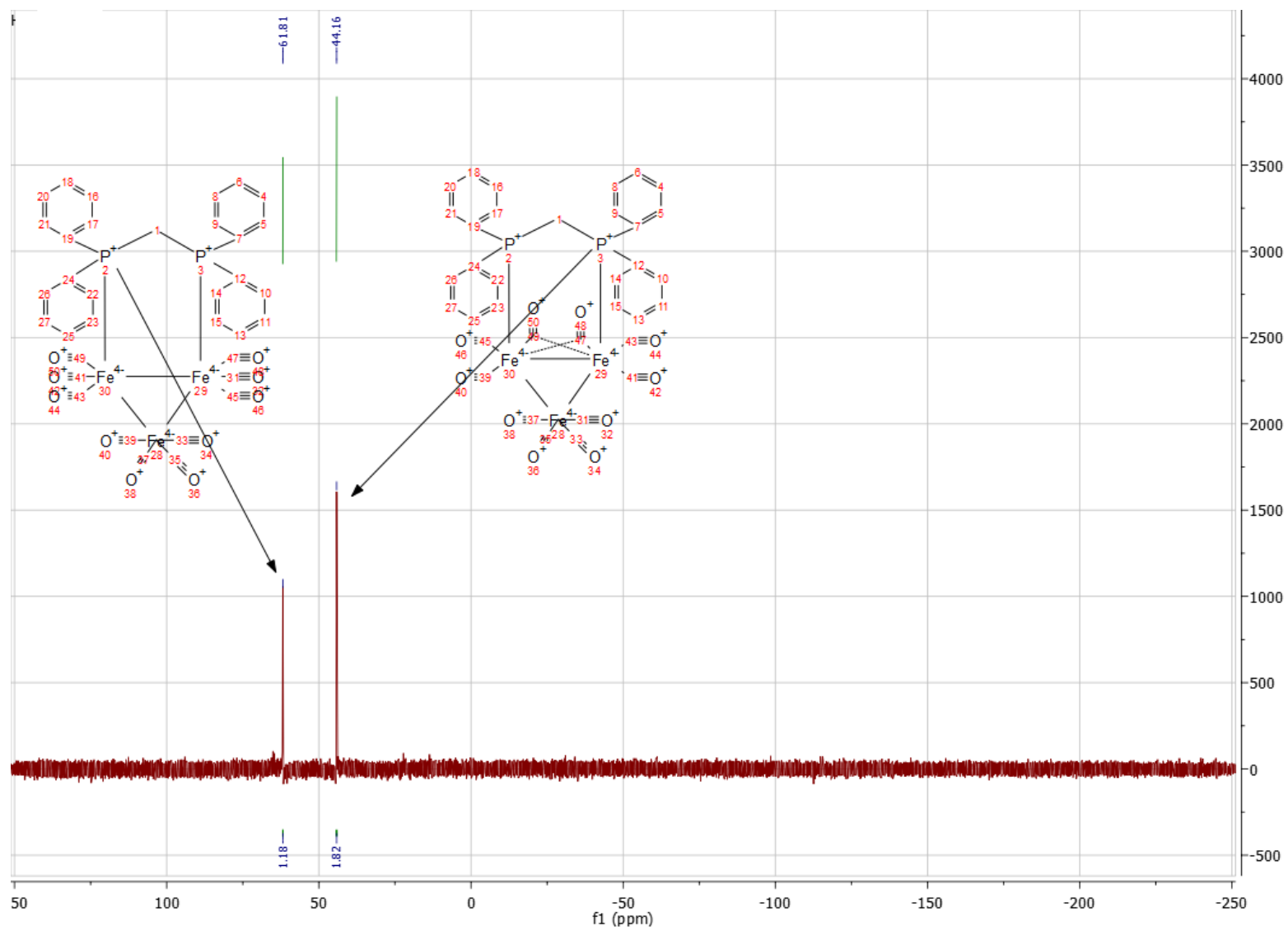
## APPENDIX 3 $^{31}\text{P}$ -NMR SPECTRA

### $^{31}\text{P}$ -NMR Spectrum of $[\text{Fe}_2(\text{CO})_4(\mu, \eta^2\text{-dppp})_2]$ (6)



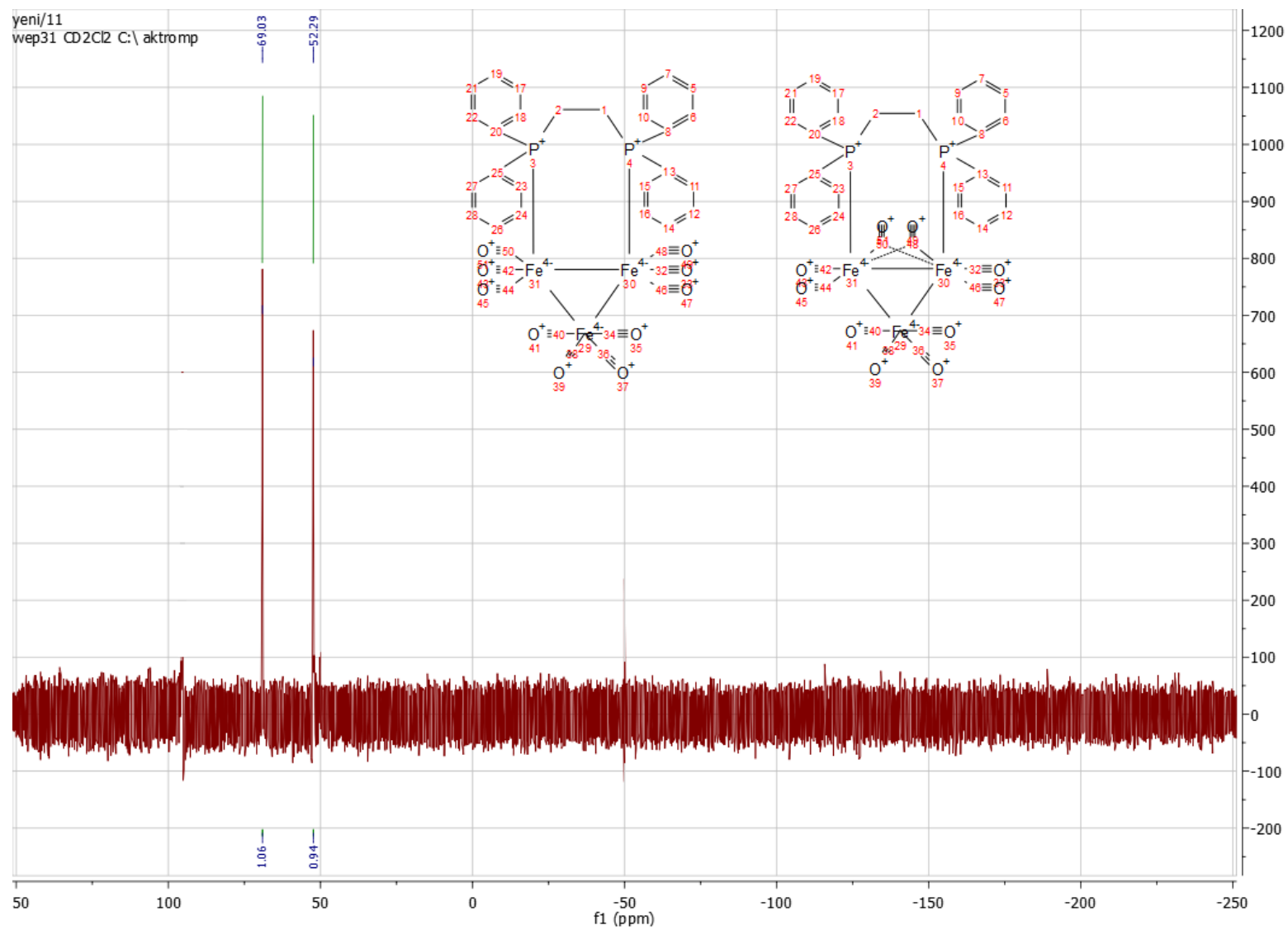
## APPENDIX 3 $^{31}\text{P}$ -NMR SPECTRA

### $^{31}\text{P}$ -NMR Spectrum of $[\text{Fe}_3(\text{CO})_8(\mu\text{-CO})_2(\mu,\eta^2\text{-dppm})]$ (7)



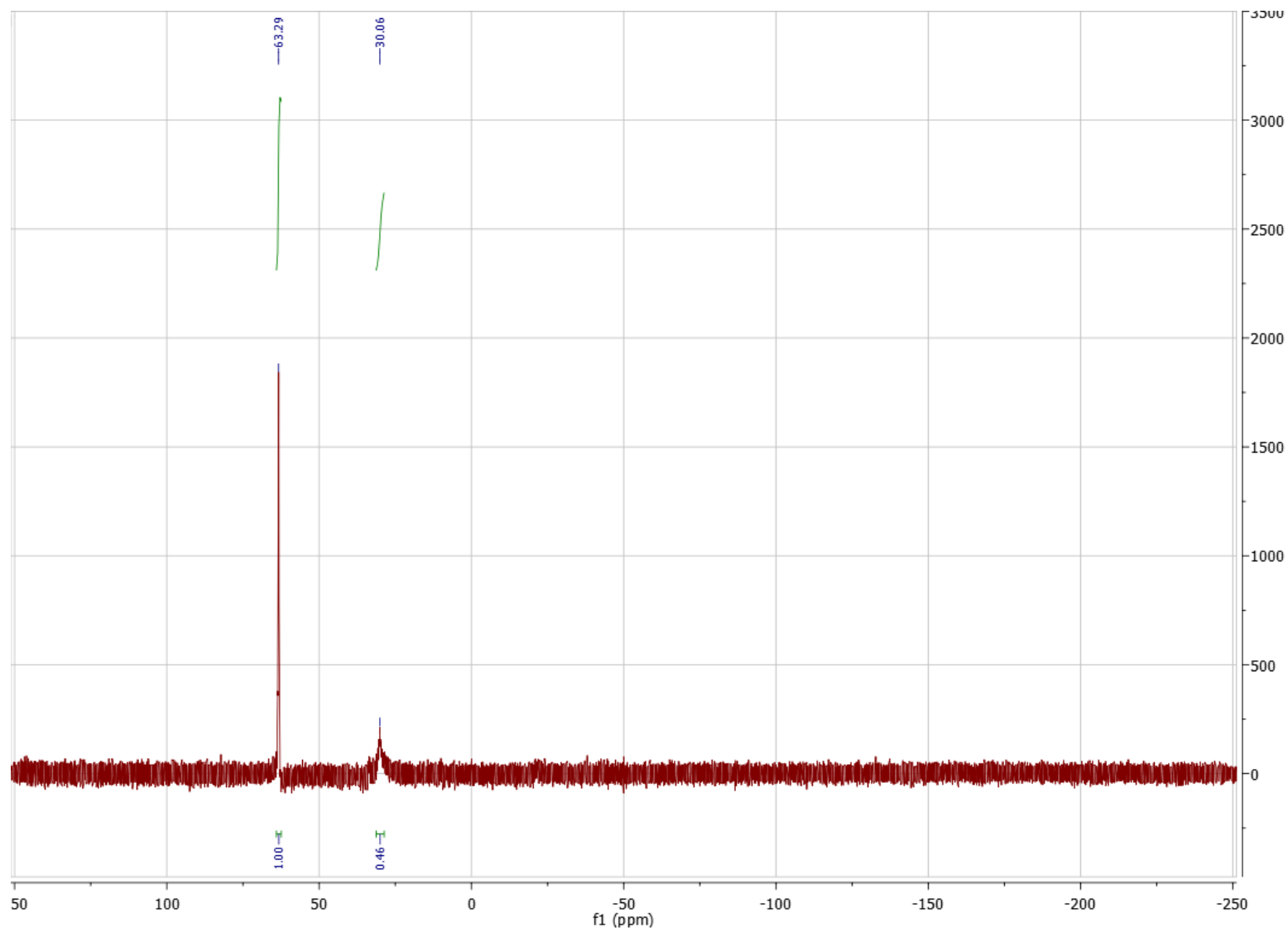
## APPENDIX 3 $^{31}\text{P}$ -NMR SPECTRA

### $^{31}\text{P}$ -NMR Spectrum of $[\text{Fe}_3(\text{CO})_8(\mu\text{-CO})_2(\mu,\eta^2\text{-dppe})] (8)$



## APPENDIX 3 $^{31}\text{P}$ -NMR SPECTRA

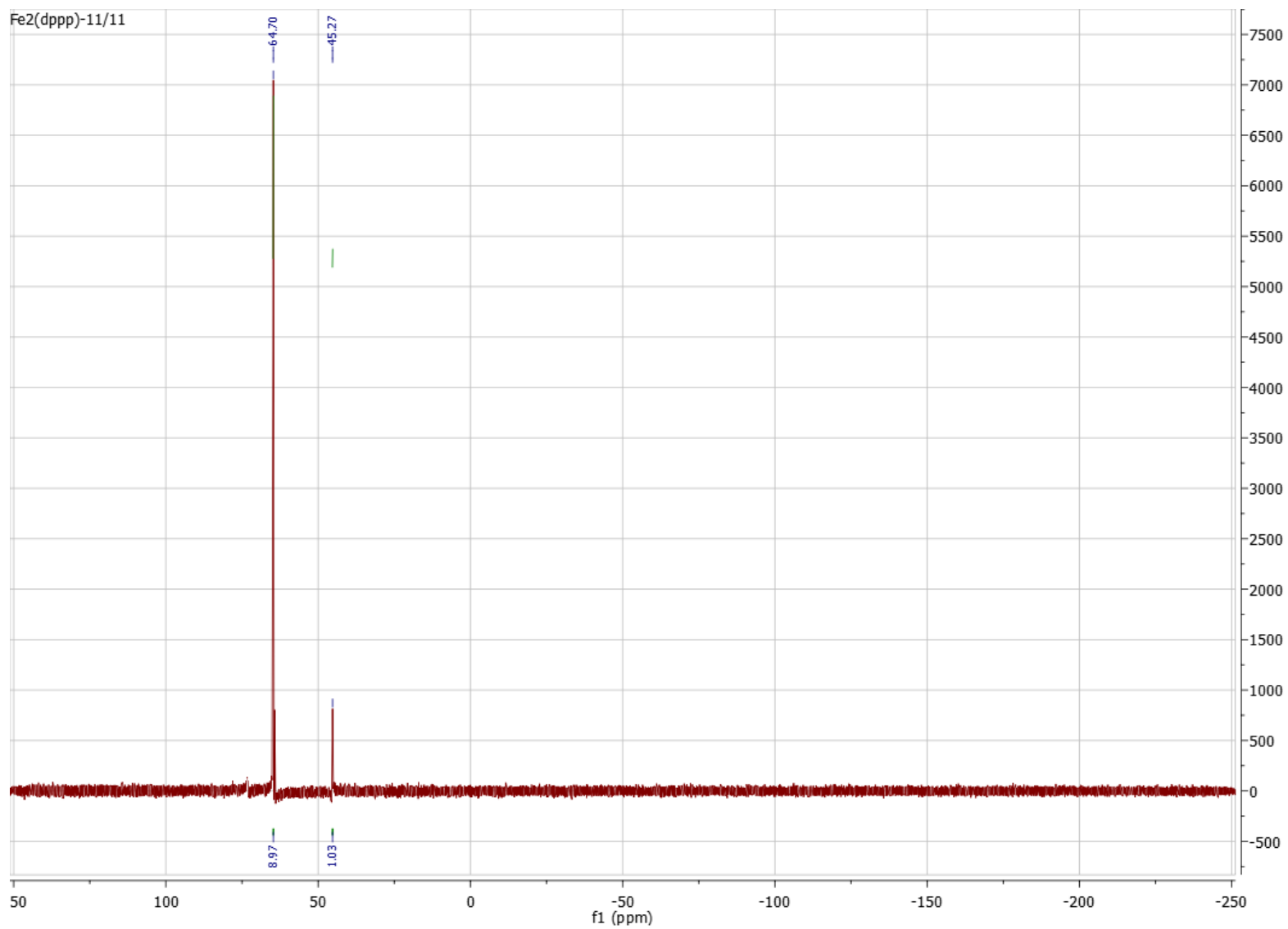
### $^{31}\text{P}$ -NMR Spectrum of $[\text{Fe}_3(\text{CO})_8(\mu\text{-CO})_2(\mu,\eta^2\text{-dppp})]$ (9)





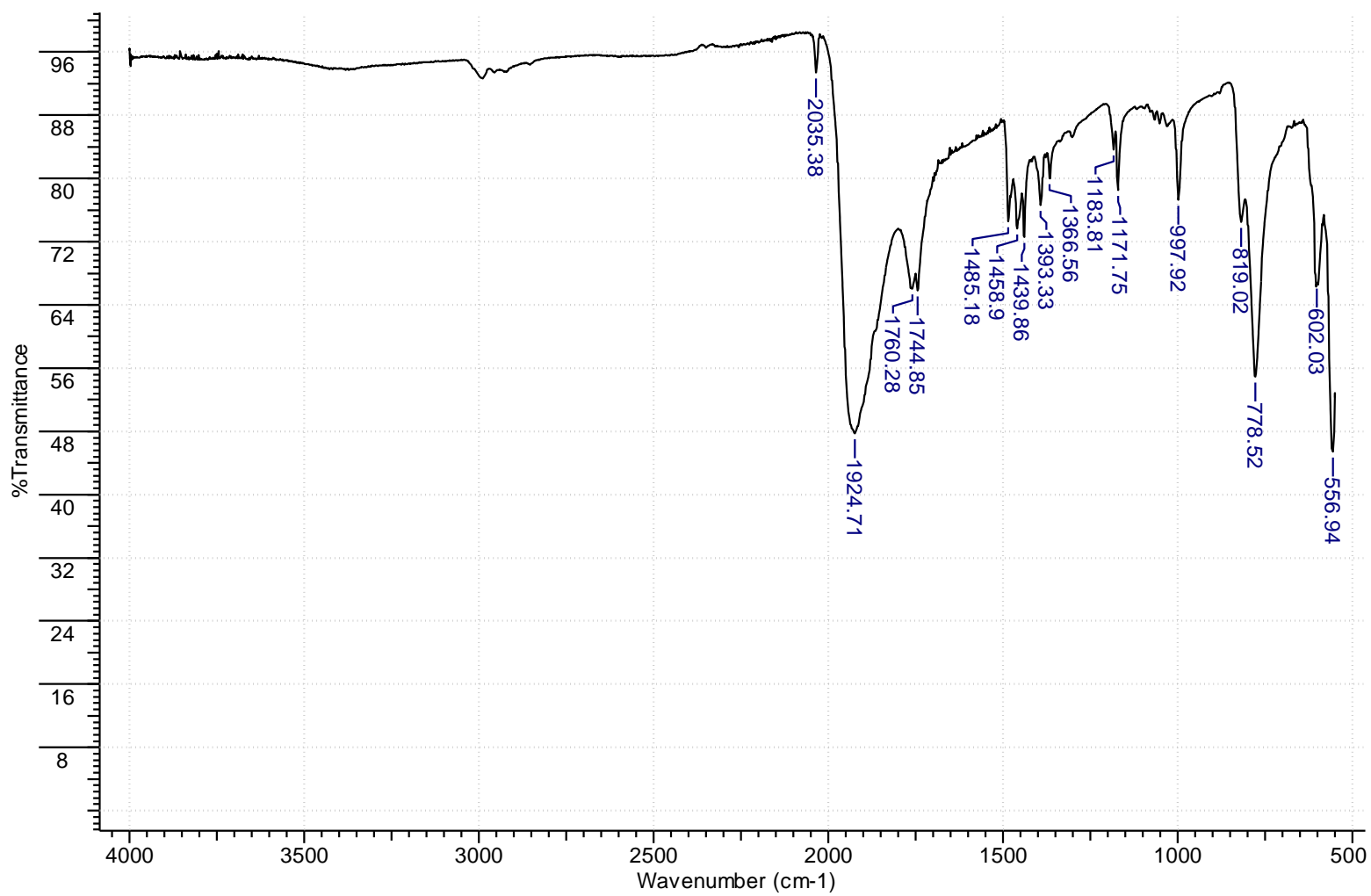
## APPENDIX 3 $^{31}\text{P}$ -NMR SPECTRA

### $^{31}\text{P}$ -NMR Spectrum of $[\text{Fe}_2(\text{CO})_4(\mu\text{-CO})_3(\mu,\eta^2\text{-dppp})]$ (10)



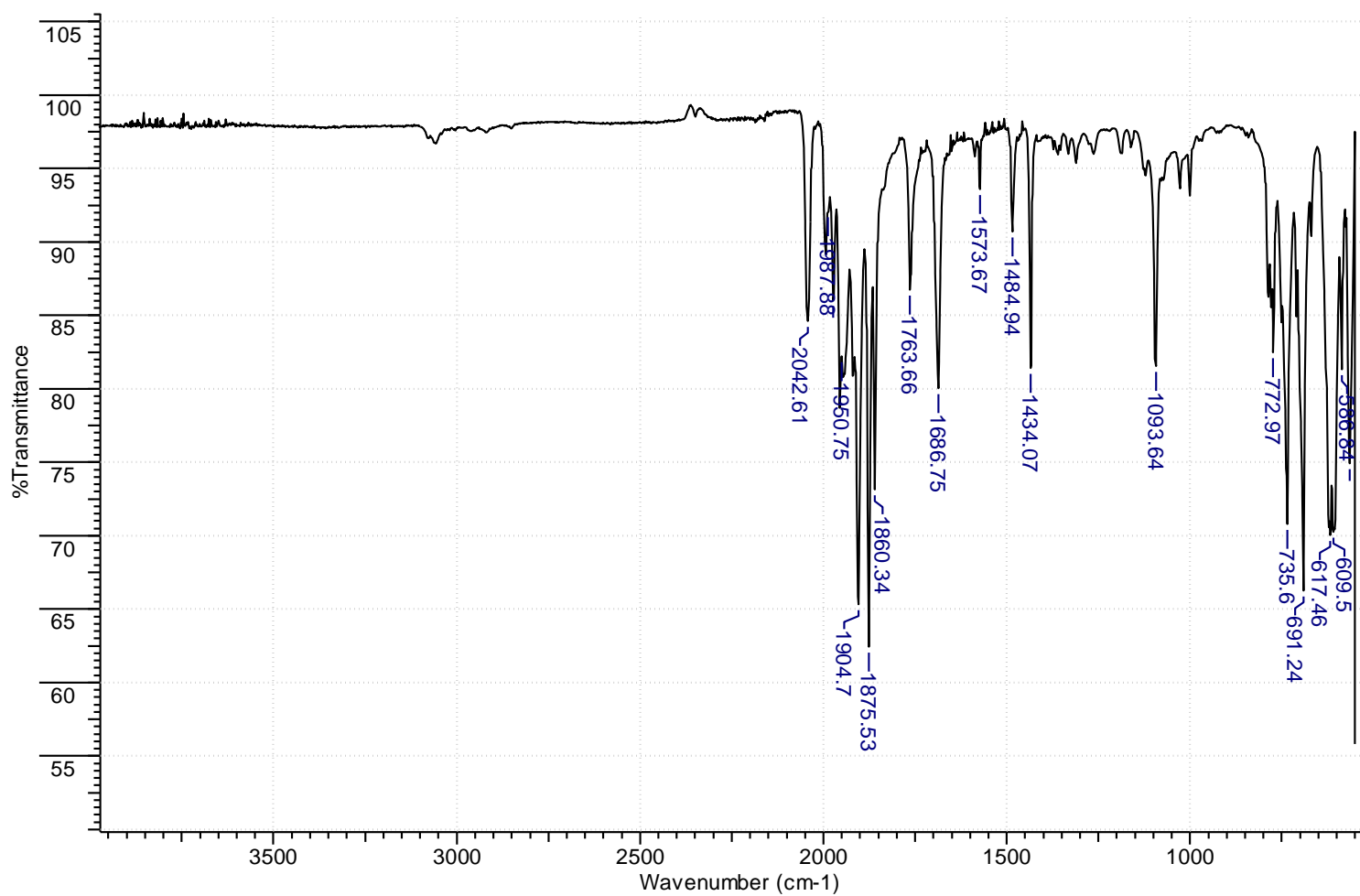
## APPENDIX 4 FTIR SPECTRA

### FTIR Spectrum of $[\text{Et}_4\text{N}]_2[\text{Fe}_6\text{C}(\text{CO})_{16}]$ (1)



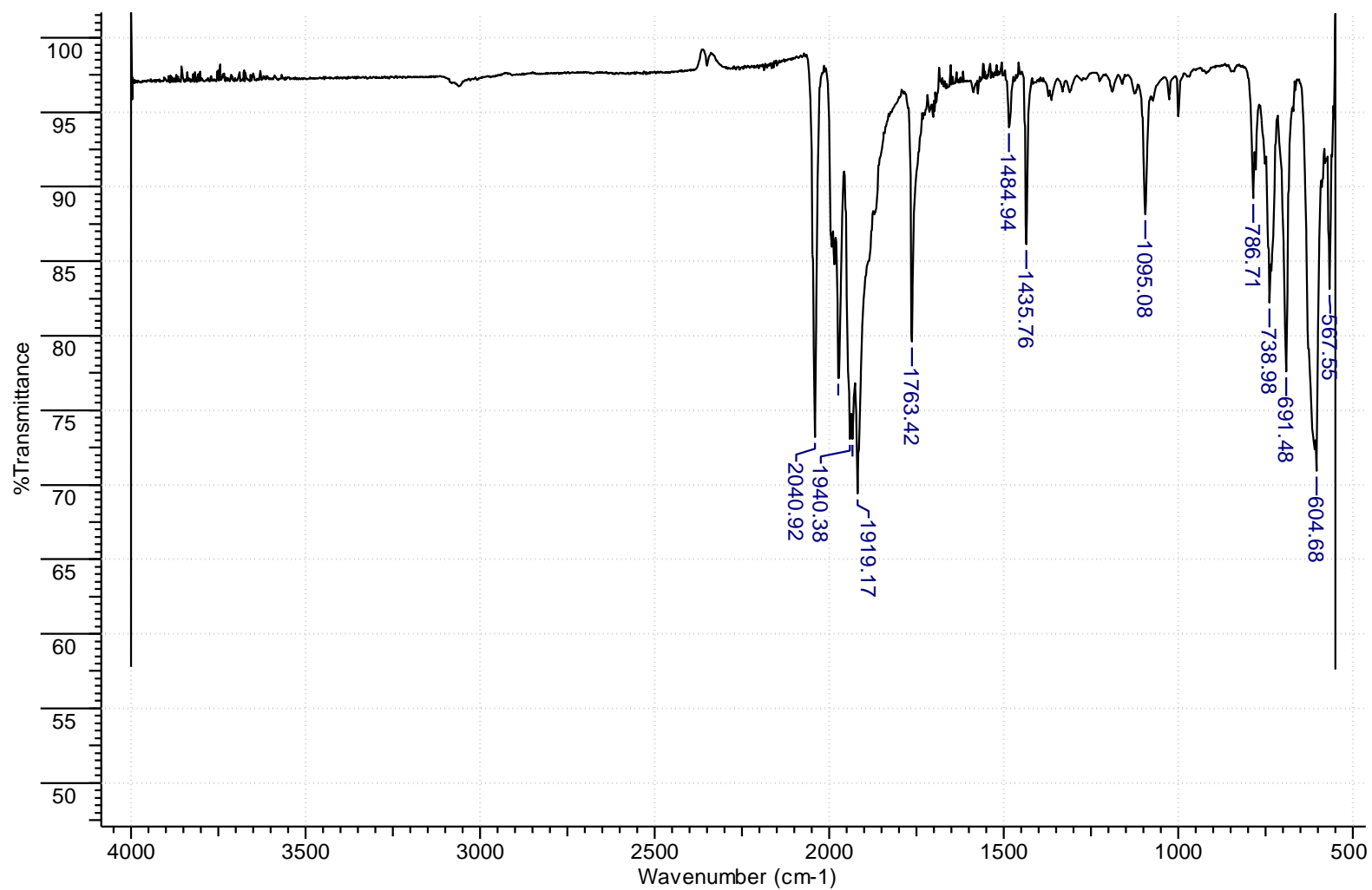
## APPENDIX 4 FTIR SPECTRA

### FTIR Spectrum of $[\text{Fe}_2(\text{CO})_4(\mu\text{-CO})(\mu,\eta^2\text{-dppm})_2]$ (2)



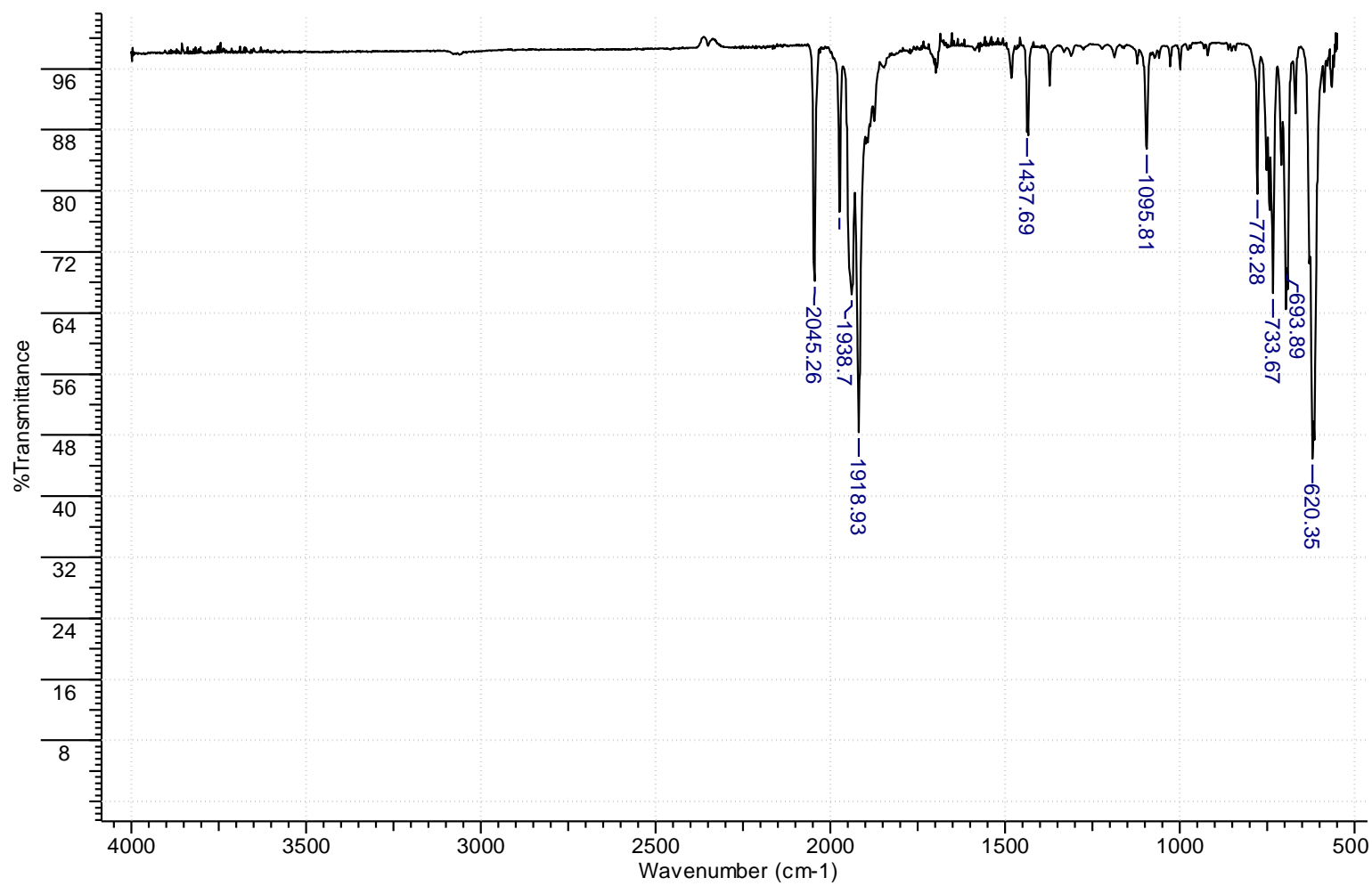
## APPENDIX 4 FTIR SPECTRA

### FTIR Spectrum of $[\text{Fe}_2(\text{CO})_4(\mu\text{-CO})_3(\mu,\eta^2\text{-dppm})]$ (3)



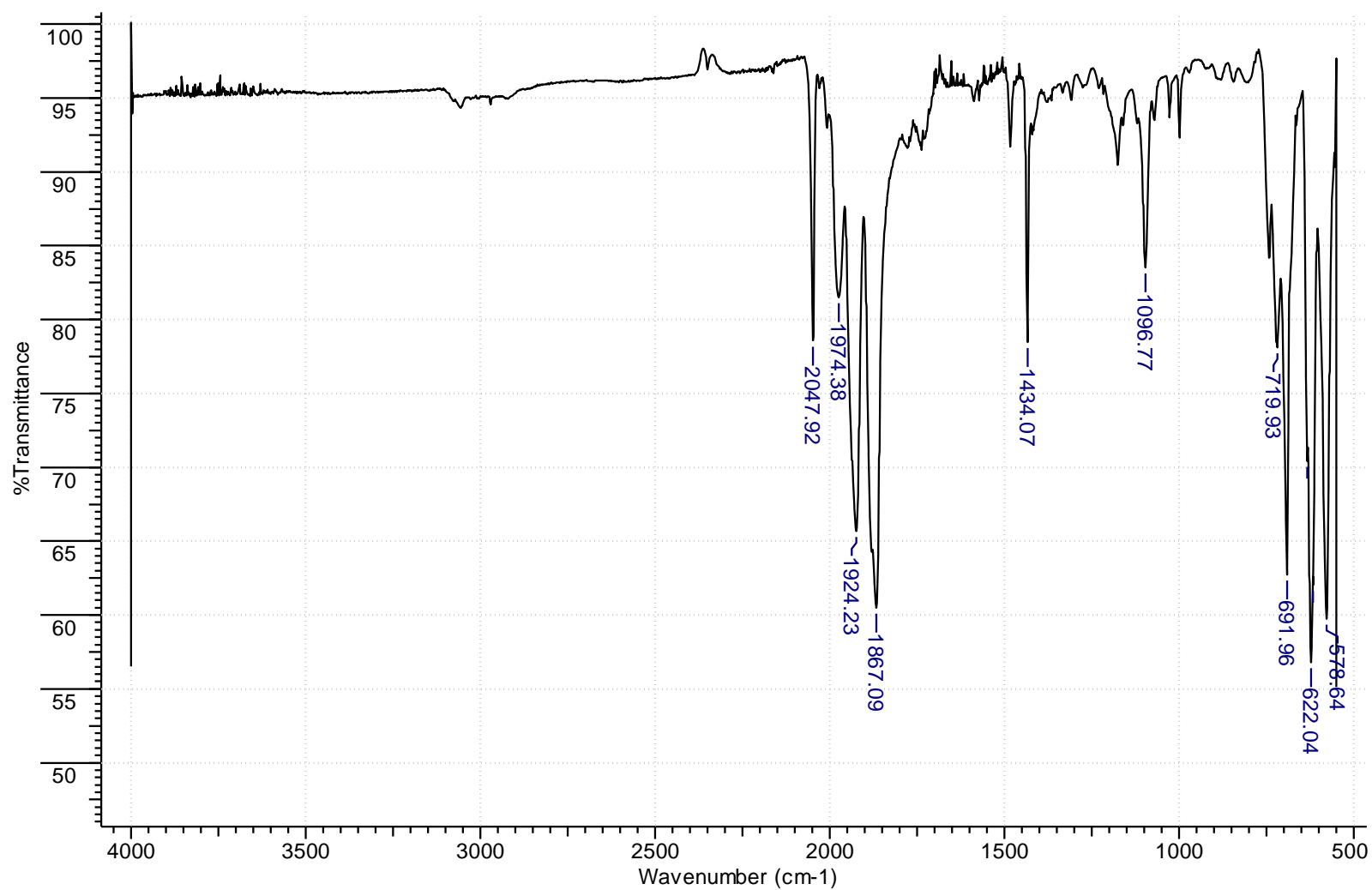
## APPENDIX 4 FTIR SPECTRA

### FTIR Spectrum of [Fe(CO)<sub>4</sub>(dppm)] (4)



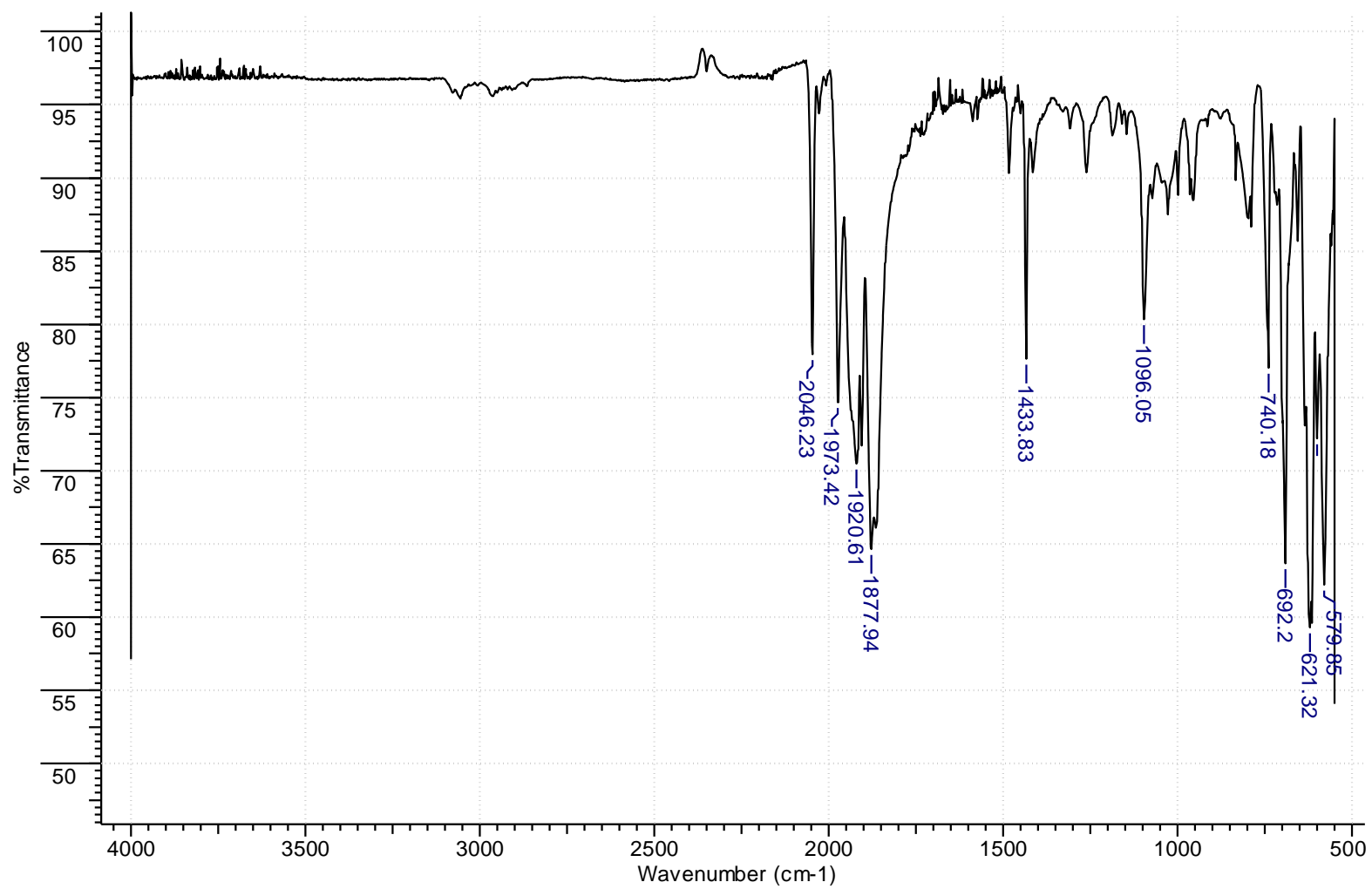
## APPENDIX 4 FTIR SPECTRA

### FTIR Spectrum of $[\text{Fe}_2(\text{CO})_4(\mu, \eta^2\text{-dppe})_2]$ (5)



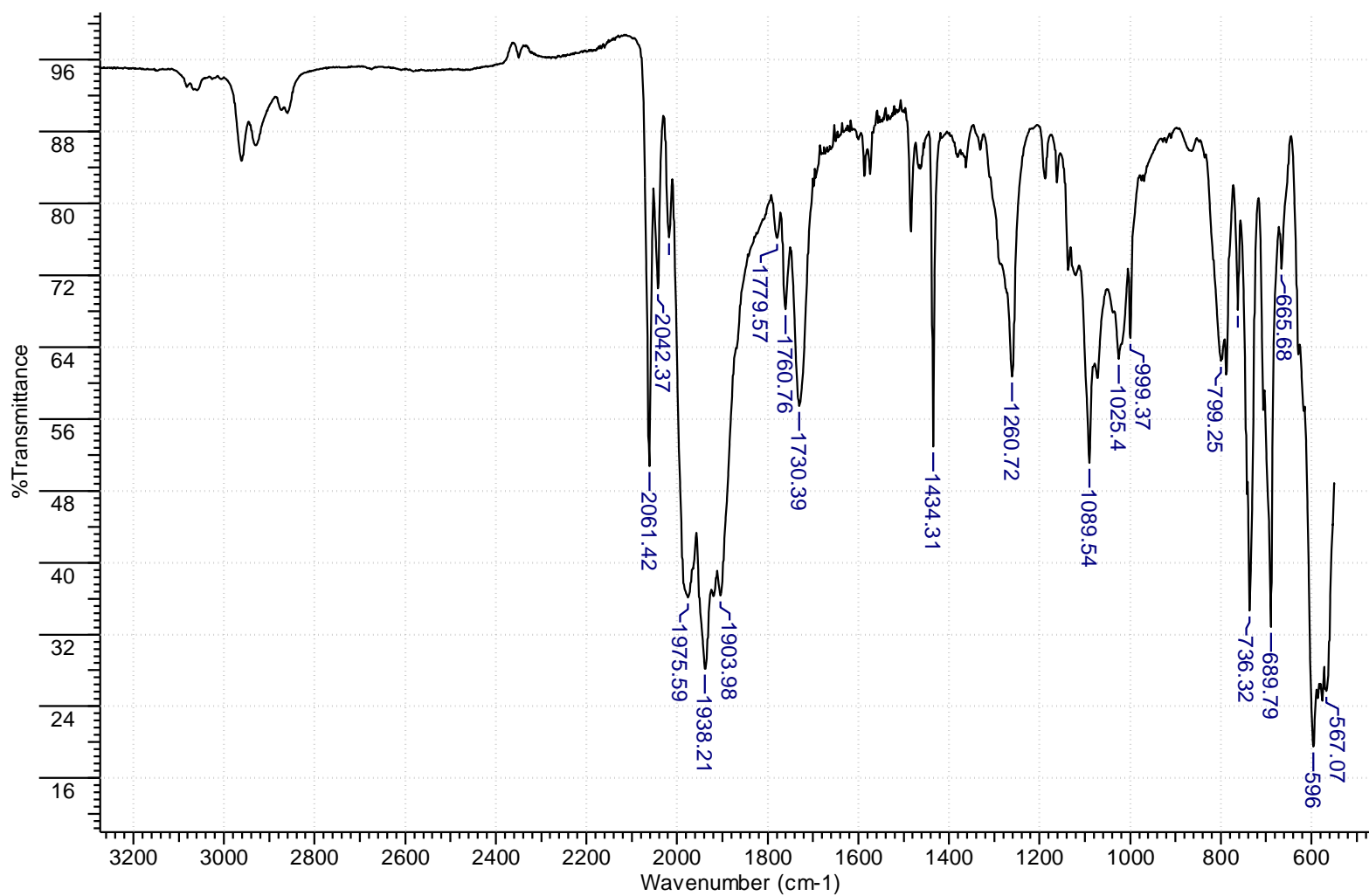
## APPENDIX 4 FTIR SPECTRA

### FTIR Spectrum of $[\text{Fe}_2(\text{CO})_4(\mu, \eta^2\text{-dppp})_2]$ (6)



## APPENDIX 4 FTIR SPECTRA

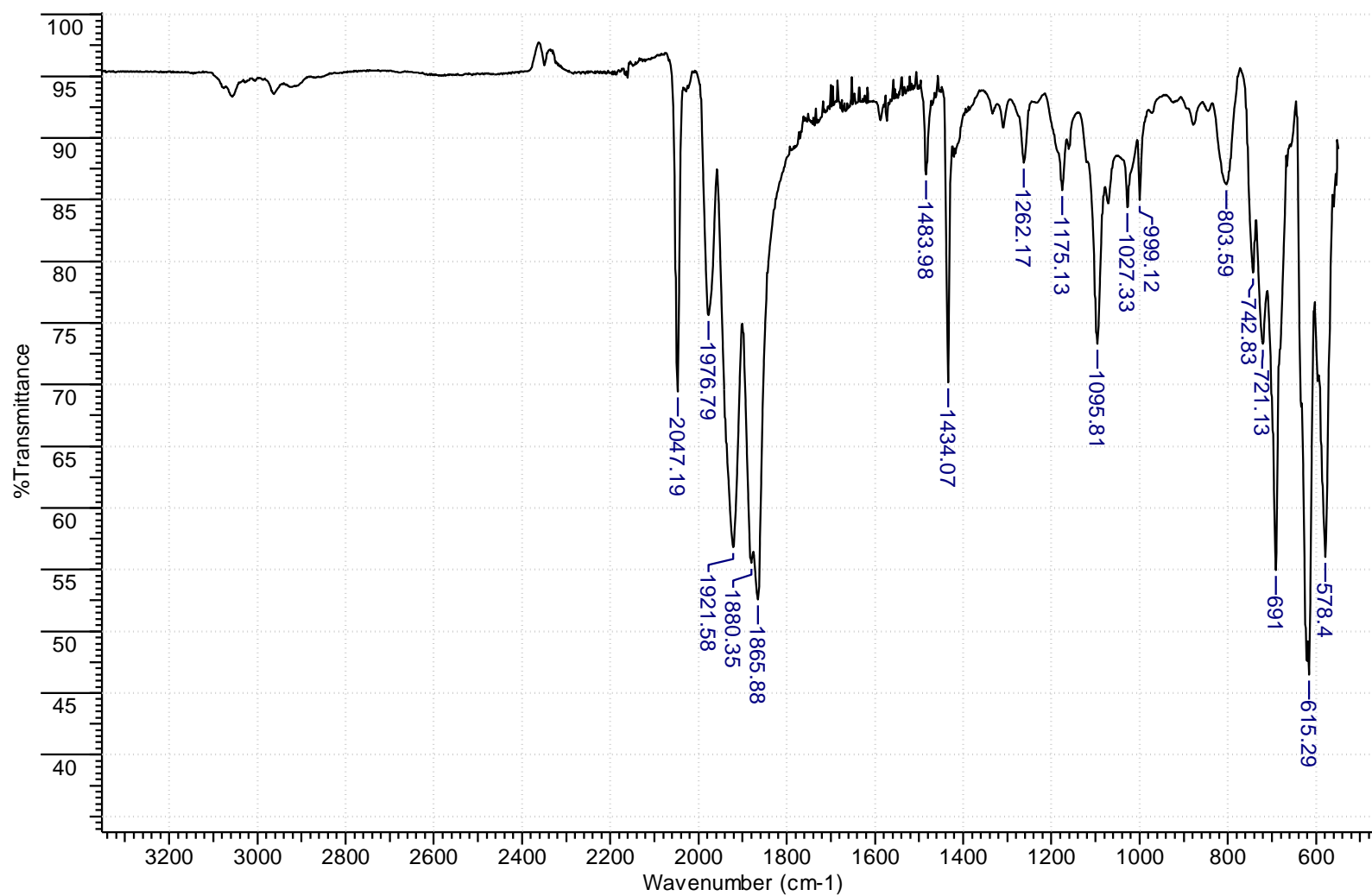
### FTIR Spectrum of $[\text{Fe}_3(\text{CO})_8(\mu\text{-CO})_2(\mu,\eta^2\text{-dppm})]$ (7)





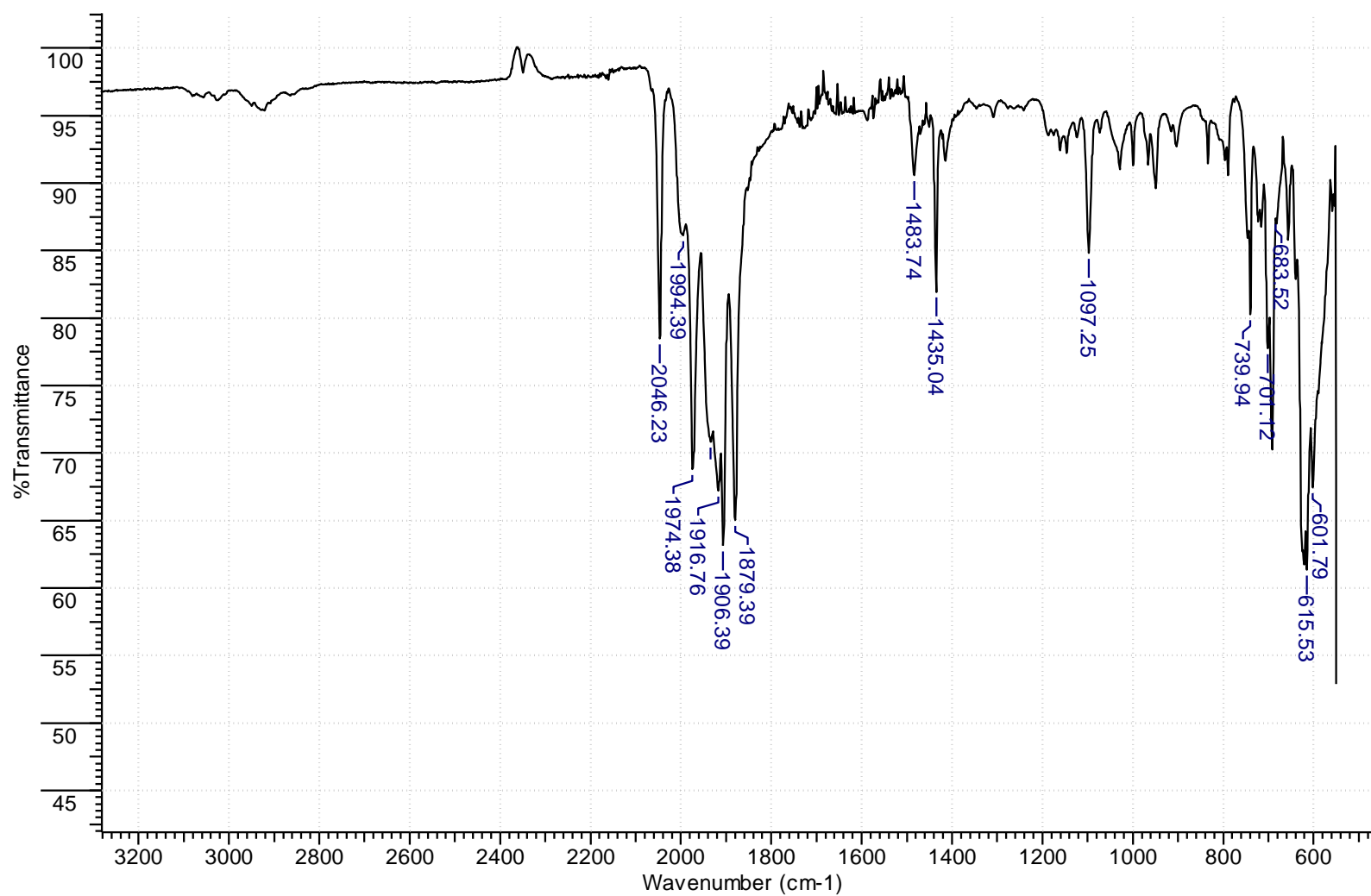
## APPENDIX 4 FTIR SPECTRA

### FTIR Spectrum of $[\text{Fe}_3(\text{CO})_8(\mu\text{-CO})_2(\mu,\eta^2\text{-dppe})]$ (8)



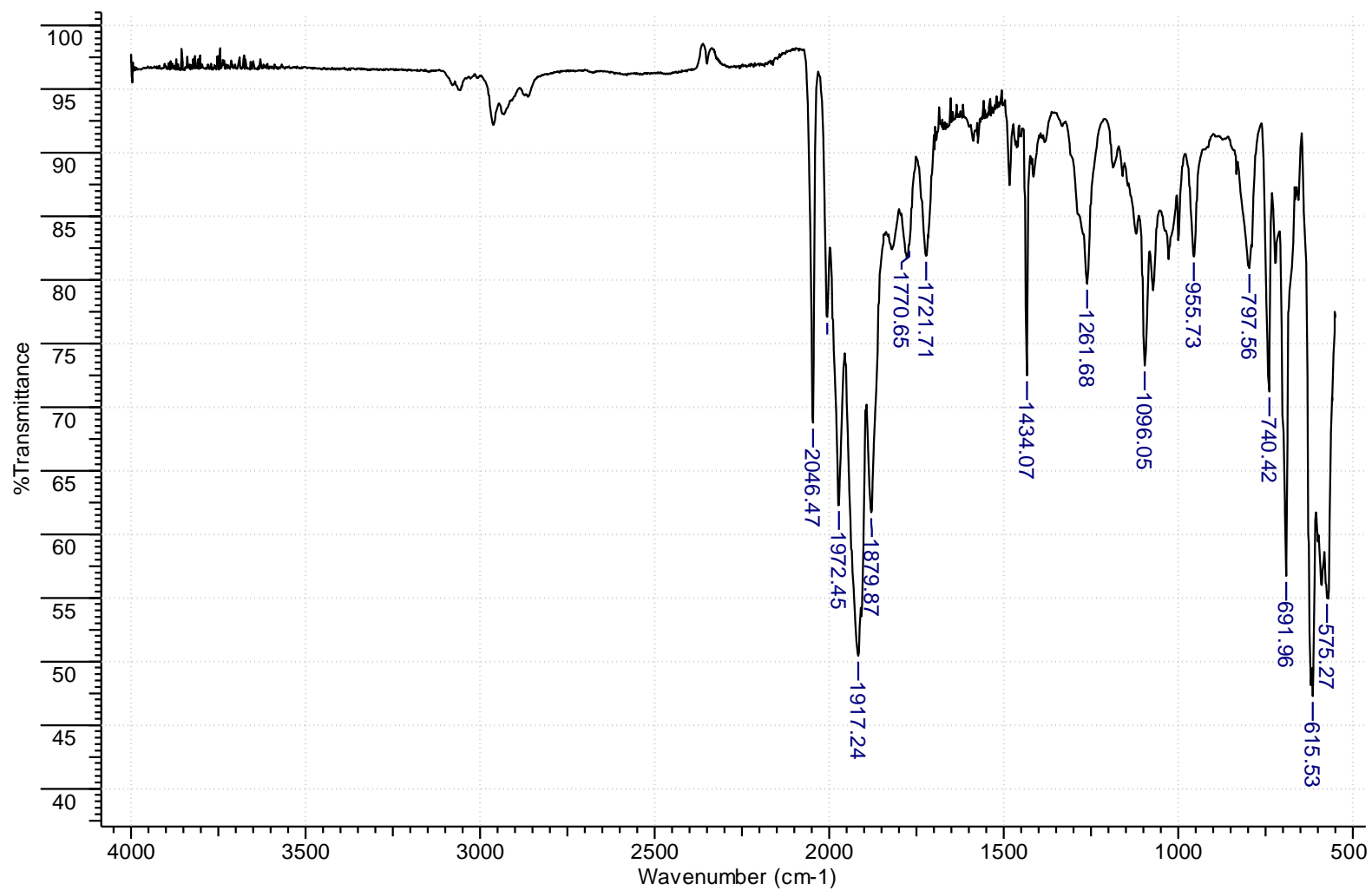
## APPENDIX 4 FTIR SPECTRA

### FTIR Spectrum of $[\text{Fe}_3(\text{CO})_8(\mu\text{-CO})_2(\mu,\eta^2\text{-dppp})]$ (9)



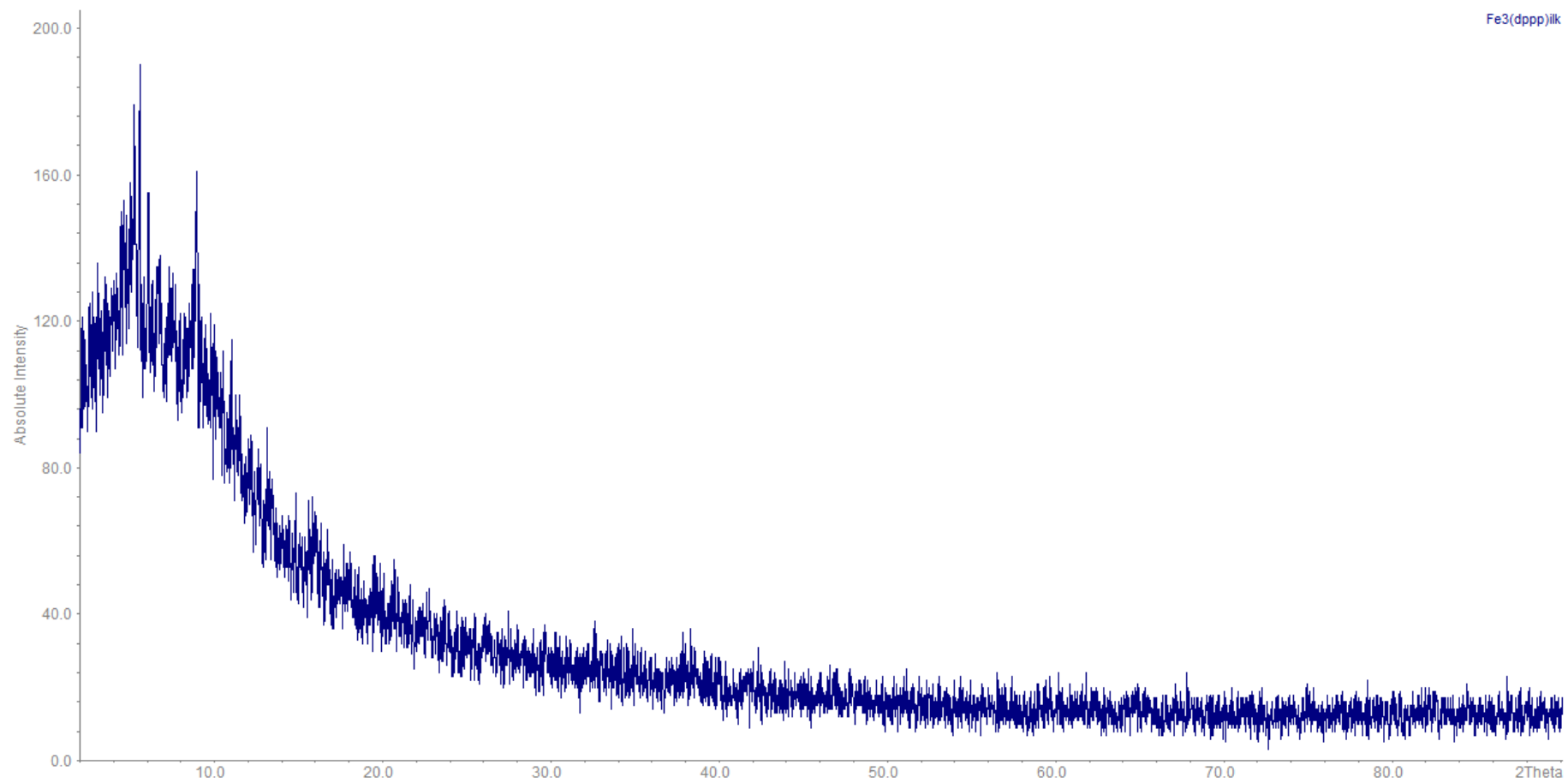
## APPENDIX 4 FTIR SPECTRA

### FTIR Spectrum of $[\text{Fe}_2(\text{CO})_4(\mu\text{-CO})_3(\mu,\eta^2\text{-dppp})]$ (10)



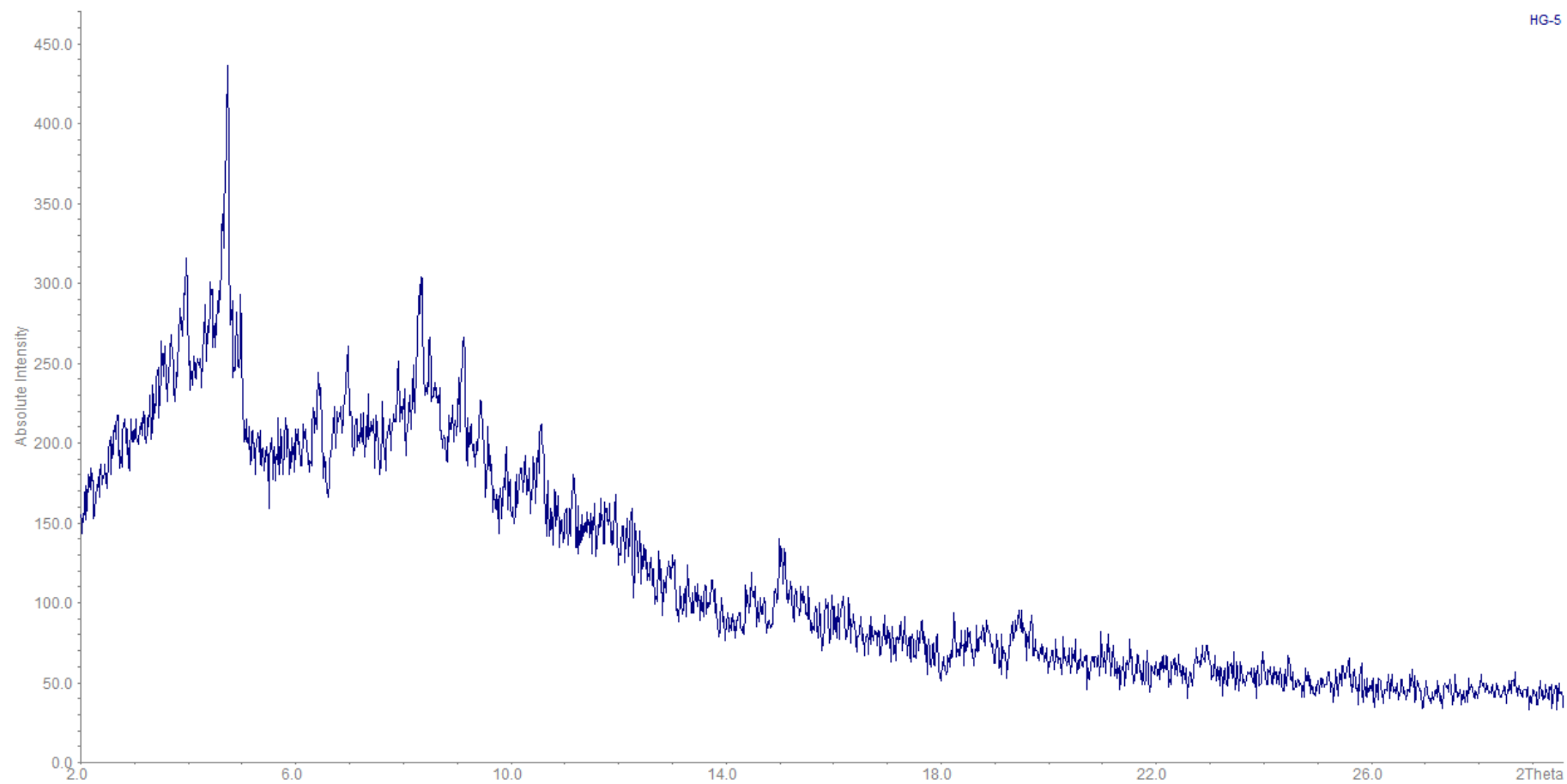
## APPENDIX 5 X-RAY POWDER SPECTRA

### X-Ray Powder Spectrum of [Et<sub>4</sub>N]<sub>2</sub>[Fe<sub>6</sub>C(CO)<sub>16</sub>] (1)



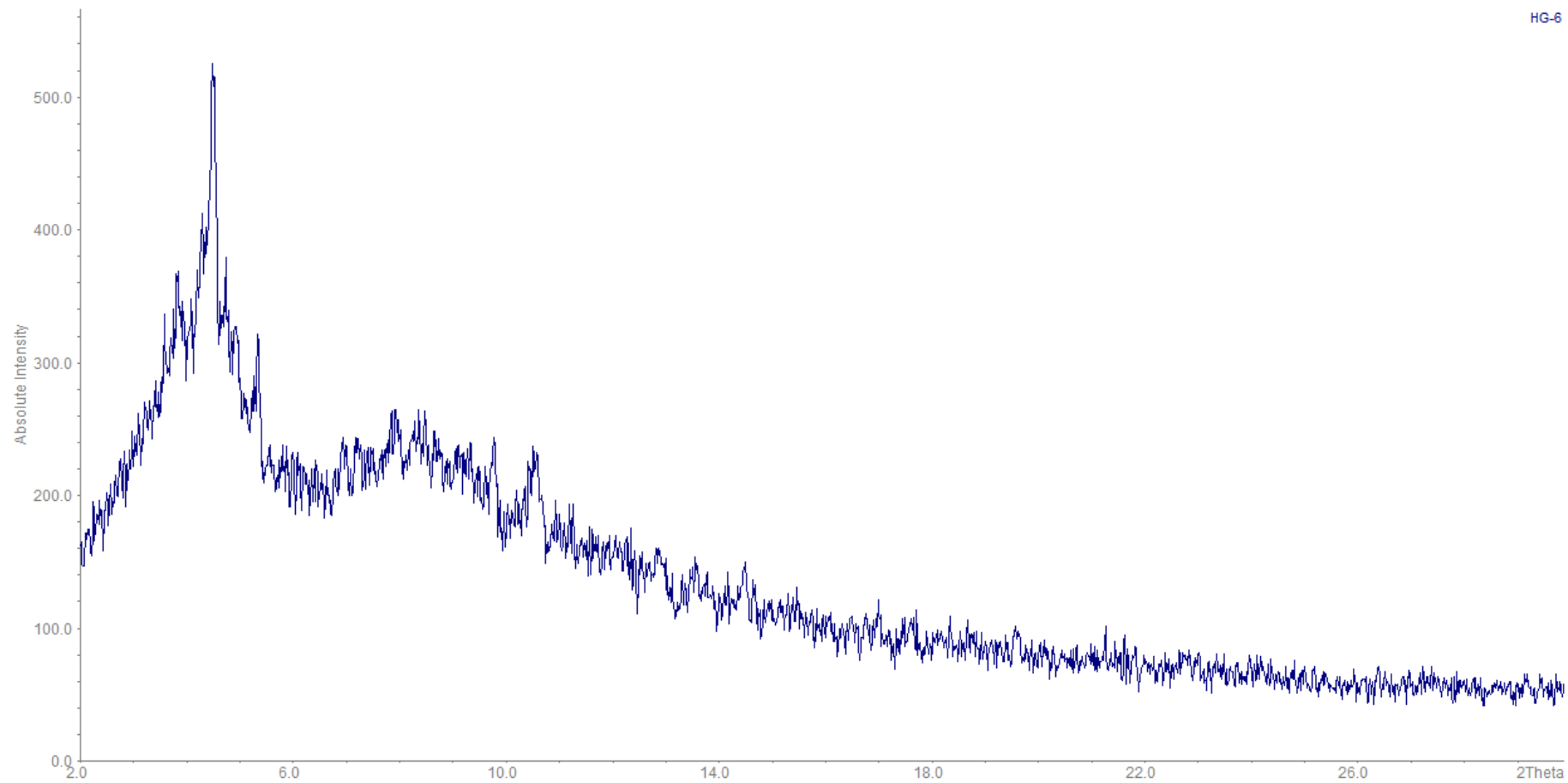
## APPENDIX 5 X-RAY POWDER SPECTRA

### X-Ray Powder Spectrum of $[\text{Fe}_2(\text{CO})_4(\mu\text{-CO})(\mu,\eta^2\text{-dppm})_2]$ (2)



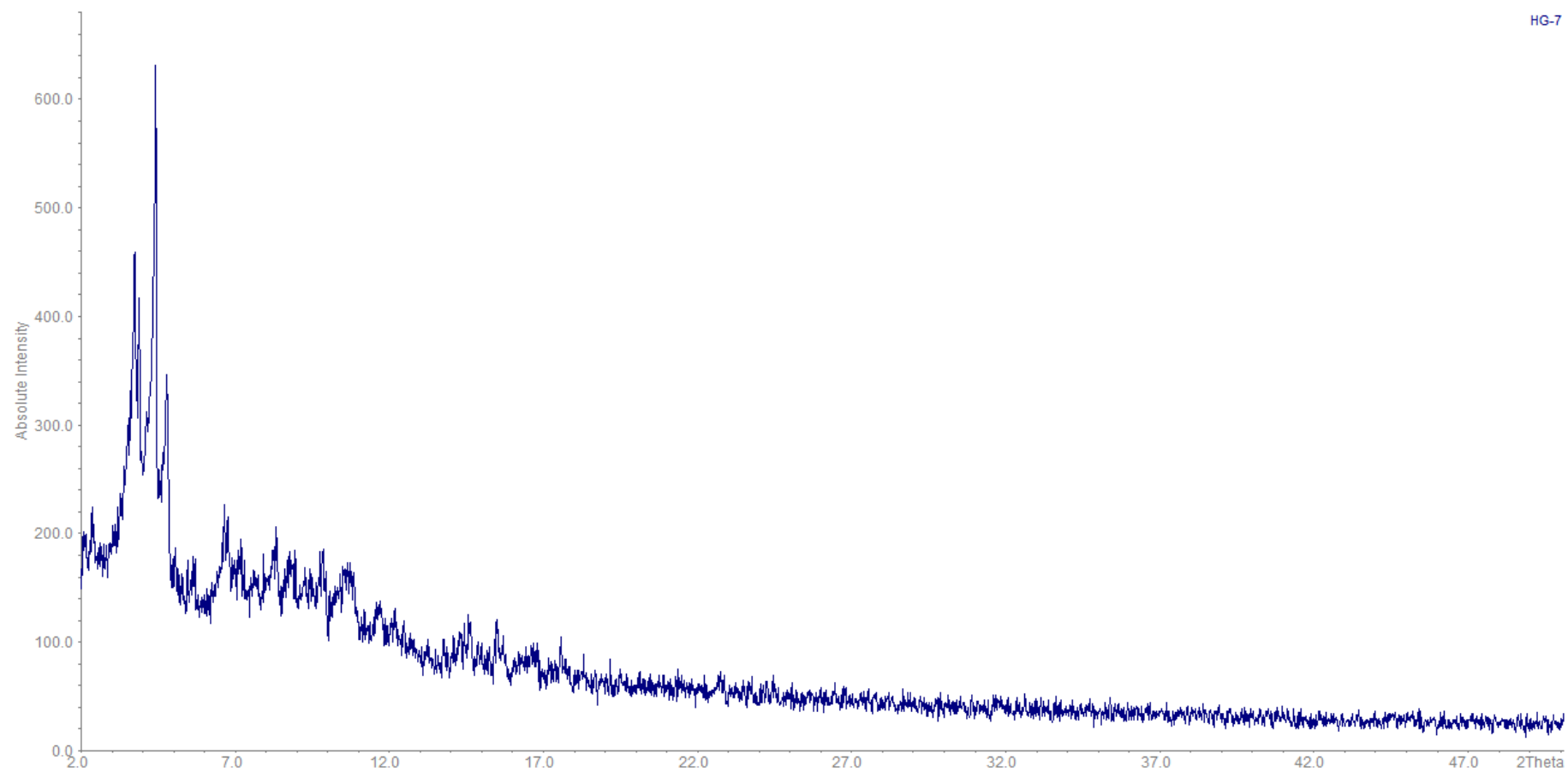
## APPENDIX 5 X-RAY POWDER SPECTRA

### X-Ray Powder Spectrum of $[\text{Fe}_2(\text{CO})_4(\mu\text{-CO})_3(\mu,\eta^2\text{-dppm})]$ (3)



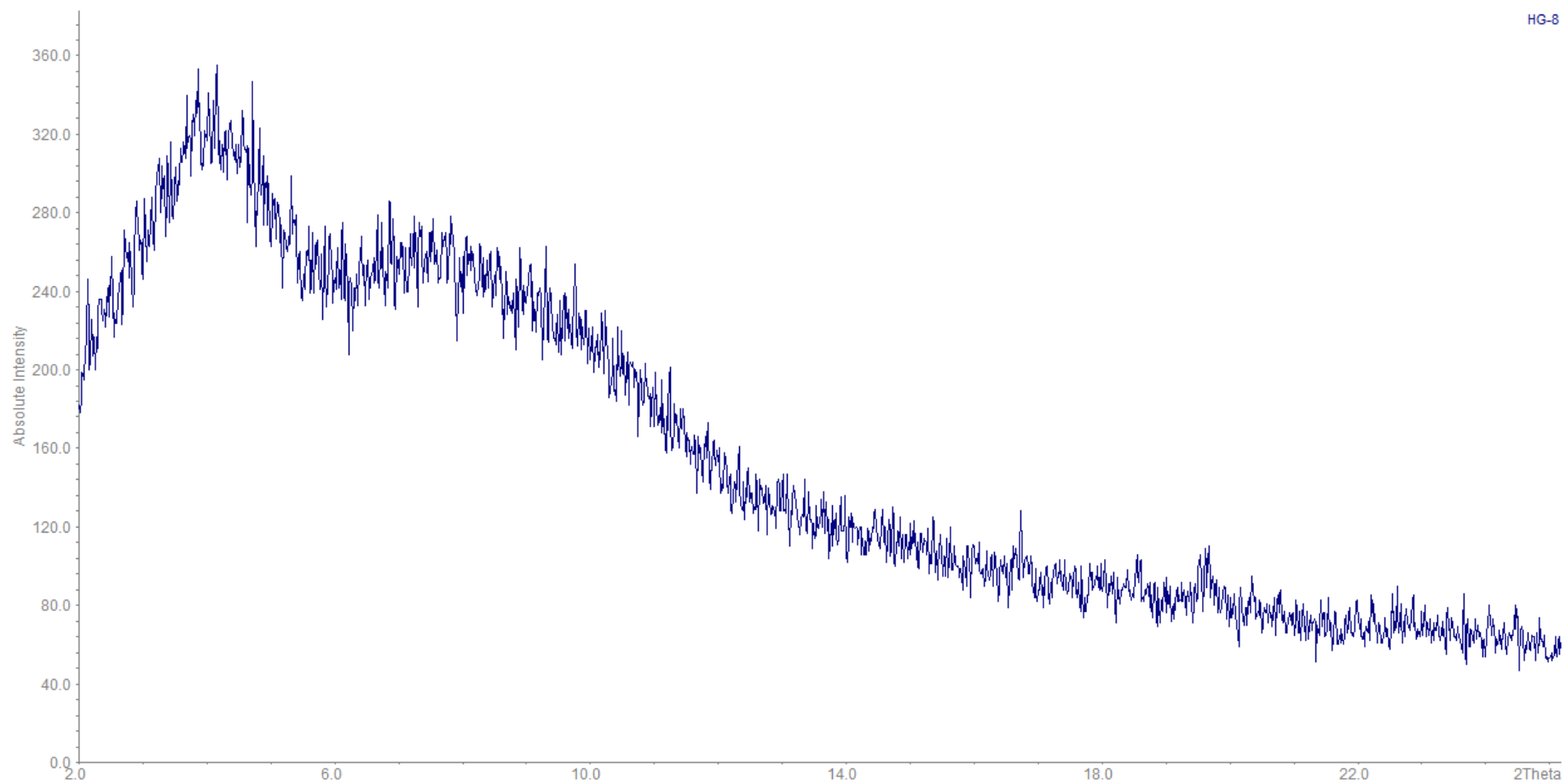
## APPENDIX 5 X-RAY POWDER SPECTRA

### X-Ray Powder Spectrum of [Fe(CO)<sub>4</sub>(dppm)] (4)



## APPENDIX 5 X-RAY POWDER SPECTRA

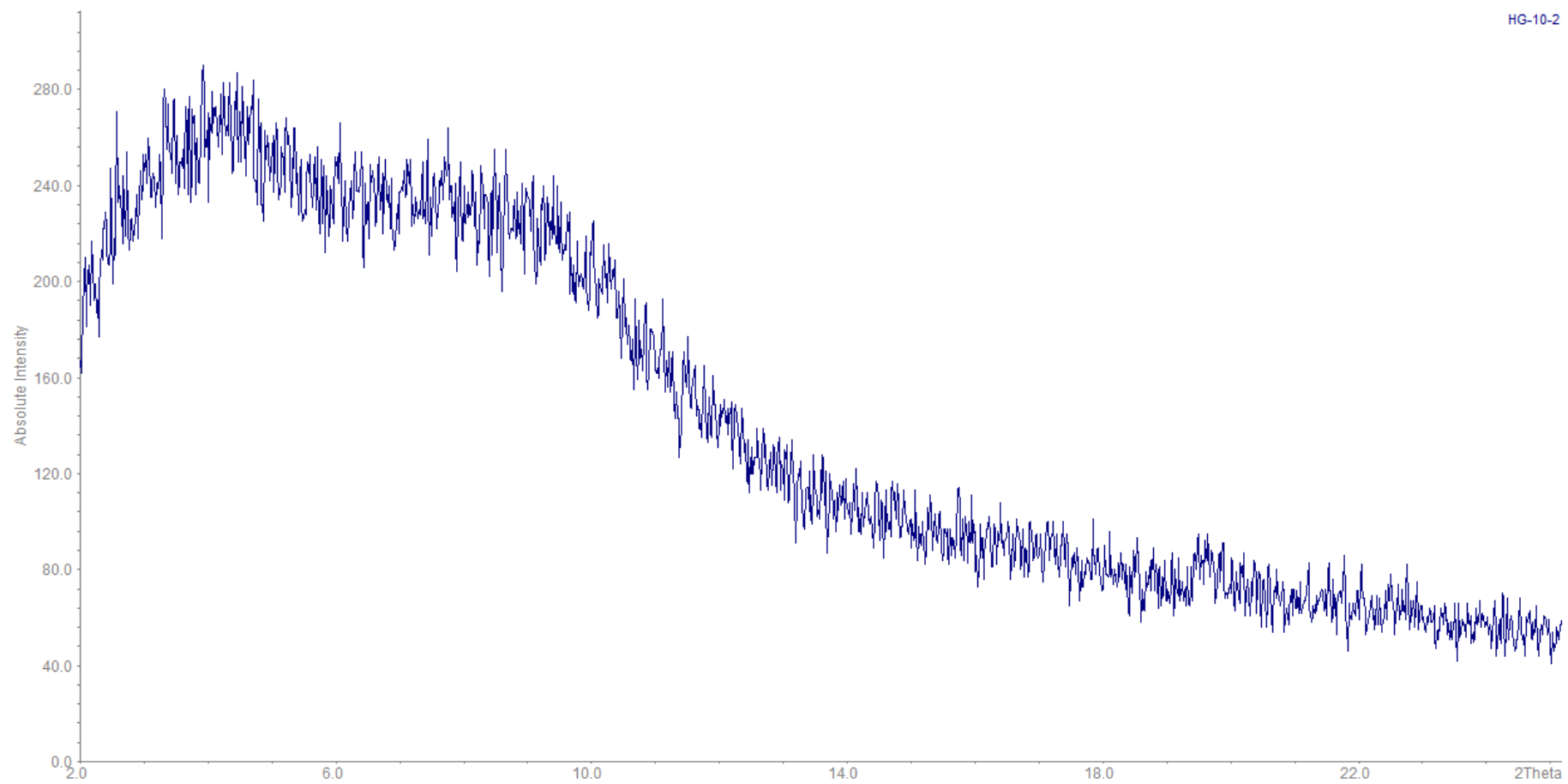
### X-Ray Powder Spectrum of $[\text{Fe}_2(\text{CO})_4(\mu, \eta^2\text{-dppe})_2]$ (5)





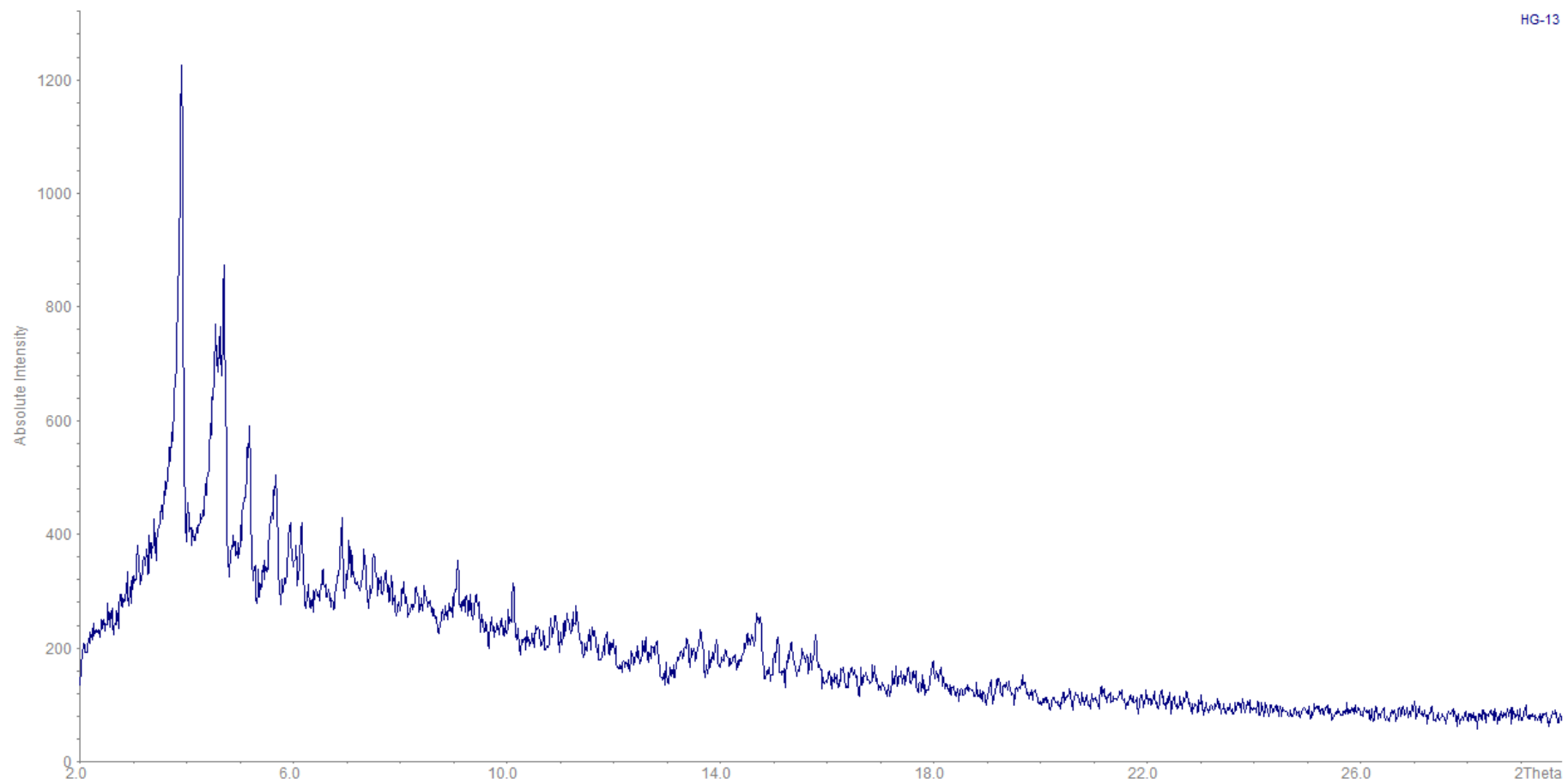
## APPENDIX 5 X-RAY POWDER SPECTRA

### X-Ray Powder Spectrum of $[\text{Fe}_2(\text{CO})_4(\mu, \eta^2\text{-dppp})_2]$ (6)



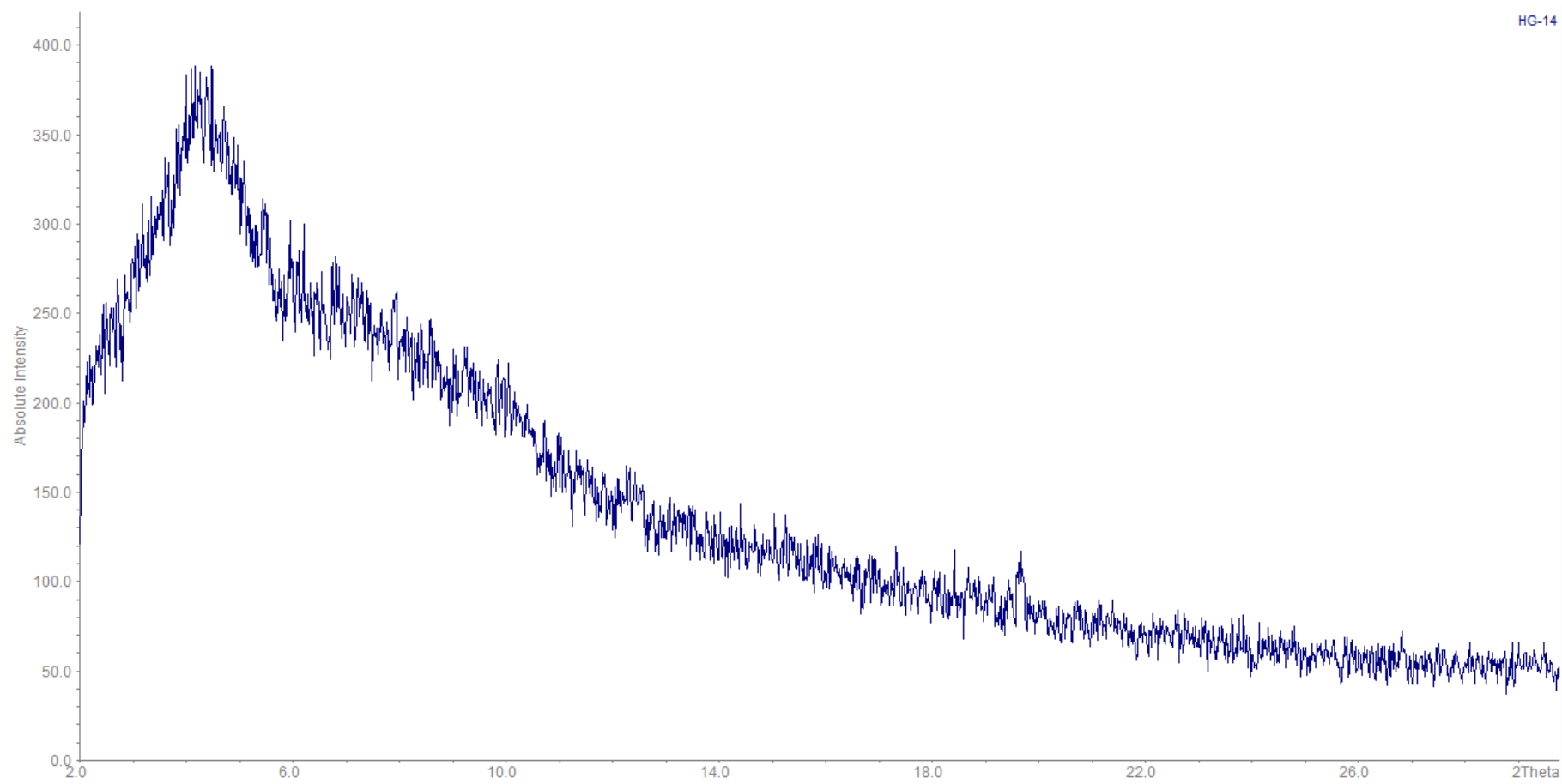
## APPENDIX 5 X-RAY POWDER SPECTRA

### X-Ray Powder Spectrum of $[\text{Fe}_3(\text{CO})_8(\mu\text{-CO})_2(\mu,\eta^2\text{-dppm})]$ (7)



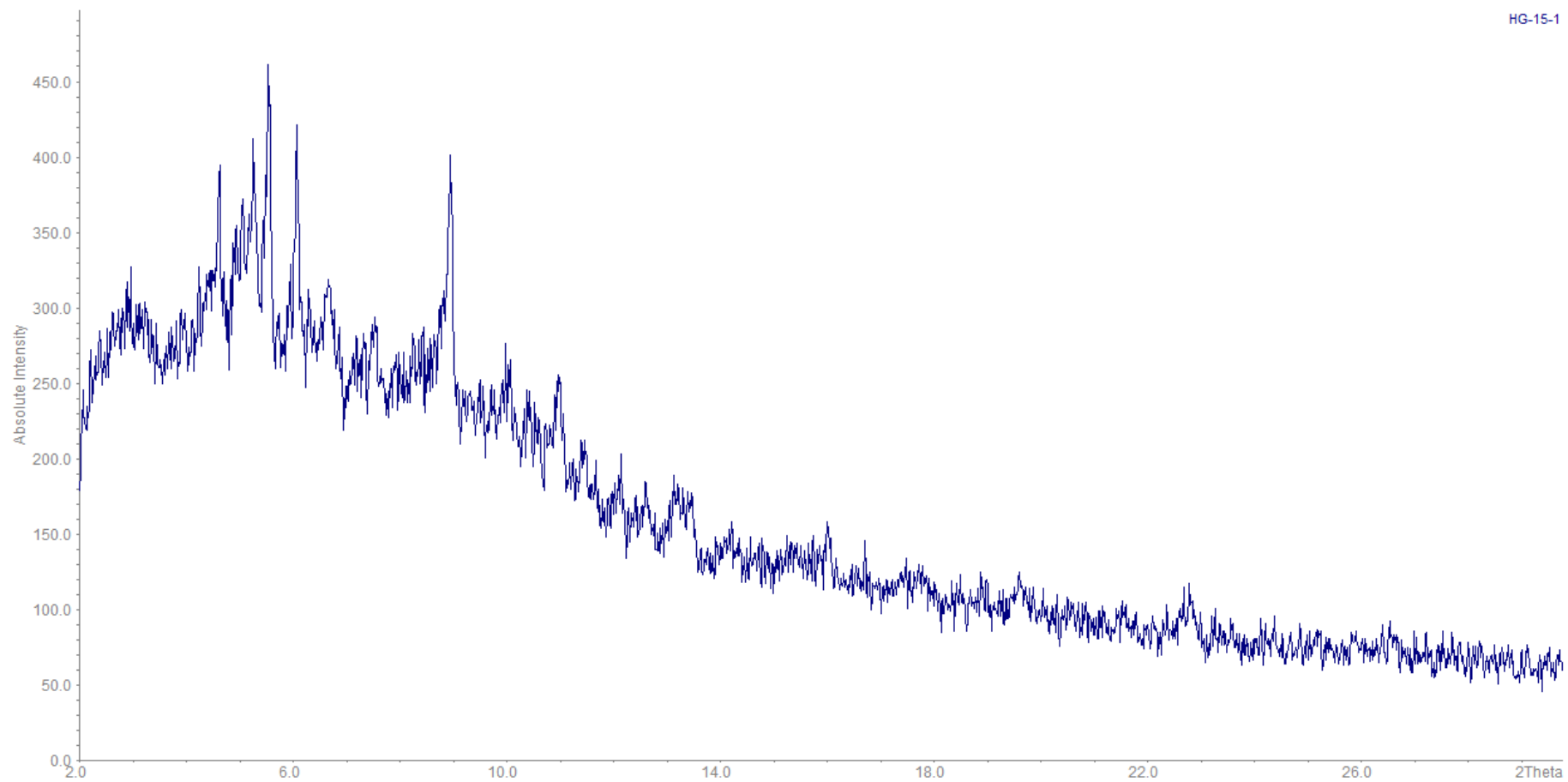
## APPENDIX 5 X-RAY POWDER SPECTRA

### X-Ray Powder Spectrum of $[\text{Fe}_3(\text{CO})_8(\mu\text{-CO})_2(\mu,\eta^2\text{-dppe})]$ (8)



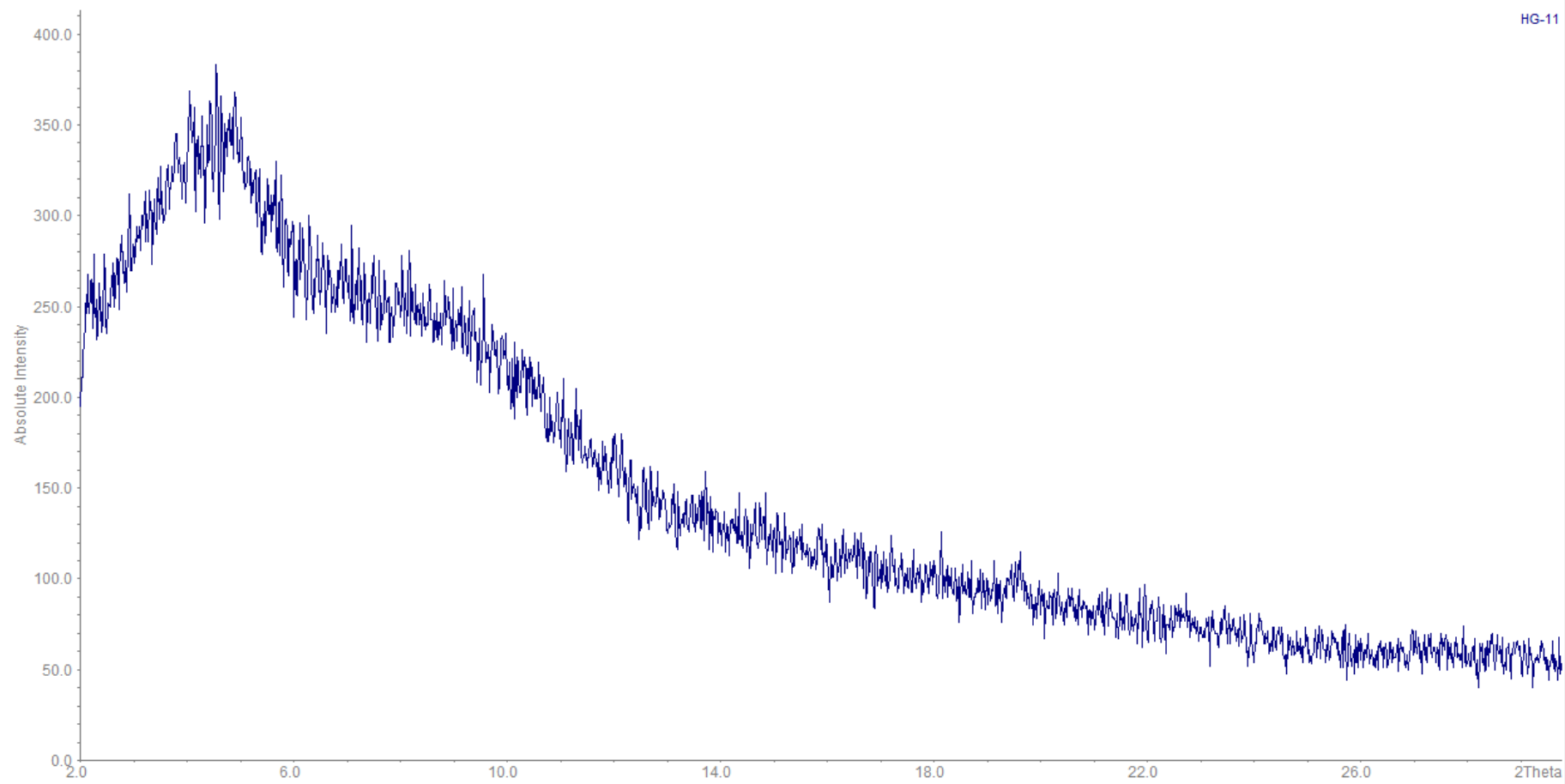
## APPENDIX 5 X-RAY POWDER SPECTRA

### X-Ray Powder Spectrum of $[\text{Fe}_3(\text{CO})_8(\mu\text{-CO})_2(\mu,\eta^2\text{-dppp})]$ (9)



## APPENDIX 5 X-RAY POWDER SPECTRA

### X-Ray Powder Spectrum of $[\text{Fe}_2(\text{CO})_4(\mu\text{-CO})_3(\mu,\eta^2\text{-dppp})]$ (10)



## DECLARATION

---

Hiermit bestätige ich, dass die der Fakultät für Chemie der Technischen Universität München zur Promotionsprüfung vorgelegte Arbeit mit dem Titel: "The Synthesis, Characterization and Performance of Well-Defined Iron Carbonyl Catalysts" im Lehrstuhl für Strukturanalytik in der Katalyse unter Anleitung und Betreuung von Prof. Moniek Tromp erstellt und bei der Abfassung nur die gemäß § 6 Abs. 5 angegebenen Hilfsmittel benutzt worden sind. Die Dissertation ist in keinem anderen Prüfungsverfahren als Prüfungsleistung vorgelegt.

*München, 28.05.2015*

Hüseyin Güler

## ACKNOWLEDGMENTS

---

Foremost, I would like to thank my advisors Prof. Moniek Tromp for providing me with the opportunity of my PhD at the Technical University of Munich. She has been actively interested in my work and has always been available to advise me.

I want to thank present and past members of my department: Dr. Fatemeh Ahmadi, Jan Samson, Dr. Rowena Thomas and Venkatesh Subbiah for giving me an introduction into the lab and for sharing their knowledge.

I especially thank my mom, dad, and brother. My hard-working parents have sacrificed their lives for my brother and myself and provided unconditional love and care. I love them so much, and I would not have made it this far without them. My brother has been my best friend in my life, and I would thank him for all his advice and support.

For the non-scientific side of my thesis, thanks to Ismail Ceylan and Mustafa Akyel for advising of the life in Munich. Thanks to Irfan Temur, Umut Güney, Emrah Karakoc and Inan Karasoy for many evenings filled interesting discussions, for the accommodation, cigarettes, beer, and the great trips, and for enjoyable card games.

## CURRICULUM VITAE

---

Name : Hüseyin Güler  
Address : Schinkel Str. 4 80805 Munich / GERMANY  
Birth : 07.10.1985 in Sivas / TURKEY  
Tel : +49 0151 47138083  
E-mail : hueseyin.gueler@tum.de

### ***Education***

<u>1999 - 2003</u> : Can Lisesi (Canakkale)	High School
<u>2003 - 2009</u> : Hacettepe University / Chemistry Teaching	Bachelor
<u>2009 - 2011</u> : Ankara University / Inorganic Chemistry	Master
<u>2011 - 2015</u> : Technical University of Munich	PhD

### ***Work Experience***

06/2007-07/2007: EUAS Thermic Reactor / Chemistry lab / Internship

05/2010-05/2011: Scientific and Technical Research Council of Turkey (TUBITAK)  
grand No: TBAG 210T122

09/2011-02/2015: PhD Candidate / Catalysis Research Center / Chair of Catalyst  
Characterisation / Technical University of Munich

### ***Areas of interest***

Cluster Science, Spectroscopy, Analytical Chemistry, Homogeneous Catalysis,  
Surface Chemistry, Heterogenous Catalysis,



## ***Project***

2009-2010: Schiff bases with macrocyclic parents and their complexes

2010-2011: The condensation reactions of new 4-Cyanobenzoyloxy-derivatives with 4-Aminoantipyrinen and 4 alkaline aminobenzo-15-Crown-5 and crown ether-metal complexes / THESIS

2011-2015: The Synthesis, Characterisation and Performance of Well-Defined Iron Carbonyl Catalysts / THESIS

## ***Publication***

The synthesis, molecular structure, FT-IR and XRD spectroscopic investigation of 4-[(2-[(2-furylmethyl)imino]methyl)-4-methoxyphenoxy)methyl]benzonitrile: A comparative DFT study. **Journal of Molecular Structure (2011), 991(1-3), 12-17.**

Syntheses, spectroscopic and structural characterizations and metal ion binding properties of Schiff bases derived from 4'-aminobenzo-15-crown-5. **Polyhedron (2012), 31(1), 688-696.**

Novel bis-crown ethers and their sodium complexes as antimicrobial agent: synthesis and spectroscopic characterizations. **Medicinal Chemistry Research (2014), 23(8), 3652-3661.**